DNA MATERIALS FOR DIAGNOSTIC APPLICATIONS

A Dissertation

Presented to the Faculty of the Graduate School

of Cornell University

In Partial Fulfillment of the Requirements for the Degree of

Doctor of Philosophy

by

Roanna Clarissa Ruiz

August 2015

DNA MATERIALS FOR DIAGNOSTIC APPLICATIONS

Roanna Clarissa Ruiz, Ph.D.

Cornell University 2015

The extraordinary controllability of DNA nanostructures provides great potential for nanotechnology and biotechnology, with diverse applications including drug delivery, sensing, and materials synthesis. However, DNA-based systems are limited in their real-world applications, particularly with respect to diagnostics. In particular, they are high complexity, require expensive equipment, and have specific operation conditions. To overcome these challenges, recent work has demonstrated the power of integrating DNA and microfluidics. The multifunctionality, controllability, and design versatility of DNA make it incredibly well suited for the detection of nucleic acid targets, chemicals, and small molecules. Moreover, microfluidic technology is ideal for clinical and point-of-care (POC) detection by providing small, highly controlled, self-contained systems for executing DNA-based reactions with high accuracy and precision. Thus, in this Dissertation I discuss two important themes underlying the use of DNA materials for diagnostics: 1) DNA is a remarkable structural polymer that enables controlled assembly of multifunctional probes for multiplexed detection, and 2) DNA's biological role in enzymatic amplification can be harnessed for engineering novel POC detection strategies. This fusion of "structure" and "function" exemplifies the power of DNA as both a genetic and generic material, and it will ultimately lead to great advancements in the field of nucleic acid diagnostics.

BIOGRAPHICAL SKETCH

Roanna Ruiz received a Bachelor of Science degree in Engineering Sciences from Harvard University in 2009. As an undergraduate focusing in Biomedical Engineering, Roanna was fortunate enough to work on exciting research projects under the guidance of excellent Harvard Professors and mentors: George M. Whitesides, Eric Mazur, and Hanspeter Pfister. During her time at Harvard, Roanna performed research in nanotechnology, physics, and computer science – all of which inspired her to enter graduate school and seek an advanced degree. Roanna then moved to Ithaca, NY to attend Cornell University, where she earned a Master of Science degree in Biomedical Engineering while pursuing a Doctor of Philosophy degree in Biomedical Engineering. Upon entering graduate school, Roanna joined the research group of Professor Dan Luo to investigate the use of DNA nanotechnology for biomedical applications. At Cornell, Roanna developed skills in engineering DNA nanostructures and creating microdevice systems for medical diagnostics applications. She was also the recipient of three competitive research fellowships: the Cornell Sloan Minority Fellowship (2009), the NDSEG Fellowship (2011), and the NSF Graduate Research Fellowship (2012). Roanna will be joining the life sciences management consulting firm IMS Consulting Group from July 2015 as a consultant. She is excited to apply the knowledge and expertise she has developed in graduate school towards biotechnology and pharmaceutical industry work.

To my family and friends

ACKNOWLEDGMENTS

I would like to express my deep appreciation for the valuable guidance and advice provided by my academic advisor and committee chair, Professor Dan Luo. His mentorship during my time at Cornell was instrumental in shaping my development as a researcher, while also enabling me to grow professionally. Without his continued support and guidance, my Ph.D. degree would not have been possible. I am also incredibly grateful to my committee members, Professor Harold Craighead and Professor Barbara Baird, both of whom provided insightful and thoughtful feedback on my research projects. Furthermore, I am honored and thankful for the fellowship awards I received from Alfred P. Sloan Foundation, U.S. Department of Defense, and National Science Foundation. Many thanks are due to my fellow Luo Lab members as well. Specifically, I would like to thank Edward Rice, Shogo Hamada, Mark Hartman, Thua Tran, Jason Kahn, Shawn Tan, Natt Kiatwuthinon, Ken Yancey, Songming Peng, Tom Derrien, and Duo An for their helpful suggestions and advice. Last but not least, my heartfelt gratitude goes to my parents, Professor Victoria Herrera and Professor Nelson Ruiz-Opazo, my brother Nick Ruiz, and my boyfriend, Alex Dubec. Their unwavering support and love has helped me to continue to work hard, set high standards, and achieve ambitious goals.

TABLE OF CONTENTS

LIST OF FIGURES

CHAPTER 1

INTRODUCTION

In this Dissertation, I will use DNA materials as a powerful tool for nucleic acid diagnostics. In particular, I will demonstrate how the intrinsic advantages of DNA – precise controllability, versatile functionalization, and ease of manipulation – can be maximized to achieve advanced and novel diagnostic capabilities. In the introduction, I will discuss how different DNA topologies (linear, branched, and networked) have been applied towards DNA material assembly, and explore fundamental strategies behind DNA-based detection. Next, I will discuss the integration of branched DNA nanomaterials with a microbead-array device for multiplexed diagnostics. I will then explain how enzymatically amplified DNA materials can be leveraged with microfluidics for point-of-care (POC) applications. Finally, I will outline how and why DNA materials have become a highly versatile tool for improving and evolving current diagnostic approaches.

1.1 DNA topologies for nanoscale material assembly

Historically, DNA has been commonly understood as a genetic material whose main function is the encoding and storage of genetic information. However, in recent decades the fields of molecular genetics and nanotechnology have spurred the rise of DNA as a generic material useful for assembling complex, multifunctional structures. In particular, DNA has a unique set of physical and chemical properties that enable it to serve as a structural polymer for bottom-up nanoscale material assembly.[1] These properties not

only provide important advantages in self-assembly, but they also make DNA a material unlike any other polymer found in biology.

Physically, the composition and structure of DNA is both precisely controllable and highly predictable. Single-stranded DNA (ssDNA) is composed of four bases – Adenine (A), Tyrosine (T), Guanine (G) and Cytosine (C). Unlike other polymers whose individual monomer units are arranged randomly, these base subunits can be organized in any order. Furthermore, the bases follow a set of base-pairing rules whereby it is energetically favorable for binding between A/T and G/C complements over other combinations. Therefore, two ssDNA strands with complementary sequences will recognize and bind to each other (hybridize) to form a double-stranded DNA duplex (dsDNA) with high affinity and predictability. These concepts are summarized in **Figure 1.1**. Furthermore, the DNA hybridization process is both reversible and repeatable. Two ssDNA may be separated at elevated temperatures (denatured) and re-hybridized at lower temperatures (renatured). These denaturing and renaturing steps can be repeated multiple times to facilitate certain DNA reactions, such as polymerase chain reaction (PCR). With the advent of solid phase synthesis and recombinant DNA technologies, ssDNA can now be mass produced in virtually any sequence order and at a variety of lengths – making DNA a potent material that can be "pre-programmed" to generate structures in a specific and controllable way with regards to base organization, sequence length, and binding affinity.

Chemically, DNA can be engineered and functionalized using a broad range of chemical processes and modification techniques. DNA itself stands apart from other polymers in that it can be processed with angstrom level accuracy using biochemical techniques[2] and it can be chemically synthesized with an error rate as low as 1 per 10,000

nucleotides.[3,4] In addition, an extensive library of thousands of enzymes have been characterized and made available for the precise editing of both ssDNA and dsDNA.[5] Different enzymes may be used to cleave and ligate DNA at specific sites with single-base precision, which greatly facilitates the generation of both monodisperse DNA strands and higher-ordered DNA materials. A variety of bio-functional groups (fluorescent labels, quenchers) and chemical moieties (primary amines, alkynes, thiols and biotins) can also be attached to synthetic DNA for added functionality. The modified DNA may be subsequently conjugated to additional inorganic and organic materials as well, such as gold nanoparticles,[6-12] proteins,[13-19] and polymers.[20-25] These layers of modifications create a mosaic of possibilities in the function, behavior, and structural composition of DNA materials.

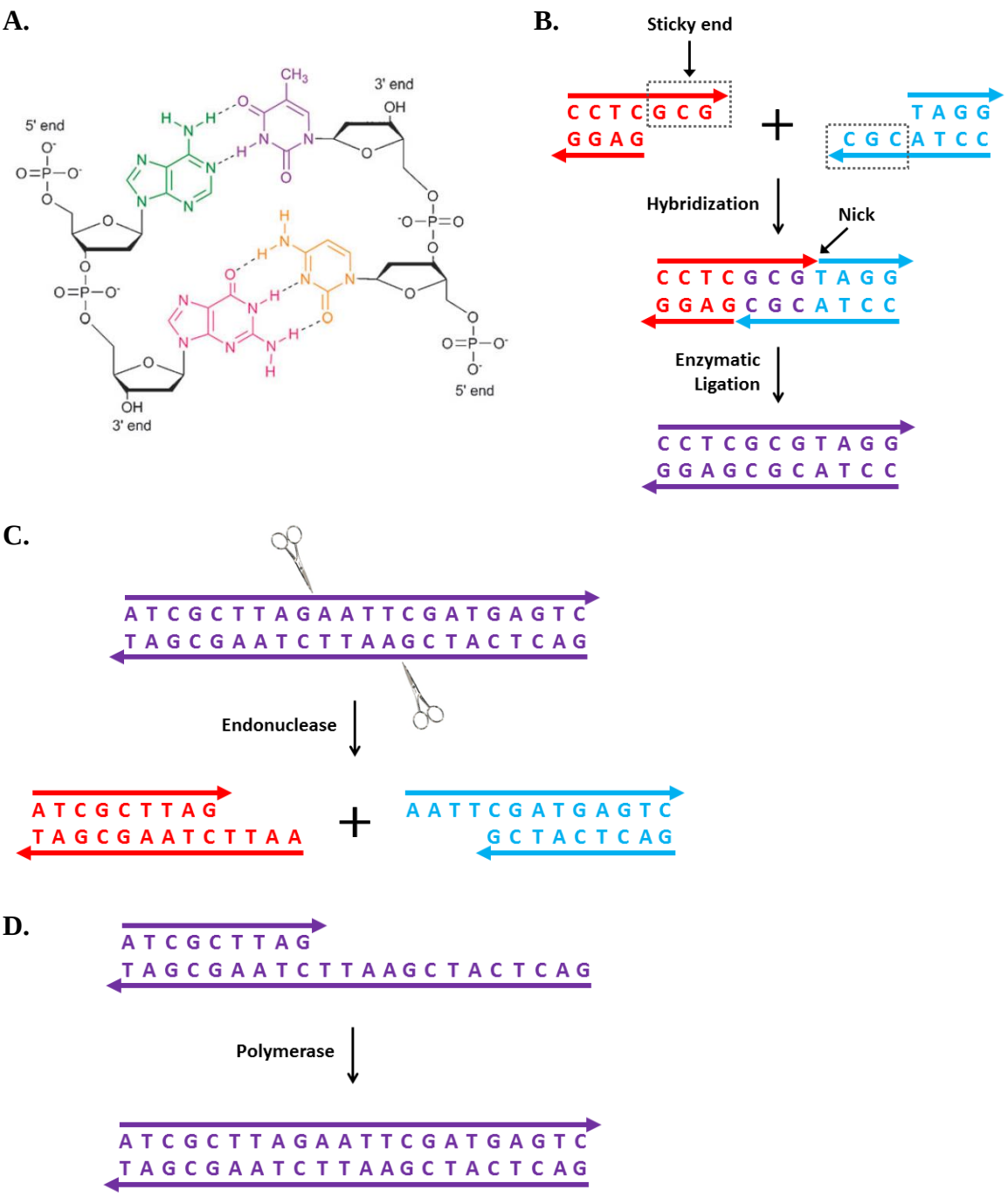

Figure 1.1 Principles of DNA self-assembly and DNA manipulation strategies

A) The Watson-Crick base-pairing rules mean that Adenine (A) pairs with Thymine (T) and Guanine (G) pairs with Cytosine (C). **B)** Two dsDNA can be linked by hybridization of sticky ends. The nick between the two dsDNA can be chemically linked by enzyme ligation, resulting in a single dsDNA. Arrows indicate the 5' to 3' direction of DNA. **C-D)** Enzymes may also be used to manipulate and control DNA. For example, endonuclease

(C) can be used to cut one dsDNA into two discrete pieces at a specific sequence. Furthermore, polymerase **(D)** can be used to elongate one ssDNA strand using a precursor strand as a template.

1.1.1 *Linear DNA topology*

DNA materials can be divided into three main topologies: linear, branched, and networked. (**Figure 1.2**) The most fundamental topology, linear DNA, is the naturally occurring form of DNA. It provides a simplicity and versatility that enables the design and development of many complex structures. Interestingly, linear DNA can be used to assemble one-dimensional (1D) materials (DNA nanowires, DNA nanotubes), two-dimensional (2D) materials (DNA tiles, DNA origami), and three-dimensional (3D) materials (DNA box, DNA tetrahedra). Additionally, linear DNA can be functionalized both internally and on the 3' or 5' ends, making it an optimal template for organizing and patterning functional moieties such as gold nanoparticles (AuNPs), quantum dots (QDs), carbon nanotubes (CNTs), and proteins. By interconnecting multiple linear DNA carrying different functional moieties, sophisticated patterns and multifunctional structures can be engineered for entirely new applications that would otherwise not have been possible.

Linear DNA was first used as a generic material for the organization and assembly of nanoparticles (NPs). One of the earliest examples was that of Mirkin and coworkers, who functionalized AuNPs with thiol-modified DNA (forming DNA-AuNP conjugates) to arrange the AuNPs into macroscopic hybrid materials.[26,27] By exploiting the site-specific recognition feature of DNA hybridization, DNA was used to rationally direct the formation of larger assemblies in a controlled manner – paving the way for the fabrication of more advanced materials. The programmable assembly power of linear DNA was further developed by Mirkin and colleagues when they utilized the precise binding of DNA-AuNP conjugates to form novel 3D AuNP crystalline materials.[28] Interestingly, the crystalline state (face-centered-cubic vs. body-centered-cubic) of these microstructures was

determined by the different ssDNA sequences attached to the nanoparticles, free ssDNA linkers, and the absence or presence of a single-base "flexor" unit. In a similar study, Gang and coworkers reported 3D body-centered-cubic nanoparticle structures.[29] Additional work in this area has led to the production of chiral DNA-AuNP nanostructures with pyramidal and tetrahedral geometries.[30] Linear DNA has served as a highly effective nanoscale organizer for other materials as well, including patterning of DNA-protein (streptavidin) conjugates in 2D arrays,[31] formation of multi-enzyme complexes on linear DNA templates,[32] and organization of quantum dots.[33-36]

Building upon this foundation, Mirkin and coworkers developed customized DNA-AuNPs for highly sensitive, colorimetric detection of DNA.[37,38] In short, two different sets of non-complementary, thiolated ssDNA were attached to AuNPs, each partially-matching to a specific DNA target. These DNA-AuNPs were homogeneously distributed in solution and would only aggregate in the presence of matching target DNA, which served as a hybridization linker between the two types of DNA-AuNPs. This aggregation reaction yielded a visible color change from red to purple and achieved a detection limit of 10 femtomoles of target with the naked eye. Detection using hybridization between "capture" DNA and "target" DNA (or RNA) is incredibly useful thanks to the predictability and specificity inherent in all DNA interactions. In addition to colorimetric detection, DNA has been used for highly sensitive electrochemical identification of nucleic acid targets. In particular, these strategies take advantage of the specific binding interactions between complementary DNA target and capture probes in solution, in addition to the high surface area of DNA nanostructures – both of which significantly increase the sensitivity of electrochemical read-outs.[39,40] Fang and coworkers, for instance, used hybridization-based

detection with an array of nanostructured electrochemical sensing elements to identify messenger RNA (mRNA) for prostate cancer screening.[41] Additional surface-based electrochemical detection systems utilize the programmable folding of nucleic acid nanostructures as functional nanoscale target-activated switches.[42,43]

Linear DNA-based detection was at first limited by the quantity of linear DNA used – whether it be the quantity of DNA capture probes, or the amount of available nucleic acid target. These obstacles were overcome through the incorporation of DNA amplification schemes with uniquely designed linear DNA binding configurations tailored for specific amplification cycles. Enzyme-based DNA amplification takes advantage of the natural biological roles of both DNA and enzymes, but adapts them for the purpose of exponentially increasing the amount of DNA sequences (e.g. target DNA) in a detection system. One of the most popular enzymatic amplification methods is PCR, which is a standard technique in clinical and laboratory settings and has also been adapted for low-resource, POC sample detection.[44,45] Despite its widespread use, the repeated thermal cycling steps in PCR necessitates the use of expensive heating and temperature sensing equipment, in addition to greater device and process complexity, all of which are major impediments to creating POC DNA detection systems. Isothermal DNA amplification, on the other hand, uses enzymes optimized for lower isothermal temperatures – making it an ideal strategy for interfacing with small portable systems such as microfluidic devices. A variety of isothermal amplification strategies exist today, but some of the most common include loop-mediated isothermal amplification (LAMP), nucleic acid sequence-based amplification (NASBA), rolling-circle amplification (RCA), and helicase dependent amplification (HDA). These methods utilize linear DNA in a variety of ways, such as using

DNA loops, hairpins, and lock-and-key formations to trigger the enzymatic polymerization and growth of new DNA strands. These strategies exploit the selective molecular recognition properties of DNA to not only accurately identify their target, but also precisely direct the amplification process step-by-step so as to achieve more informative and quantitative results than other detection methodologies.

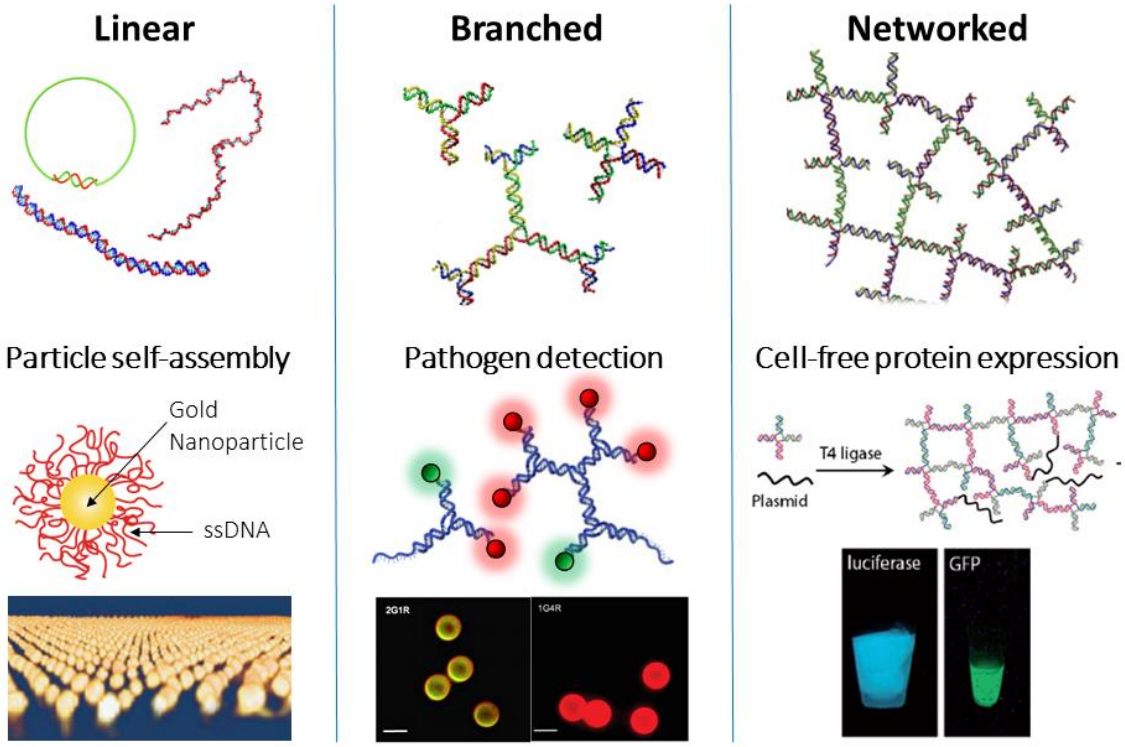

Figure 1.2 Three main topologies of DNA and their real-world applications

Linear, branched, and networked are the three main topologies of DNA. Linear DNA has been used to coat nanoparticles and guide their self-assembly, branched DNA has been used to develop molecular probes for pathogen detection, and networked DNA has been used to create protein-producing hydrogels.

1.1.2 *Branched DNA topology*

Although linear DNA is a versatile building block for assembling a variety of structures, its simple format can lead to certain structural and topological limitations. To overcome these constraints, branched DNA was developed. Branched DNA offers several unique advantages over linear DNA, including an inherent multivalency through which different functional moieties may be attached to different branches. Additionally, branched DNA can be designed to assemble into either isotropic or anisotropic structures by using different sticky end "connectors" on separate branches. Therefore, many unique functionalities and physical conformations can be built into a single branched DNA nanostructure – a capability that is very difficult to achieve with linear DNA alone. Furthermore, the hybridization and ligation of multiple branched DNA structures can be precisely controlled to yield complex 2D and 3D assemblies. By treating branched DNA as nanoscale "building blocks," entirely new DNA materials can be assembled at lower cost since only a small set of ssDNA sequences are required per building block. In contrast, many more linear DNA molecules would have been required to form the same complex DNA material, with the additional concern of an increased rate of incorrect and nonspecific binding interactions. Despite the greater utility of branched DNA architectures, much less is known regarding the material properties and behaviors of branched DNA as compared to linear DNA.

Seeman and colleagues pioneered the first branched DNA nanostructures by mimicking the four-armed Holliday junctions that exist transiently in cells. By designing DNA sequences with partial complementary regions and strategically placed sequence-symmetry constraints, Seeman's group created highly stable, synthetic four-armed DNA

structures[46] that did not exhibit the characteristic instability of traditional Holliday junctions (which is necessary for facilitating branch point migration during genetic recombination in cells).[47] This pivotal work inspired a broad range of novel branched DNA shapes, such as DNA cubes,[48] hexagons,[49] and octahedrons,[50] in addition to DNA catenanes and knots.[51] Further development led to more rigid motifs based on the concept of crossover hybridization, in which two or three DNA helices were interlinked using cross-allocation of multiple DNA strands. Using this strategy, double-crossover[52] (DX), triple-crossover[53] (TX), and paranemic crossover[54] (PX) architectures were formed. Seeman's initial biomimetic four-armed branched DNA nanostructure has now grown into a broad library of branched DNA conformations that can be tailored for a variety of biomedical and biological applications.

Another fundamental branched DNA structure is dendrimer-like DNA (DL-DNA). DL-DNA is an extremely versatile building block for two main reasons: 1) it has the same advantages of traditional chemical dendrimers, (multivalency, tunable size, and diverse architecture),[55] and 2) it deviates from chemical dendrimers in that it can be specifically programmed by DNA sequence design to generate tunable, multifunctional, anisotropic nanostructures containing a variety of functional moieties. Building upon this concept, our group developed novel branched Y-shaped, X-shaped, and T-shaped DNA by strategically engineering DNA sticky ends (ssDNA overhangs at the ends of dsDNA which are free to hybridize and connect two dsDNA together).[56] In particular, Y-shaped DNA (Y-DNA) was assembled from three separate ssDNA (Ya, Yb, Yc), with each ssDNA containing partial complementary sequences to the other two ssDNA. (**Figure 1.3**) When equal moles of the three ssDNA were combined in solution, they preferentially hybridized to each other and

formed Y-DNA nanostructures at almost 100% yield. Amazingly, these structures were very robust – Y-DNA remained stable with no sign of degradation after 30 days at 4˚C. T-shaped and X-shaped DNA (T-DNA and X-DNA, respectively) were also self-assembled using a similar method. In addition to monodisperse and robust self-assembly, the multiple branch-ends of branched DNA can be attached to different functional groups and/or sticky ends, enabling programmable design and assembly of complex and multifaceted branched DNA materials.

Specific design features are needed to direct the binding between DNA structures and generate higher-generation branched DNA assemblies with specific properties. In particular, non-palindromic sticky ends must be used on each branch instead of palindromic sticky ends. By definition, palindromic sticky ends contain the same exact 5' to 3' sequence as their matching complementary DNA sequence. For instance, a 5'-GAATTC-3' sequence will bind to any other 5'-GAATTC-3' sequence, which could lead to self-hybridization and uncontrolled self-assembly of larger structures. In contrast, non-palindromic sticky ends will never self-ligate, thus enabling highly precise control of binding between DNA nanostructures. To build a stable, multi-generation branched DL-DNA structure, our group used non-palindromic sticky ends and enzymatic ligation.[57] (**Figure 1.3**) More specifically, non-palindromic sticky ends were used for a single core Y-DNA (G0), to which an additional three peripheral Y-DNA (with complementary sticky ends to the core Y-DNA) were hybridized and ligated. This process formed a first-generation of DL-DNA (G1). Higher generation structures (up to six generations) were produced by repeatedly ligating peripheral Y-DNA to the prior generation.

DL-DNA, like other branched DNA building blocks, has a number of exciting biomedical and biological applications. One noteworthy example is that of Nishikawa and coworkers, who loaded DL-DNA with GACGTT sequences to specifically activate murine immune cell secretion of various cytokines and promote the production of immunoglobulin.[58,59] The increased number of DL-DNA branches supplied a higher dosage of GACGTT sequences, which yielded a significantly stronger immunostimulatory response compared to linear DNA with the same sequence. This was one of the first instances in which structure-dependent immunostimulatory activity enhancement was achieved. Because it is extremely difficult to use conventional polymeric materials to form anisotropic branched structures,[60] our group used DNA nanostructures to developed anisotropic, branched, and crosslinkable monomeric units (ABC-monomers) for performing sensitive pathogen detection.[61] On different branch points these ABC-monomers carried different color combinations of QDs, photo-crosslinkable moieties, and sticky ends for ligation to a target DNA. The sticky ends were designed to hybridize with specific pathogen DNA targets and form dimers. After ultraviolet (UV) illumination, the dimers polymerized through their built-in crosslinkable groups and formed spherical particles with unique fluorescent-QD identification signals. (**Figure 1.4**) Dimer formation and, by association, UV-polymerization could not have occurred in the absence of the DNA target, making this a uniquely target-driven polymerization detection strategy. Additional branched DNA assemblies (formed from Y-DNA) have been designed with three different functional moieties: a lipid molecule for self-assembly, a fluorescent dye for imaging, and a complementary DNA for target recognition and binding. These Y-DNA structures self-assembled into liposome like structures, called DNAsomes, which could be applied toward

multiplexed drug delivery.[62] Our group has also developed branched DNA nanobarcodes with distinct fluorescence color-codes for multiplexed pathogen detection. These nanostructures will be the focus of **Chapter 2** of this Dissertation. Overall, the modular assembly feature of branched DNA, combined with the predictable binding and functionalization of multiple branch arms, allows for a powerful assembly and design versatility not yet achieved in conventional polymers. A myriad of designs and assembly conformations can be created using branched DNA building blocks, and as DNA synthesis and DNA conjugation processes become more widespread, a vast library of multifunctional DNA architectures could arise for building DNA-based materials beyond the nanoscale.

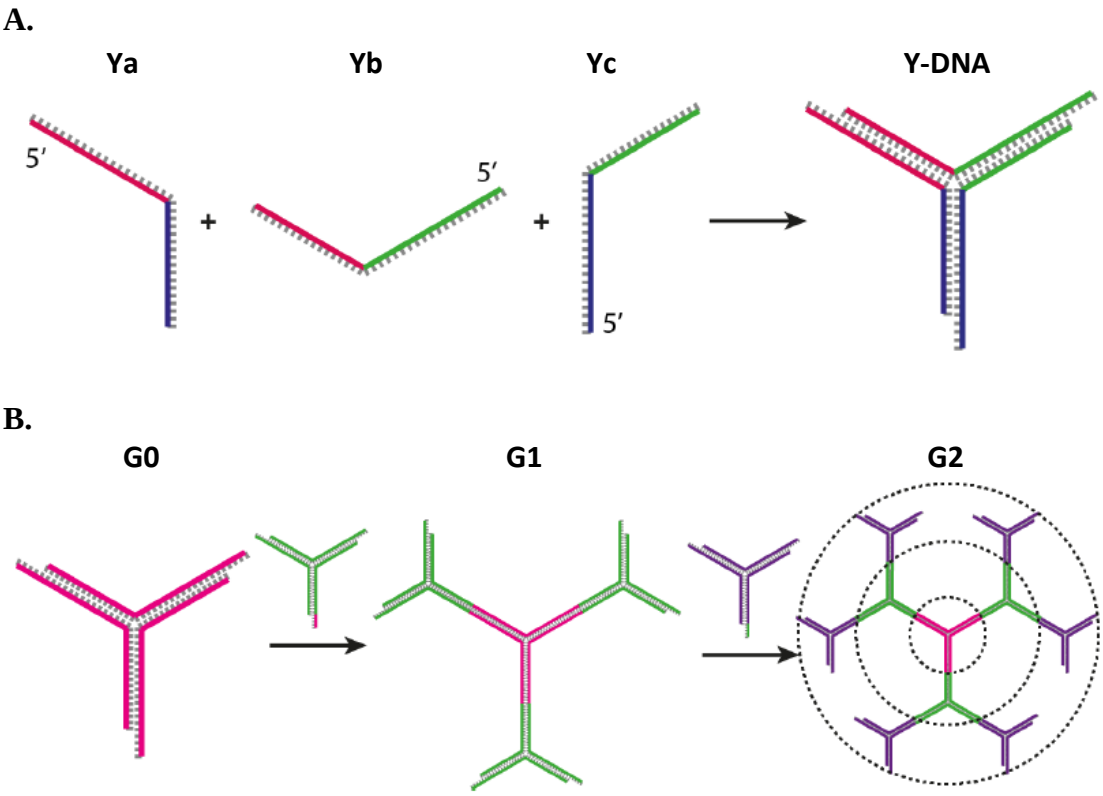

Figure 1.3 Schematic of Y-DNA and dendrimer-like DNA (DL-DNA) formation

A) Three partially complementary ssDNA (Ya, Yb, Yc) recognize and hybridize to each other to assemble Y-DNA (G0). **B)** By incorporating non-palindromic sticky ends into the core Y-DNA (G0), peripheral Y-DNA can specifically bind to the core Y-DNA in a controlled manner to assemble DL-DNA (G1) through DNA hybridization and ligation. Using this strategy, higher generations of DL-DNA can be assembled by adding more layers of peripheral Y-DNA.

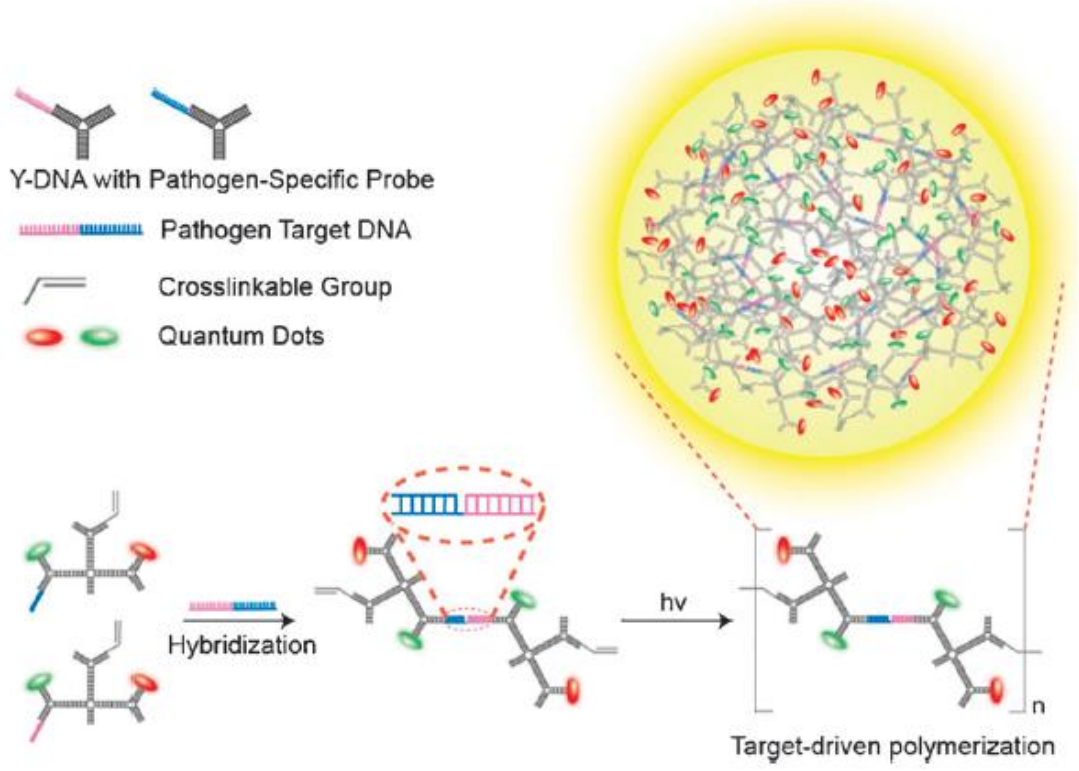

Figure 1.4 Schematic of target-driven polymerization using branched anisotropic DNA nanostructures

Branched anisotropic DNA nanostructures form crosslinked dimers only in the presence of the correctly matching (complementary) pathogen target. Upon UV illumination of the dimers, large aggregate structures are assembled through target-driven polymerization. These aggregates can be easily visualized with fluorescence microscopy imaging.

1.1.3 *Networked DNA topology*

While linear and branched DNA have been used to achieve complex and higher-ordered DNA assemblies, one challenge still remains: bulk scale formation of DNA materials in the micro- to millimeter size regime. Toward that end, the networked DNA topology was developed. Networked DNA can be 2D or 3D, and it is typically formed from DNA that cross and/or interconnect either covalently or non-covalently. Some examples of 2D networked DNA structures include DNA tiles, DNA periodic lattices, and DNA origami. Although these 2D structures are incredibly complex and rigid, they are limited in their ability to mass-produce or mass-assemble bulk 3D materials. Therefore, networked DNA hydrogels were developed. Not only can DNA hydrogels be formed in 3D by hybridization and/or ligation of numerous discrete DNA building blocks, but they can also be assembled via chemical or physical crosslinking. Interestingly, bulk 3D hydrogels have been found to exhibit unusual mechanical properties not seen in conventional hydrogels made from other polymers.[63] Moreover, the high-yield and large-scale capabilities of networked DNA, coupled with the multifunctionality and controllability of DNA, have greatly expanded the utility of DNA as a structural polymer.

2D networked DNA structures were the first step towards achieving 3D bulk DNA materials. These 2D DNA structures have served as optimal planar templates for the precise patterning of AuNPs, QDs, proteins, and other small particles in uniform arrays. For instance, combinations of multiple branched DNA motifs (DX, TX, and PX) have been used to construct DNA tiles. DNA tiles have similar shapes to Y-DNA and X-DNA, and can have more intricate formats (e.g. star-shaped) for the assembly of more complex 2D structures. A variety of 2D ordered patterns, such as periodic hexagonal,[64] cross-shaped,[65]

and star-patterned[66] lattices were developed using interlocked DX DNA tiles. (**Figure 1.5**) Furthermore, by modifying the structural flexibility at particular tiles and junctions a variety of 3D structures including tetrahedra,[67] octahedra,[68] and buckyballs[69] have been built. Additional planar structures called DNA origami have been formed from folding a long single strand of viral DNA in the presence of multiple smaller "staple" DNA strands. DNA origami has proved to be a highly versatile building block that has been used to form 3D origami boxes,[70] logs and gears.[71,72]

DNA networks are especially interesting because one can specifically engineer branched DNA monomers to form both 2D and 3D morphologies – a structural versatility that cannot be realized with conventional polymers. Many networked structures have been developed, and one of the most fascinating is DNA hydrogels. Traditional non-DNA hydrogels are bulk scale materials with great potential in a number of areas – they have been utilized in biomedical applications such as drug delivery,[73-78] cell encapsulation,[79-83] 3D cell culture,[84-87] and tissue engineering.[88-93] DNA hydrogels, in contrast, have a lesser presence in these exciting applications despite the fact that DNA is an excellent biocompatible and biodegradable biomaterial. The predominant challenge for the field of DNA technology is synthesizing DNA materials in bulk scale for advanced real-world applications.

To create DNA materials at bulk scale, synthesis efficiency and total yield must be carefully tuned and maximized. Certain networked DNA materials such as gels, spheres, and fibers, are more easily synthesized at bulk scale – very similar to synthetic polymers. With proper design considerations, networked DNA can be synthesized into these formats with high efficiency and yield. Further still, networked DNA can be constructed from either

pure DNA or from DNA combined with additional polymer materials. In this way, the unique features of both DNA and polymers can be incorporated into the final hybrid material. In general, there are three main approaches for assembling bulk scale DNA networks: enzyme ligation, chemical crosslinking, and physical interactions.

Using enzyme ligation, our group invented a bulk scale DNA hydrogel made of branched X-DNA monomers.[94] (**Figure 1.6**) This DNA hydrogel was the first example of a DNA gel formed entirely by enzymatic catalysis, and it was assembled through hybridization and ligation between palindromic sticky ends on the X-DNA. More importantly, its gelation process introduced unique capabilities that conventional hydrogels do not have. Because the gelation was catalyzed by an enzyme, T4 ligase, the DNA hydrogel could be synthesized under physiological conditions (aqueous environment, neutral pH, room temperature, etc.). This feature provided a critical advantage in that it enabled *in situ* encapsulation of a variety of materials – small molecule drugs, therapeutic proteins, live cells, etc. – and it eliminated the harsh drug-loading steps and denaturing conditions common in other gels. To that end, we demonstrated that the DNA hydrogel could successfully encapsulate and culture both Chinese hamster ovarian cells (adherent cells) and Hela S3 cells (floating cells) without any loading step. Moreover, by tuning the concentrations and types of X-DNA used in the initial reaction mixture, one can precisely tune the physical properties of the hydrogel such as rigidity and pore size. These hydrogels were non-toxic and biodegradable as well. Altogether, this combination of features provided a novel route for controlled encapsulation, storage, and delivery of materials through a networked DNA format.

Similarly, Liu and coworkers used the molecular recognition capability between DNA structures to make DNA hydrogels that responded to pH stimuli.[95] Instead of using palindromic sticky ends, Y-DNA were designed with i-motifs, or intermolecular lockable DNA sequences, on the branch ends. These i-motifs had stretches of two or more protonated and unprotonated cytosines, and in the presence of specific pH changes a phase switchable capability was exhibited by the i-motifs. More specifically, the i-motif is a cytosine rich sequence that is unprotonated at pH > 8, in which case they cause the Y-DNA to repel each other. On the other hand, when the pH value becomes slightly acidic the i-motifs become partially pronated and cause hydrogen bonds to form between protonated and unprotonated cytosines.[96] The result of this change was the formation of a DNA hydrogel within minutes due to slight pH changes. Rapid transformation of DNA binding structures within a DNA hydrogel provides another advantage in that it can quickly release cargos trapped within the hydrogel, such as AuNPs. In more recent work, Liu and coworkers developed another type of DNA hydrogel with unique thermal and enzymatic responsiveness properties.[97]

Besides using DNA hydrogels for cell culture and drug release, our group harnessed DNA's genetic function to create the first ever cell-free protein producing DNA hydrogel (P-gel).[98] The P-gel was composed of X-DNA and linearized plasmids that were covalently ligated together by T4 DNA ligase. The X-DNA served as a scaffold, while the plasmid functioned as the gene for encoding protein production. After incubating the P-gel with the necessary components for creating proteins (transcription/translation-related enzymes, amino acids, ATPs), the P-gel produced up to 300-fold more proteins than conventional solution-based systems (SPS). (**Figure 1.7**) The P-gel achieved enhanced protein

production efficiency because the hydrogel matrix could protect and improve gene stability, increase local gene concentration, and increase enzyme turnover rate as a result of the closer proximity of genes. Since the P-gel can produce proteins entirely without cells, it can also generate proteins that are extremely difficult to produce in conventional cell-based protein expression systems, such as toxic and membrane proteins. The P-gel is an excellent example of how exploiting both the genetic and generic functions of DNA, can be used to create novel functionalities which cannot be achieved by any other material. This work was further advanced by the development of a scaled-up P-gel particle microfluidic system which could create a large quantity of DNA hydrogel microspheres.[99] Since these P-gel microspheres had a greater surface area than the original P-gel, elevated levels of high-throughput cell-free protein production could be achieved. Indeed, the P-gel not only demonstrated that complex transcription and translation processes can be replicated outside the cell, but it also showed that bulk scale DNA hydrogels can be used for the mass production of biologically relevant and medically important materials.

In addition to using enzymes to interconnect DNA together, chemical crosslinking is a useful approach for the assembly of pure DNA and hybrid DNA-polymer networks. Our group, for instance, achieved nanoscale 3D DNA spheres by photo-crosslinking branched X-DNA.[100] More specifically, a photo-crosslinkable moieties were attached to X-DNA monomers. Upon exposure to UV illumination, the X-DNA monomers were crosslinked into monodisperse DNA nanospheres that were internally networked. The surface charge and size of the nanospheres were specifically controlled by varying the initial X-DNA monomer concentration.

Chemical crosslinking has also been used to assemble hybrid hydrogels from both DNA and polymers. For instance, DNA and polyacrylamide (PAAm) were combined to generate hydrogels for controlled drug release.[101,102] In these works, two different acrydite-modified ssDNA was copolymerized with acrylamide monomers, thus enabling their incorporation into the PAAm chains. These ssDNA-conjugated PAAm chains were then mixed with additional ssDNA crosslinkers which hybridized to and crosslinked the ssDNA-PAAm conjugates to assemble a hybrid DNA-PAAm hydrogel. To achieve switchable sol-gel phase transitions in the DNA-PAAm hydrogel, many ssDNA with complementary sequences to the crosslinker ssDNA were introduced. The additional ssDNA removed the crosslinker ssDNA from the gel matrix, thus releasing the networked structure and changing its state. The resulting switchable material has shown strong applications in controlled drug release. Another type of polyacrylamide-DNA hybrid gel was used for colorimetric detection of mercury.[103] In this case DNA was designed to contain many thymine bases, two of which could bind to Hg2+. The resulting DNA gel showed yellow fluorescence in the absence of Hg2+, and green fluorescence when exposed to small amounts of Hg2+. These hybrid DNA hydrogels demonstrate the tremendous design specificity and utility of using DNA materials for real-world detection applications.

The third approach for constructing DNA networks is through physical interactions, such as entanglement of long ssDNA or enzymatic amplification and weaving of DNA fibers. For example, stable and intertwined DNA fibers were formed by random entanglement of long ssDNA.[104] First, aqueous DNA solution was injected into a coagulation bath with room-temperature hydrophilic ionic liquid (RTIL), which served as a condensing agent to enhance coagulation and DNA fiber formation. Using a wet spinning

process with the RTIL, compact toroids were formed from DNA bundles, and then these toroids were further entangled into a stable DNA fiber. Interestingly, these DNA fibers resisted endonuclease digestion due to their highly entangled networks – a feature that can be extremely useful for constructing stable, biocompatible composites.

DNA entanglement generates remarkably unique DNA materials when combined with enzymatic DNA amplification. Our group recently invented a DNA hydrogel with highly unusual mechanical properties that are unprecedented in conventional gels.[105] We used a polymerase enzyme (ϕ29) to elongate DNA chains and weave them noncovalently into a physical hydrogel. In particular, the ϕ29 enzyme is a bacteria phage polymerase capable of DNA chain elongation and displacement.[106] Through careful design of the precursor ssDNA strands, a ϕ29 can be used to elongate and interweave numerous DNA fibers into a 3D network. Amazingly, we discovered that the resulting 3D DNA material had liquid-like properties when taken out of water and solid-like properties when in water. This work will be further discussed in **Chapter 3** of this Dissertation.

Production of long DNA or RNA strands can be used for self-assembly of other materials as well. Qi et al. demonstrated that RCA can be used to produce a ‘‘DNA glue’’ that directs the programmable assembly of Poly(ethylene glycol) (PEG) hydrogel cubes into complex, 3D micro- and macroscale structures.[107] First, DNA primer-modified PEG hydrogels were prepared and RCA was performed to generate giant ssDNA strands on the surface of the hydrogels. These ssDNA contained numerous repeating complementary sequences so that the hydrogel cubes could bind together through complementary hybridization. Upon mixing the hydrogel cubes in solution with agitation, a variety of different multi-hydrogel objects (dimers, chains, T-junctions, and squares) with sizes

ranging from 30 μm – 1 mm were achieved. It is important to note that enzymatic elongation is not only limited to DNA. RCA has also been used to create novel siRNA microsponge structures for siRNA delivery and treatment.[108] Hammond and colleagues designed a unique RCA reaction using a T7 promoter as the primer and T7 RNA polymerase. This system produced long RNA products that self-assembled into microscale RNA spheres with sponge-like morphologies. Overall, these uniquely designed DNA and RNA materials provide capabilities that linear and branched DNA could not achieve in their isolated and discrete forms.

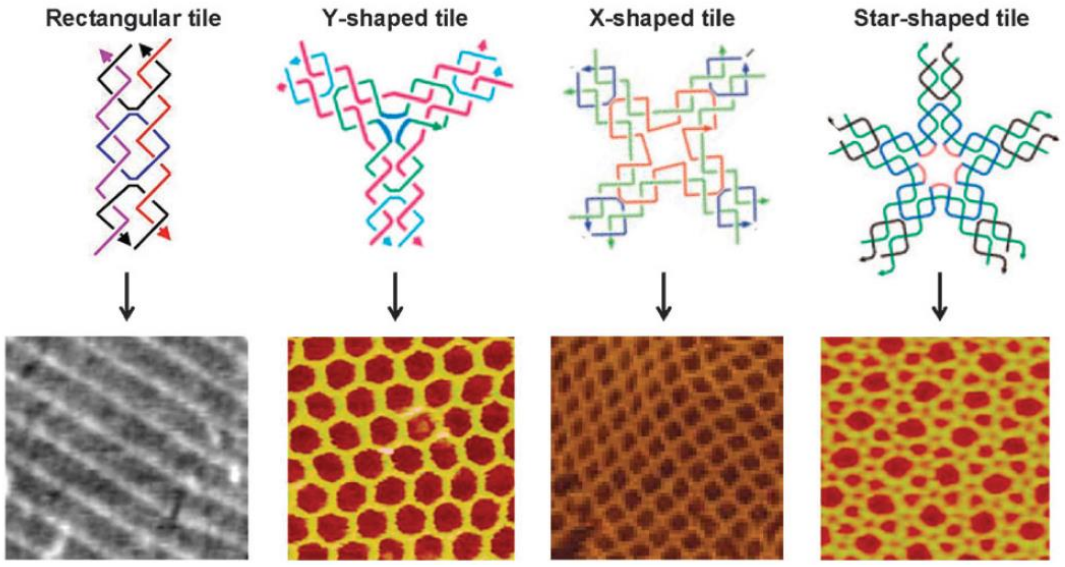

Figure 1.5 Diagram of DX DNA tiles and their 2D lattice structures

Different DX DNA tiles can be made into rectangular, Y-, X-, and star-shapes. Uniform and periodic 2D lattice structures can be self-assembled from numerous monomer DX DNA tiles.

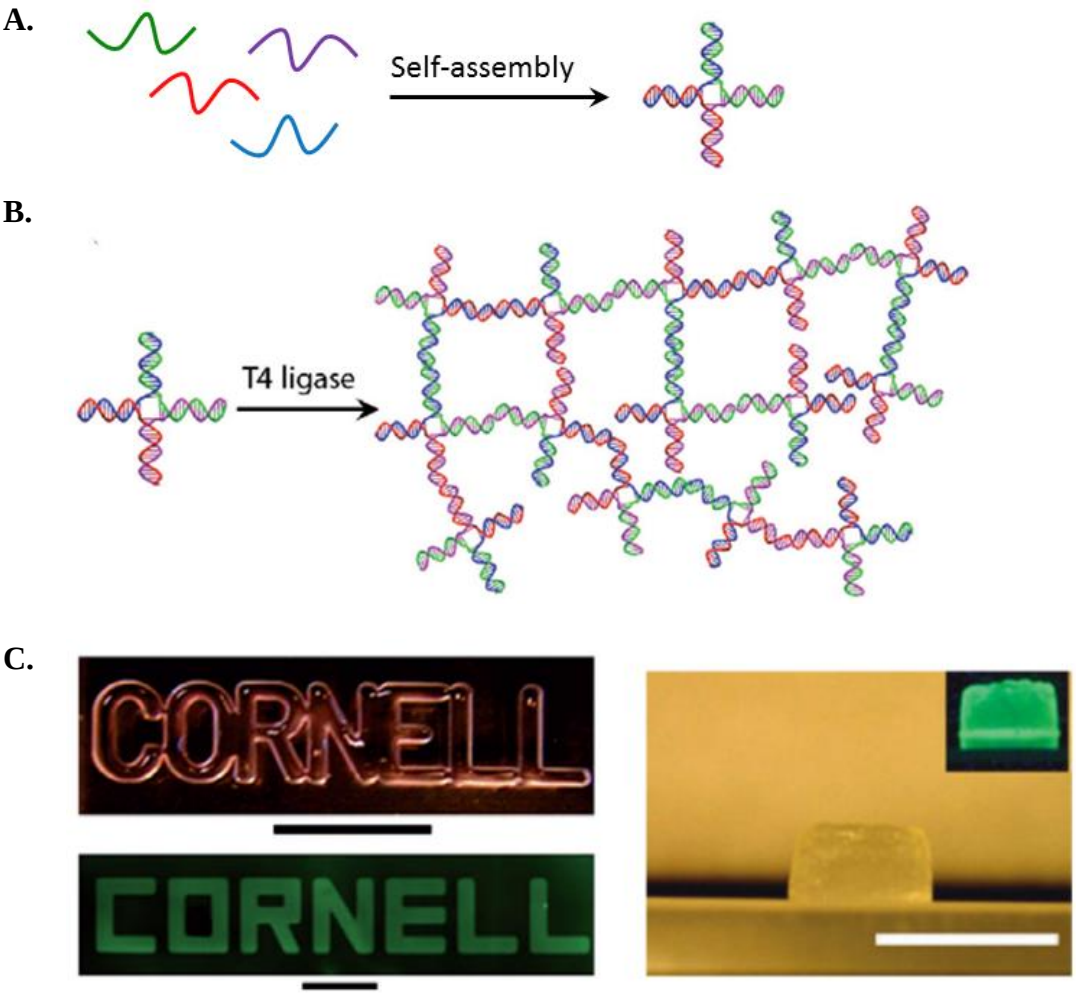

Figure 1.6 Self-assembly of DNA hydrogel from X-shaped DNA (X-DNA)

A) First, the X-DNA nanostructure is self-assembled by hybridization of linear DNA strands that are partially complementary to each other. **B)** Numerous X-DNA carrying sticky ends are then connected together using T4 DNA ligase. **C)** Images of the resulting DNA hydrogel demonstrate that it has a robust structure which maintains its shape and furthermore it can achieve centimeter-scale bulk dimensions. Scale bars are 1 cm.

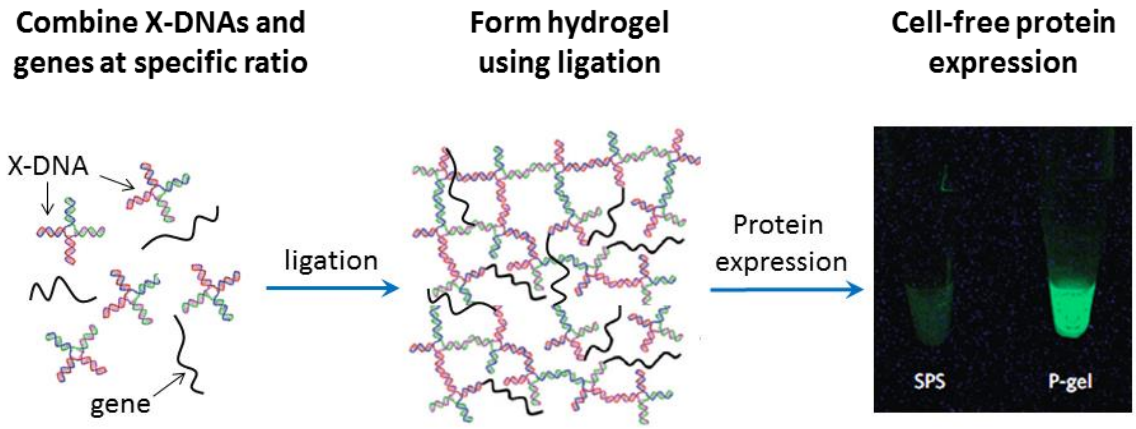

Figure 1.7 Illustration of P-gel formation from X-DNA and plasmid genes

Individual X-DNA and plasmid genes are combined at a specific ratio and ligated together to form the bulk DNA hydrogel. Next, all the necessary machinery for protein production are added and the DNA hydrogel was incubated at 24˚C for several hours. As seen in the image on the right, P-gel outperformed the standard SPS protein production reaction in producing a model protein, GFP.

1.2 Microfluidic strategies for DNA processing and analysis

Microfluidics, a technology based on the manipulation and engineering of fluids at sub-millimeter scales, has huge potential in a broad array of fields including biology, chemistry, physics, and engineering. The topic of microfluidics has gained tremendous attention in academia and industry – nearly 75,000 articles have been published on microfluidics,[109] and over 6,600 microfluidics-related patents have been filed in the U.S. alone.[110] Microfluidics has several critical advantages – precise fluid control, rapid processing and analysis, low volume consumption, etc. – that make it an attractive system for biomedical and biological applications. From these advantages, a variety of microfluidic platforms have emerged with a range of features (micropumps,[111-113] microvalves,[114] micromixers,[115,116] microsieves,[117,118] etc.) and a range of exciting applications (POC diagnostics, gene sequencing, cell culture, cell sorting, drug screening, protein crystallization, chemical synthesis, etc.). Indeed, microfluidics is a toolbox of unique devices and functionalities that can be used to not only develop new innovative methods and products, but it can also be used to improve the efficiency and accuracy of standard laboratory techniques.

Microfluidics has shown tremendous potential for improving diagnostics and biological research. Numerous microfluidic platforms have been created for the detection and study of small molecules, nucleic acids, proteins, and even dangerous substances and toxins. These systems have employed a range of nanoscale agents, such as nanoparticles, quantum dots, carbon nanotubes, and synthetic DNA nanostructures. While many strategies have been developed, it is also important to select a universal target that can be consistently identified across different pathogen species and different generations or

strains. To achieve this goal, nucleic acids such as DNA or RNA are prime candidates. The main unifying factor between viruses and bacteria is that they all contain unique, species-specific genetic material made of either DNA or RNA. Capitalizing upon this fact, in addition to leveraging the precision of micro- and nano-scale microfluidics, leads to the emergence of highly advanced, multifunctional DNA/RNA detection systems.

DNA nanotechnology is inherently small scale, and it affords unique advantages which cannot be achieved by microfluidics alone. More specifically, DNA structure and behavior is precisely controllable, there are a wide range of manipulation techniques available, and DNA is capable of storing information for programmable operations such as self-assembly and temporary binding interactions. DNA is also increasingly being used to organize and pattern both organic and inorganic nanomaterials, making it ideal for building hybrid materials and integrated systems. Furthermore, DNA is the "molecule of life" and it is intrinsically linked to many biological functions. Thus, it is the optimal interface through which one can address and control biological material, such as other DNA and RNA, proteins, and enzymes. That said, DNA nanotechnology has certain limitations, such as its expensive cost and the fact that it is often restricted to laboratory settings, where reactions are typically performed in controlled environments and closed solution tubes. Hence, scaling up reactions and reducing processing and handling for real-world applications can be prohibitively difficult.

The structural, biological, and self-assembly advantages of DNA can be combined with the precision and versatility of microfluidics to improve and re-define modern sensing and diagnostics. A summary of some of the advantages of DNA and microfluidics is shown in **Table 1.1**. With the increased growth of DNA nanotechnology in recent decades, a

myriad of assembly and manipulation techniques have emerged to make DNA a highly accessible engineering material. Microfluidics, in turn, is a highly innovative field that encompasses a variety of device materials, components, designs, and fluid manipulation techniques. Microfluidics helps overcome DNA's limitations by being portable, compact, inexpensive, and highly efficient at processing fluids and performing reactions quickly. Together, integrating DNA nanotechnology with microfluidics can lead to the creation of powerful diagnostics tools and methodologies that have far-reaching implications for both clinical and non-clinical settings.

Advantages of DNA	Advantages of Microfluidics
▪ Precise sequence design ▪ Programmable binding ▪ Many DNA processing enzymes ▪ Ease of commercial synthesis ▪ Chemical stability ▪ Diverse modification options ▪ Biological importance and role ▪ Attain 1D, 2D, and 3D structures ▪ Isotropic & anisotropic capabilities	▪ Precise fluid manipulation ▪ Low volume consumption ▪ Fast reaction kinetics ▪ Diverse design possibilities ▪ Portable and compact ▪ Low cost ▪ Easily merge with other technologies ▪ Rapid processing and analysis ▪ Ease of use ▪ Autonomous capabilities

Table 1.1 Summary of the advantages of DNA and microfluidics

1.2.1 *Integration of microfluidics and DNA for point-of-care diagnostics*

Pathogen detection platforms are an invaluable tool in many different areas such as drug discovery, clinical diagnostics, medical research, disease outbreaks, and food safety. In fact, the detection and diagnosis of infectious disease is critically important today. The World Health Organization recently reported that, after cardiovascular disease, infectious diseases are the second leading cause of mortality throughout the world.[119] This problem is particularly severe in developing countries with limited access to centralized labs and clinics. Moreover, despite the strong progress in improving health conditions in developed countries, there are still pathogen detection challenges in food industry, pathogen outbreaks, and sexually transmitted diseases.[120]

Conventional methods for pathogen detection often involve cell or bacteria cultures, PCR tests, and immunoassays. While these methods are the gold standard in clinical labs and hospitals, they have critical drawbacks such as being labor intensive, needing special training, and requiring between a few hours to several days to complete. Microfluidics has the potential to surmount these obstacles and improve upon current pathogen detection methods. Microfluidic devices can be made into infinitely different designs, and furthermore they are portable, easy to use, and have the distinct advantage of reducing reaction times due to faster heat and mass transfer within the fluid-filled microchambers. Additionally, microfluidic platforms use lower sample volume and exhibit incredibly precise control of minute fluid volumes without requiring a laboratory setting, which makes them perfect for achieving POC diagnostics.

POC diagnostics, or testing that is performed at or near the site of the patient, is an extremely powerful method that can expand the access and efficiency of diagnostics far

beyond hospitals and centralized laboratories. POC detection of nucleic acids is of particular interest given the extreme importance of DNA and RNA as diagnostic targets for many health care applications. Important nucleic acid detection applications include genotyping and genetic prognostics, expression profiling, monitoring new disease outbreaks (H7N9,[121,122]) and identification of infectious disease and cancer.[123-128] What makes nucleic acids incredibly exciting as detection biomarkers is that they have several practical advantages which immunological biomarkers (e.g. antibody-based) do not have. For instance, nucleic acids facilitate straightforward design of specific recognition elements (primers and probes) and they have predictable and controllable molecular behaviors (binding affinity, structure, melting temperature etc.). In addition, nucleic acids have intrinsic compatibility with enzymatic amplification methods such as PCR, which enables extremely sensitive detection.

From an engineering perspective, POC detection represents an exciting and complex challenge that could benefit a great deal from nanotechnology-enabled functionalities and capabilities.[129-132] For instance, metal nanoparticles (e.g. AuNPs) have been widely used for various biosensing applications,[133,134] particularly for their unique nanoscale characteristics such as their high degree of polyvalency and plasmonic properties.[135,136] Furthermore, other engineered nanomaterials such as nanowires, carbon nanotubes, and quantum dots have been used for imaging[137-139] and electrochemical sensing applications.[140,141] Although these materials are useful for detection, they cannot interface with nucleic acid targets as efficiently or as controllably as synthetic nucleic acids. To address this challenge, a diverse array of synthetic DNA nanostructures have been designed to form nanoscale assemblies that selectively recognize and interact with

target nucleic acids for detection purposes.[142-144] DNA has also been used to create hybridization-based circuits and reaction networks for enzyme-free target amplification.[145] With these advantages as well as many others not mentioned here, DNA nanotechnology will continue to play a critical role in the growth and evolution of POC diagnostics.

To understand and pursue next-generation POC diagnostics, one must understand the fundamental steps of POC detection and, furthermore, investigate how DNA materials can be used to enhance each step of the process. Three operational steps are typically required for POC detection: 1) sample preparation, 2) target amplification, and 3) signal read-out. While the first step of detection (sample preparation) is very important, this is a complex area that is beyond the scope of this section. Of the three steps in the POC diagnosis process, I focused on target amplification and signal read-out in my Dissertation research work. These two steps require careful engineering and a sharp clinical perspective, especially with regards to nucleic acid detection. In addition, these steps can hugely benefit from the advances of DNA nanotechnology and microfluidics. The main challenge in merging DNA with microfluidics is seamlessly integrating these two technologies, and their respective advantages, into one platform without sacrificing critical features such as sensitivity, efficiency, portability, and cost. This Dissertation will focus on DNA materials for diagnostics applications, and it will be underlined by an investigation into how the advantages of DNA can be maximized to enhance the two core POC detection steps of target amplification and signal read-out. Ultimately, this work will lay new groundwork for engineering and developing innovative, next-generation diagnostics.

1.2.2 *DNA amplification strategies*

Once the initial sample preparation step is finished, POC nucleic acid detection requires target amplification to achieve clinically relevant sensitivity from small amounts of target molecules.[146,147] Although the target amplification step can introduce substantial engineering and operational complexity, it is important for at least two fundamental reasons: 1) target amplification relaxes the constraints on the downstream signal read-out step, and 2) increasing target concentrations promotes faster kinetics for hybridization and mass transport, which reduces the time required for read-out and diagnosis. With regards to integrating DNA nanotechnology with POC diagnostics, two main approaches are used for target amplification: enzyme-based, and enzyme-free.

Enzyme-based target amplification involves the use of enzymes with predictable and well-understood behaviors, through which a specific target can be multiplied many times over (e.g. exponentially). One of the most popular enzymatic amplification methods, PCR, is widely used in hospitals and clinical laboratories. Because of its broad use, PCR has also been adapted for POC detection.[148,149] In particular, a considerable body of work has been applied toward the development of microfluidic-based PCR systems, which improve upon standard PCR by providing reduced power consumption, smaller sample volumes, and faster kinetics and heat transfer properties.[150-152] Despite these advantages, the thermal cycling steps needed to perform PCR require expensive and complex heating, temperature sensing, and control systems, all of which are undesirable and even detrimental for POC applications. Therefore, a substantial amount of research has been devoted to developing strategies which avoid thermal cycling, such as isothermal amplification and enzyme-free amplification methods.

Unlike PCR, isothermal amplification operates at one constant temperature. Because of this capability, isothermal amplification has fewer equipment and control requirements, making it an optimal process for incorporation into microfluidic POC technology. A variety of isothermal amplification strategies have been developed – some of the most popular include nucleic acid sequence-based amplification (NASBA), loop mediated isothermal amplification (LAMP), and rolling-circle amplification (RCA). These three methods are illustrated in **Figure 1.8**.

NASBA is a well-established isothermal amplification strategy that has been used in a variety of applications since its first publication in 1991.[153] The distinctive feature of NASBA is its excellent ability to amplify single-stranded RNA (ssRNA) targets instead of DNA. Furthermore, while most target amplification methods generate dsDNA, NASBA generates ssRNA products that can hybridize to complementary DNA probes for downstream capture or labeling. In general the NASBA process uses a mixture of reverse transcriptase, RNase H, and T7 RNA polymerase to amplify ssRNA sequences. More specifically, NASBA performs amplification by a cyclical process: 1) forming DNA–RNA hybrids with reverse transcriptase, 2) selectively degrading only the RNA strand of the hybrid using RNase H, 3) creating dsDNA with reverse transcriptase, and 4) generating numerous copies of ssRNA using T7 RNA polymerase. As a result, NASBA requires three different enzymes, which could increase procedural complexity. Zhao et al. used NASBA to demonstrate a low cost and potentially disposable device that achieved quantitative detection.[154] This method achieved multiplexed target detection using less than one hundred cells in a liter of solution. NASBA has also been used for the simultaneous amplification of mRNA and miRNA, with applications for cancer screening.[155]

LAMP is a technique that is becoming increasingly popular for POC applications. The LAMP method involves a single isothermal enzyme, and it typically lasts less than an hour. In general, the LAMP procedure includes four ssDNA primers which are used in a cyclical amplification process based on spontaneous formation of stem-loop DNA structures.[156] (**Figure 1.8**) More specifically, this system uses the strand displacement property and DNA polymerization activity of ϕ29 polymerase to continuously amplify DNA. The resulting products are heterogeneously amplified, and they exhibit multiple bands in an electrophoresis gel. A broad range of pathogens have been detected with the LAMP assay, including malaria,[157,158] HIV,[159] and multiple bacteria.[160] A number of LAMP assays for bacterial,[161-164] viral,[165-167] fungal,[168-170] and parasite[171-173] detection have exhibited performance equal to or better than PCR, immunoassay or culture-based diagnostic methods. Additionally, LAMP was successfully used for sensitive and specific detection of Cryptosporidium species in PCR-negative samples.[174] Real-time monitoring of the LAMP reaction can be achieved by measuring solution turbidity changes resulting from complex formation of pyrophosphate and divalent metallic ions, and by fluorescence through a calcein indicator.[175] A key challenge for the LAMP method is a tendency for false positive results arising from accidental amplification of non-target DNA sequences. To overcome this problem, researchers have utilized sequence-specific fluorescence probes such as molecular beacons to add an additional layer of specificity.[176] Another concern is that LAMP is highly dependent on the careful design of multiple complex primers[177] which can lead to undesirable complications in assays.[178]

Similar to LAMP, RCA utilizes the high processivity capability and strand-displacement activity of ϕ29 DNA polymerase. Unlike LAMP, the RCA process uses a

circular ssDNA template to continuously generate very long ssDNA products.[179,180] (**Figure 1.8**) Interestingly, the ssDNA product is composed of tandem-repeats of the initial circular template – thus, careful sequence design can lead to cyclical and exponential amplification of a small amount of target. Because RCA requires a circular template to perform amplification, this method is uniquely well-equipped for the amplification of circular DNA molecules found in nature such as plasmids and certain viral genomes. Moreover, the speed and sensitivity of RCA can be greatly enhanced through the addition of short primers that bind to repeat sequences in the amplified RCA product. These secondary primers trigger additional rounds of amplification reactions, which greatly increases the amplification rate and can yield a billion-fold or more copies of the template in under an hour. Amazingly, this process has been shown to detect as few as ten target molecules.[181] To further increase the sensitivity of RCA, researchers have designed repeated hairpin structures within the RCA products to provide specific DNA segments where DNA dyes like SYBR Green can preferentially bind.[182] RCA can also be used to detect miRNA by generating ssDNA products containing DNAzymes.[183] These DNAzymes induced a color signal which allowed for highly sensitive detection of zeptomole amounts of target miRNA.

Although enzymes, such as polymerases, are highly effective at nucleic acid target amplification, they present certain challenges for POC detection. Specifically, many enzymes are unstable in POC settings because they require special conditions such as refrigeration for transport, storage, and handling. In response to this, enzymes have been lyophilized or stabilized in a gel format to improve stability.[184] Enzymes can also be sensitive to sample contamination which can lead to unreliable detection results (false

positives or false negatives). Alternatively, enzyme-free amplification strategies offer a unique DNA-based method that avoids the typical detection challenges associated with enzymes.

One interesting enzyme-free amplification strategy uses DNAzymes and/or RNAzymes (ribozymes), which are non-protein-based DNA and RNA catalysts with enzymatic properties. For example, ribozymes with ligase activity[185,186] as well as RNA-cleaving DNAzymes[187,188] have been successfully implemented for amplification. Additionally, DNAzymes and/or ribozymes have been used in a combined approach with conventional enzymes. Tang and colleagues, for instance, recently developed a versatile RNA detection method based on cleavage by DNAzyme and signal amplification.[189] This method used two types of DNAzymes to detect RNA, and it was capable of achieving both colorimetric and real-time fluorescence detection read-outs.

To achieve completely enzyme-free target amplification (without DNAzymes or ribozymes, which can be sensitive to reaction conditions), DNA hybridization can be applied as an amplification mechanism using the concept of strand displacement.[190-193] **Figure 1.9 A** illustrates the strand displacement process, in which an initiator strand (Sc) binds to a partially complementary strand (P), creating a toehold which allows a third perfectly complementary strand (S) to bind , displace and release the partial complementary strand (P) back into solution. The rate of strand displacement can be controlled several ways, including the use of a catalyst component, as shown in **Figure 1.9 B**.[194,195] A catalyst enables amplified control over the production of output DNA, and it can also be applied to autocatalytic systems (**Figure 1.9 C**).[196] Furthermore, amplification using strand displacement has been incorporated into DNA logic gate circuits,[197,198] and the controlled

use of toehold regions has been shown to enhance the specificity of nucleic acid hybridization.[199] These unique capabilities could be very useful in the future development of programmable nucleic acid networks for molecular detection.

As a variation on these main non-enzymatic approaches, hairpin structural motifs have been engineered for strand displacement applications. For example, hybridization chain reaction (HCR) uses hairpins to produce long dsDNA as an output.[200] This system was implemented *in situ* for visualization of mRNA expression in zebra fish embryos.[201] Yin et al. further used the hairpin motif to design diverse types of reactions, including a scheme for exponential target amplification that is triggered by an initiator strand.[202] Overall, hairpin-based motifs provide a great amount of modularity, which enables the development of reaction systems tailored for a particular set of detection requirements.

Although exciting work is being done on enzyme-free amplification, current enzyme-free methods are still in their early stages of development. Some enzyme-free systems are prohibitively complex for POC applications, and moreover their performance may be inferior relative to more established enzyme-based approaches. As a step toward improved detection, enzyme-free hybridization methods have been combined with isothermal enzymatic strategies in hybrid systems that exploit the advantages of both.[203] Allen et al. used a catalytic hairpin assembly (CHA)-based device combined with LAMP to create an inexpensive and portable paper microfluidic device.[204] Similarly, by combining LAMP with CHA-based non-enzymatic circuit Li et al. increased the specificity of the LAMP reaction. [205] By introducing an "AND" gate in this system they detected as few as ten molecules per microliter.

Taken together, these developments in both isothermal and enzyme-free amplification form a strong foundation for the development of sensitive and robust POC detection systems. To build upon this work, it is important to focus on the signal read-out stage as well. Signal read-out can be achieved by several different means, but the underlying requirement is the same – the select read-out method must be carefully engineered to merge with and improve upon the target detection strategy in order to achieve a truly optimized POC detection platform.

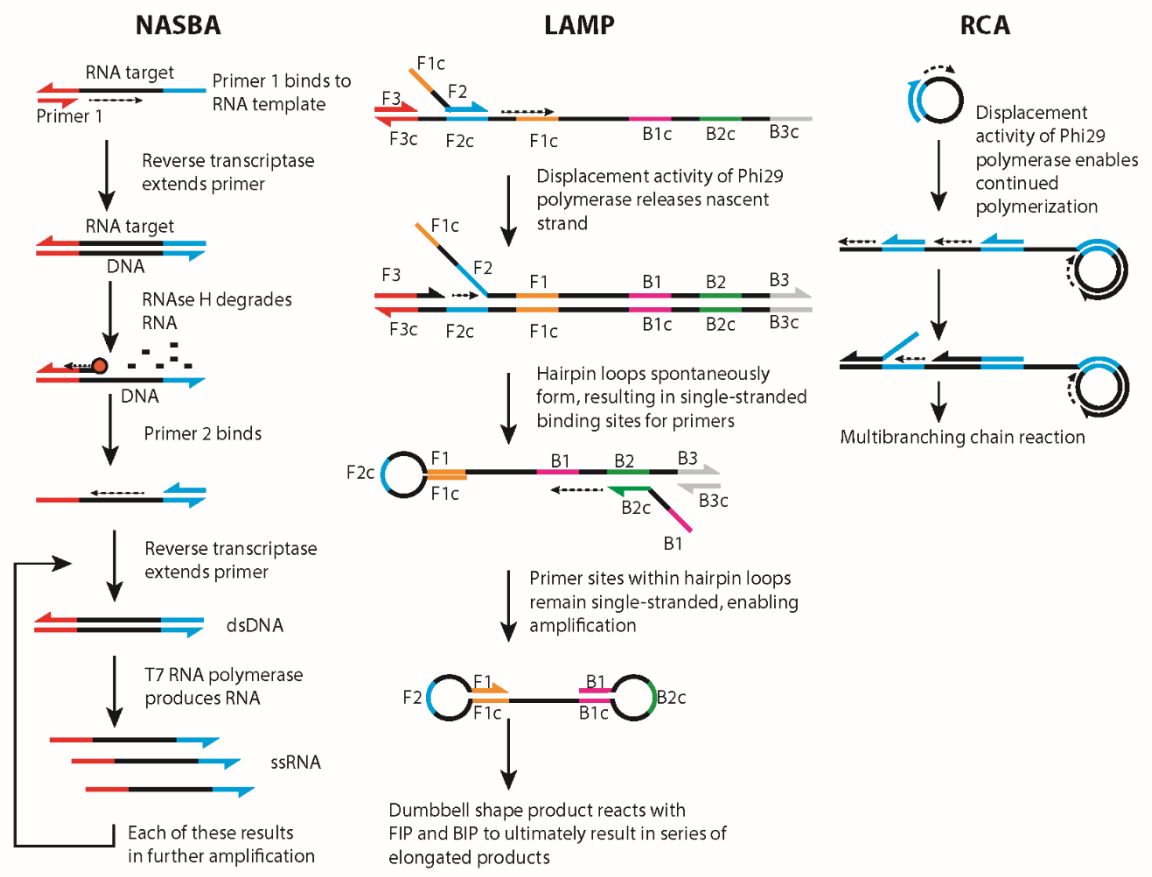

Figure 1.8 Schematic of isothermal nucleic acid target amplification methods

NASBA, LAMP, and RCA are some of the most popular isothermal nucleic acid amplification methods. NASBA is well-established for specific amplification of RNA targets. LAMP involves a stem-loop format and requires only a single enzyme, whereas most isothermal amplification methods require at least two. RCA uses a unique circular template for continuous amplification, and it is optimal for detection of circular and single-stranded DNA targets.

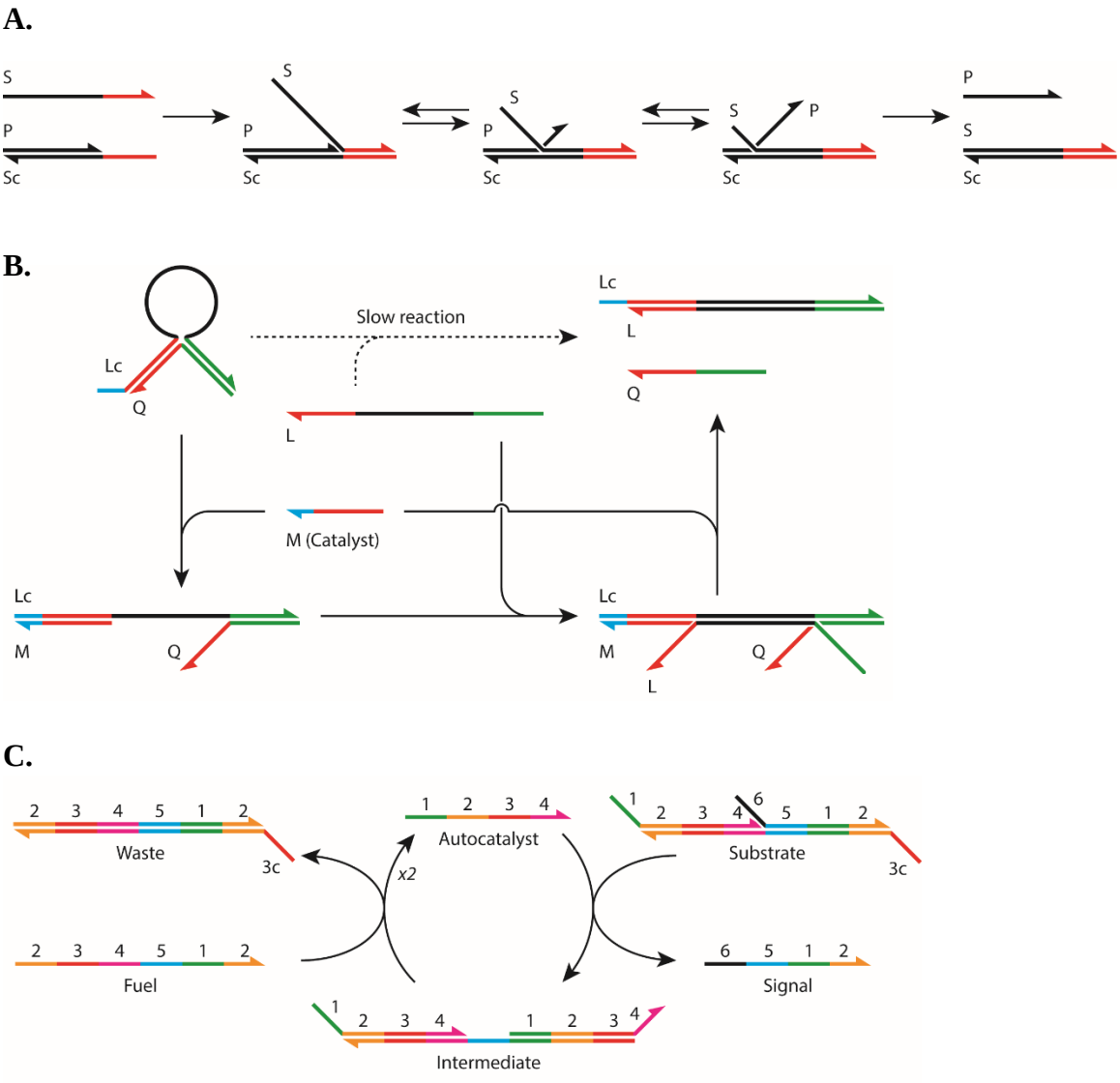

Figure 1.9 Enzyme-free amplification strategies using DNA hybridization

A) Basic schematic for strand displacement. Strand S replaces strand P as it hybridizes with strand Sc. Consequently, P is released into solution as a single strand. **B)** Catalyst-mediated strand displacement. Catalyst M kinetically enhances the reaction from fuel complex to output and waste. The catalyst (M) helps open the initial fuel complex (Lc-Q) into an intermediate formation (Lc-Q-M), which can more easily react with the fuel strand's complement (L). This reaction leads to the final stable state (L-Lc; waste DNA), and as a result the output single-stranded DNA (Q) and catalyst (M) are popped out using this reaction as a driving force. **C)** Autocatalytic reaction based on strand displacements. The substrate contains signal DNA and inactive (hybridized) catalyst. The active catalyst releases the signal from the substrate, and then the fuel strand releases both catalysts. As a result, one reaction cycle doubles the number of catalyst and produces one signal molecule.

1.2.3 *DNA signal read-out strategies*

Following target amplification, it is important to have clear, unambiguous read-out of the detection results. To achieve this goal in a range of POC environments, the signal read-out must be redesigned to overcome the mobility and equipment challenges facing laboratory-bound detection methods such as gel electrophoresis and cell or bacteria cultures. Innovations in nanotechnology introduce many interesting opportunities for improved POC signal read-out. For example, nanomaterials can act as labels for fluorescence or electrochemical detection, nanofunctionalized sensing surfaces can enable higher binding capacities, and nanoscale phenomena such as fluorescence resonance energy transfer and plasmon resonance can dramatically increase detection sensitivity. For nucleic acid detection, some of the most popular read-out modalities include naked eye and optical sensor methods.

Naked eye read-out is incredibly important in POC detection applications because it can be easily operated by untrained personnel. Additionally, it is highly accessible to almost any low resource environment because it is not constrained by a need for expensive, complicated equipment. That said, the simplicity of naked eye read-out causes some limitations, such as reduced quantitative capability and lower sensitivity. One strategy for making naked eye read-out more powerful is combining this method with DNA nanotechnology. Technologies such as DNA-functionalized nanoparticles and DNA amplification methods have been integrated with naked eye read-out to achieve a level of specificity and sensitivity that matches the performance of optical and electrochemical methods.

The lateral flow assay (LFA) is among the most common POC diagnostic formats today, and it typically employs naked eye read-out methods.[206,207] LFA has key advantages of low cost, rapid results, and simple format. It has also been broadly used for many applications including pregnancy testing, infectious disease detection, and clinical diagnosis of heart attacks and strokes. In general, LFA devices are chromatographic platforms in which the sample is driven through the platform by capillary force and the results are read visually by the naked eye. Typically, carriers or labels (functionalized AuNPs, latex microparticles, or liposomes) are used to generate the visual result, which is usually a colored band that can be seen without any visual apparatus. LFA devices are traditionally used for immunological detection, but more recent studies have adapted LFA devices to exploit the specificity of DNA hybridization to capture and detect nucleic acid targets in a manner similar to the original, antibody-based LFA assays.

A number of recent LFA-based approaches have achieved convenient portable read-outs of nucleic acid targets.[208-210] For example, Baeumner et al. demonstrated RNA detection in a test strip format with nanomolar detection levels,[211] and Carter and Cary achieved sub-femtomole sensitivity in an LFA format using latex microparticles.[212] To improve the performance of the nucleic acid LFA format, Lie et al. modified AuNPs with DNA hairpin nanostructures that only opened in the presence of the correct target, which achieved greater specificity than linear ssDNA alone.[213] This system was tested on human genomic DNA, and it achieved naked eye read-out at target concentrations as low as ten attomolar in thirty minutes. Rohrman et al. also designed a nucleic acid LFA device combined with a gold enhancement solution that increased the size and optical absorbance of the AuNP probes.[214] This strategy was used to quantitatively monitor HIV viral load in

patients over a clinically relevant range. Many of the LFA-based concepts and technologies have been extended and developed for paper-based microfluidics as well.[215-218]

Another naked eye read-out strategy uses nanoparticle aggregation instead of binding to a surface region on a lateral flow strip. More specifically, AuNPs are covalently modified with capture probe ssDNA that specifically hybridize to target DNA molecules. These hybridization reactions form large nanoparticle assemblies and networks, which causes a red-to-purple color change (due to the plasmonic properties of the metal nanoparticles) that is visible by the naked eye.[219] The hybridized samples can furthermore be spotted onto a solid support for easy visualization. AuNP aggregation has also be used following a target amplification step, such as NASBA,[220] LCR,[221] and other enzyme-assisted amplification methods,[222] and it can also be used to detect total RNA or specific mRNA targets as well.[223] In addition to disordered aggregates, DNA-modified AuNPs may be designed to assemble into discrete architectures with specific interparticle distances.[224,225] This enhanced design control takes advantage of the programmability of DNA, and it could lead to more sophisticated colorimetric read-out platforms with finely tuned color changes as a response to specific targets.

Although naked eye read-out has great applicability in POC detection, it is limited in its quantitative capability and in the detection of extremely small amounts of target molecules. Optical enhancement is incredibly useful for overcoming these challenges because it amplifies and strengthens the read-out signal. Examples of optical sensor read-out modalities include absorbance, scattering, and fluorescence – all of which have been employed for detection of nucleic acid targets. Traditional laboratory-based optical methods are becoming the standard in clinical analysis, but they often use optics that can

only be operated by highly trained personnel. Fortunately, advances in portable optics such as LEDs, optical micro- and nanofibers, and miniaturized sensors, have fueled the translation of optical systems into portable, low-complexity formats that are ideal for POC.[226,227] In addition, progress in micro- and nanofabrication facilitates the integration of microfluidic devices and optics in an integrated microchip format (e.g., lensless imaging) which can lead to innovative platforms for future POC diagnostics.[228]

Laboratory-based imaging techniques, such as fluorescence microscopy, are very important for characterization and analysis of nucleic acids. High resolution microscopy is able to discern single molecules of DNA,[229] and microscopes are also important for imaging spatially defined systems such as microarrays and microwells. Although microscopy equipment affords great resolution and control of imaging read-out, it can be difficult to use (and even acquire) for POC settings. To avoid using complex and expensive equipment without sacrificing resolution and control, progress has been made in designing POC-based imaging methods.[230] For example, low cost and portable implementations of bright field and fluorescence microscopes have been developed,[231-233] successfully demonstrating miniaturized, POC-adapted versions of conventional microscopes. Lens-free imaging systems are also an exciting advancement in POC imaging, since these systems have the potential to significantly reduce instrumentation requirements and thus improve portability.[234-236] Furthermore, smartphone devices have been interfaced with microscopy,[237-239] and in some investigations smartphones have been successfully applied to colorimetric read-out of various biomarkers,[240-242] including DNA.[243]

Nanotechnology has made great strides in improving fluorescence detection because it has been applied towards the generation of fluorescence labels, markers, and

detection systems with novel target isolation and identification mechanisms. For example, fluorophore-labeled branched DNA nanostructures were constructed to create color-coded DNA nanobarcodes for multiplexed detection,[244,245] as well as produce light-driven aggregation of DNA nanostructures for detection applications.[246] In addition, fluorescence-labeled DNA nanostructures have been integrated with PCR to perform simultaneous amplification and multiplexed labeling in a single step.[247] Fluorescence-labeled branched DNA structures can also form complexes with cationic polymers, enabling fluorescence resonance energy transfer that has high potential as a label for biosensing applications.[248] Further work has applied DNA nanostructures as multiplexed fluorescent labels for protein detection as well.[249] Overall, employing highly precise DNA architectures with multifunctional moieties for both target detection and read-out is a powerful strategy for diversifying and adapting fluorescence imaging for novel, portable diagnostic systems.

1.3 Significance of this dissertation

DNA nanostructures are amazingly versatile tools for the design and construction of multifunctional materials. Their implementation in diagnostics is particularly exciting because the critical benefits of DNA (multifunctionality, controllability, design versatility) are incredibly well suited for the detection of nucleic acid targets, chemicals, and small molecules. That said, some challenges remain, such as reducing the complexity and strict operation and manipulation requirements of DNA-based systems. In general, it is difficult to remove DNA materials from a clinical environment; many DNA reactions require complex thermocycling equipment, refrigeration, highly trained personnel, and other laboratory-bound processes. The advent of microfluidics has helped overcome these obstacles by providing a precisely controlled, self-contained system for DNA-based reactions. Indeed, the fusion of DNA nanotechnology and microfluidics has immense potential for the development of cutting-edge diagnostics – as long as the sum of both technologies yields superior diagnostic capabilities that could not be attained with either technology alone. I argue that with careful design and in-depth knowledge of both research areas, DNA materials and microfluidics can be seamlessly integrated into novel diagnostic platforms capable of performing multiplexed pathogen detection and sensitive POC diagnosis without increased complexity or operation requirements.

This Dissertation will highlight two innovative projects whose core theme is the application of DNA materials in diagnostics. First, **Chapter 2** discusses the use of fluorescence-encoded DNA nanostructures in a microbead-array system for multiplexed detection of pathogen targets. Multiplexed diagnostics faces key limiting factors, such as the fact that detection labels are typically limited to a single color, and standard detection

technologies are often restricted to single-target, one-time use. I aimed to address these issues in two ways: 1) by using branched DNA nanostructures to engineer a versatile, multi-color barcode labeling system, and 2) by integrating these nanostructures into a portable, re-usable microfluidic device that performs rapid multiplexed pathogen detection. This platform utilizes DNA nanostructures as sensitive molecular-recognition probes without the added complexity or high-temperature requirements of standard methodologies such as PCR. The multiplexed capability has been successfully validated using real clinical patient samples, and furthermore we have demonstrated sensitivity levels similar to clinical methods such as ELISA.

Second, **Chapter 3** discusses the investigation and implementation of an isothermal DNA amplification strategy within a microfluidic device for POC detection of DNA and RNA viral targets. One challenge in DNA-based detection is incorporating target amplification within a POC platform without sacrificing detection sensitivity or accuracy. I sought to overcome this challenge by designing a target-triggered isothermal DNA amplification system and combining it with hydrodynamic flow to generate 2D periodic DNA patterns as a detection read-out. These DNA patterns can be quickly stained with silver solution and visualized with the naked eye. Furthermore, this novel room-temperature reaction system can maintain accurate detection to as low as 150 fM of nucleic acid target. To the best of our knowledge, this is the first time hydrodynamic flow has been combined simultaneously with enzymatic amplification to achieve periodic DNA patterns. In addition to demonstrating a broad detection range and high sensitivity, we have achieved accurate detection of both DNA and RNA viruses from raw crude leaf samples. Our diagnostic platform could revolutionize agriculture diagnostics, where there is a severe lack

of detection systems for on-site identification of plant disease. Furthermore, this device could easily translate to clinical detection of pathogens from human and animal samples.

Taken together, these two projects represent an interdisciplinary approach to pathogen diagnostics. I have designed two completely different systems which exploit DNA's ability to act as both a structural polymer for self-assembly, and as a biological molecule which can initiate reactions with enzymes and genetic material. The significance of this body of work stems from its universal applicability – these detection systems could easily be adapted toward diagnosing disease in a number of hosts (such as humans, animals, and plants) and a number of environments (clinical hospitals, field clinics, and even farms or wildlife environments). More importantly, this Dissertation demonstrates the successful fusion of DNA materials and microfluidics in innovative systems that achieve multiple capabilities that are difficult to combine in standard diagnostic methodologies today. Ultimately, these DNA-based platforms provide valuable insight into new strategies for improving pathogen detection and for successfully translating DNA-based diagnostics for real-world use.

CHAPTER 2

MULTIPLEXED DIAGNOSTICS USING A DNA NANOBARCODE MICROBEAD-ARRAY DEVICE

2.1 Overview and background

The extraordinary controllability of synthetic DNA nanostructures affords great advantages in nanotechnology and biotechnology,[250-253] with important applications including self-assembly,[254-257] sensing,[258-260] and DNA-based materials.[261-264] However, solution-based reactions using DNA nanostructures are limited in their real-world execution, particularly with respect to diagnostics, because they are time consuming, require expensive equipment, and use large volumes of reagents. To overcome these drawbacks recent work has demonstrated the tremendous advantages of combining DNA and microfluidics, which has led to many innovative platforms including droplet-based, paper microfluidics, and DNA-nanoparticle-based systems.

In this chapter, I will discuss a novel approach that combines our previously-reported branched DNA building blocks[265,266] with a new microfluidic microbead-array platform for achieving multiplexed detection of viral and bacterial targets. Our DNA nanobarcodes have been redesigned for greater detection resolution in a microfluidic format and for expanding the number of multiplexed labeling probes that can be used simultaneously in one test. In addition, the microfluidic device has been specifically engineered to enhance the reaction kinetics and improve the read-out of our DNA-based diagnostic system. This platform has the unique advantage of being able to detect multiple

targets simultaneously in under 30 minutes and using only 20 µl of reagent volume (including the target sample). Furthermore, it provides additional advantages of a straight-forward microarray-like read-out (while avoiding the fabrication complexity typical of DNA microarrays) and the ability to be re-used at least 7 times without sacrificing diagnostic accuracy and performance.

Branched DNA nanostructures are highly effective detection probes because they directly interface with pathogen DNA or RNA, thus removing the need for intermediaries which can introduce experimental error. They also have the added strength of being very controllable; their binding specificity can be fine-tuned with optimized (more stringent) buffer conditions to remove non-specific binding events. Furthermore, this system is extremely modular. Simple Y-DNA structures can be combined in a deliberate, programmable fashion (through enzymatic ligation) to self-assemble increasingly complex DNA architectures, each carrying a unique fluorescence-code label and a target-specific binding region. Overall, the rapid read-out microbead-array in our microfluidic device and the highly programmable, modular DNA detection probes make this platform a potent tool for multiplexed detection with strong applications in clinical diagnostics.

2.1.1 *Dendrimer-like DNA nanostructures for detection*

DNA is a polymeric material that possesses many desirable chemical and physical properties. With the myriad of enzymes available to manipulate DNA,[267,268] there is great potential for using DNA as a generic material instead of a genetic material. Since almost all naturally occurring DNA molecules are either linear or circular, one must first create additional shapes of DNA to act as basic building blocks for assembling larger and more complex DNA materials. It is particularly important that DNA building blocks are designed

to readily incorporate into larger structures in a controlled manner so that different structures can be made at high yield and monodispersity for downstream use.

To this end, our group achieved controlled assembly of dendrimer-like DNA (DL-DNA) from Y-DNA building blocks.[269] The synthesis of Y-DNA and the self-assembly of DL-DNA were robust and efficient; the resulting DL-DNA was highly stable and monodisperse. Because each ssDNA can be conjugated to different moieties, the final DL-DNA structures are multivalent and can be either isotropic or anisotropic. This structural versatility yields endless possibilities when used for the generation of multifunctional entities. As described previously, Y-DNA were formed from three ssDNA in a one-pot approach. Using densitometry, the total yield of Y-DNA was estimated to be close to 100%. Importantly, synthesized Y-DNA demonstrated high stability with no observed degradation after 30 days at 4˚C, making these nanostructures optimal candidates for building intricate architectures for downstream sensing and labeling. DL-DNA was assembled by the ligation of Y-DNA molecules whose sequences were designed such that each Y-DNA bound in a controlled fashion. Specifically, ligation sequences were non-palindromic to prevent self-ligation or unintended binding from occurring. Moreover, the ligation was programmed to be one directional, such that a "base" Y-DNA (G0) would only bind to first generation Y-DNA (G1), the outer branches of the first generation Y-DNA would only bind to second generation Y-DNA (G2), and so on. (see **Figure 1.3** in the **Introduction**)

Modular and systematic assembly of materials from DNA building blocks is extremely useful for the development of diagnostic probes. This "mix and match" assembly strategy, coupled with the programmability of DNA binding, makes DNA a powerful

vehicle for designing unique labels and binding mechanisms. Furthermore, the high specificity and sensitivity of DNA (able to distinguish single base pair mismatches) provides an impressive molecular recognition capability that is essential for accurate detection. Rapid, multiplexed, sensitive, and specific molecular detection is of great demand in gene profiling, drug screening, clinical diagnostics and environmental analysis.[270-272] One of the main challenges in multiplexed detection is identifying each specific detection-reaction with a distinct label or 'code'.[273] There are two main strategies for detection encoding: 1) positional encoding, which involves assigning every potential reaction to a particular location on a solid phase support such as a DNA microarray,[274-276] and 2) reaction encoding, in which every possible reaction is uniquely tagged with a code, typically optical or particle based.[277-280] Although these methods are quite popular, the micrometer size, polydispersity, complex fabrication process, and non-biocompatibility of current codes restrict their real-world use.[281-283]

Our lab developed a novel detection strategy by synthesizing DL-DNA-based, fluorescence-intensity-coded nanostructures (DNA nanobarcodes) that contained a built-in fluorescence code and detection probe for molecular recognition.[284] First, fluorescence-labeled Y-DNA were synthesized from three ssDNA, one carrying a sticky end and the other two labeled with either fluorophore(s) or a molecular detection probe. After hybridization, the resulting fluorescence-labeled Y-DNA (**Figure 2.1 A**) were incorporated into the peripheral-outer layer of fluorescence-labeled DL-DNA, or DNA nanobarcodes. Both dye type and dye number were precisely controlled to create a unique fluorescence intensity-code (**Figure 2.1 B**). These probes were decoded based on the ratios of different fluorescent dyes (e.g. 2 red to 1 green dye) present in the DNA nanobarcodes (**Figure 2.1**

C). During assembly, molecular recognition elements (e.g., DNA or RNA probes, or even antibodies) could be built into DNA nanobarcodes for a variety of detection applications.

These DNA nanobarcode probes were applied towards multiplexed detection of DNA from several pathogens using dot blotting, fluorescence, and flow cytometry. The successful synthesis and application of DNA nanobarcodes demonstrates two novel concepts: 1) multiplexed detection can be achieved by identifying fluorescence intensity ratios instead of fluorescent colors, and 2) DL-DNA can be used as both structural scaffolding and functional molecular probes. Results have shown that detection was sensitive (attomole level) and rapid. Furthermore, the DNA nanobarcodes are biocompatible and their nanoscale size enables more rapid access to targets in solution. Despite these achievements, our previous DNA nanobarcode strategy had drawbacks in that it was limited to solution-based testing and involved complicated read-out systems such as flow cytometry, which required special training and expensive equipment. Even with the simple dot-blot format, tests were constrained to one-time use and read-out of the fluorescence intensity codes had diminished precision.

To improve upon this strategy, I implemented a platform that converted the DNA nanobarcode detection system from a solution phase format (which is restricted to laboratory settings and highly trained personnel) to a portable, easy-to-use, quick read-out microfluidic device format. This is the first time DNA nanobarcodes have been used in a microfluidic device, and furthermore this detection strategy stands apart from other methods by simultaneously incorporating both positional and optical encoding. In particular, microbeads were organized within the microfluidic chamber into a 2D array format, similar to a standard DNA microarray but on a smaller (micron-sized) scale. The

microbeads enable fluorescence signal amplification by providing a surface upon which targets and DNA nanobarcodes can bind and become concentrated. Overall, this system improves upon conventional detection systems by combining features that are typically difficult to achieve in a single platform: 1) it enables continuous and rapid flow-through exchanges of buffers and reagents, 2) the microscale chamber improves reaction kinetics to reduce detection times, 3) this system can be re-used at least seven times without negatively impacting detection performance, and 4) this platform is inexpensive, costing less than $2 overall.

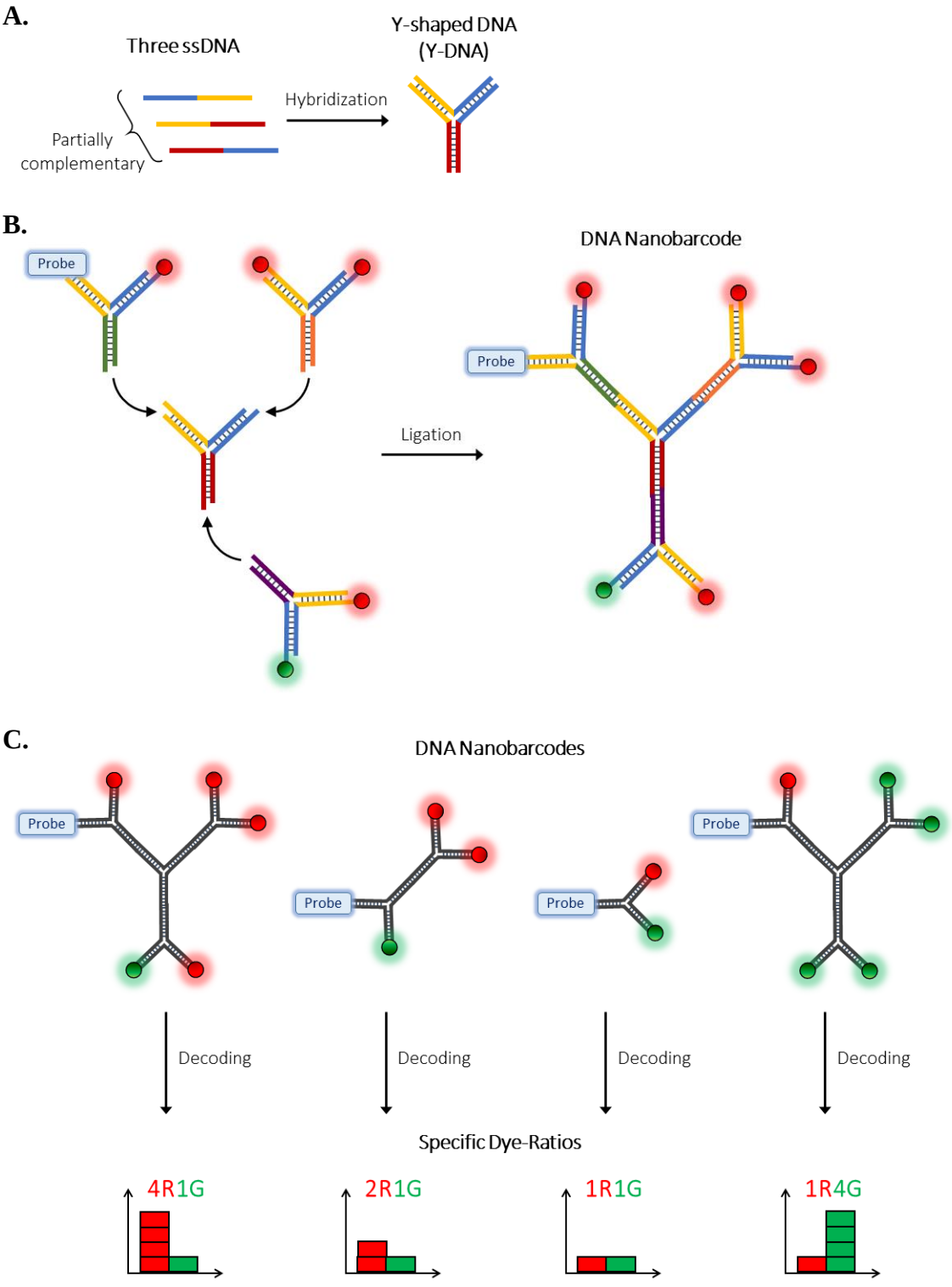

Figure 2.1 Illustration depicting DNA nanobarcode synthesis with dye-ratios

A) Illustration of the self-assembly of a Y-DNA building block. Three separate ssDNA are used – one or more carry fluorescence dyes and another has an overhang sequence which

acts as a molecular detection probe for a pathogen target. These ssDNA are partially complementary to each other and thus they hybridize together in a controlled manner to self-assemble into the Y shape. **B)** The Y-DNA are combined together into the branched DNA nanobarcode structure using sticky end ligation. **C)** Schematic of DNA nanobarcode decoding. Each DNA nanobarcode carries a unique fluorescence intensity code made of different amounts of red and green dyes, and this code is used to identify a target based on a preassigned code library.

2.1.2 *Microfluidic cell and particle trapping systems*

Controlling small particles and cells in free solution is an important goal in biology, engineering, and nanotechnology. In particular, the ability to organize and manipulate micro- to nanoscale objects in highly tunable microfluidic environments (with precise chemical, thermal, and spatial control) enables the generation of high-resolution biological studies and diagnostic assay platforms. These systems employ various trapping mechanisms to hold cells or particles in place, such as acoustic, electrokinetic, and magnetic fields, in addition to pressure-driven flow and centrifugal force. Overall, these microfluidic platforms can be separated into two general categories: cell trapping and particle trapping.

Some of the core advantages of microfluidic trapping systems include rapid and precise buffer exchange and easy manipulation of numerous discrete objects. In particular, controlled confinement of a specific number of cells per trapping structure is important for high precision biological studies. Trapping systems have been designed to investigate single cell response, cell fusion, and tumor spheroid behavior – all of which can be challenging to perform in bulk scale cultures where non-uniform environments and cell-cell contact can influence results. For example, Di Carlo et al. performed high-throughput analysis of single cell behavior in a microfluidic device with an array of U-shaped capture elements.[285] Pressure-driven flow loaded cells into the array, whose trapping structures were designed to trap only one cell per trap. HeLa cells were successfully cultured in this array (similar to controls) and 85% of the cells stayed in their original trap positions for over 24 hours. This trapping array concept was further developed by the Voldman group,

who combined and array of deeply recessed traps with reverse flow steps to perform single cell pairing tests and cell fusion studies.[286]

Building upon previous work, Luke P. Lee and colleagues achieved self-assembly of uniform spheroid arrays and characterization of spheroid dynamics in one microfluidic platform.[287] Cancer cells were hydrodynamically trapped and compacted together in an array through continuous perfusion, eventually forming many 3D tumor spheroids (7,500 spheroids/cm^2) with a narrow size distribution. This platform reliably assembled uniform spheroid arrays for anticancer drug screening and long-term tumor monitoring, which may provide a more realistic model than monolayer culture of *in vivo* tumors. In addition, platforms have been designed for quantification of tumor cell death over time. This was achieved by tracking the differences in stochastic cell death sensitivity in the microfluidic device, a phenomenon which is often undetectable in conventional end-point analysis devices such as flow cytometry.[288] New trapping platforms have expanded beyond cells towards large-scale organization and analysis of hundreds of drosophilia embryos[289,290] and the encapsulation of individual live *C. elegans* in series for behavior study and characterization in response to neurotoxin assays.[291] Together, the highly precise control of fluid perfusion conditions (flow rate, flow time, chemical gradients etc.), and the transparent, rapid read-out nature of PDMS-based devices create a powerful strategy for gathering continuous, high-throughput, and real-time measurements.

In addition to cells and small organisms, microfluidic systems have been used for organizing and trapping particles (e.g. microbeads) for detection applications. One of the main challenges of traditional solution-based detection assays is that they require laborious, time-intensive fluid mixing procedures in which specific reagents and/or washes must be

introduced sequentially one at a time. Particles, such as microbeads, remove these laborious procedures and improve detection reaction execution by providing high surface-to-volume ratios and enabling rapid mixing, holding, and transport of particles depending on specific screening goals.

To advance microbead trapping technology further, microfluidic processors have been produced for parallel manipulation of numerous particles and for performing multi-stage fluidic reactions. For instance, a microfluidic micropost-railing system was reported which transports and holds microbeads in distinct, adjacent laminar flow streams for rapid fluidic mixing and assaying.[292] In total, 48 discrete fluidic mixing stages were performed on microbeads in parallel without the need for external observation or regulation. Following these reactions, beads were immobilized in separate trapping arrays for fluorescence visualization and signal detection. Another microfluidic system developed by Sochol et al. integrated both microfluidic mixing of mobile microbeads and hydrodynamic microbead arraying for simultaneous detection of multiple bio-molecules.[293] This system had four parallel reaction chambers for mixing and detection, and it was successfully utilized for detection of three distinct DNA oligonucleotide sequences from the Hepatitis C viral genome with single base-pair mismatch specificity. Microfluidic platforms such as these greatly increase the parallelization of reactions and improve microbead handling for many different applications, including bio-molecule detection, clinical diagnostics, and drug screening.

In addition to microfluidic flow, other mechanisms have been employed to trap microbeads for analysis and sensing applications. Lilliehorn and colleagues, for instance, created a device that enabled ultrasonic capture of microbead clusters using ultrasonic

microtransducers.[294] Beads were flowed into discrete chambers and trapped using acoustic forces in standing waves, and they could then be shuttled between different chambers as a means for performing more complex biological assays. Burger et al. developed a different system for performing multiplexed immunoassays on microbeads which was based on a centrifugal microfluidic platform.[295] An array of V-cup barriers were radially arranged for trapping microbeads with nearly 100% capture efficiency and high retention. Furthermore, since the beads were individually located in a well-defined array in the same focal plane, multiplexed assay read-out was simple and straightforward. To achieve PCR-free DNA detection, Dubus et al. developed a microelectromagnetic trap for confining biosensing magnetic beads in a small volume for rapid and ultrasensitive detection of DNA.[296] This system achieved a detection limit of ~200 target copies in a volume of 150 µl, and it offers the possibility for fast multi-target DNA detection in POC settings.

Although many trapping strategies are available, some of these methods are limited to particles with specific material properties, and they can also be restricted by having a complex setup that is difficult to operate. With these concerns in mind, I have developed a novel microfluidic microbead-array platform that organizes over a thousand microbeads in a uniform array by hydrodynamic trapping. This system has been used to detect five DNA targets simultaneously in a single chamber, and moreover it does not require expensive equipment or many detection steps. Furthermore, the versatile DNA nanobarcode probes, low fluid volume requirement, simple design and operation, and the ability to create large arrays of particles for high-throughput analysis, make this system uniquely adapted for rapid multiplexed pathogen sensing and read-out.

2.1.3 *Diagnostic approach*

The diameter of DNA nanobarcodes is approximately 30 nm, which is significantly below the detection limit of optical microscopy. Thus, polystyrene microbeads (10 μm diameter) were used as a substrate for amplifying the DNA nanobarcode fluorescence signals for imaging and read-out. The microbead-based signal amplification strategy and detection format are shown in **Figure 2.2**. In this system, two sets of ssDNA probes were used: 1) biotin-labeled ssDNA (capture probes) which were surface bound to superavidin-functionalized microbeads, and 2) target-specific ssDNA (reporter probes) that were built into the DNA nanobarcode structure. Each batch of microbeads was functionalized with a single type of capture probe, which was partially complementary to a region of a pathogen target DNA. Multiple types of microbeads were mixed to form a library of microbeads for multiplexed detection. The reporter probes were complementary to another region of a pathogen target DNA, which was different than that of the capture probe binding region. Therefore, both capture probe and reporter probe hybridized to the target DNA by sandwiched hybridization. Because each microbead could accommodate a large number of sandwiched complexes on its surface, DNA nanobarcode fluorescence signals were accumulated on the microbead surface for higher-intensity read-out.

Rather than perform the detection assay in solution, which can be time consuming and laborious, we used a microfluidic device with an array for trapping and organizing the microbeads for multiplexed detection. (**Figure 2.3** and **Figure 2.4**) Microfluidic devices afford many advantages, such as low sample volume, enhanced reaction kinetics, and simple read-out. In our diagnostic assay, the microbeads are first trapped in a uniform array, and then the sample reagents (wash buffer, target sample mix, etc.) were flowed into the

chamber to perform detection. In short, the target DNA is hybridized onto matching capture probes on the bead surfaces, and then DNA nanobarcodes matching the target DNA are bound. After sufficient time for hybridization, the entire bead surface should be specifically coated with a single type of DNA nanobarcode probe, indicating successful detection of a designated target. Washing steps were used between each hybridization step to prevent nonspecific binding phenomena. The resultant microbeads were first evaluated individually by fluorescence microscopy, and the overlay color images are shown in **Figure 2.5**. We expanded our detection probe library to include more DNA nanobarcode ratios, and some of these probes were used for detecting samples that contained DNA from four different pathogens: Streptococcus pyogenes, Human Rhinovirus, Human Coronavirus, and Influenza A virus.

The fluorescence intensity ratio is the basis for decoding the DNA nanobarcodes, which can generally be written as the function *aGbR*. Under the same conditions, the fluorescence intensity ratio λ between a single green (g) and a single red (r) dye is constant ($\lambda = g/r$). In turn, the total green and red fluorescence intensities (G and R, respectively) of a microbead bound with DNA nanobarcodes may be calculated by formulas $G = (a \times g)$ and $R = (b \times r)$, respectively. Thus, the total fluorescence intensity ratio (K) between red and green fluorophores ($K = R/G$) can be used to calculate the code number, a/b, using the formula $a/b = 1/(K\lambda)$. When G and R are measured using our microbead-array microfluidic detection platform, K can be calculated by measuring the average fluorescence ratio for all the microbeads in the array that match a single target. It is important to note that the slope of a two-color (green-red) scatter plot of the microbead-array data (where one data point represents the average fluorescence ratio (R/G) of a single bead) will be the same for one

type of DNA nanobarcode, regardless of target concentration. Therefore, multiple DNA nanobarcode labels remain distinguishable from each other on a green-red scatter plot by their different slopes. Our platform's detection capabilities can be further expanded by using different sized microbeads and also by modifying the microbead surface-binding capacity (partially-blocking the surface), both of which will be discussed in the results section.

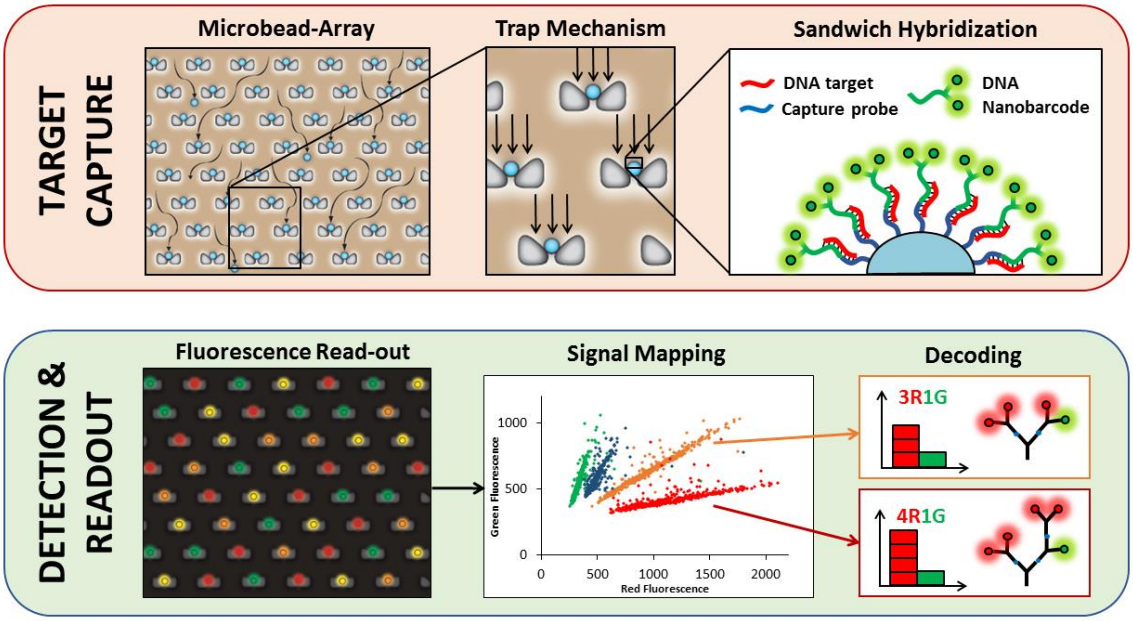

Figure 2.2 Schematic of the diagnostic approach used in the DNA nanobarcode microbead-array system

Target capture and identification is performed on the surface of the microbeads through a sandwich hybridization process. In general, the matching DNA target will hybridize to the ssDNA capture probes that are pre-bound to the microbead surface, and subsequently a DNA nanobarcode labeling probe will hybridize to a separate free region of the captured DNA target sequence. Detection and read-out involve fluorescence imaging of the microbead-array, collecting the average fluorescence dye-ratio intensities for the collection of trapped microbeads, and plotting this information on a scatter plot of red vs. green dye intensity. From the plot, the fluorescence ratio can be easily decoded to identify the detected target.

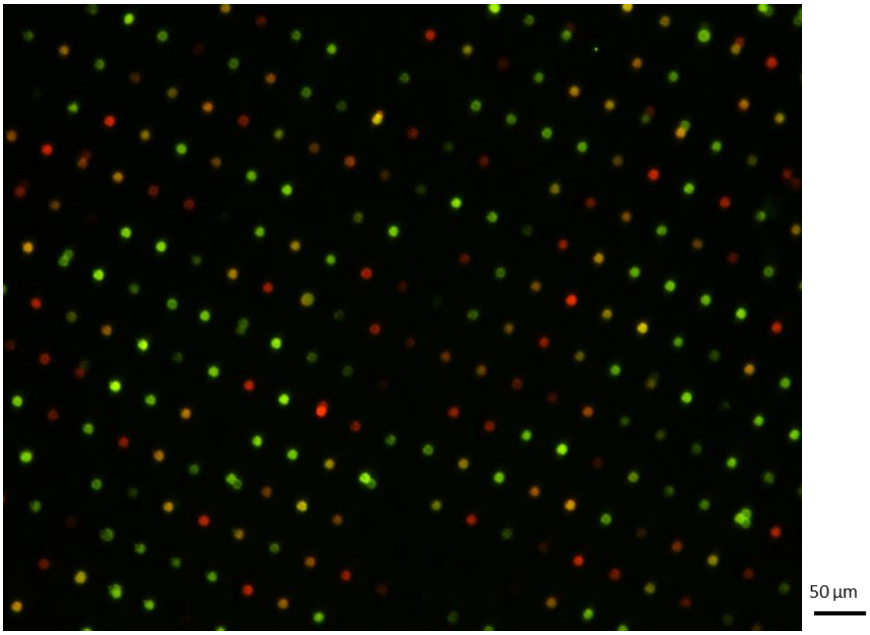

Figure 2.3 Multiplexed read-out with the DNA nanobarcode microbead-array

Image of the DNA nanobarcode microbead-array after performing multiplexed detection of pathogen DNA. Several different DNA nanobarcode intensity ratios are clearly visible even with naked eye from these images, as seen by the color variation.

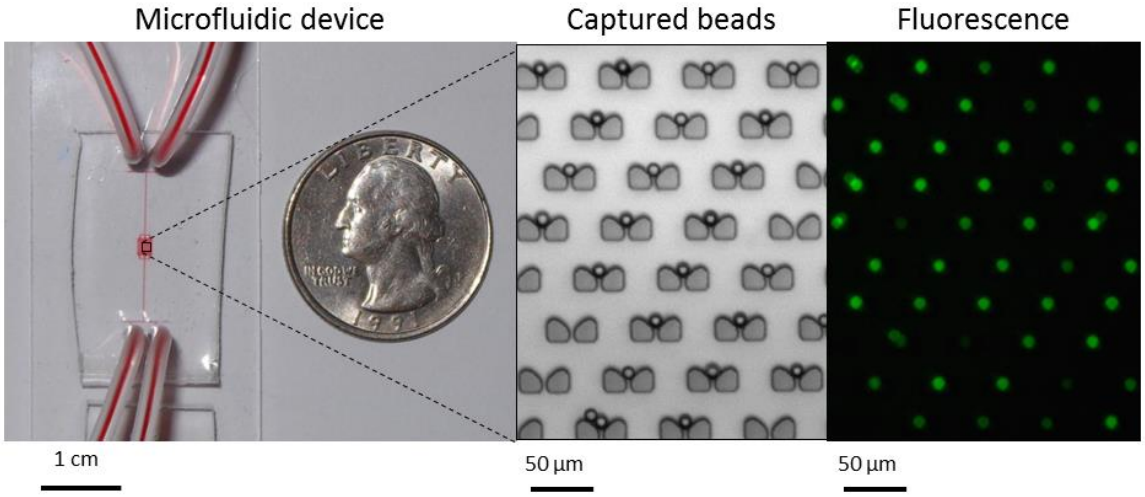

Figure 2.4 Images of the microfluidic device and microbead-array chamber

Image of the DNA nanobarcode microfluidic device and a high magnification image of a section of the microbead-array. Bright field imaging (center panel) reveals that the majority of traps contain only single microbeads, which helps isolate the nanobarcode signals and

avoid intensity ratio blending. Fluorescence imaging (right) reveals that the microbeads can be clearly organized and visualized in a uniform array for easy read-out.

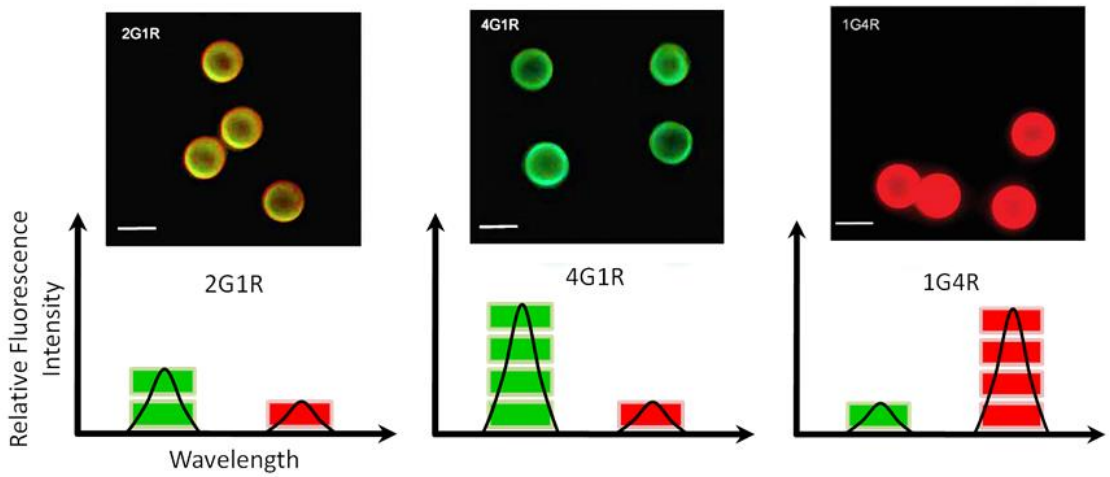

Figure 2.5 Fluorescence images of microbeads after DNA nanobarcode labeling

These images demonstrate that the DNA nanobarcodes and DNA targets uniformly hybridize to the microbeads. Each color is depicted by a different fluorescence dye ratio as shown by the plots under each microbead image. Furthermore, these images show that the DNA nanobarcode signals can be amplified by concentrating the DNA nanobarcodes on the microbead surface.

2.2 Materials and methods

2.2.1 *Chemicals, materials, and DNA sequences*

T4 DNA ligase was purchased from New England Biolabs (Beverly, MA). DNA hybridization buffer was purchased from Sigma Aldrich (St. Louis, MO). Polystyrene microbeads were purchased from Bangs Laboratories (Fishers, IN). Dow Corning 184 Sylgard Silicone Elastomer (PDMS) was purchased from Fisher Scientific (Waltham, MA). Hamilton Gastight syringes (250 µl volume) were purchased from Hamilton Company (Reno, NV). Microfluidic syringe pumps were purchased from Harvard Apparatus (Holliston, MA). Custom-designed oligonucleotides were commercially synthesized and PAGE purified (Integrated DNA Technologies, Coralville, IA). The oligonucleotide sequences used in forming Y-DNA, DNA nanobarcodes, and the DNA-coated microbeads are listed in the following tables.

DNA Nanobarcode Sequences	
Name	5' - 3' sequence
Ya-H	/5Phos/AACGTGGATCCGCATGACATTCGCCGTAAG
Ya-AF488	/AF488/TGGATCCGCATGACATTCGCCGTAAG
Ya-AF546	/AF546/TGGATCCGCATGACATTCGCCGTAAG
Yb-e	/5Phos/GCAACTTACGGCGAATGACCGAATCAGCCT
Yb-d	/5Phos/ATGCCTTACGGCGAATGACCGAATCAGCCT
Yb-AF488	/AF488/CTTACGGCGAATGACCGAATCAGCCT
Yb-AF546	/AF546/CTTACGGCGAATGACCGAATCAGCCT
Yc-h	/5Phos/CGTTAGGCTGATTCGGTTCATGCGGATCCA
Yc-E	/5Phos/TTGCAGGCTGATTCGGTTCATGCGGATCCA
Yc-D	/5Phos/GCATAGGCTGATTCGGTTCATGCGGATCCA
Yc-InfA	GTCAGAGGTGACAAGATTGGTCTTTTTAGGCTGATTCGGTTCATGCGGATCCA
Yc-HRV	CCAAAGTAGTCGGTCCCATCTTTTTAGGCTGATTCGGTTCATGCGGATCCA
Yc-CoV	CTCTGTCACATTTTGGATAATCCCATTTTTAGGCTGATTCGGTTCATGCGGATCCA
Yc-HSV	CCTGCTGCTTGTCCAGGATTTTTAGGCTGATTCGGTTCATGCGGATCCA
Yc-Strep	GCCGTGTCTCAGTCCCAGTGTGTTTTTAGGCTGATTCGGTTCATGCGGATCCA

Table 2.1 List of sequences used for DNA nanobarcode formation

Microbead Capture Probe Sequences	
Name	5' - 3' sequence
Bead-InfA	/5Biosg/TTTTTTTAGCGTGAACACAAATCCTAAAATTCC
Bead HRV	/5Biosg/TTTTTTTAGGAAAAAGTGAAACACGGACAC
Bead-CoV	/5Biosg/TTTTTTTGGCCATTATCCTAAGCATGTTAGG
Bead-HSV	/5Biosg/TTTTTTTGAGTTACACACGACCTTGATGG
Bead-Strep	/5Biosg/TTTTTTTTTCCCTACTGCTGCCTCCCG

Table 2.2 List of sequences used to functionalize polystyrene microbeads

Synthetic DNA Target Sequences (Derived from real pathogens)	
Name	5' - 3' sequence
Target-InfA	GACCAATCTTGTCACCTCTGACTAAGGGAATTTTAGGATTTGTGTTCACGCT
Target-HRV	GATGGGACCGACTACTTTGGGTGTCCGTGTTTCACTTTTTCCT
Target-CoV	TGGGATTATCCAAAATGTGACAGAGCCATGCCTAACATGCTTAGGATAATGGCC
Target-HSV	TCCTGGACAAGCAGCAGGCCGCCATCAAGGTCGTGTGTAACTC
Target-Strep	CACACTGGGACTGAGACACGGCCCAGACTCCTACGGGAGGCAGCAGTAGGGAA

Table 2.3 List of sequences used for synthetic pathogen DNA targets

2.2.2 *Sample Preparation from patients with acute pharyngitis*

Influenza A, Human Rhinovirus, Human Coronavirus, and Streptococcus pyogenes samples were obtained from pediatric subjects, age range 0 to 18 years, males and females, in accordance with IRB rules and regulations. Samples were collected in the form of nasopharyngeal swabs and used to prepare viral and bacterial cultures. These cultures were grown and prepared for shipment in the Microbiology Department at New York Presbyterian Hospital (NYPH)–Weill Cornell Medical Center (WCMC) in New York City, NY. Samples were completely de-identified prior to overnight transport to our Ithaca-based laboratory. The QIAamp Cador Pathogen Mini Kit (Qiagen, Valencia, CA) was used for extraction and isolation of viral and bacterial nucleic acid material from patient sample cultures for DNA nanobarcode detection reactions in the microbead-array device.

2.2.2 *Preparation of DNA-coated microbeads*

Streptavidin-coated 10 µm diameter polystyrene microbeads were suspended in wash buffer (40 mmol NaCl in 40 mL TE, 0.05% TritonX-100) and washed 3 times at 1200 RCF for 3 min. Biotinylated linear ssDNA capture probes (10 µM) were added to 10 µl of concentrated microbeads and incubated with rotation for 1.5 hours at room temperature. Following incubation, the ssDNA-functionalized microbeads were washed in wash buffer 3 times at 1200 RCF for 3 min to remove excess unbound ssDNA capture probes. Final microbeads were resuspended in 200 µl wash buffer and stored at 4˚C prior to use.

2.2.3 *Fabrication of microfluidic devices*

The microfluidic devices were fabricated using a standard soft lithography process at the Cornell Nanoscale Science and Technology Facility (Ithaca, NY). First, a CAD

design was transferred to a chrome-glass mask using a Heidelberg Mask Writer DWL2000 (Heidelberg Instruments Inc., Woburn, MA). A 16 μm thick layer of negative photoresist, SU-8 2015 (MicroChem, Newton, MA), was spin-coated onto a clean 4 inch Silicon (Si) wafer, which was then pre-baked at 90˚C for 3 min. Microfluidic features were defined using contact photolithography (Contact Aligner, ABM, Scotts Valley, CA) with an exposure time of approximately 15 sec. The Si wafer was post-baked at 95˚C for 4 min and developed for 3 min in SU-8 developer (Microchem, Newton, MA). The finished Si wafer mold was plasma oxidized and coated with an anti-stiction coating through molecular vapor deposition of (perfluorooctyl) trichlorosilane (FOTS) (MVD 100, Applied Microstructures, San Jose, CA).

Using the developed photoresist as a negative master, the microfluidic devices were micromolded with silicone elastomer, poly(-dimethylsiloxane) (PDMS), at a 10 : 1 (base : curing agent) ratio (Sylgard 184, Dow Corning, Corning, NY). After curing at 70˚C for 1.5 hours, the PDMS was removed from the mold and individual devices were cut from the PDMS. Ports for tubing connections were punched at inlet and outlet locations, and then the PDMS devices were covalently bonded to PDMS-coated glass microscope slides (Fisher Scientific, Pittsburgh, PA) via plasma oxidation. These devices were specifically designed to trap and hold an array of 10 μm diameter streptavidin-coated polystyrene microbeads (Bangs Laboratories, Fishers, Indiana). Due to the polydispersity of the beads (and to prevent bead clumping), the heights of the microchannels were set at 16 μm. The bead-trapping microposts were approximately 17 x 6 μm in dimension, and the gaps between microposts were 2 μm. The array of trapping features can hold approximately 1000 microbeads simultaneously in as single device, with typically one bead per trap.

Figure 2.4 in ***Section 2.1.3*** shows the device array with trapped microbeads, both using bright field and fluorescence imaging.

2.2.4 *Self-assembly of DNA nanobarcodes*

Branched Y-DNA nanobarcodes were prepared according to previously published methods from our group.[297] Briefly, DNA nanobarcodes were synthesized by first self-assembling discrete Y-DNA, and then ligating specific Y-DNA together to form larger dendrimer-like DNA nanobarcodes. To form the Y-DNA, equal molar amounts of three corresponding ssDNA strands, each partially complementary to the others, were mixed and annealed together by a highly controlled heating and gradual cooling process. To form fluorescence dye-labeled Y-DNA, commercially synthesized ssDNA conjugated to fluorophores were used. To assemble the DNA nanobarcodes, fluorescence-labeled Y-DNA and target-binding Y-DNA (all carrying at least one ssDNA sticky end) were mixed together and ligated overnight at 16˚C using T4 DNA ligase.

2.2.5 *Fluorescence microscope imaging*

An Olympus BX61 fluorescence microscope (Olympus America, Melville, NY) was used to obtain high resolution fluorescence images of the DNA nanobarcode-labeled microbeads within the microbead-array microfluidic device. Following a detection reaction, the device was separated from the infusion syringes and immediately transferred to the fluorescence microscope for imaging. Extended exposure times were used to image the microbead-array and distinguish DNA nanobarcode fluorescence ratios, ranging from 2 to 6 seconds.

2.2.6 *DNA nanobarcode microbead-array device detection protocol*

The microfluidic device was pre-filled with nuclease free water and all air bubbles were removed from the internal chambers. Next, ssDNA-conjugated microbeads (whose sequences specifically match the desired target(s)) were flowed into the chip and trapped in the microbead-array trapping features. DNA target samples were mixed with hybridization buffer stock to achieve 1x buffer and subsequently flowed into the device at 0.5 µl/min. Harvard Apparatus syringe pumps were used to control the fluid flow. The sample was continually infused into the device for a 12 minute period to allow for hybridization between the pathogen DNA/RNA and the microbeads. Following target hybridization, fluorescence-coded DNA nanobarcodes (matching the pathogen target but non-complementary to the microbeads) were flowed through the chip at 0.5 µl/min for 12 minutes to allow for hybridization. Once these steps are completed, the device is imaged using an Olympus BX61 Microscope. To calculate the DNA nanobarcode fluorescence ratio codes, raw fluorescence images were processed using ImageJ software (NIH, Bethesda, MD) and the average fluorescence intensity was measured over the circular area of each microbead in the array. This process is summarized in **Figure 2.2** in ***Section 2.1.3***.

2.2.7 *Experimental setup*

All microbead-based experiments were conducted in a room temperature environment (20–25˚C) and without any thermal heating or cycling. Prior to device operation, nuclease free water was perfused into the microbead-array chamber for a 10 min incubation period. For all detection experiments, two syringe pumps were used to control the input flow rates, one for a stringent wash solution and the other for the solutions and reagents necessary in the detection process (microbead suspension, target sample solution,

DNA nanobarcode probe solution, etc.). For multiplexed detection in the microbead-array system, a mixture of targets and a select panel of DNA nanobarcode probes were used as the sample and detection probe solutions, respectively.

During operation, syringe pumps were used to control the input flow rates (set at 0.2 µl/min for the wash solutions; 0.5 µl/min for all other DNA suspensions) during continuous flow-loading of the homogenous fluids. Experimental testing was completed after approximately 30 min, corresponding to reagent/suspension volumes of 15 µl and wash solution volumes of 5 µl. To decode the DNA nanobarcode fluorescence signals, the device was imaged with an Olympus BX61 fluorescence microscope for approximately 4 sec and raw image data of the microbead-array was analyzed using ImageJ software. In brief, the average red and green fluorescence intensity over the circular area of a bead was measured, then the average fluorescence ratio was calculated per bead to determine which target was captured on a particular bead.

The negative control experiments were also run using the microfluidic microbead-array device. Different negative controls were performed to confirm accurate DNA hybridization-based detection, including an unrelated target control (having a totally different, non-matching sequence), unrelated DNA nanobarcode control, and unrelated bead capture sequence control. Additionally, control tests for nonspecific binding (e.g. using microbeads and DNA nanobarcodes only) confirmed that nonspecific binding does not significantly contribute to detection signals.

2.3 Results and discussion

2.3.1 *Characterization of the DNA nanobarcode detection system*

The DNA nanobarcode system has a few key parameters which need to be optimized for achieving accurate and sensitive nucleic acid detection. First, accurate and specific DNA nanobarcode hybridization was confirmed against negative controls. More specifically, triplicate tests were performed for three scenarios: a) positive (matching) DNA nanobarcodes that are complementary to the targets captured on the microbeads, b) control DNA nanobarcodes that are unrelated and do not match the DNA targets, and c) tests with no target present, to check for nonspecific binding between the DNA nanobarcodes and the microbeads. **Figure 2.6 A** demonstrates that DNA nanobarcode detection is indeed accurate and significantly different from the negative controls.

Additionally, it is critical that the DNA target specifically and accurately hybridizes to the ssDNA-coated microbeads. In a similar manner to the DNA nanobarcode tests, we took FAM-labeled synthetic ssDNA probes and performed two sets of triplicate tests: a) positive test in which complementary ssDNA targets bind to matching ssDNA probes on the microbeads, and b) negative controls in which unrelated (non-matching) ssDNA targets were used with the same ssDNA-coated microbeads. Our results in **Figure 2.6 B** indicate that the hybridization was accurate and significantly different from the negative controls. Overall, these results confirm that the DNA sandwich hybridization detection approach between microbeads, ssDNA targets, and DNA nanobarcodes can be successfully employed within this microfluidic detection platform.

It was also important to optimize the flow rate for maximum DNA hybridization between all components of the microfluidic detection strategy. Performing a series of tests

with all conditions held constant, we varied the microfluidic flow rate and then imaged the microbead-array to evaluate the relative intensity of the DNA nanobarcode read-out. Since we had already defined the ideal solution conditions for DNA hybridization, the flow rate was the only parameter directly impacting the final read-out intensity. As seen in **Figure 2.6 C**, we found that the 0.5 µl/min flow rate produced the highest overall binding between the detection probes and the DNA target, as represented by the higher average fluorescence intensity in comparison to the other sample tests.

After establishing the optimal conditions for maximum detection, we evaluated the point at which the hybridization becomes saturated for a range of target concentrations. This was necessary because it helped determine at what time point we could clearly distinguish different target concentrations from each other. This time measurement served as a guideline for determining hybridization flow time periods in the final detection platform. As seen in **Figure 2.7**, the different target concentrations (1, 10, and 100 nM) reached hybridization saturation at 50 – 60 minutes and maintained their level of binding for long flow periods up to 3 hours. Achieving the maximum time of 3 hours without any loss in hybridization is an important indicator that we achieved specific and secure hybridization between the target and detection probes. Moreover, we found that the lower limit of hybridization time is approximately 12 minutes, at which point we can still maintain a significant difference between different target sample concentrations.

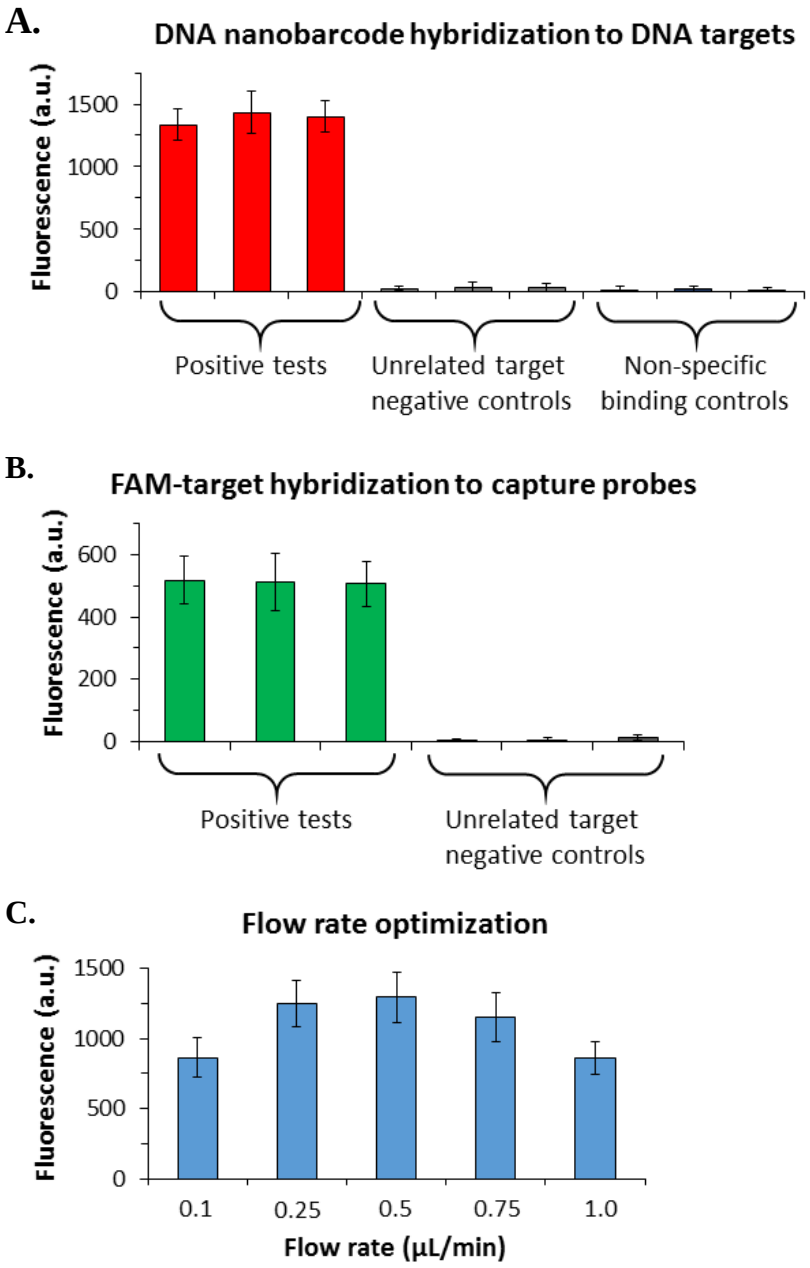

Figure 2.6 DNA nanobarcode system characterization data

A) Evaluation of positive control DNA nanobarcode hybridization (correctly matching to the DNA target) compared to two negative controls: 1) DNA nanobarcodes that are unrelated to the DNA target, and tests with no target present to investigate for nonspecific binding phenomena. **B)** Evaluation of correct target hybridization to microbeads compared to negative controls (non-matching targets) **C)** Flow rate optimization results after performing a series of identical tests at different flow rates. The average fluorescence over a set of microbeads was measured as an indicator for the number of DNA nanobarcodes that were correctly hybridized to DNA targets captured on the microbeads.

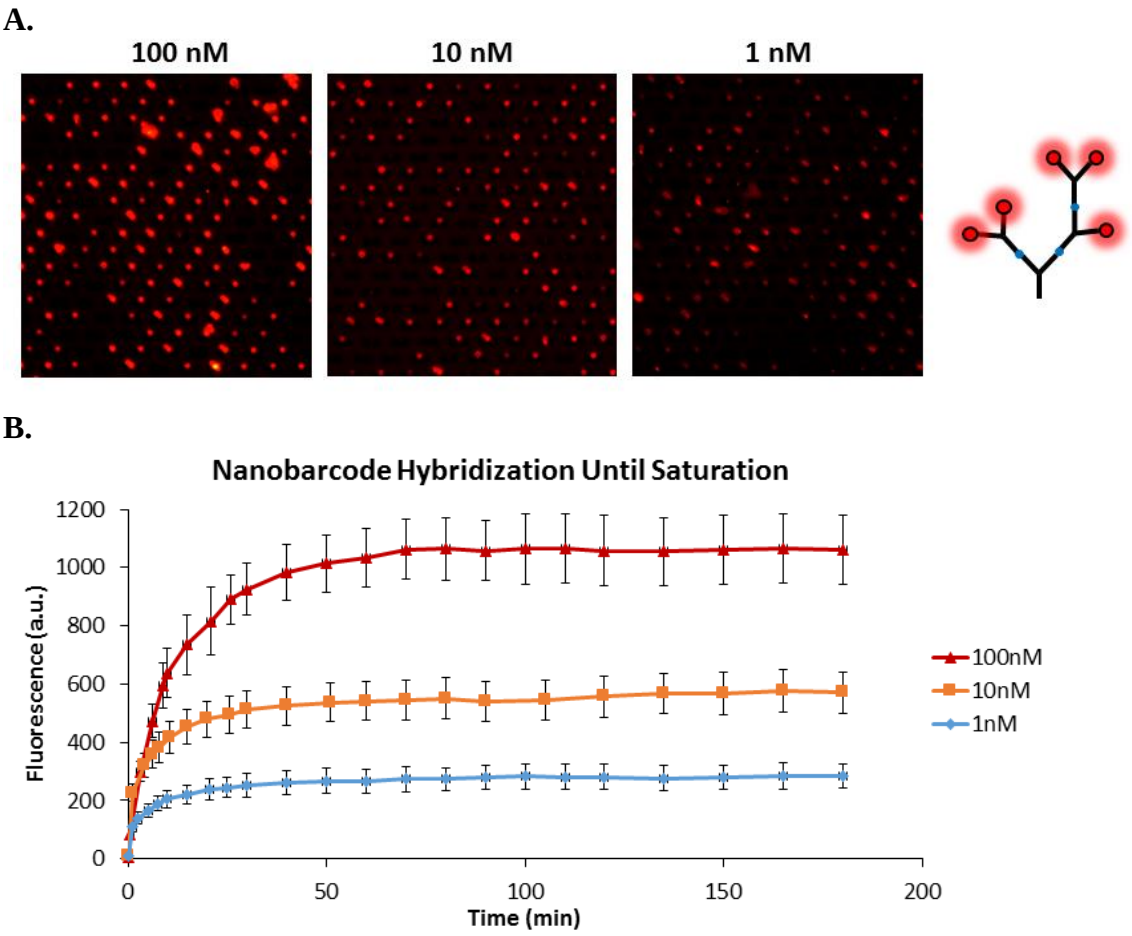

Figure 2.7 DNA nanobarcode hybridization saturation results

A) Fluorescence images of the microbead-array detection results for different target concentrations. These results show the relative intensity differences when each test reaches its saturation point. **B)** Time-lapse graph of average fluorescence intensity measurements over time for three tests with different initial DNA target concentrations.

2.3.2 *Bead intensity-coding to expand probe library*

DNA nanobarcodes employ different ratios of red and green dyes to label different targets. To expand the probe library, we created another labeling strategy by tuning the number of detection probes that are bound to the surface of the microbeads. More specifically, we used a ratio of "blocked" (non-binding) detection probes to "unblocked" (correctly binding to the desired target) detection probes to tune final overall fluorescence intensity on the microbeads. In this manner, we can use the same fluorescence ratio across a set of DNA nanobarcodes and only need to alter the bead surface binding capacity to differentiate multiple targets from each other. Examples of this intensity difference are shown in **Figure 2.8 A**. To further confirm that the ratio of blocked vs. unblocked bead capture probes does not negatively affect overall detection, we tested negative control samples against positive detection tests as seen in **Figure 2.8 B**.

We built an additional dimension of target labeling that did not require any extra fluorescence dyes and greatly reduced the cost and assembly complexity for the DNA nanobarcode probe library. Experimentally, we achieved accurate and clearly distinguishable detection of up to 3 synthetic targets using 0%, 50%, and 80% partially-blocked microbeads. This, combined with a potential DNA nanobarcode probe library of over 48 different dye-ratio combinations, yields a diverse and large probe library which is equal to or greater than other detection probe libraries available today. Moreover, the intrinsic benefits of highly controllable and modular DNA self-assembly makes the rational design of these probes both highly consistent and incredibly versatile.

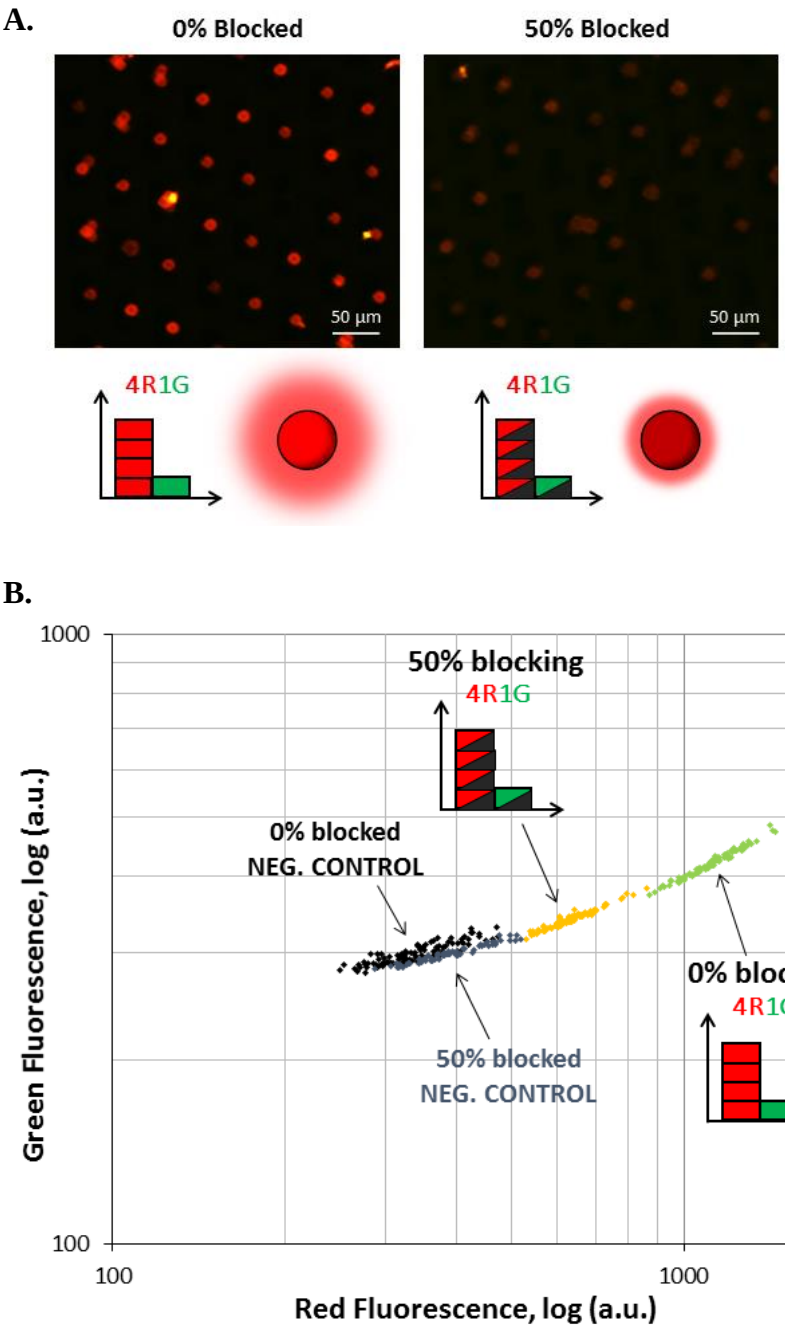

Figure 2.8 Bead-blocking intensity encoding results using the microbead-array

A) Fluorescence images of the microbeads at 0% blocking (all probes bind to the target) and 50% blocking (only half the probes specifically bind to the target). **B)** Scatter plot of the microbead data using 0% and 50% blocking of the microbead surface, as compared to the negative controls (unrelated, non-binding DNA target).

2.3.3 *Design and characterization of the DNA nanobarcode library*

Two types of fluorescent dyes, Alexa Fluor 488 and Alexa Fluor 546, were used to label the ssDNA used to assemble DNA nanobarcodes. For our detection purposes, we constructed seven different nanobarcodes (coded as 4R1G, 3R1G, 2R1G, 1R1G, 1R2G, 1R3G, and 1R4G) where each number refers to the quantity of each dye molecule (R = red, G = green) in one DNA nanobarcode. These different branched DNA nanobarcode structures are depicted symbolically in **Figure 2.9 A**. To verify the DNA nanobarcode color ratios, sample detection tests were performed for each individual DNA nanobarcode type and the resulting microbead-arrays were imaged and normalized to each other. To confirm that the microbead partial-blocking strategy works, we also designed 50% blocked microbeads. Sample images of each microbead dye-ratio color are shown in **Figure 2.9 A**. The microbead intensity and fluorescence dye ratio differences are clearly visible and discernable from one another, indicating that our strategies for implementing an extended detection probe library work as expected.

In addition to taking sample images of microbeads with DNA nanobarcodes bound to them, we mapped the microbead fluorescence intensity ratios for each bead on a red-green scatter plot. The average red and green fluorescence intensity measured across the total area of a particular microbead correlates to an X and Y value, respectively, in the scatter plot. Each dot represents a single bead, and in total hundreds of beads in the microfluidic device array are measured and plotted. As seen in **Figure 2.9 B**, microbeads carrying the same DNA nanobarcode ratio form a cluster of points with a linear trajectory. Because this plot has logarithmic axes, these dot clusters are in roughly parallel lines that can be clearly distinguished from each other. This logarithmic plot enables highly precise

mapping of the microbead-array fluorescence intensities and rapid identification of different targets through the separate nanobarcode dot-cluster locations.

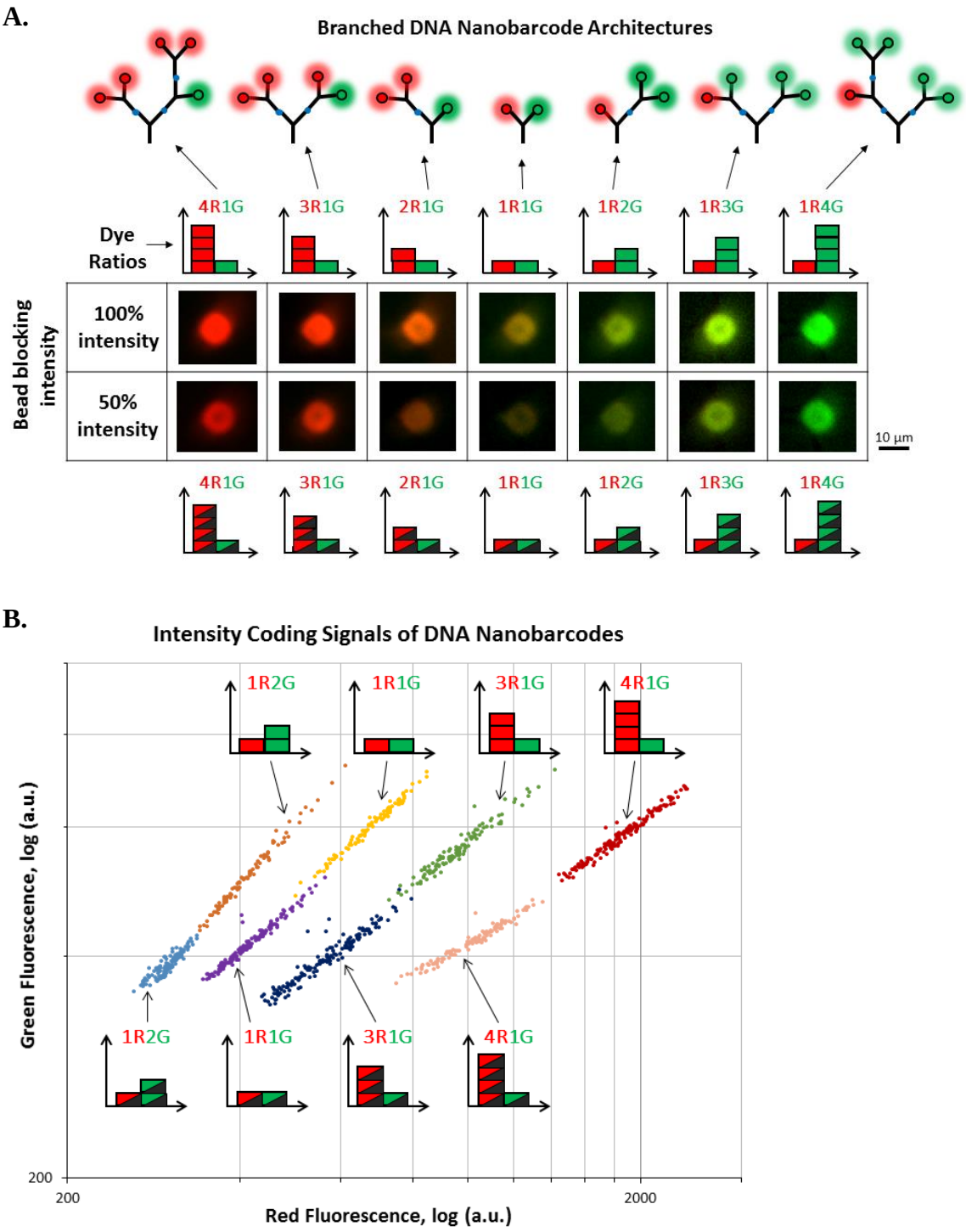

Figure 2.9 Fluorescence microbead read-out for DNA nanobarcode probe library

A) DNA nanobarcode probe library spectrum using different combinations of red and green fluorescence dyes and microbead surface intensity-blocking. The top row includes schematic drawings of the DNA nanobarcode branched structures, and corresponding dye

ratios and microbead images are shown in the row below. **B)** Scatter plot (logarithmic axes) of the collective microbead data for each DNA nanobarcode binding test. Each set of test data contains measurements for over 200 microbeads. Both 0% blocked and 50% blocked microbeads were used to provide two stratified levels of DNA nanobarcode detection within the graph.

2.3.4 *Microbead-array resetting for performing multiple tests per device*

One of the challenges in developing portable, rapid diagnostics is that many of these tests are limited to one-time use, which can increase the cost and diminish the utility of a diagnostic. To overcome this obstacle, we developed a protocol to "reset" the DNA nanobarcode microbead-array system in a rapid fashion by washing the microbeads with a formamide (FA) solution. In molecular biology, FA is a commonly used denaturing agent for DNA. Most denaturing agents interact with the hydrogen bonds (H-bonds) in the DNA double helix, and FA is especially known for its ability to form H-bonds and to compete efficiently with the H-bonds between Watson–Crick base pairs.[298] Different studies have reported that FA lowers the melting temperature of free DNA in solution by 0.60% to 0.73˚C/% FA (v/v).[299-301]

Capitalizing upon this well-known behavior and the rapid reaction kinetics within microfluidic devices, we achieved rapid denaturation of all hybridized DNA targets and DNA nanobarcodes in the microbead-array in less than 1 minute. As seen in the scheme of **Figure 2.10 A**, we can trace the average fluorescence intensity of a large number of microbeads over time as the DNA nanobarcodes bind to the captured targets, and also demonstrate that FA wash quickly denatures all the DNA targets and DNA nanobarcodes. This hybridization-denaturation cycle can be graphed in relation to time, as seen in **Figure 2.10 B**. Remarkably, we discovered that we can repeat the hybridization-denaturation cycle at least seven times – effectively "resetting" the device without any significant loss in hybridization and detection performance. Furthermore, using this protocol we could reliably reset the microbead-array three times for a range of target concentrations including 1, 10, and 100 nM. **Figure 2.10 C-F** show these results and compares them to negative

controls. As expected, the negative controls (which involve unrelated and non-matching targets and DNA nanobarcodes) exhibit a plateaued line that is significantly different from the peaks shown by the positive detection tests.

From the perspective of nucleic acid detection, this resetting capability is unique – many DNA-based detection systems are restricted to one-time use, which can create a significant amount of waste. Instead, we have designed a microfluidic microbead-array system that facilitates rapid buffer exchange and byproduct removal. Not only does rapid buffer exchange allow for precise control of DNA probe hybridization through a series of increasingly stringent buffer washes, but it also allows for rapid FA solvent washes that are fast enough to avoid damaging the PDMS-based microfluidic device. Particularly in low-resource settings and third-world field clinics, re-usable devices are critically important for maintaining long-term health care capabilities in areas that cannot afford buying numerous disposable devices. Our device helps fill this need, and furthermore it achieves sensitive and specific multiplexed detection in a single test with a detection limit that is similar to commercially available antibody-based devices.

A.

Order	Step
1	DNA target binding
2	Nanobarcode binding
3	50% Formamide wash

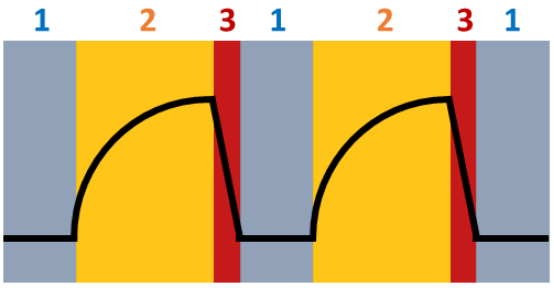

B.

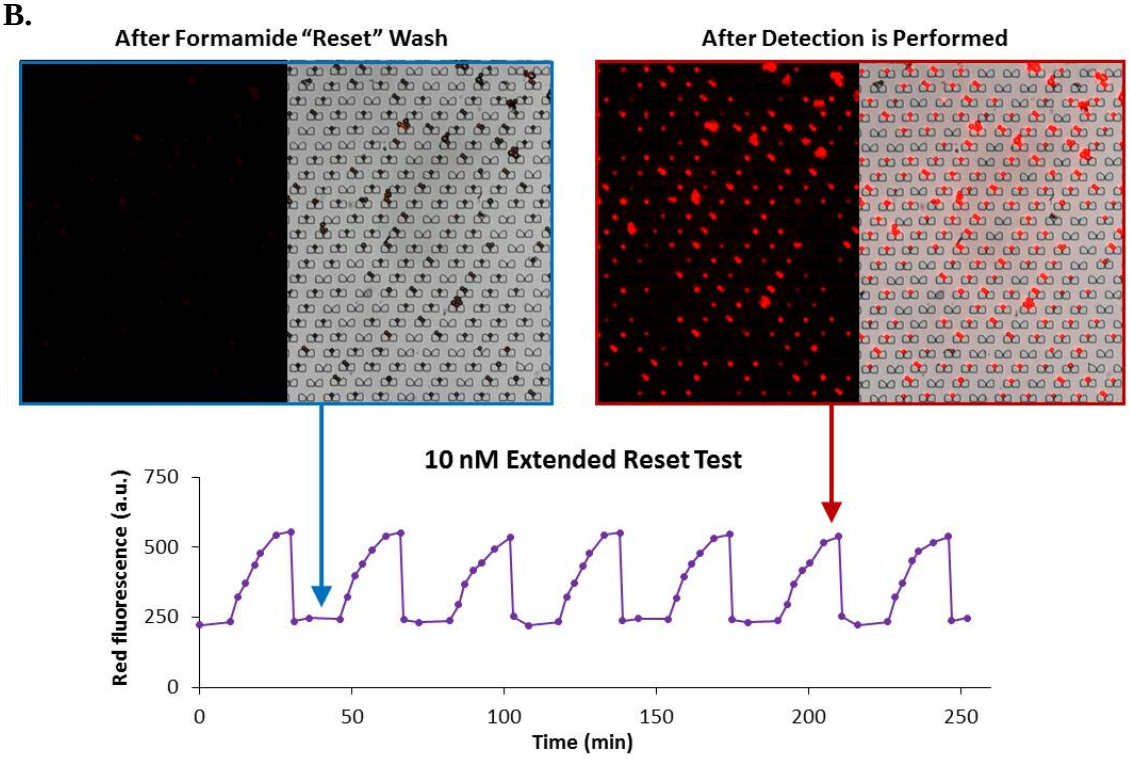

C.

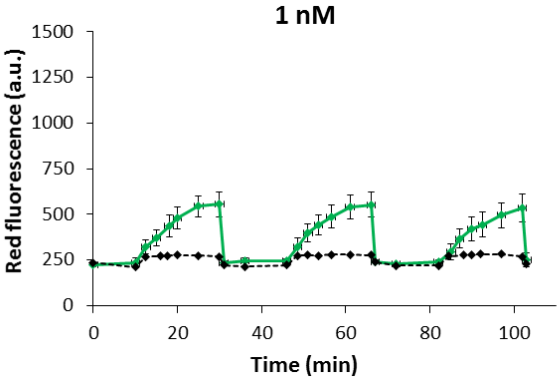

D.

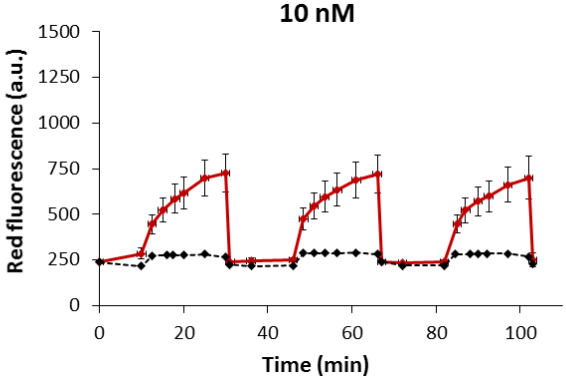

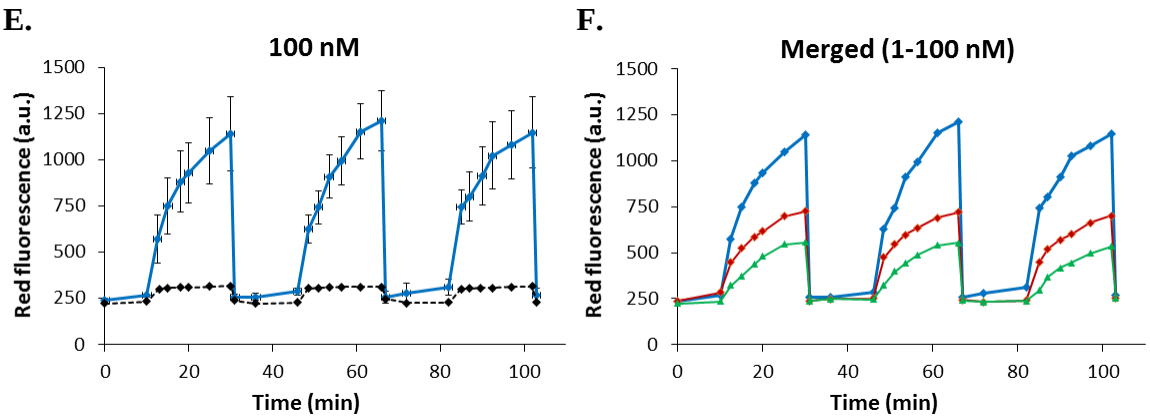

Figure 2.10 Resetting the DNA nanobarcode microfluidic device

A) Schematic of the steps involved in resetting the DNA nanobarcode microfluidic device after performing detection. **B)** Graph depicting successful resetting of the microfluidic device up to 7 times. Sample images show the microbead-array at the peak (maximum binding between beads, DNA targets, and nanobarcodes) and the trough (post-formamide wash dehybridization) of the graph. **C-F)** Fluorescence intensity data for three-time reset tests across three different target concentrations (1, 10, and 100 nM).

2.3.5 *Multiplexed detection of a panel of targets*

To verify that our DNA nanobarcode microfluidic device can achieve consistent detection of a range of target samples, we tested a titration of DNA targets at concentrations ranging from 1 nM to 1000 nM. To also demonstrate that the multiplexed detection accuracy is consistent across the detection range, each target titration test used two different synthetic DNA samples with sequences from two different viral genomic DNA targets. As seen in **Figure 2.11 A-D**, we successfully performed simultaneous detection of two targets for the entire range of target samples. For these tests, the average fluorescence intensities (red and green) were measured per microbead and plotted in a scatter plot with x and y axes representing red and green dye intensities, respectively. As expected, the microbeads form linear clusters with distinct slopes. Because these plots have linear axes, the linear clusters are not parallel and their slopes are unique for each DNA nanobarcode fluorescence ratio code. The different slopes helps to clearly delineate the different pathogen targets in a multiplexed test read-out. All the data was plotted together in **Figure 2.11 E**, which demonstrates the consistency across different target amounts and also distinguishes the two linear cluster-lines representing the two different DNA targets.

As with most multiplexed detection systems, it is important to test the system with different numbers of targets to confirm the system is accurate and specific. In addition to two targets, we performed simultaneous multiplexed detection tests for 3, 4, and 5 different DNA targets. **Figure 2.12 A-B** show the 3-target detection test with the actual fluorescence images from the microbead-array. The three separate linear clusters can be clearly identified and do not exhibit significant signal overlap, and furthermore the corresponding fluorescence images reveal the individual fluorescence dye ratios by the distinct color

differences (red vs. green vs. yellow-orange) in the microbeads. Increasing the number of targets to 4 and 5 does not diminish the detection signal read-out magnitude, and moreover the slopes remain consistent across the different detection tests. (**Figure 2.12 C-D**) In fact, the data points (each point representing one microbead) conform closely to a specific linear trajectory and generate a thick cluster of points along this line. In summary, these graphs indicate that our DNA nanobarcodes specifically detect multiple targets in a single device without significant signal overlap. This is a critical feature, particularly for multiplexed detection of a panel of pathogens that exhibit very similar clinical symptoms in patients.

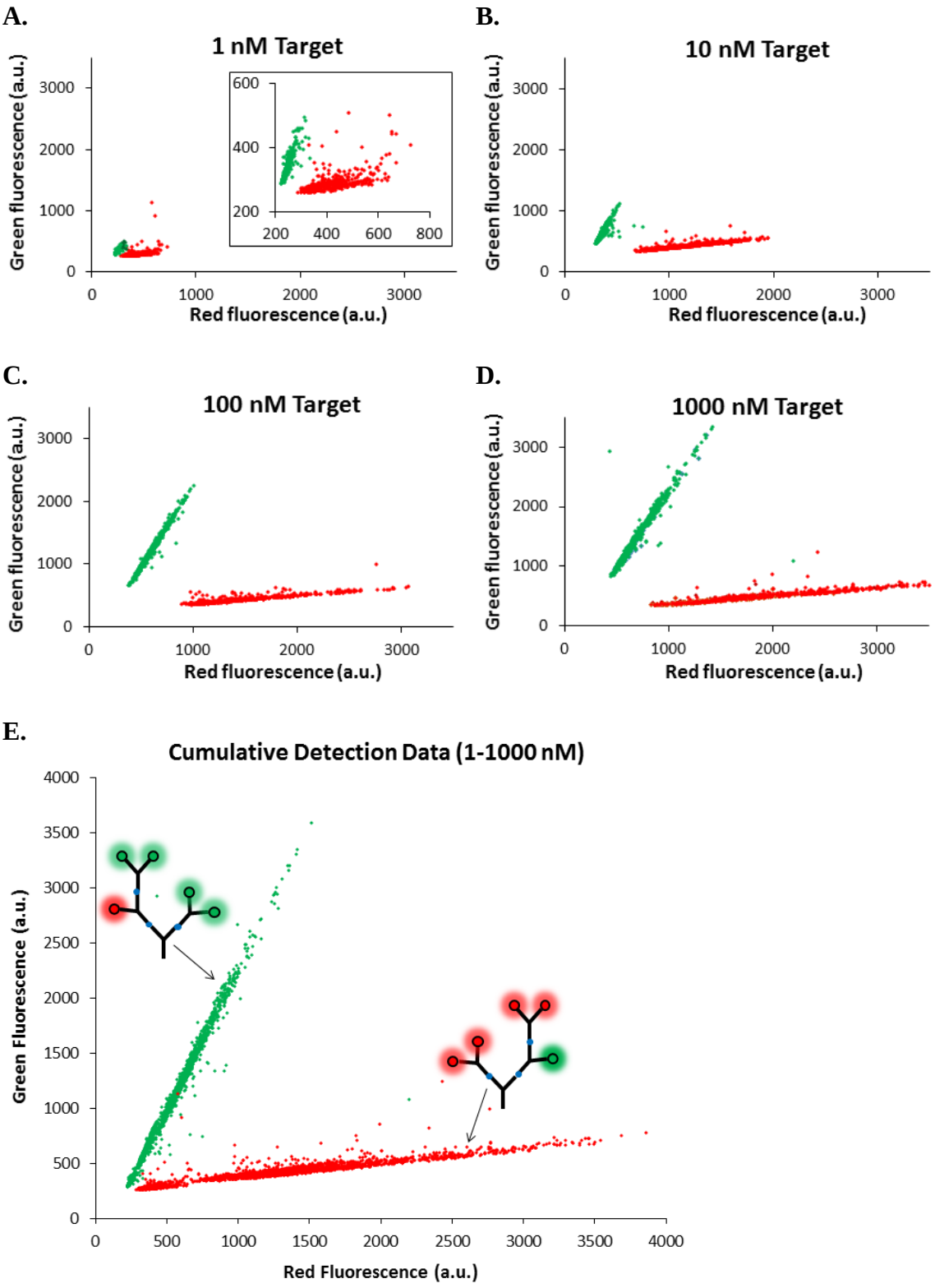

Figure 2.11 Multiplexed detection of DNA targets across different concentrations

A-D) Scatter plots of microbead-array data for 1, 10, 100, and 1000 nM DNA target detection tests (each plot shows aggregate data for triplicate tests). **E)** Cumulative graph

showing all data from the plots in **A-D.** The lines representing each DNA nanobarcode label are clearly distinguished and consistent across the different target concentrations.

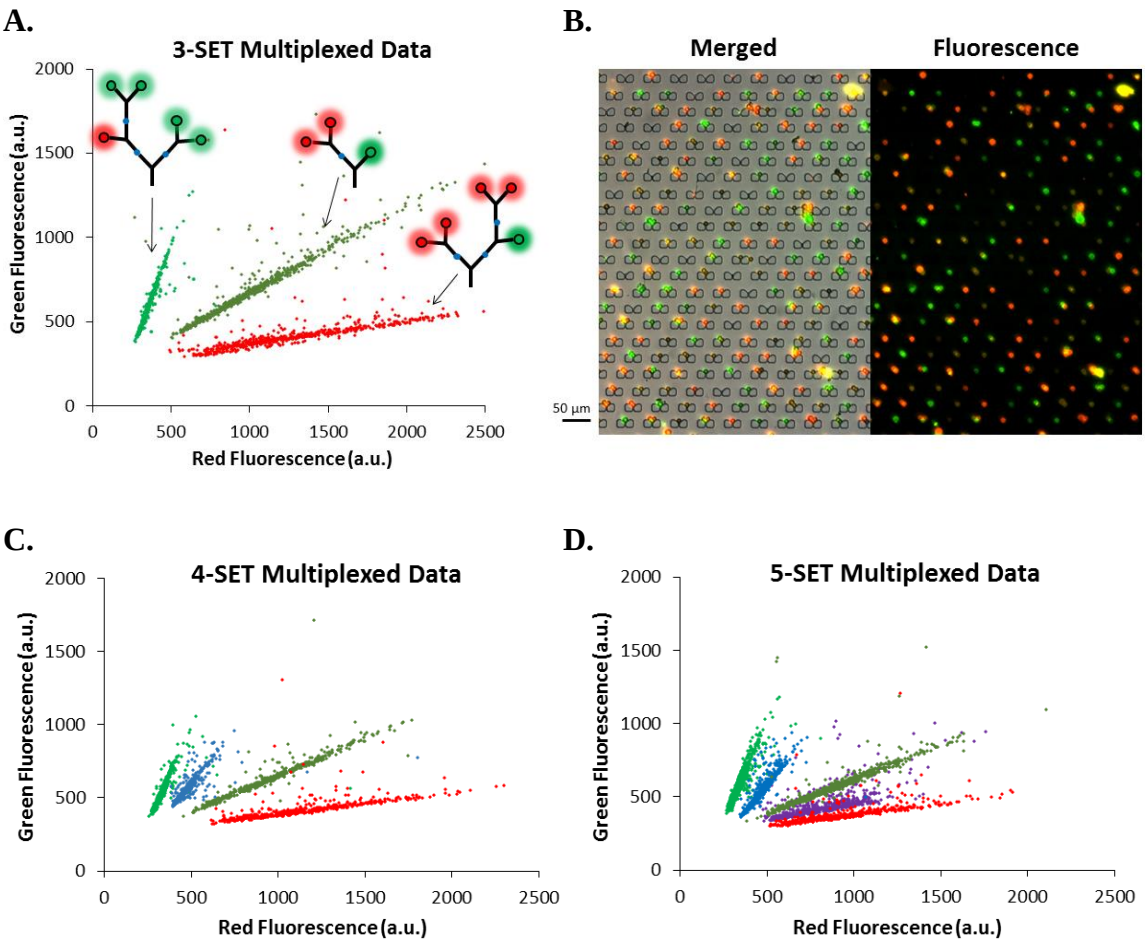

Figure 2.12 Multiplexed detection of 1-5 targets in the microbead-array device

A) Scatter plot depicting collected multiplexed data for three targets, using three different DNA nanobarcode ratio code labels. **B)** Corresponding merged bright field and fluorescence images of the microbead results for the 3-target multiplexed detection test. **C)** Scatter plot depicting collected multiplexed detection data for 4 different DNA targets. **D)** Scatter plot depicting collected multiplexed detection data for 5 different DNA targets.

2.3.6 *Detection limit of the microbead-array system*

Confirming accurate and sensitive detection at low target amounts is important for any clinical diagnostic system. We investigated the detection limit of the DNA nanobarcode microbead-array system by preparing synthetic DNA target samples with sequences drawn from Influenza A virus. Beginning with 1 nM, we prepared a titration of decreasing concentrations: 1 nM, 500 pM, 200 pM, 100 pM, 50 pM, 20 pM, and 10 pM until a detection limit was reached. Performing the standard detection reaction and using optimized hybridization conditions with wash steps, we discovered that the lower detection limit for the DNA nanobarcode platform is 50 pM. Beyond this point, the positive detection microbead-array data (10 and 20 pM) is not distinguishable from the negative control (unrelated target) data. Altogether, this data shows that we can achieve sensitive detection of DNA targets down to 50 pM, which is comparable in sensitivity to standard clinical detection methods such as ELISA. **Figure 2.13** depicts the microbead fluorescence data for these lower target amount titration tests. Our platform consistently detects up to 5 targets simultaneously, can achieve low-picomolar levels of detection, and can be reused more than 7 times without sacrificing performance. In all, these features create an effective, long-lasting detection platform that can have a significant impact on the clinical diagnosis of many types of viral and bacterial pathogens.

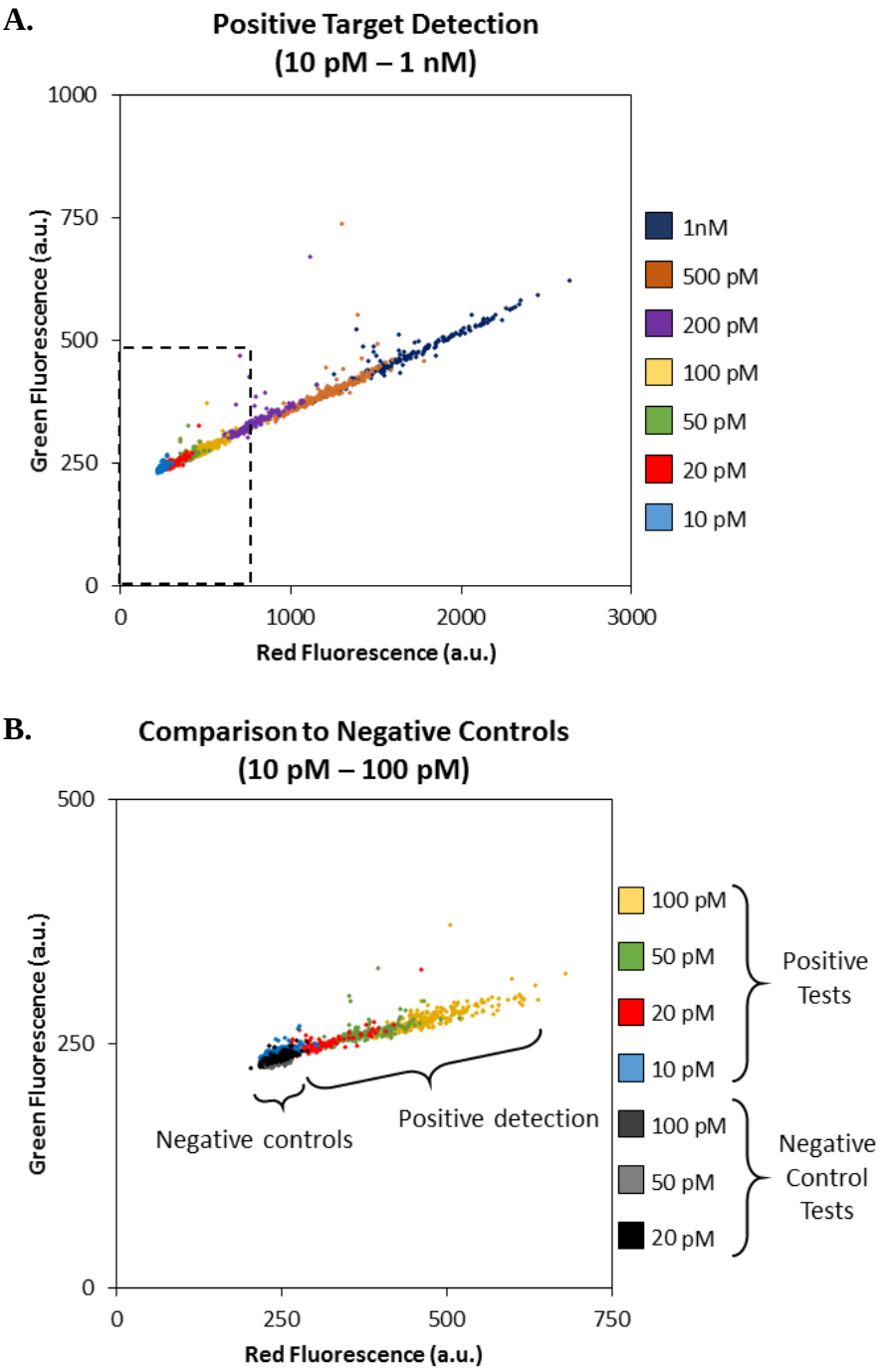

Figure 2.13 Detection limit for the DNA nanobarcode microbead-array system

A) Scatter plot of the collected microbead fluorescence intensity data for a target titration range of 10 pM – 1 nM. **B)** Scatter plot of collected microbead data comparing positive detection tests to negative controls at low target concentrations (10 – 100 pM). The negative controls are only distinguishable from positive detection tests at 50 pM DNA target concentration and higher, signifying that 50 pM is the detection limit.

2.3.7 *Statistical analysis of DNA nanobarcode results*

To further confirm our aforementioned observations, we performed statistical analysis on the multiplexed and detection limit data. We collected DNA nanobarcode red and green fluorescence intensity data for three synthetic pathogen DNA targets (labeled Target 1, Target 3, Target 5) that were used in triplicate multiplexed tests. For each microbead, we plotted the measured red and green intensities on an x-y axis. As expected, these points clustered and spread along three specific lines, each of which delineated a specific DNA nanobarcode label and, correspondingly, a particular pathogen target.

Based on our experimental observations, we used a linear regression method to fit a line to the data points collected for each target. Different targets are distinguished by different lines. (**Figure 2.14**) Therefore, we can statistically test whether the fitted slopes from the target data are significantly different. As a quick check, we calculated 95% confidence intervals (CI's) for each of the slopes in **Table 2.3**. From the table, with 95% in confidence, we concluded that the three slopes were positive (because the lower bounds of their confidence intervals were positive). We also confirmed that the three slopes were significantly different from each other (because their CI's did not overlap). These results further validate the accuracy of our multiplexed DNA nanobarcode detection platform.

We then statistically examined our positive and negative control detection tests for the titration of samples with low target concentrations. **Figure 2.15** presents three scatter plots with this data. In the left panel, the green dots represent data from the negative control 20 pM tests, and the blue dots represent data from the positive 20 pM detection tests. The middle and right panels depict the 50 pM and 100 pM positive and negative control detection data, respectively.

Considering these plots, we aimed to statistically verify that the positive test read-out data at low target concentrations (i.e., blue dots in these three cases) is discernable from the read-out data from negative control tests (i.e., the green dots). This can be considered a cluster analysis problem which has a few available analysis methods. Since we are particularly interested in obtaining a significant testing level (indicated by p-value), we choose the method by Liu et al.[302] with an open source software (R) implementation package *sigclust*. The statistical test is whether the green and blue dots come from the same cluster (or distribution), which serves as the null hypothesis. Using the *sigclust* software package, we obtained p-values (0.647, 0, and 0) for the three panels of data from the left to right in **Figure 2.15**. Thus, at the significant level of 0.05, we concluded that we could not distinguish the positive detection tests from the negative control tests for the 20 pM Target test. In contrast, the positive detection tests in the other two cases (50 pM and 100 pM Targets) were significantly different from the corresponding negative control tests. Together these statistical analyses further verify that the lower detection limit of our DNA nanobarcode microfluidic diagnostic platform is 50 pM.

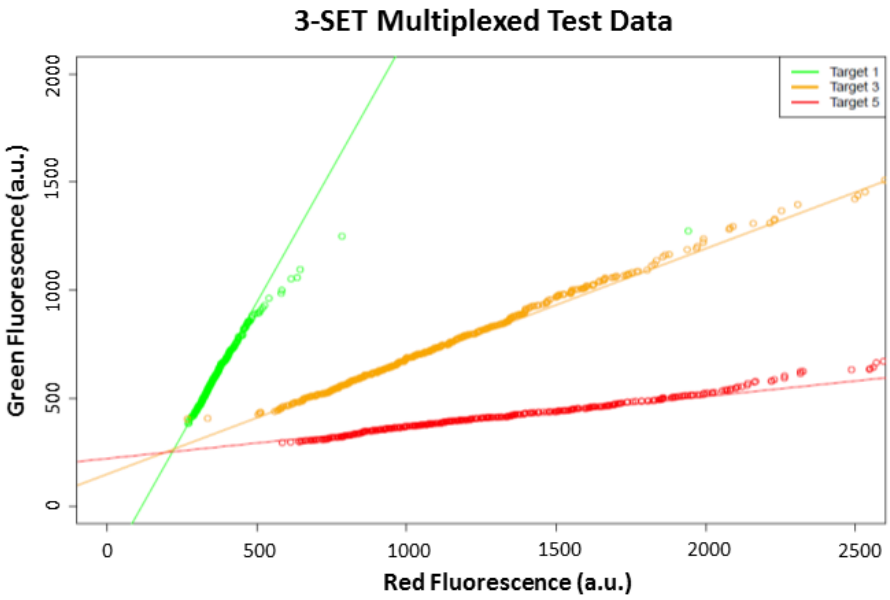

Figure 2.14 Scatter plots of three different target samples with three fitted lines

The graph shows that the collected microbead fluorescence read-out data conforms to distinct linear trends. Three fitted lines were drawn for each cluster of data points (different color for each target). These fitted lines provide information (e.g. a consistent and well-defined slope) for easy identification and decoding of the DNA nanobarcode detection read-out.

Target	Slope	Confidence Interval (CI)
1	2.454	(2.39, 2.469)
3	0.522	(0.518, 0.525)
5	0.144	(0.140, 0.147)

Table 2.3 Estimated slopes and 95% confidence intervals (CI's) for 3-target multiplexed detection tests

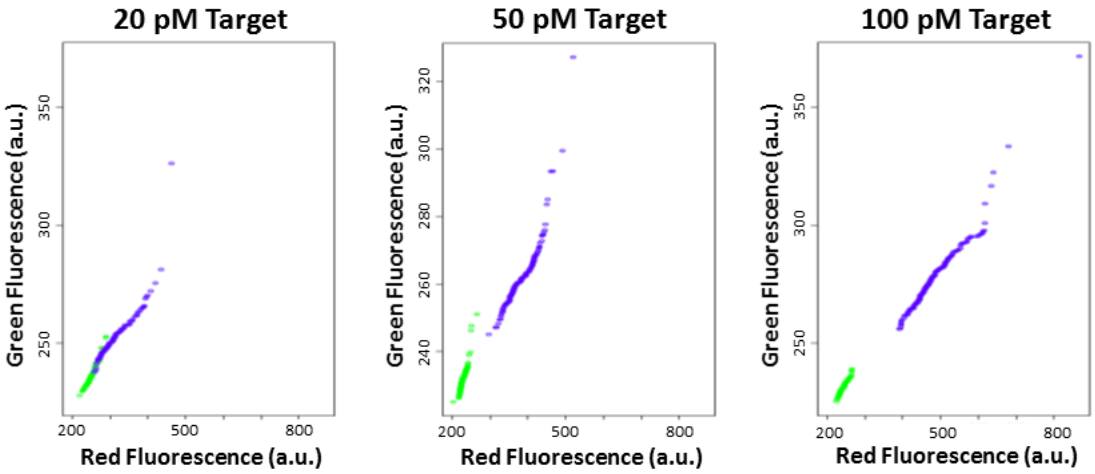

Figure 2.15 Scatter plots for 20, 50, and 100 pM detection tests

Scatter plots of three tests investigating picomolar-range DNA target detection. Blue dots represent positive detection test microbead data, and green dots represent the negative control microbead data for the corresponding target concentration.

2.3.8 *Detection of viral pathogens from real patient samples*

To test the real-world application of our DNA nanobarcode microbead-array diagnostic device, we used real patient samples from pediatric patients exhibiting *acute pharyngitis* (sore throat) symptoms. We chose *acute pharyngitis* patients because these symptoms can be caused by both viral and bacterial pathogens. In particular, we selected five pathogens causing *acute pharyngitis* for our DNA nanobarcode detection panel: Human Coronavirus, Human Rhinovirus, Influenza A, Herpes Simplex Virus, and Streptococcus pyogenes. Only one of these pathogens (Streptococcus pyogenes) requires antibiotic treatment – in the other cases, antibiotics are not required. One of the main concerns behind diagnosing *acute pharyngitis* is that misdiagnosis and improper administration of antibiotics for the wrong pathogen infection could lead to severe health issues and even death in pediatric patients. Therefore, accurate and informative multiplexed detection devices are needed to quickly rule-out the pathogens that do not require antibiotic treatments from the ones which require antibiotic treatments.

One of the main goals of our diagnostic system is to distinguish multiple pathogens in a single test. We first demonstrated this capability using synthetic pathogen targets, and next we sought to use real viral samples from clinical patients. To demonstrate this capability, we used two de-identified viral culture samples which were prepared from nasopharyngeal swabs. The nasopharyngeal swabs were used on pediatric patients with *acute pharyngitis* symptoms, as part of standard clinical diagnosis procedures. Our collaborator at Weill Cornell Medical Center, Dr. Christine Salvatore, collected the nasopharyngeal swabs and prepared the viral cultures for overnight shipment. Upon receiving the samples, we performed DNA/RNA extraction using the QIAamp Cador

Pathogen Mini Kit, and subsequently used these processed samples for multiplexed detection within the microbead-array diagnostic platform. Two nucleic acid samples from different viruses were flowed in series into the microfluidic device and allowed to bind to the microbeads using optimized hybridization conditions. Then, we infused the microbead-array with a panel of five different DNA nanobarcode probes, which were flowed individually and separated by stringent wash steps. Only the correctly matching DNA nanobarcode probe (that is, having a complementary sequence) will hybridize to its designated pathogen DNA target.

Figure 2.16 shows our detection results. In the graph, two distinct clusters of data points are visible. Each data point represents the average red and green fluorescence measurements for each bead following multiplexed detection. Based on our prior analysis of multiplexed detection tests using synthetic pathogen DNA samples, we can decode these clusters based on their specific slopes and locations in the scatter plot. We determined that these two clusters match two types of DNA nanobarcodes: 4R1G and 1R4G, which represent Influenza A virus and Human Rhinovirus, respectively. In summary, this data demonstrates that our system accurately detected two different viruses from real pediatric patient samples within a single device.

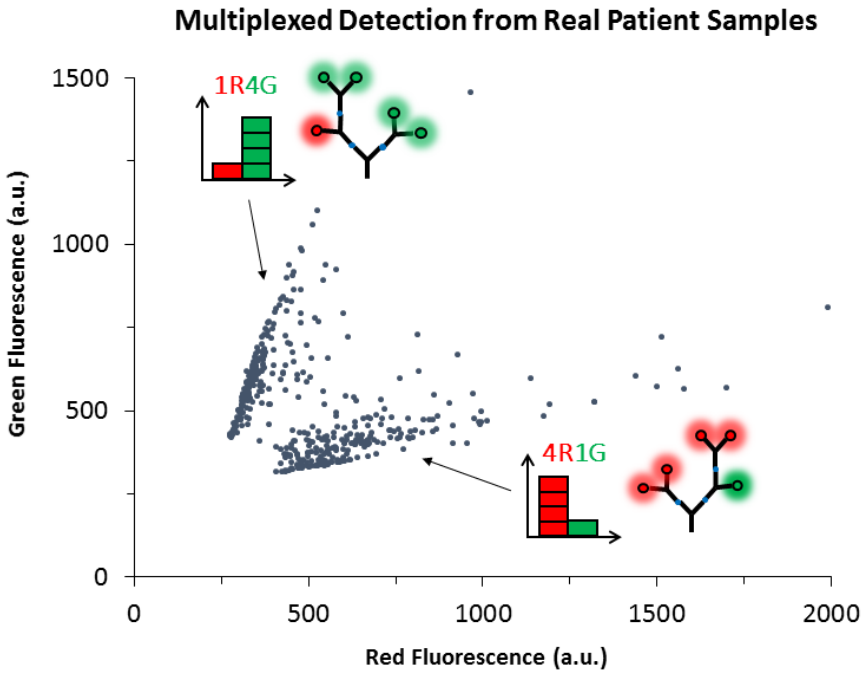

Figure 2.16 Multiplexed pathogen detection from real patient samples

Viral cultures from nasopharyngeal swabs were used as sources of DNA/RNA pathogen material. Following DNA/RNA extraction, the nucleic acid material was flowed into the microbead-array and allowed to hybridize to the capture probes on the microbeads. A panel of DNA nanobarcodes were then introduced and allowed to hybridize to all captured pathogen targets. Each DNA nanobarcode was flowed individually and washed with a stringent wash buffer to prevent nonspecific binding. The final results depicted in the graph here reveal two clusters, which were decoded to the 4R1G and 1R4G DNA nanobarcodes based on their slopes and locations in the plot. These DNA nanobarcodes represent Influenza A and Human Rhinovirus, respectively. The results demonstrate accurate detection of two different pathogens from real patient samples.

2.4 Conclusion

We have successfully created a system incorporating fluorescence-encoded DNA nanostructures in a microbead-array device that achieves multiplexed detection of pathogens. The DNA nanobarcode probe library was expanded by incorporating bead surface intensity-coding, through which a single DNA nanobarcode probe can be used to distinguish multiple targets without any additional dye labels. This, combined with a potential DNA nanobarcode probe spectrum of over 48 different dye-ratio combinations, yields a diverse probe library which is equal to or greater than other detection probe series available today. Moreover, the added advantage of highly controllable and modular DNA self-assembly makes the rational design of these probes both highly consistent and incredibly versatile.

We also discovered a remarkable resetting capability in our DNA nanobarcode system. Taking advantage of the rapid reaction kinetics within microfluidic devices and the strong DNA-denaturing property of formamide, we successfully repeated pathogen detection tests seven times in a single device without reducing detection performance. This resetting capability is very important because many DNA-based detection systems are restricted to one-time use, which can lead to a high amount of waste and additional costs for buying many more detection devices. Particularly in low-resource settings, outside field conditions, and third-world areas, it is critical to have re-usable devices that have extended lifetime without sacrificing detection accuracy. Our device does this, and furthermore it can perform multiplexed detection simultaneously in a single test. We achieved specific detection of 1, 2, 3, 4, and 5 DNA targets simultaneously, and have confirmed sensitive DNA detection within our diagnostic device for a target concentration range of 50 pM – 1

μM. Integrating multiplexed detection with a low detection limit is a critical feature, particularly for sensitive detection of a panel of pathogens which exhibit very similar clinical symptoms in patients.

In all, our platform utilizes branched DNA nanostructures as molecular-recognition probes for multiplexed detection in a microfluidic microbead-array format. It is a uniquely engineered system that avoids introducing the typical complexity and temperature cycling requirements in conventional diagnostic methods such as PCR and cell culture. Our work will significantly expand the DNA-based diagnostics repertoire, and it has immense potential for real-world clinical applications. In particular, it would be extremely useful for screening difficult to detect (and difficult to distinguish) bacterial and viral pathogens, a procedure which necessitates rapid and accurate diagnosis in order to protect patients from misdiagnosis and severe health complications.

CHAPTER 3

POINT-OF-CARE DIAGNOSTICS USING A SILVER-ENHANCED ISOTHERMAL DNA AMPLIFICATION SYSTEM

3.1 Overview and background

Rolling-circle amplification (RCA) is a powerful and versatile isothermal nucleic acid amplification strategy that is increasingly used in the development of bioassays and diagnostics. From a materials science perspective, the sequence engineering flexibility of RCA makes it useful in preparing highly-ordered nanoarchitectures and novel materials. More specifically, RCA products can be tailor-designed by manipulating the circular template, resulting in the generation of complex structures such as DNA origami,[303] nanotubes,[304] and DNA-based metamaterials.[305] Form a clinical perspective, the robust amplification of long ssDNA with repeating tandem segments makes RCA a simple way to exponentially increase low amounts of target and achieve easy-to-detect levels without the need for expensive thermocycling equipment.

Although RCA-based nanotechnologies have been used in a variety of applications such as biodetection, drug delivery, and the design of bioelectronics circuits, there is still a need for integrating RCA-based systems within more portable and accessible formats. Microfluidics is a technology that offers not only portability and ease-of-use, but also precise control of reagents and reaction steps. In this chapter, I will discuss the engineering of a microfluidic approach that combines RCA-based amplification of DNA/RNA targets with 2D DNA pattern formation to create a diagnostic platform with enhanced detection

sensitivity and POC read-out capabilities. Although this strategy was inspired by our previously-reported DNA meta-hydrogel research,[306] it differs from this past work in that it utilizes pure RCA under continuous microfluidic flow. In this way, single-stranded RCA products can be organized and weaved into a 2D DNA network within a micropost array in a highly robust and reproducible manner.

To the best of our knowledge, this is the first time RCA and microfluidic flow have been combined to construct 2D patterns as uniquely identifiable read-out signals for pathogen detection. This platform has been successfully used for the detection of plant virus pathogens from raw crude leaf extracts using less than 35 µl of reagents (including target sample) and in room temperature conditions. To achieve POC detection, I incorporated a silver staining methodology following the assembly of 2D DNA patterns within the microfluidic device. The resulting stained DNA product was easily viewed with the naked eye, and it could also be rapidly imaged using a generic smartphone camera. Overall, this system represents a significant step forward in POC detection because it integrates robust isothermal DNA amplification, flow-guided DNA nanopatterning, and naked eye silver staining strategies.

3.1.1 *Rolling-circle amplification for detection*

Rolling-circle amplification (RCA) is a straight-forward and efficient enzymatic amplification process that uses a DNA or RNA polymerase enzyme to generate long ssDNA or ssRNA products. During the RCA process the polymerase continuously adds nucleotides (nt) to a primer that is hybridized to a circular template. Over time, long ssDNA products can be generated in a few hours with tens to thousands of tandem repeats as the polymerase moves along the circular template and simultaneously displaces the newly

generated DNA strand. (**Figure 1.8** in **Chapter 1**) Among the polymerases that are used, ϕ29 DNA polymerase is most popular because of its exceptional processivity and strand displacement capability. In fact, research has shown that ϕ29 can process a very complex circular DNA template with topological constraints, four-way junctions and even multiple cross-overs.[307,308] ϕ29 can remain functional for 24 hours without a decrease in activity and it also has a low overall error rate (1E-6 – 1E-7).[309] Moreover, ϕ29 is highly robust and can function stably at low temperatures (up to 0˚C) and high ionic conditions (up to 100 mM) without a decrease in strand displacement or elongation performance.[310]

The RCA primer is also an important consideration as well. The RCA primer can be RNA or DNA, and it is often used as a target molecule that is detected with molecular level sensitivity through hybridization between the primer and the DNA template. In this strategy, the target DNA is used as a ligation template for a linear DNA probe (called a padlock probe) that is only ligated and circularized when it perfectly hybridizes to the correctly matching target. (**Figure 3.3** in ***Section 3.1.3***) T4 DNA ligase is typically used to ligate and circularize the padlock probe for performing RCA. Under standard reaction conditions, this enzymatic reaction is highly sensitive to mismatches – thus, the circularization reaction is extremely specific and can only occur if both template arms hybridize correctly and specifically to the target sequence. The fact that both ends of the probe must be fully hybridized to the target nucleic acid promotes extremely high detection selectivity.[311-314] Even a single mismatch in the ligation junction prohibits the circularization of the probe, which makes the padlock probe strategy an effective means for detecting single nucleotide polymorphisms (SNPs) and mutations.[315-317] Because the two template arms for ligation belong to the same molecule, the padlock probes are also

useful for highly multiplexed genetic assays because cross-reactive ligated probes generate linear sequences that cannot be amplified through RCA.

In addition, RCA is a powerful tool because it brings unique features that cannot be realized by traditional amplification methods such as PCR. For example, RCA can be conducted at a constant temperature (25-37˚C) in solution, on a solid support or in a complex biological environment (e.g., inside a cell).[318,319] Additionally, the repeat sequences within RCA products (which are complementary to the circular DNA template) can be custom-designed for downstream assembly of nanostructures and macroscale DNA materials. For instance, by careful design of the RCA template, these DNA products can incorporate functional sequences including DNA aptamers,[320,321] DNAzymes,[322,323] and restriction enzyme sites.[324,325] Multifunctional materials with diverse properties can also be assembled from these RCA products by attaching ssDNA with a functional moiety (such as a fluorophore, biotin, nanoparticle, antibody, etc.),[326-329] making RCA-based materials incredibly useful for sensing, biorecognition, and drug delivery.

For detection and diagnostics applications, RCA methodologies can be divided into two themes: solution phase and solid phase. In solution phase RCA, the RCA primers are present in solution from the start and the generated RCA products are homogeneously and dynamically free in the reaction solution, sometimes serving as triggers to initiate additional amplification cycles. Solution-based RCA has been utilized extensively for many applications involving the detection and analysis of nucleic acids, proteins, and other small molecules. For instance, Faruqi et al. used this strategy for high-throughput genotyping 10 SNPs in human genomic DNA. They discovered that SNP scoring by ligation exhibited a 100,000 fold discrimination against probes mismatched to the SNP.[330]

In addition to DNA, the padlock probe RCA approach has also been successfully applied towards detection of mRNA,[331] microRNA (miRNA),[332-334] and DNA methylations.[335,336] RCA can also be integrated with other enzymes for enhanced detection capabilities. Haiyun Liu et al. developed a process which incorporates nicking endonuclease with RCA, and using this method they achieved highly specific and sensitive detection of miRNA at the zmol level. In general, standard RCA amplified the target isothermally, and nicking reactions generated many copies of short ssDNA products which acted as "triggers" for additional amplification rounds. By generating a long ssDNA product that can be accessible for a range of manipulation techniques (chemical, enzymatic, etc.), RCA has become a potent and versatile detection strategy.

It is important to note that RCA is not constrained to solutions in small containers such as microcentrifuge tubes, which is a common drawback for other detection reactions. For example, Nilsson and colleagues used RCA for *in situ* genotyping in whole cells for both genomic DNA and mRNA.[337,338] Smolina et al. also achieved RCA *in situ* in whole cells to detect X- and Y-specific sequences on human chromosomes using PNA to locally open target dsDNA sites and enable padlock probe access and circularization.[339,340] In addition to nucleic acids, solution phase RCA has been broadly used for the detection of proteins and small molecules. The general strategy involves target binding-induced generation of RCA primers or circular templates. Ou et al., for example, developed a unique sandwich immunoassay in which an antibody functionalized liposome (containing multiple RCA primer copies inside) is captured by a target antigen and lysed to release the primers for performing RCA detection.[341] In similar immunoassays, other carriers can be used to supply many RCA primers for the protein detection assay such as: AuNPs for on-

nanoparticle RCA,[342] and streptavidin-conjugated antibodies for cascade signal amplification RCA.[343]

Conformational change can also be harnessed for performing RCA-based protein detection. Structure-switching DNA aptamers, for example, can be circularized upon interaction with a specific target. Ellington and coworkers used an aptamer that changes its structure only when binding to PDGF, which allows T4 DNA ligase to react with the aptamer, perform ligation, and generate a circular template for RCA.[344] Interestingly, DNA aptamers were also applied toward the detection of cocaine. In brief, cocaine induced a conformational change in the aptamer by forming a complex with it, and this caused the release of a short complementary sequence that further acted as a padlock probe and primer in RCA.[345] Another common RCA-based protein detection strategy is in situ proximity ligation (PL). In this approach, oligonucleotides tethered to antibodies against the two epitopes of a target protein (or protein complex) form a circular DNA template exclusively when bound in close proximity with the target. These proximity-initiated DNA templates allow localized RCA reactions to occur for *in situ* visualization and detection in cell lines and clinical specimens.[346] Combining RCA with the PL method has also been used to detect short RNA at the single cell level and cell surface markers.[347,348]

In contrast to solution phase RCA, solid phase RCA is performed on a surface such as glass, micro- or nano-beads, microwell plates, microfluidic device chambers and even paper strips. Solid phase RCA strategies bring several unique advantages including simple separation of the target from complex solutions, high-throughput analysis capability, and simple transition into POC environments. For example, surface-tethered DNA oligonucleotides can be used to capture target nucleic acids and make these targets

accessible to primer-templated ligation for a surface-initiated RCA reaction. Ali, et al. used this strategy for DNA detection on a paper strip,[349] and it has also been utilized in electrochemical detection of DNA mutation on magnetic beads.[350] In addition, Konry et al. described a high-density microarray for simultaneous detection of proteins and DNA via RCA.[351] Capture antibodies were immobilized on fluorescently encoded microbeads and a sandwich assay was performed for target proteins IL-6 and IL-8 using biotin-labeled secondary antibodies. Biotinylated capture DNA probes were then attached to the detection antibodies using an avidin bridge, enabling a padlock DNA probe to hybridize to the target DNA and become ligated for performing RCA.

Innovative detection platforms are being developed to harness the detection power of RCA and also incorporate more informative read-out signals as well. For example, Doyle and coworkers demonstrated a multiplexed, quantitative detection system for miRNAs on encoded hydrogel microparticles.[352] The miRNA targets were captured on gel-embedded probes on the microparticles, and surface-based RCA was performed with subfemtomolar sensitivity. Each microparticle was graphically encoded to have spatially segregated chemical regions for both encoding and target capture. The selective labeling of only those miRNAs that have been specifically captured and concentrated on immobilized probes has advantages over bulk enzymatic and chemical detection methods, such as higher efficiency, lower cost, and reduced labeling bias.[353,354] Lee et al. also reported a robust, sensitive, self-assembled optical diffraction biosensor that combines surface-based RCA and magnetic microbeads as a signal enhancement method.[355] Microcontact printed streptavidins were arranged on a surface in 15 μm wide alternating lines, and they were used to specifically capture and detect platelet derived growth factor

B-chain (PDGF-BB). Aptamers were used as a template for ligating the padlock probes for RCA. The resulting concatameric RCA product would hybridize to biotinylated ssDNA which was used to capture streptavidin-labeled magnetic beads. Overall, the signal from trapped PDGF-BB was amplified by the concatameric RCA product, and the diffraction intensity and microbead density on the surface varied as a function of PDGF-BB concentration. These self-assembled bead patterns allow visual analysis of molecular binding events under a simple bright field microscope without a need for complicated imaging systems.

3.1.2 *RCA-based DNA hydrogels and DNA materials*

In addition to detection, RCA systems can be integrated with DNA building blocks for self-assembly purposes. By combining RCA with DNA nanostructures, many materials can be created with unusual properties and functionalities that other nanoscale probes and linear DNA structures cannot achieve. Recently the Luo Lab used a ϕ29 polymerase enzyme to elongate DNA chains and weave them noncovalently into a hydrogel (termed meta-hydrogel).[356] The scheme of the hydrogel formation process is shown in **Figure 3.1**. Remarkably, this meta-hydrogel exhibited liquid-like properties when taken out of water and solid-like properties when in water. In addition, after complete deformation the hydrogel could return to its original shape upon the addition of water. Unlike conventional hydrogels, which have amorphous internal structures,[357-359] the meta-hydrogel has a hierarchical internal structure containing dense bird nest-like structures that are woven together by DNA. (**Figure 3.2**) This meta-hydrogel was used to create an electric circuit that used water as a switch, and furthermore it could find strong real-world applications in drug release, cell therapy, electric switches and flexible circuits.

In a different approach, the Hammond group invented a delivery vehicle that is simultaneously both carrier and cargo using rolling-circle transcription (RCT).[360] More specifically, they used RCT to create long, pure RNA interference (RNAi) polymers that self-assembled into nanoscale sheets of hairpin RNAs, which eventually formed microsponge-like particles over time. These RNAi-microsponges were assembled from cleavable RNA strands, which were only cleaved after cellular uptake whereby the cell's natural RNA machinery could convert the stable hairpin RNA structures into siRNA. This process enables the siRNA to remain protected during delivery and transport into the cell cytoplasm. A single microsponge contains over half a million copies of siRNA, making it a highly potent vehicle for cellular delivery of siRNA at low cost and with a relatively straight forward assembly process.

As previously discussed, DNA is an incredibly adaptable and programmable building block for assembling well-defined nano- and microscale architectures. RCA-generated DNA products are especially attractive for constructing multifunctional materials because they are well-suited for a number of roles such as: periodic assembly, bridging nano- and micro-scale regimes, and creating multivalent synthetic ligands. In particular, the repeating tandem sequences in RCA products are complementary to the DNA circular template, and thus they carry a predefined sequence order and can be produced at high yield for large-scale periodic assembly. One of the early examples of RCA-based templated assembly was 1D periodic assembly of DNA functionalized AuNPs, which were complementary to RCA products.[361,362] RCA has also been performed on the surface of AuNPs to generate a 3D scaffold for extended periodic assembly with a second batch of AuNPs.[363] Other particles can be arranged on RCA products as well. For example,

Willner and coworkers grew metallic nanowires by assembling glucose oxidase (GOx)/AuNP seed conjugates on RCA products.[364] Willner's group continued their work by reporting an RCA product containing thrombin and lysozyme aptamer sequences, which facilitated the organized assembly of multiple proteins through aptamer–protein binding.[365]

In addition to periodic arrays of particles, RCA products can be used to assemble large architectures with high precision and accuracy. Sleiman and coworkers generated DNA nanotubes using a backbone scaffold made of RCA products. More specifically, these RCA scaffolds were used for the assembly of triangular DNA "rung" structures incorporating stimuli responsive block copolymers and a set of linking strands.[366,367] Additionally, Fan and colleagues developed a range of DNA structures such as 1D nanowires, and 2D nanoplates and multilayer 3D nanoribbons using RCA products as guiding backbones and a few staple strands.[368,369] Overall they demonstrated that the RCA circular template design, its molar ratio to staple strands, and the concentration of the RCA products can be modified to precisely tune the size, structure and configuration of the final nanostructures. Because RCA can be extended to 2D and 3D structures, it can be exploited for the assembly of multifunctional architectures in solution or in microfluidic platforms. Zhao et al. created a microfluidic platform to capture and isolate rare circulating tumor cells from blood for diagnostic applications.[370] The RCA products extended tens of micrometers and contained repeating aptamer domains that bound to protein tyrosine kinase-7, which is overexpressed in many human cancer cells. The 3D DNA network improved cell capturing efficiency and furthermore the microfluidic system enabled highly precise control of important parameters including DNA graft density, length, and cell flow through for optimized diagnostic performance.

Taken together, RCA is an amazing strategy for achieving efficient isothermal amplification, single molecule sensitivity, structural versatility, and multivalency. RCA has been utilized not only for nucleic acid and small molecule detection, but it also has been applied to constructing novel architectures (ranging from 1D to 3D), drug delivery, tissue engineering, and manipulating cell biology. New technologies combining RCA and microfluidics are emerging, which adds both precise control of RCA parameters and added functionalities afforded by microfluidic technology such as low sample consumption and simple visualization. That said, the integration of these two methodologies is in its early stages and there is still a need for more sophisticated RCA patterning and more efficient read-out visualization for POC diagnostics. In the next section, I will describe my research which combines RCA and microfluidics to achieve a novel diagnostic platform with a robust, naked eye read-out and a novel DNA patterning strategy.

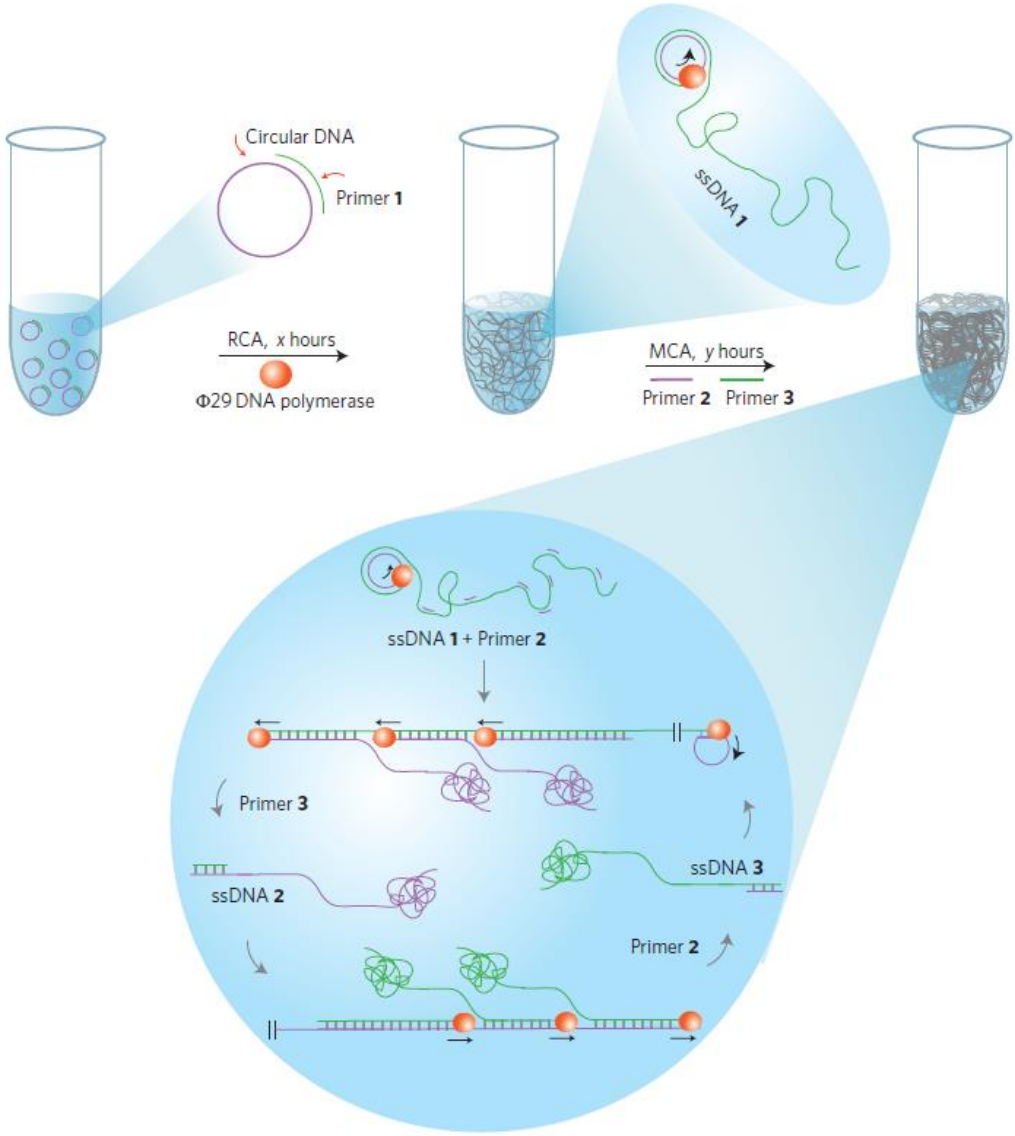

Figure 3.1 Schematic diagram of DNA meta-hydrogel synthesis

The RCA and MCA processes were carried out in two main steps. First, in the RCA (R) process, a circular ssDNA template was produced and a complementary primer for RCA (Primer 1) was hybridized to the circular template. This binding enabled ϕ29 to produce elongated ssDNA products (termed ssDNA 1: tandem repeats of the sequences complementary to the original circular ssDNA template). Second, in the MCA (M) process, which occurs after RCA, two additional primers (Primer 2 and Primer 3) were added for extra chain amplification. Primer 2 was elongated to generate ssDNA 2 (complementary to ssDNA-1). Primer 3 was used to create ssDNA 3 (complementary to ssDNA 2; thus ssDNA 3 and ssDNA 1 had exactly the same sequences). Primer 2 was therefore also able to produce more ssDNA 2 using newly synthesized ssDNA 3 as templates, leading to chain amplification.

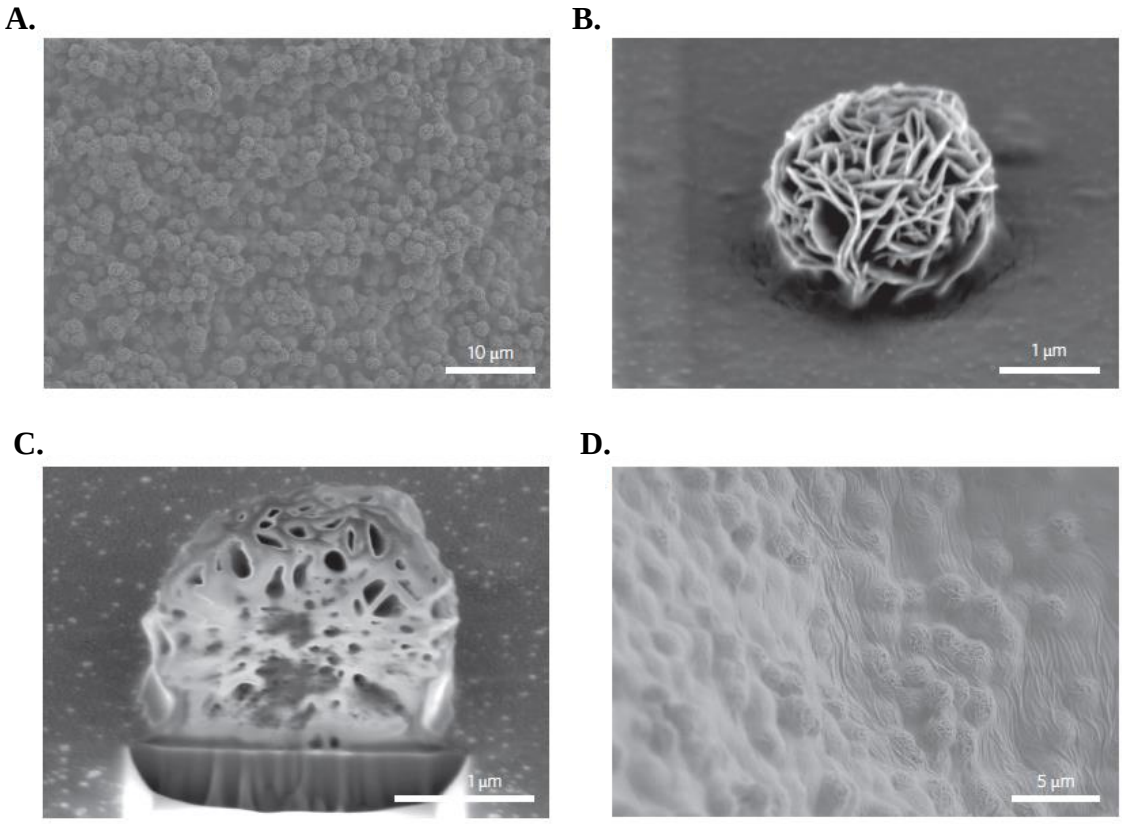

Figure 3.2 Morphology of the DNA meta-hydrogel

A) SEM images of R4M16 DNA hydrogel made by using RCA (R) and MCA (M). The numbers next to R and M represent reaction time in hours for each step, respectively. **B-C)** SEM images of an individual DNA bird nest, which was isolated from the DNA hydrogel **(B)** then cut with a focused ion beam **(C)**. **D)** SEM image for the DNA hydrogel using times of R0M16.

3.1.3 *Diagnostic approach*

I have developed a novel diagnostic system that achieves two things: 1) it uses RCA to specifically detect small amounts of DNA or RNA targets by generating an amplified detection signal, and 2) it uses microfluidics to assemble the RCA products into a periodic 2D pattern which can be quickly detected with the naked eye using silver staining. More specifically, the detection of pathogen targets in this diagnostic system begins with padlock probe RCA, through which a target (viral genomic DNA or RNA) hybridizes to a linear DNA template (padlock probe) to connect the padlock probe ends and enable ligation-based circularization. (**Figure 3.3**) After circularization, the target sample is mixed with the reagents necessary for performing RCA and then flowed slowly through a microfluidic device containing a chamber with an array of microposts. To facilitate pattern formation within the microfluidic chamber, ssDNA-coated polystyrene microbeads (10 μm diameter) were used as a substrate for capturing the circularized DNA padlock probes and anchoring RCA products as they were being generated by ϕ29 polymerase enzymes. The entire RCA reaction is performed simultaneously while the solution is continuously flowed through the microfluidic array (at flow rates ranging from 0.02 – 0.2 μl/min depending on the required detection sensitivity). Therefore, fluid flow provides a force for directing RCA growth through the micropost array. Using optimized detection conditions, microfluidic flow and DNA amplification created periodic 2D DNA patterns within the device with great precision and reproducibility for a range of target samples. **Figure 3.4** depicts the scheme for this novel diagnostic strategy.

Although our RCA detection reaction can be performed in solution within microcentrifuge tubes, the resulting RCA products from this scenario are irregular

aggregates that are difficult to image and incapable of providing quantitative or even semi-quantitative information. Rather than use solution phase reactions, I designed a microfluidic device with an array of posts for facilitating RCA-based DNA pattern formation. Importantly, the RCA pattern was used as an orthogonal signal (totally independent to other detection signals such as fluorescence) which acted as a read-out confirmation for accurate pathogen detection. To avoid using expensive or complicated equipment with our detection platform, a silver staining methodology was developed to stain the RCA DNA pattern after it was formed. Using this silver stain method the microfluidic device can be imaged with the naked eye because the silver stain causes the DNA to appear dark black within the microfluidic chamber. The silver staining methodology is well characterized and highly sensitive, and it is the perfect vehicle for achieving POC detection of viral DNA or RNA with minimal complexity and low cost.

The RCA-based diagnostic assay includes three main steps: 1) target detection using sequence-specific padlock probe ligation, 2) target amplification through a flow-guided RCA reaction, and 3) signal read-out by combining periodic DNA patterns with fluorescence or silver staining strategies. More specifically, padlock probe ligation is performed when a specific pathogen DNA (or RNA) target and a linear DNA padlock probe template hybridize together and T4 DNA ligase is introduced. Next, the pre-ligated padlock probes are combined with the reaction mix (including ϕ29 polymerase) for performing RCA. The entire solution is then slowly infused into a microfluidic device that has been prefilled with DEPC water and microbeads. One should note that microbeads are not absolutely necessary for pattern formation. By using different shapes and distances within custom-designed “no-bead” micropost arrays, RCA patterns could still be generated

from positive detection of a pathogen target. The RCA reaction mix is flowed over an extended period of time, ranging from 4 to 24 hours, and during this time the circularized padlock probe template is amplified tens to thousands of times. Interestingly, as RCA generates long ssDNA products, these products become deposited in and around the array microposts along fluid streamlines. Over time RCA-based "DNA fibers" are weaved together in a 2D network through physical entanglement and transient binding interactions between the RCA product strands. The final pattern is easily accessible to different DNA staining methods, including fluorescence and silver staining.

In agriculture, there is a critical need for portable and low cost devices which can be used in the field to accurately detect plant pathogens. Very few detection devices are commercially available to date and minimal research is being done in this area. I developed a microfluidic diagnostic system that not only helps address this problem, but also demonstrates a novel strategy for identifying nucleic acid material from any pathogen target (e.g. in humans, in animals, etc.) by the naked eye. This system was successfully used to detect two different plant virus pathogens from crude, minimally processed leaf samples derived from agricultural crops. Specifically, we targeted two common and rapid-spreading viruses: Cucumber Mosaic Virus (CMV) and Tomato Yellow Leaf Curl Virus (TYLCV). To improve the detection limit of our diagnostic, RCA reactions were performed at significantly lower flow rates and longer flow times. These extended reactions detected viral DNA and RNA targets in the femtomolar range, with a detection limit of 150 fM. In the following sections I will explain the methods and results of this research work and discuss its implications for POC diagnostics.

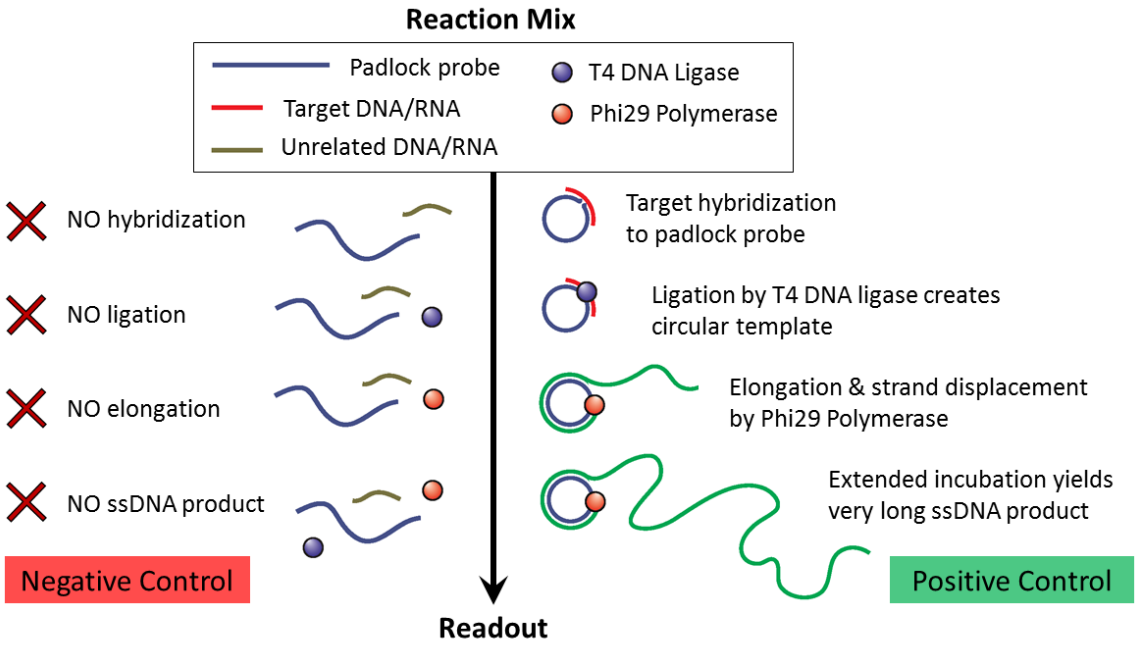

Figure 3.3 Schematic illustration of the lock-and-key RCA process

Lock-and-key RCA involves a DNA padlock probe, a nucleic acid target (DNA or RNA), and two enzymes: T4 DNA ligase and ϕ29 polymerase. The padlock probe is a linear DNA that becomes circularized only in the presence of the correctly matching complementary DNA (or RNA) target, which acts like a "key". Once the target hybridizes to the padlock probe, it enables T4 DNA ligase to circularize the padlock probe. After the padlock probe is ligated into a circular template, ϕ29 polymerase is able to use this template to generate long ssDNA in continuous tandem repeating segments. When no matching target is available, ligation cannot occur, which effectively inhibits the entire amplification process.

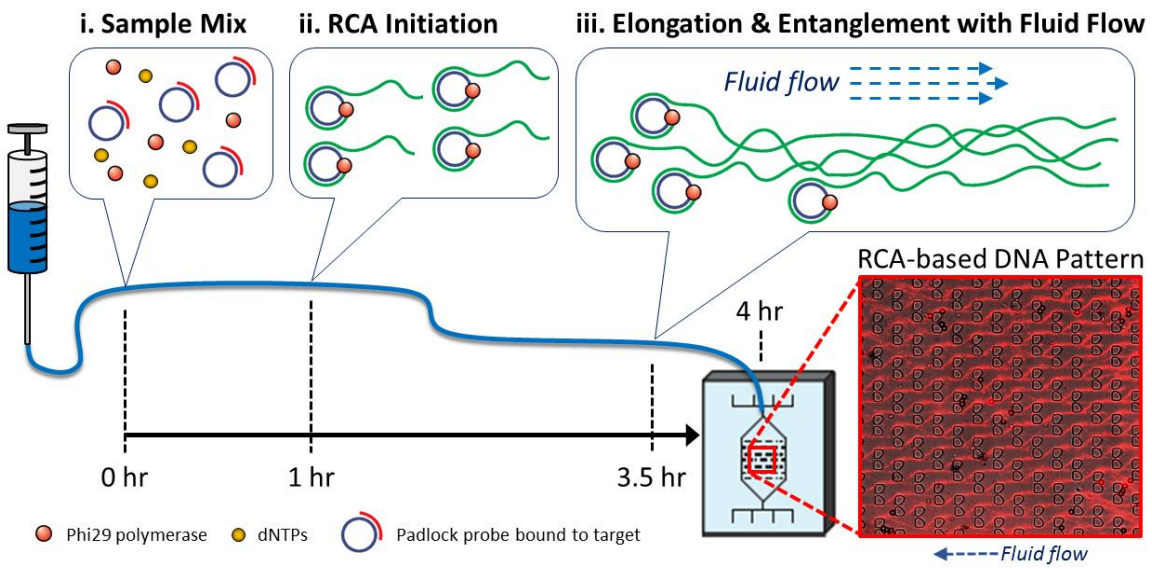

Figure 3.4 RCA-based detection with continuous flow in the microfluidic device

Our system generates uniform DNA patterns by using simultaneous RCA and fluid flow with a micropost-array microfluidic device. **(i)** First, all the reaction components are combined in a sample mixture and loaded into a syringe with long microtubing interconnecting the syringe to the microfluidic device. **(ii)** The reaction occurs over a 4 hour period, during which the sample mix continually flows at 0.1 µl/min through the microtubing and into the device. **(iii)** Over time the ϕ29 polymerase elongates the circular padlock probe, generating very long ssDNA products. Because this reaction occurs under continuous flow conditions, the ssDNA products physically entangle and form thick fibers. Due to hydrodynamic force, these DNA fibers entangle and weave around the micropost array structures, generating a 2D RCA-based DNA pattern within the microfluidic chamber which can be rapidly stained for easy detection read-out.

3.2 Materials and methods

3.2.1 *Chemicals, materials, and DNA sequences*

T4 DNA ligase was purchased from New England Biolabs (Beverly, MA). The ϕ29 polymerase kit including the enzyme, reaction buffer, DTT, and dNTPs, was purchased from Epicentre (Madison, WI). OmniPur DEPC (Calbiochem) was purchased from EMD Millipore Headquarters (Billerica, MA). Polystyrene microbeads were purchased from Bangs Laboratories (Fishers, IN). Dow Corning 184 Sylgard Silicone Elastomer (PDMS) was purchased from Fisher Scientific (Waltham, MA). Hamilton Gastight syringes (250 µl volume) were purchased from Hamilton Company (Reno, NV). Microfluidic syringe pumps were purchased from Harvard Apparatus (Holliston, MA). Custom-designed oligonucleotides were commercially synthesized and PAGE purified (Integrated DNA Technologies, Coralville, IA). The oligonucleotide sequences are listed below.

Microbead Capture Probe Sequence	
Name	5' - 3' sequence
Cap-RCA	/5Biosg/AAAAAAAAATACTGCGTTGGTACGTTAG

Table 3.1 List of sequences used to functionalize polystyrene microbeads

Padlock Probe Sequences	
Name	5' - 3' sequence
CMV-Temp	/5phos/GCCTAGGTCACACTCGATGTTCCTAACGTACCAACGCAGTATTATGGACTG CATCCAATGATGCCG
TYLCV-Temp	/5phos/CCCTCTATTTCAAGAGATGTTCCTAACGTACCAACGCAGTATTATGGACTGG GGAGATAAACAATC

Table 3.2 List of sequences used for RCA-based detection of viral DNA targets

3.2.2 *Sample preparation from plants infected with agricultural viruses*

Total nucleic acid (TNA) extraction from raw leaves: 150 mg of Tomato yellow leaf curl virus (TYLCV) infected leaf material from tomato (*Solanum lycopersicum L.*) was ground in a mortar in liquid nitrogen. 900 µl of extraction buffer (2% CTAB, 2.5% PVP-40, 2 M NaCl,100 mM Tris-HCl pH 8.0, 25 mM EDTA pH 8.0) warmed to 65˚C was added and then the sample was placed on a thermomixer with shaking for 1 hour. An equal volume of chloroform: isoamyl alcohol (24:1 v/v) was added and the tube was vortexed before centrifugation at 11,000 g for 10 min at 41˚C. The supernatant was recovered and the chloroform: isoamyl alcohol step was repeated. The supernatant was transferred to a fresh tube with 70 % vol isopropanol added and centrifuged at full speed for 15 min at 4˚C. Liquid was poured off and the resulting pellet was washed once with 500 µl of 70% ethanol by centrifuging for 2 min at full speed. The pellet was then air dried and resuspended in 50 µl sterile distilled water.

Rolling-circle amplification (RCA) for generating positive control samples: RCA of TYLCV samples for system optimization was carried out using the Illustra TempliPhi 100 Amplification Kit (GE Healthcare, Pittsburgh, PA) according to the manufacturer's instructions. 1µl of TNA mixed with 5 µl sample buffer was heated at 95˚C for 3 min, cooled to room temperature, mixed with 5 µl reaction buffer and 0.2 µl enzyme mix and incubated for 18 hours at 30˚C. 2µl of the final reaction was then digested with EcoRI to confirm restriction pattern was consistent with TYLCV.

CMV 200mer and 500mer RNA transcripts for optimization tests: Using a CMV (strain Fny) RNA3 construct 309 (Rizzo and Palukaitis, 1990) as a template, PCR was done using AccuPrime^{TM} Taq (Life Technologies, Carlsbad, CA) with the following

primers. For CMV-11c.2 probe in the movement protein ORF; forward T7 primer (p980.CMVFny3.T7.151s) CGTAATACGACTCACTATAGGGAGACTCAACAGTCC TCAGCGGCTACGTC with either (p982.CMVFny3.360as) ATAATTCACCAACAT CATATCCAGA for the 200mer amplicon or (p983.CMVFny3.660as) AATTACTACA CACGCTAGCTGTGGT for the 500mer. For CMV-8c.2 probe in the capsid protein ORF; forward T7 primer (p984.CMVFny3.T7.1526s) CGTAATACGACTCACTATAGGG AGAGTTACTACCTGATTCAGTCACGGAA with either (p986.CMVFny3.1711as) ACTCCAGATGCGGCATACTGATAAA for the 200mer amplicon or (p987.CMVFny3.2011as) GTAAGCTGGATGGACAACCCGTTCA for the 500mer. Amplicons were purified using Zymoclean™ (Irvine, CA) DNA recovery columns and quantified using a spectrophotometer. Transcriptions were carried out for 1 hour at 37˚C using 1 µg of PCR amplicon in a 50 µl reaction with 1 µl T7 polymerase (NEB, Ipswich, MA) according to the manufacturer's instructions. The reaction was then DNase treated, phenol/chloroform treated and ethanol precipitated. Pelleted RNA was resuspended in 50 µl sterile distilled water and quantified spectrophotometrically.

3.2.3 *Preparation of DNA-coated microbeads*

Streptavidin-coated 10 µm diameter polystyrene microbeads were suspended in wash buffer (40 mmol NaCl in 40 ml TE, 0.05% TritonX-100) and washed 3 times at 1200 RCF for 3 min. Biotinylated linear ssDNA capture probes (10 µM) were added to 10 µl of concentrated microbeads and incubated with rotation for 1.5 hours at room temperature. Following incubation, the ssDNA-functionalized microbeads were washed in wash buffer 3 times at 1200 RCF for 3 min to remove all excess unbound ssDNA capture probes. Final microbeads were resuspended in 200 µl wash buffer and stored at 4˚C prior to use.

3.2.4 *Fabrication of microfluidic devices*

The microdevices were fabricated using a standard soft lithography process at the Cornell Nanoscale Science and Technology Facility (Ithaca, NY). First, a CAD design was transferred to a chrome-glass mask using a Heidelberg Mask Writer DWL2000 (Heidelberg Instruments Inc., Woburn, MA). A 16 μm thick layer of negative photoresist, SU-8 2015 (MicroChem, Newton, MA), was spin-coated onto a clean 4 inch Silicon (Si) wafer, which was pre-baked at 90˚C for 3 minutes. Microfluidic features were defined using contact photolithography (Contact Aligner, ABM, Scotts Valley, CA) with an exposure time of approximately 15 sec. The Si wafer was post-baked at 95˚C for 4 min and developed for 3 min in SU-8 developer (Microchem, Newton, MA). The finished Si wafer mold was plasma oxidized and subsequently coated with an anti-stiction coating through molecular vapor deposition of (perfluorooctyl) trichlorosilane (FOTS) (MVD 100, Applied Microstructures, San Jose, CA).

Using the developed photoresist as a negative master, the microfluidic devices were micromolded with silicone elastomer, poly(-dimethylsiloxane) (PDMS), at a 10 : 1 (base : curing agent) ratio (Sylgard 184, Dow Corning, Corning, NY). After curing at 70˚C for 1.5 hours, the PDMS was removed individual devices were cut from the PDMS. Ports for tubing connections were punched at inlet and outlet locations, and then the PDMS devices were covalently bonded to PDMS-coated glass microscope slides (Fisher Scientific, Pittsburgh, PA) via plasma oxidation. These devices were designed to trap 10 μm diameter streptavidin coated polystyrene microbeads (Bangs Laboratories, Fishers, Indiana). Due to the polydispersity of the microbeads (and to prevent bead clumping), the heights of the microchannels and array chamber were set at 16 μm. A filter made of rectangular posts

was incorporated at the front of the microfluidic chamber to prevent debris from crude samples from clogging the trapping array. Each rectangular filter post was 20 x 30 μm dimension, the bead-trapping microposts were approximately 17 x 6 μm dimension, with the gaps between two bead trap halves were 2 μm. The array of trapping features can hold approximately 350 microbeads simultaneously. **Figure 3.7** in ***Section 3.3.2*** shows the final microfluidic device array design. Additional device designs for investigating DNA patterning mechanisms contained arrays completely comprised of rectangular microposts with varying inter-post spacing. (**Figure 3.21** in ***Section 3.3.8***)

3.2.5 *Synthesis of DNA patterns using enzymatic amplification and microfluidic flow*

2 μM linear DNA padlock probe template was hybridized with the designated target (or unrelated target in negative controls) using 65˚C heating for 3 min and gradual cooling (-0.5˚C/min) to room temperature. This hybridization reaction linked the two template strand ends together (lock-and-key strategy) to form a circular or padlock shape. T4 DNA ligase and T4 DNA ligase buffer were introduced to ligate these two strand ends together and form a circular DNA structure. In the case of RNA targets, RNAse inhibitor (40 units/μl) was also added during the ligation step. 10 μl of the hybridized circular DNA templates (with the target sample still present) were combined with 2 μl of ϕ29 DNA polymerase (100 units/μl) in 35 μl of sample mixture including 1X ϕ29 reaction buffer and 1 mM dNTPs. The entire sample mixture was loaded into a 1 mL plastic syringe and flowed through 12 inch long microtubing and eventually into the microfluidic device at 0.1 μl/min for 4 hours for standard reactions, and 0.02 μl/min for 24 hours for extended reactions (which increase detection sensitivity). All reactions were performed at room temperature with continual flow of the reaction mixture for the entire time period.

3.2.6 *Fluorescence microscope imaging*

An Olympus BX61 fluorescence microscope (Olympus America, Melville, NY) was used to obtain high quality fluorescence images of the DNA fiber patterns within the microfluidic devices. Following the RCA amplification-detection reaction, the DNA fiber patterns were stained with DNA-specific dye for 15 min at 0.2 µl/min. For optimization and crude leaf sample detection tests, 3X GelRed (Biotium, Hayward, CA) was used. For ssDNA-dsDNA fiber content analysis, both 3X GelRed, which is dsDNA-specific, and QuantiFluor ssDNA System (Promega, Madison, WI), which is ssDNA-specific, were used in series. Following DNA staining, the device was separated from the infusion syringes and immediately transferred to the microscope for imaging. Extended exposure times were used to image the DNA fiber patterns, ranging from 4 to 8 seconds.

3.2.7 *Silver staining within the microfluidic device*

The silver stain procedure for our microfluidic detection system uses a modified protocol from the Pierce Silver Stain Kit Thermo Scientific, Waltham, MA). For all the following steps, a syringe pump was used to infuse the solutions into the microfluidic device at 0.1 µl/min. First, the DNA pattern was washed for 5 min with ultrapure water. No fixation step was necessary for the DNA fibers since they were thoroughly assembled and entangled within the microfluidic device array. A sensitizer working solution (50 µl sensitizer with 25 ml water) was prepared and infused into the microfluidic device for 1 min, then the pattern was washed for 2 min with ultrapure water. A stain working solution (WS) was prepared from 0.5 ml Enhancer with 25 ml Stain. The WS was continually flowed into the device at 0.1 – 0.5 µl/min (depending on the thickness and density of the DNA pattern, a higher flow rate might be required) for 30 min to stain the DNA pattern.

Afterwards the DNA pattern was washed for 2 min with ultrapure water. Finally, a developer working solution (0.5 ml Enhancer with 25 ml Developer) was prepared and flowed into the device for 2 – 3 min until the DNA pattern appeared dark brown/black in color. Then stop solution with 5% acetic acid was introduced and flowed for 10 min.

3.2.8 *Tracer microbead flow mechanics study*

The microfluidic devices were prefilled with nuclease free water for 10 min incubation prior to use. An original stock of 1 μm diameter microbeads (Bangs Laboratories, Fishers, IN) was diluted 1/50x in wash buffer (40 mmol NaCl in 40ml TE, 0.05% TritonX-100) and flowed through the device at 0.05 μl/min for continuous observation of their flow paths. Using an Olympus BX61 microscope, (DIC mode, 20X objective) images were captured using an exposure time of 100 or 500 ms. Screen capture real-time images were taken at 20 fps (100 ms exposure) or 10 fps (500 ms exposure). Accumulated images over time were edited by Adobe Premiere, and the final file was exported to 10 fps video (Apple Prores 422 codec). Microbeads were tracked frame by frame using Motion software (Apple Inc.).

3.2.9 *Experimental setup*

All RCA experiments were conducted in a room temperature environment (20 – 25˚C) and without any thermal heating or cycling. Prior to device operation, DEPC-treated autoclaved water was perfused into the microfluidic chamber for a 10 min incubation period. 10 μm diameter DNA-coated polystyrene beads were pre-loaded and trapped in the microbead-array device design to enable capture of DNA ligated templates and, subsequently, initiation of DNA fiber formation. For all detection experiments, one syringe pumps was used to continually flow the reaction mix at a constant flow rate into the

microfluidic chamber. For silver staining the DNA fibers, all of the necessary reagents were infused into the microfluidic device in series for time periods similar to the reaction kit protocol instructions.

During operation, a syringe pump was used to control the input flow rates during continuous flow loading of the homogenous fluids. Experimental testing was completed after approximately 4 hours for standard tests, and 24 hours for low-target amount tests. Reaction volumes were typically 35 µl, and the same conditions were utilized for both DNA and RNA targets. To image the stained DNA fiber patterns after the detection reaction, the device was imaged with an Olympus BX61 fluorescence microscope for approximately 5 sec and raw image data of the micropost arrays were analyzed with ImageJ software. In brief, the images were normalized and contrast-adjusted to reduce background autofluorescence from the PDMS and show relative DNA fiber quantity differences between different target amounts detected.

The negative control experiments were also performed using the various microfluidic array device designs. Different negative controls were performed to confirm accurate RCA-based detection, including an unrelated target control (totally different, non-matching sequence) and unrelated microbead DNA capture sequence control. Additionally, control tests for nonspecific binding (as in, without any target present) confirmed that nonspecific binding does not significantly contribute to detection signals.

3.3 Results and discussion

3.3.1 *RCA-based DNA pattern formation in a microfluidic post-array device*

RCA is a robust enzymatic amplification process that generates long ssDNA products. Amazingly, we discovered that RCA can be performed at room temperature within a micron-sized microfluidic chamber with no decrease in enzymatic activity. Rather than use static incubation, microfluidic flow was utilized to continuously flow the RCA reaction mix through microtubing and then into the microfluidic chamber. The initial device that was used for performing RCA microfluidic reactions is shown in **Figure 3.5 A**. An array of micropost bead-traps was patterned throughout the chamber to enable microbead trapping and furthermore guide the DNA pattern formation resulting from

This process enabled both elongation and entanglement of RCA DNA products into long fibers, which were gradually guided and deposited into the microfluidic micropost array chamber. Upon reaching the microfluidic chamber, the micropost array provided a structural organization mechanism through which the DNA fibers could be arranged into a 2D periodic pattern. The RCA DNA fiber pattern is shown in **Figure 3.5 B**. Interestingly, the DNA fibers form specifically around the micropost trapping structures in linear waves with a diagonal trajectory, similar to the streamlines that define the fluid flow through the array. This micropost and flow-guided wave pattern can be seen in **Figure 3.5 C**. To the best of our knowledge, this is the first time RCA-based DNA products have been simultaneously generated and organized into a 2D periodic array using continuous microfluidic flow through a micropost array. The unique features of the 2D DNA pattern – periodic wave trends, growth through and around the microposts, etc. – are outlined in **Figure 3.6**.

A.

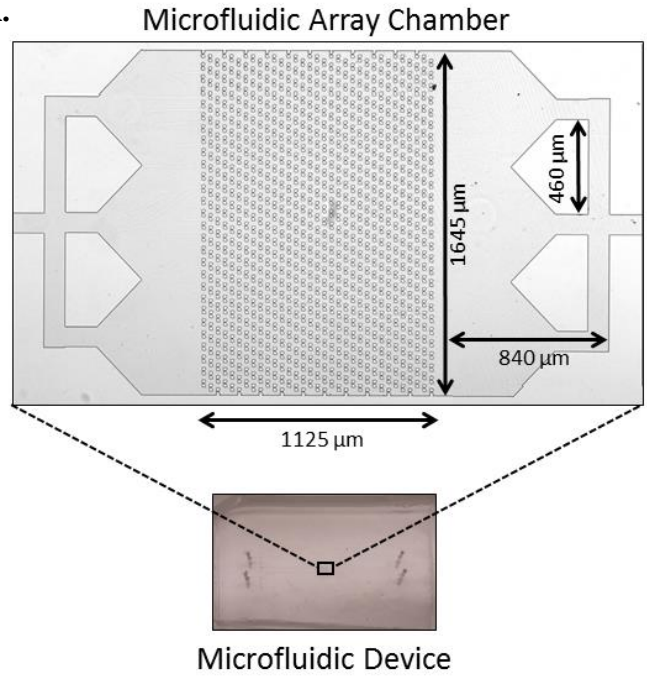
Microfluidic Array Chamber
460 µm
1645 µm
840 µm
1125 µm
Microfluidic Device

B.

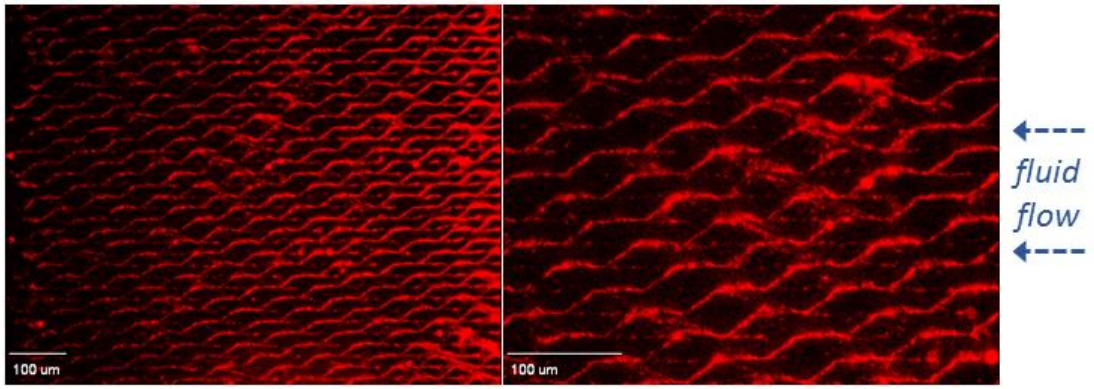
Red Fluorescence Image of DNA Fibers
100 um
100 um
fluid
flow

C.

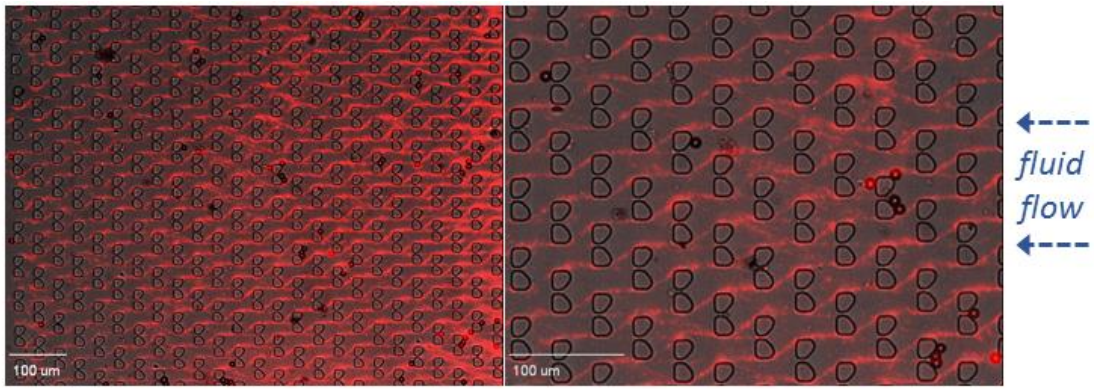
Merged Fluorescence & Brightfield Image of DNA Fibers
100 um
100 um
fluid
flow

Figure 3.5 Initial RCA-based DNA pattern results from positive detection of nucleic acid targets

A) Dimensions of the microfluidic array chamber. **B)** Fluorescence image of the DNA pattern resulting from performing RCA under continuous slow flow conditions. **C)** Merged fluorescence and bright field image of the DNA pattern from **(B)**, which reveals that the pattern is guided by the micropost array pattern geometry.

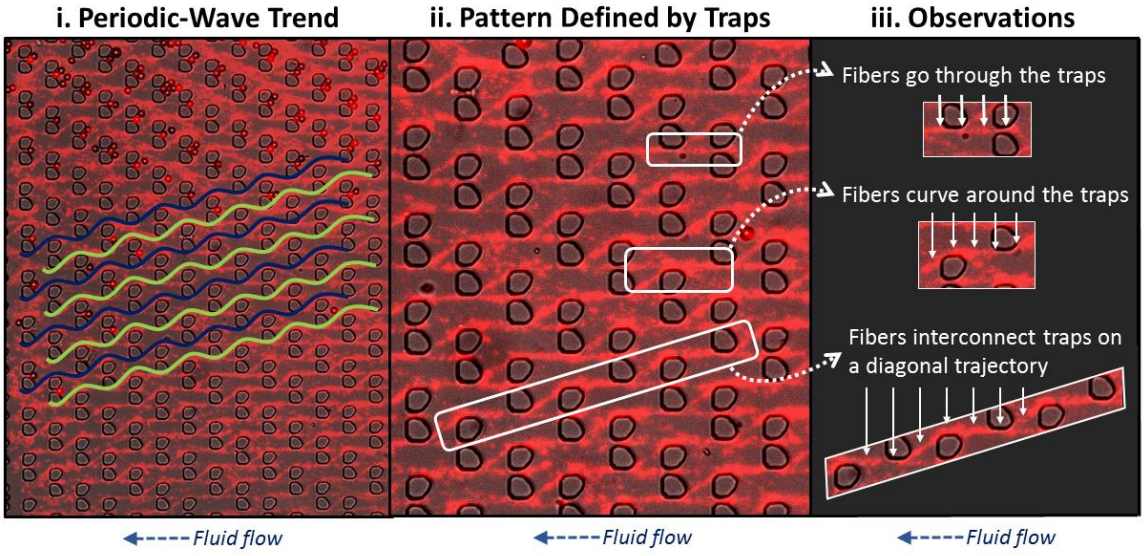

Figure 3.6 Examination of the main characteristics of RCA-based DNA patterns

i) A periodic wave-like trend is clearly formed by the entangled and entwined DNA fibers. **ii-iii)** The micropost bead traps serve as guides for both fluid flow and DNA pattern formation. DNA fibers form both through and around the microposts.

3.3.2 *Device and flow rate optimization*

To optimize the device for more sensitive and rapid pathogen detection, we reduced the size of the micropost array chamber by 60% to concentrate DNA pattern formation in a more confined space. By reducing the overall micropost array area, the detection pattern "signal" was amplified because it was not spread over such a large area. Therefore, the DNA fibers accumulate and entangle more rapidly, which leads to thicker fibers that can be visualized in a shorter period of time. The miniature microfluidic device and resulting RCA DNA patterns are shown in **Figure 3.7 A-B**. It is important to note that we also added a filter array at the beginning of the micropost array chamber. This filter of microposts was added to trap debris from crude target samples and prevent it from damaging the DNA pattern read-out. Interestingly, the DNA fiber pattern also forms in the filter array, and thus the micropost filter served as a second location for pattern concentration and detection signal read-out.

Although RCA generates very long ssDNA, ssDNA is nanometer scale and cannot be visualized individually even when stained with a fluorescence dye. To theoretically confirm that the DNA fibers in the 2D DNA pattern are not single but multiple entangled ssDNA, we calculated the theoretical length possible of the ssDNA product generated by RCA. Taking into account the length of one base (0.34 nm) and the maximum reported RCA product length of 800 kb, the maximum length possible for ssDNA generated by one ϕ29 polymerase enzyme is 272 μm. The miniature micropost array device achieved DNA fibers with an average length of ~1140 μm, which is significantly greater than the reported single ssDNA RCA product length; therefore, the DNA fibers within the device are formed from multiple entangled ssDNA RCA products. **Figure 3.7 C-D** depict the chamber

dimensions and a sample DNA fiber length measurement. The continuous microfluidic flow of the RCA sample mix at a very slow flow rate likely contributes to entanglement of the DNA products on a wave-like path, causing the DNA to form long uniform fibers rather than irregular clumps or aggregates.

In addition to determining the composition of the DNA fiber pattern, it is important to understand the effect of fluid flow on DNA pattern generation. A series of detection experiments were performed, all conditions held constant except for the flow rate that was used to infuse the RCA sample into the microfluidic device. 15 nM target samples were used in the sample mix and positive detection tests were performed for each flow rate condition. As seen in **Figure 3.8**, as the flow rate increased from 0.01 µl/min to 1 µl/min the resulting RCA pattern decreased in intensity and thickness. There appears to be an upper limit to the flow rate titration as well – above 0.2 µl/min, no DNA pattern was formed. Our system aims to achieve rapid and efficient POC detection of plant viruses, and thus detection time and flow rate must be carefully balanced such that a dense DNA pattern read-out will be reliably and quickly generated. We found that a RCA detection experiment performed at 0.1 µl/min for 4 hours consistently identifies plant virus targets over a broad range of target concentrations. The results of these tests will be explained in ***Section 3.3.5***.

A.

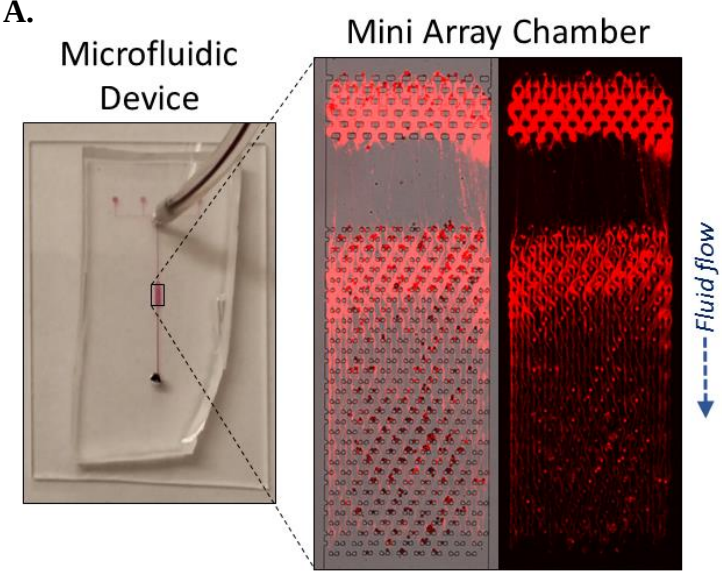
Microfluidic Device
Mini Array Chamber
Fluid flow

B.

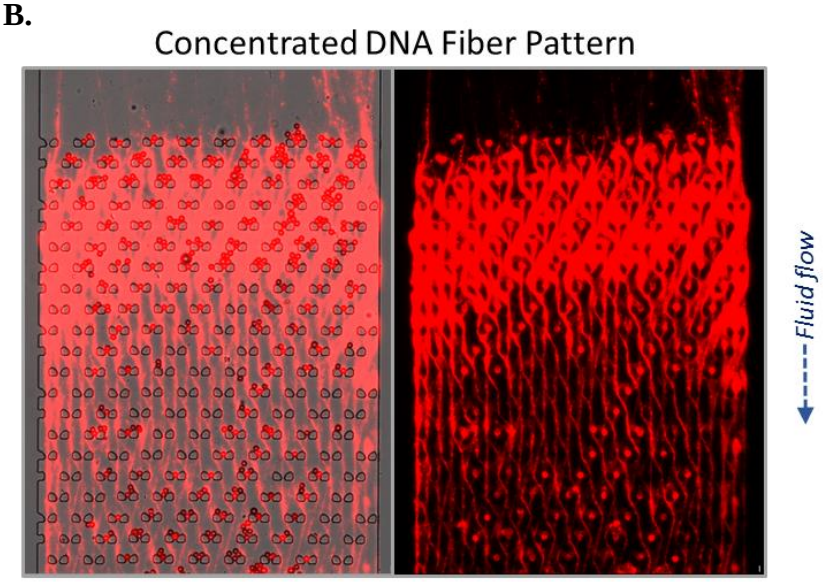
Concentrated DNA Fiber Pattern
Fluid flow

C.

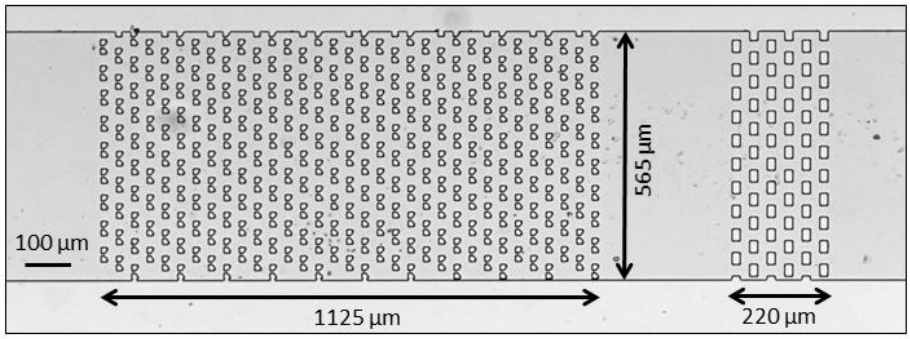
565 µm
100 µm
1125 µm
220 µm

D.

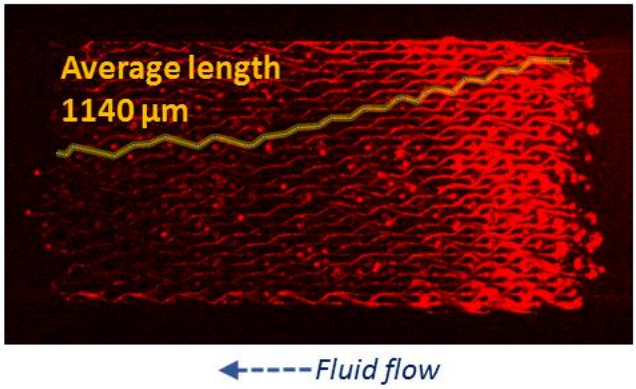

Figure 3.7 RCA-based detection in a miniature microfluidic device

The images above depict RCA-based detection in the miniature microfluidic device. The miniature device was designed to contain both a micropost array for guiding DNA pattern formation and a filter array for preventing debris from entering the chamber and inhibiting uniform DNA pattern growth. **A-B)** Image of the miniature microfluidic device array and the resulting DNA pattern after performing RCA detection. **C-D)** Dimensions of the miniature device and average length measurement of the longest DNA fibers assembled in the microfluidic chamber array.

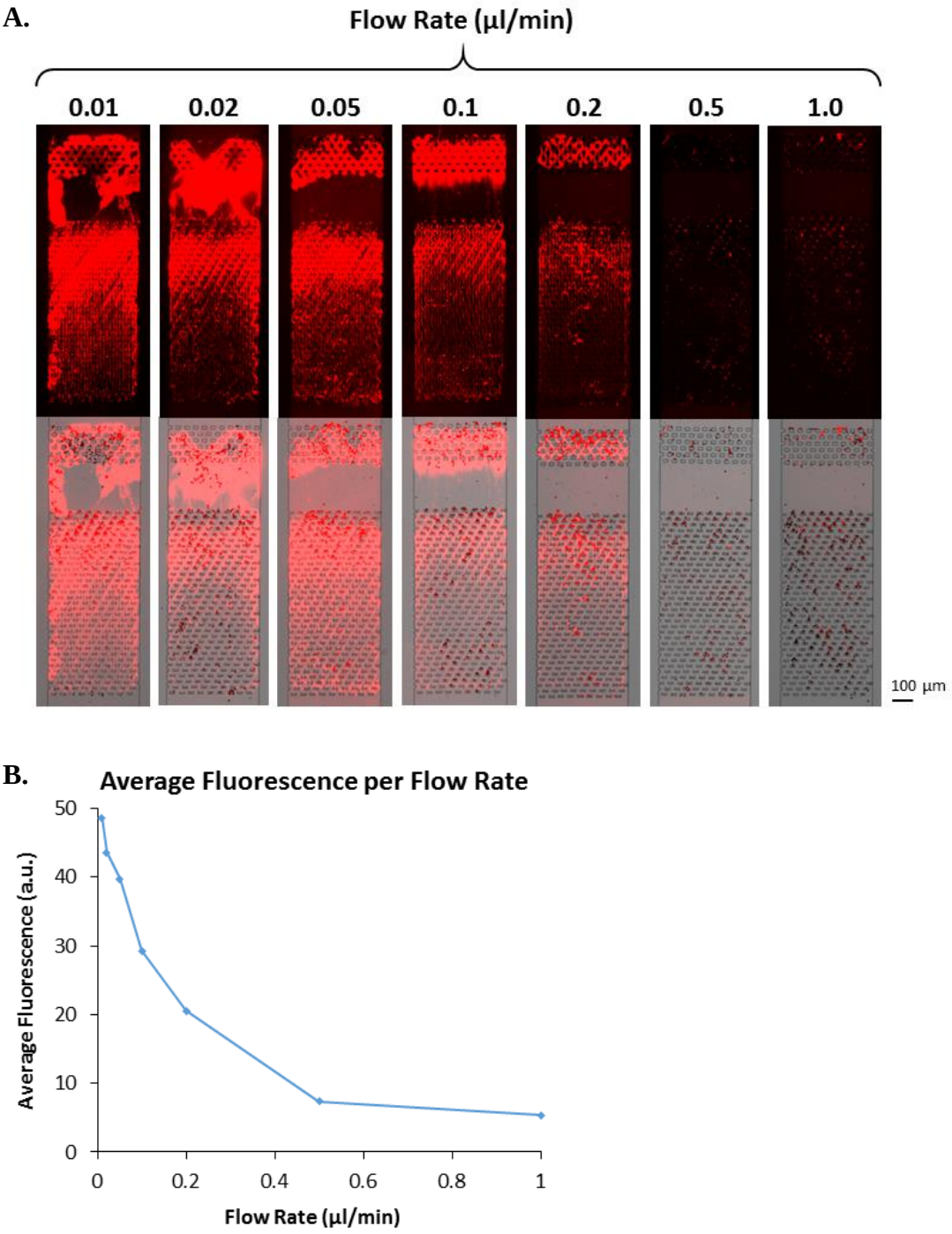

Figure 3.8 Effect of flow rate on RCA-based DNA pattern formation

To evaluate the effect of flow rate on DNA pattern formation, we performed a series of tests with varied flow rates. **A)** Fluorescence images of the resulting DNA patterns from a titration of tests, where all conditions were held constant except the flow rate for the sample mix. The flow rate range was 0.01 – 1.0 µl/min. **B)** Graph of the average fluorescence intensity measured over the total area of the DNA pattern in relation to the flow rate used.

3.3.3 *Characterization of ssDNA and dsDNA content in the DNA pattern*

We discovered that at high target concentrations the DNA fiber pattern becomes very thick and dense, particularly at the beginning of the micropost array and filter sections. Interestingly, the individual entangled DNA fibers become so entwined and enmeshed together they form a dense network similar to an entangled DNA hydrogel. To further investigate the composition of the DNA pattern in these thick dense regions, we stained a DNA pattern generated from a 150 nM target sample mix with both a ssDNA-specific green dye and a dsDNA-specific red dye. **Figure 3.9 A-B** depict the separate green and red fluorescence stain results, both as images and 3D surface plots.

Using the raw fluorescence images for each dye staining result, 3D surface plots were generated to better depict the relative intensity differences between the two staining tests. These plots show that the majority of the DNA pattern is formed from ssDNA (as expected), and additionally they indicate that the very dense regions of the DNA pattern are comprised of dsDNA. The dsDNA most likely forms due to binding between short complementary segments within the DNA products, which are tandem repeating copies of the initial padlock probe circular template. **Figure 3.9 C** shows the ssDNA and dsDNA imaging results for the entire microfluidic array.

To prove that dsDNA only forms after the ssDNA RCA products become densely entangled, this test was repeated for a lower target sample concentration of 15 nM. All conditions were held constant, and the resulting DNA pattern was similarly stained with ssDNA and dsDNA dyes. **Figure 3.10** shows the fluorescence and 3D surface plot results. These experiments confirm that little to no dsDNA forms at low target concentrations, which do not generate highly dense DNA fiber patterns within the micropost array.

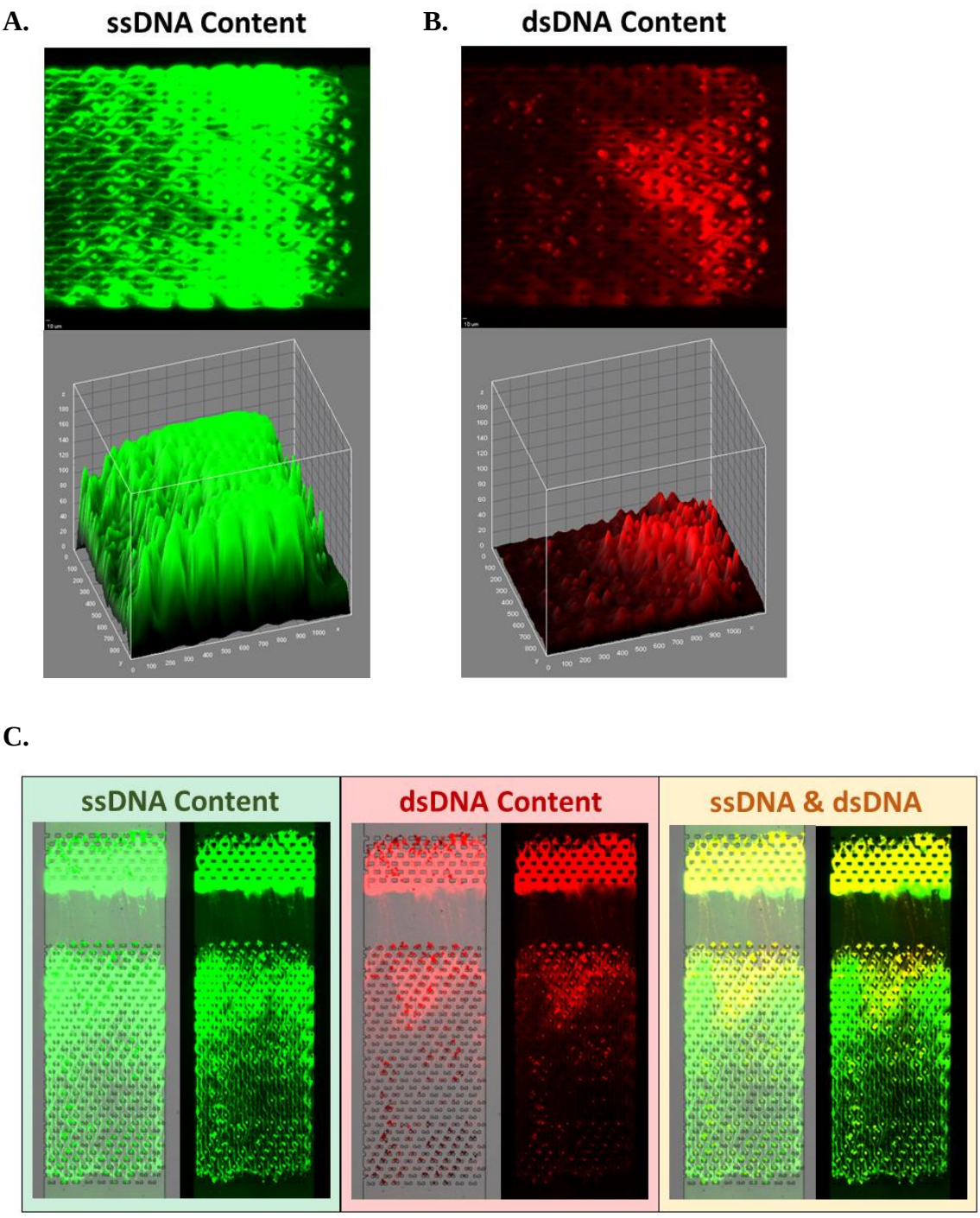

Figure 3.9 Fluorescence evaluation of ssDNA and dsDNA content in DNA pattern for a 150 nM target sample

These images depict the approximate ssDNA and dsDNA amount in the DNA patterns generated from a 150 nM nucleic acid target sample. **A)** ssDNA was stained with a green ssDNA-specific dye and imaged with a fluorescence microscope. Using the raw

fluorescence image, a 3D surface plot was generated using ImageJ software to show the magnitude of the fluorescence intensity over the area of the pattern. **B)** dsDNA was stained with a red dsDNA-specific dye and imaged with a fluorescence microscope. Using the raw fluorescence image, a 3D surface plot was generated using ImageJ software. **C)** Fluorescence images of the array depicting only ssDNA (green), only dsDNA (red), and both ssDNA and dsDNA (yellow).

A.

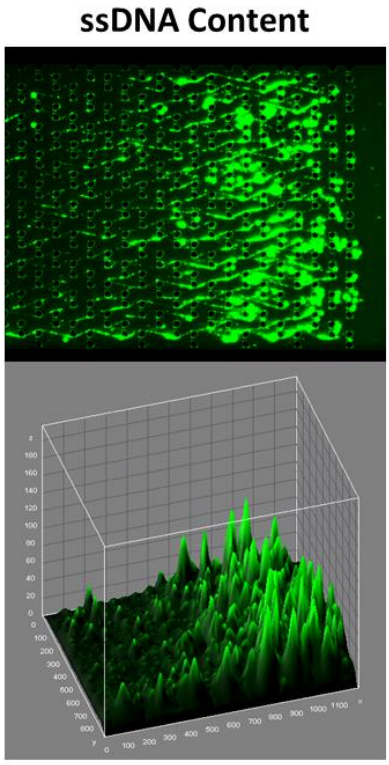

B.

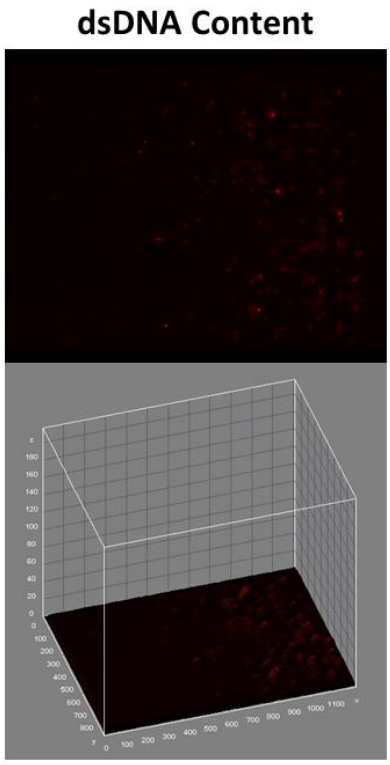

C.

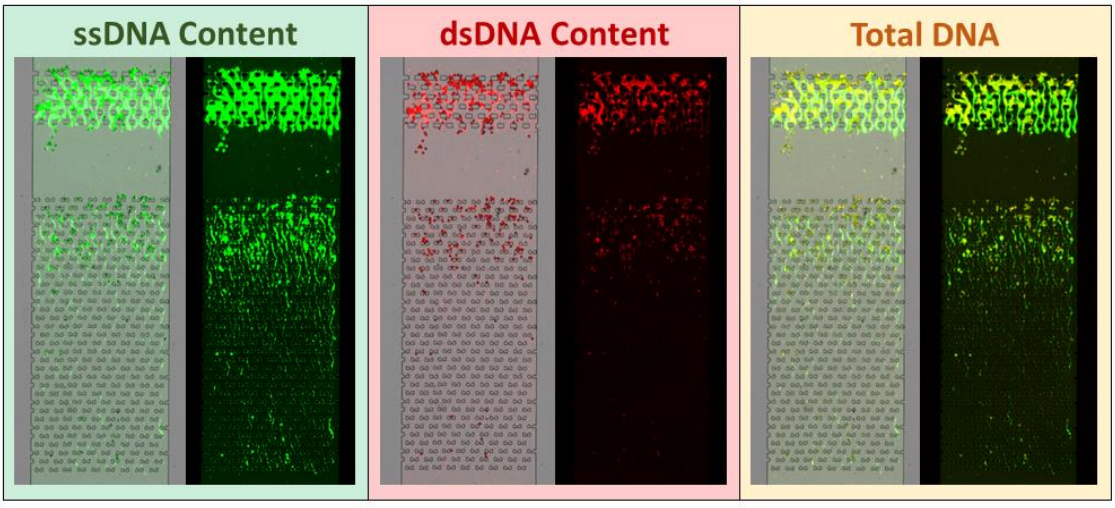

Figure 3.10 Fluorescence evaluation of ssDNA and dsDNA content in DNA pattern for a 15 nM target sample

These images depict the approximate ssDNA and dsDNA amount in the DNA patterns generated from a 15 nM nucleic acid target sample. **A)** ssDNA was stained with a green ssDNA-specific dye and imaged with a fluorescence microscope. Using the raw fluorescence image, a 3D surface plot was generated using ImageJ software to show the magnitude of the fluorescence intensity over the area of the pattern. **B)** dsDNA was stained with a red dsDNA-specific dye and imaged with a fluorescence microscope. Using the raw fluorescence image, a 3D surface plot was generated using ImageJ software. **C)** Fluorescence images of the array depicting only ssDNA (green), only dsDNA (red), and both ssDNA and dsDNA (yellow).

3.3.4 *DNA pattern dependency on microbeads and microfluidic flow*

Performing RCA in a microfluidic system is an innovative strategy for creating a hydrodynamic force that directs RCA product self-assembly. Although the ideal temperature for the ϕ29 enzyme is 30˚C, ϕ29 activity and performance is still highly optimized at room temperature conditions. As soon as the detection sample mix is combined and taken off ice, the ϕ29 polymerase begins processing the circular padlock probes that are hybridized to matching ssDNA pathogen targets. Because of this, the RCA reaction initiates at time = 0 min, and continues for the entire 4 hour detection period.

Since RCA initiates immediately upon mixing the RCA reagents and setting up the detection system, DNA fibers will begin to form and entangle with each other inside the microtubing prior to reaching the microfluidic chamber and microbead-array. The microbeads were incorporated into the detection system to act as tethers for capturing circular padlock probes and providing starting points for RCA growth. That said, we sought to test whether the microbeads were required for pattern formation. By performing identical paired tests (at 150 nM and 15 nM target concentrations) both with and without microbeads, we confirmed that RCA-based DNA pattern formation in the microfluidic device is not dependent on the presence of microbeads. In fact, the resulting DNA patterns were similar in density and fiber thickness for each pair of with- and without-microbead tests, as seen in **Figure 3.11**.

To determine that microfluidic flow is required for pattern formation, the detection protocol was modified such that the entire 4 hour RCA reaction was performed in the absence of fluid flow. In short, the reaction was performed in a microcentrifuge tube for 4 hours, then the ϕ29 enzymes were heat-inactivated, and then the entire sample mix was

flowed through microtubing and into the microfluidic device for another 4 hours. The entire process is depicted in **Figure 3.12**. Since the RCA reaction was performed in a static environment, no hydrodynamic force was available to simultaneously organize the ssDNA products while they were being generated by ϕ29. Amazingly, using these modified conditions we discovered that the resulting DNA product in the microfluidic device formed large clumps and aggregates near the inlet of the array chambers, as seen in **Figure 3.13 A-B**. No uniform DNA patterns were observed, thus verifying that continuous microfluidic flow is required for the formation of the DNA fiber pattern read-out. This is highly unusual, particularly because DNA self-assembly both at the nano- and macro-scale typically occurs in a static, self-contained solution environment. Thermal cycling is often used to facilitate DNA self-assembly, but this is a closed process that does not directly control the structural assembly of DNA. Rather, DNA self-assembly in thermal cycling processes depends on predefined complementary sequence binding to guide formation. Our detection system, on the other hand, harnesses microfluidic flow as a hydrodynamic force to directly control and evenly distribute the physical entanglement reactions between DNA fibers to self-assemble wave-like, periodic DNA patterns.

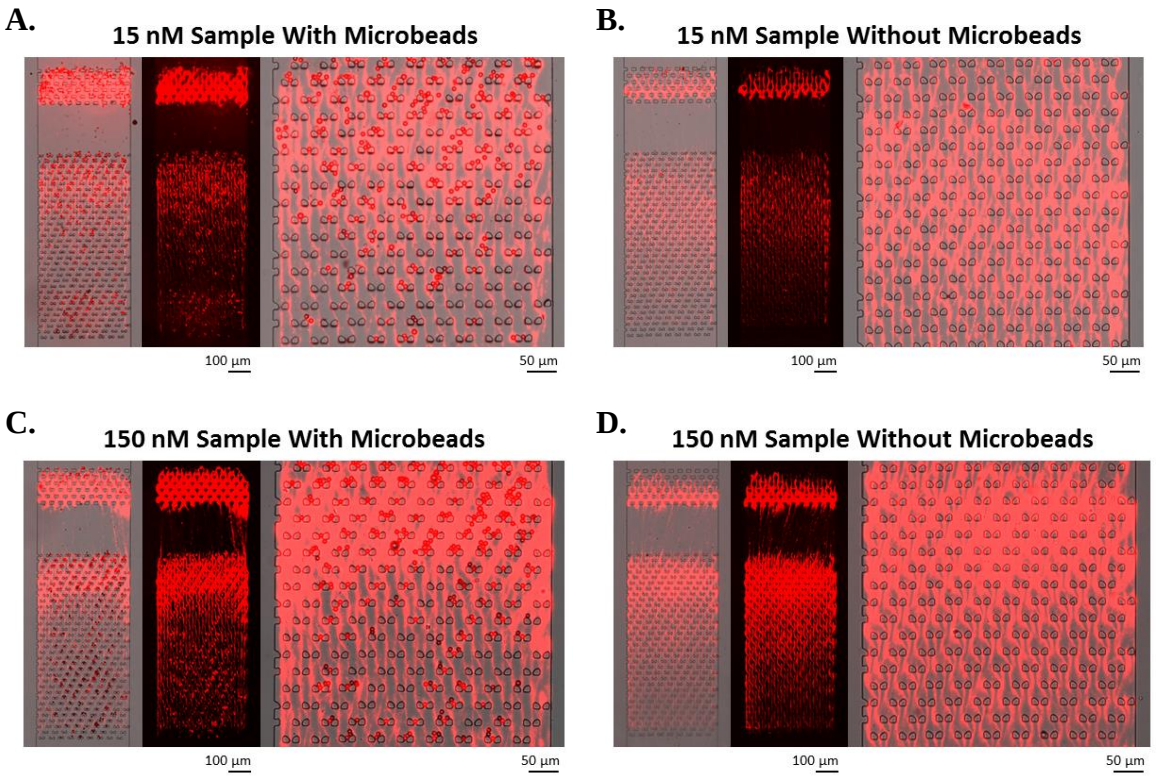

Figure 3.11 Fluorescence images of DNA fiber patterns formed with and without microbeads present in the array

To evaluate DNA pattern formation dependency on microbeads, we performed paired detection tests (15 and 150 nM) in the microfluidic devices both with and without microbeads. Fluorescence and merged bright field images of the resulting DNA patterns are shown above. **A-B)** DNA patterns generated from a pair of 15 nM target sample positive detection tests, one with beads **(A)** and without beads **(B)**. **C-D)** DNA patterns generated from a pair of 150 nM target sample positive detection tests, one with beads **(C)** and without beads **(D)**.

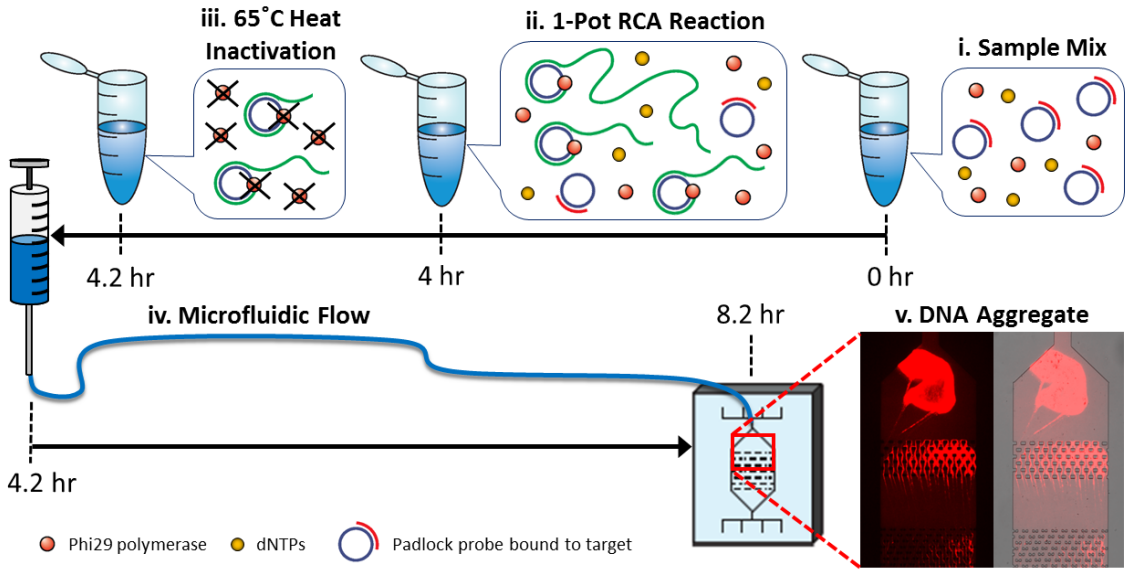

Figure 3.12 Schematic illustration of RCA-based detection after separating the RCA reaction from fluid flow

To evaluate whether fluid flow is required for DNA pattern formation, we completely separated the RCA reaction step. A static microcentrifuge tube was used to perform RCA for 4 hours **(i-ii)** and then the ϕ29 enzymes were heat-inactivated **(iii)**. Next, the sample mix was loaded into a syringe and slowly flowed through microtubing and into the microfluidic device for a duration of 4 hours **(iv)**. The final result **(v)** shows a large DNA aggregate and no uniform DNA pattern. This suggests that DNA pattern formation requires simultaneous fluid flow during the RCA reaction.

A.

B.

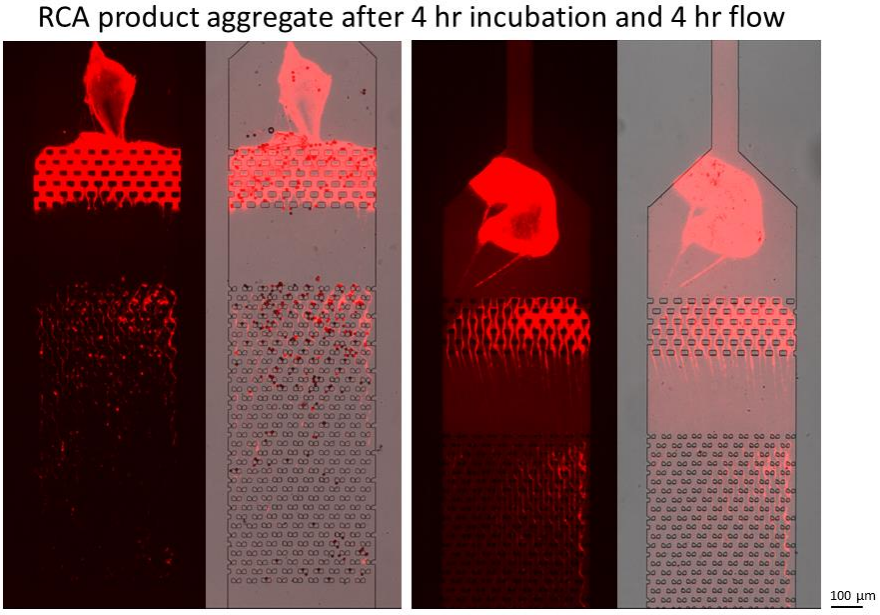

Figure 3.13 Fluorescence images of DNA products generated by performing RCA without fluid flow

A) DNA products were removed from the microcentrifuge tube after a 4 hour RCA reaction in a static environment, stained with a red fluorescence dye, and imaged on a glass slide. DNA aggregates are present, but no periodic pattern was exhibited. **B)** Image of the microfluidic chamber after DNA products (following enzyme heat inactivation) were flowed through microtubing and into the device. Large aggregates were deposited near the chamber inlet and a full uniform DNA pattern was not achieved.

3.3.5 *Detection limit and range across different target concentrations and types*

One of the main priorities for establishing a pathogen diagnostic system is determining detection reliability and consistency across a range of sample concentrations. We performed a series of positive detection tests for a target sample titration range of 0.015–1500 nM. For comparison, a series of negative control detection tests were also performed for the same titration range. As shown in **Figure 3.14**, DNA fiber patterns were achieved for all positive target sample tests across the entire titration range. The negative controls (which used unrelated nucleic acid targets with completely different sequences) revealed no DNA patterns, indicating that detection was accurate for all detection tests across this broad sample range.

To quantify the DNA pattern thickness and density as it relates to target concentration, average fluorescence intensity was measured over the total area of the array chamber for each target sample and plotted on a graph with a logarithmic x-axis. These results show that we achieved a roughly linear dynamic range over five orders of magnitude for target concentrations. These graphical results are shown in **Figure 3.14**.

It is important to note that the titration of detection experiments described above were performed using our standard detection protocol, which involves 4 hours of continuous fluid flow at 0.1 µl/min. These conditions were carefully balanced so that detection time was relatively quick while the resulting DNA pattern was also dense enough for clear visualization and read-out. ϕ29 polymerase is a highly robust enzyme, and it can retain high amplification activity over a period of 24 hours. We capitalized upon this extended 24 hour time period of activity to perform extremely sensitive detection of very low target sample concentrations. More specifically, we designed a modified “extended”

detection protocol the in which the RCA reaction was run for 24 hours of continuous flow at a significantly lower flow rate (0.02 µl/min). As shown in **Figure 3.15**, detection of positive target samples was achieved down to a detection limit of 150 fM. Interestingly, beyond this detection limit no pattern forms. These results provide a unique "yes or no" result that is entirely based on the existence of a visual pattern. In a way, the 2D DNA pattern acts as a cognitive signal that instantly provides a "yes" answer to the viewer for a quick read-out of the detection results.

As with the higher target concentration titration tests, a generally linear dynamic range was achieved over several orders of magnitude. In total, we achieved accurate detection of positive pathogen target samples with consistent negative control results across a concentration range spanning seven orders of magnitude. This is impressive especially for a room temperature detection reaction that requires zero input or manipulation after the experiment is initiated. The broad detection range, coupled with the simplicity and consistency of the DNA pattern read-out, makes this system a powerful platform that could be used in a wide variety of clinical and non-clinical environments.

A.

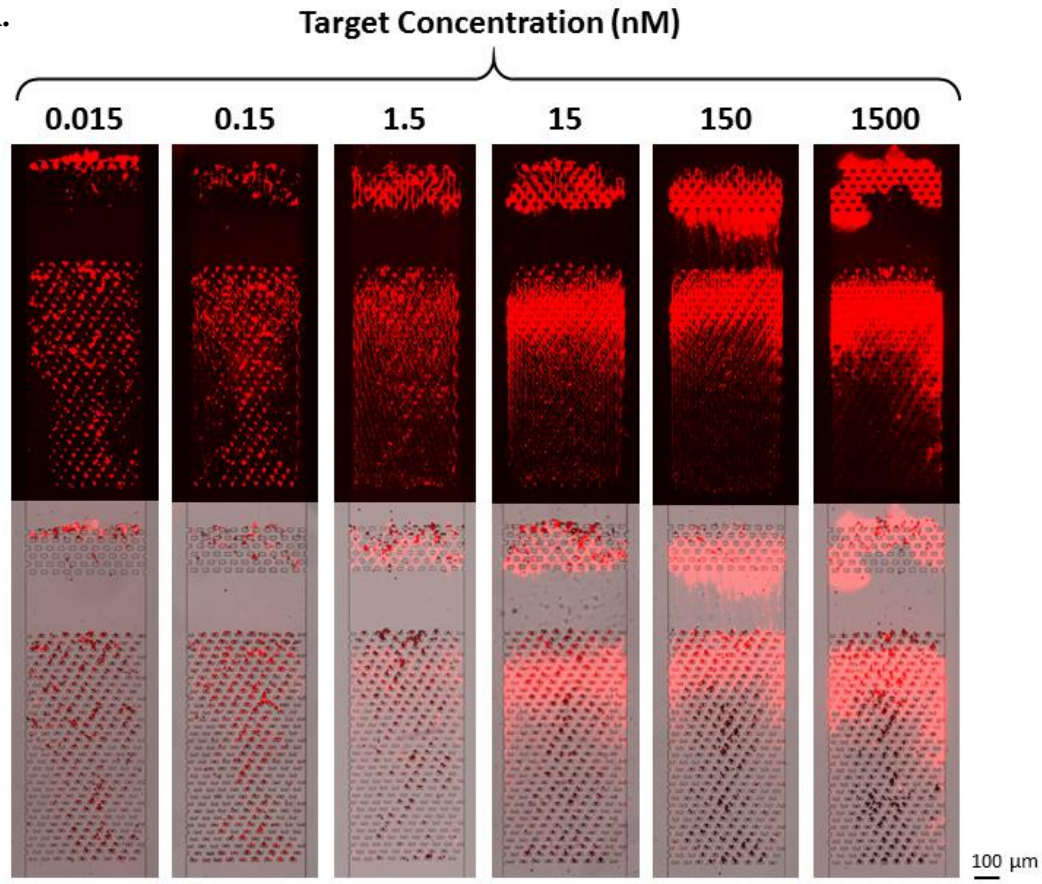
Target Concentration (nM)
0.015
0.15
1.5
15
150
1500
100 µm

B.

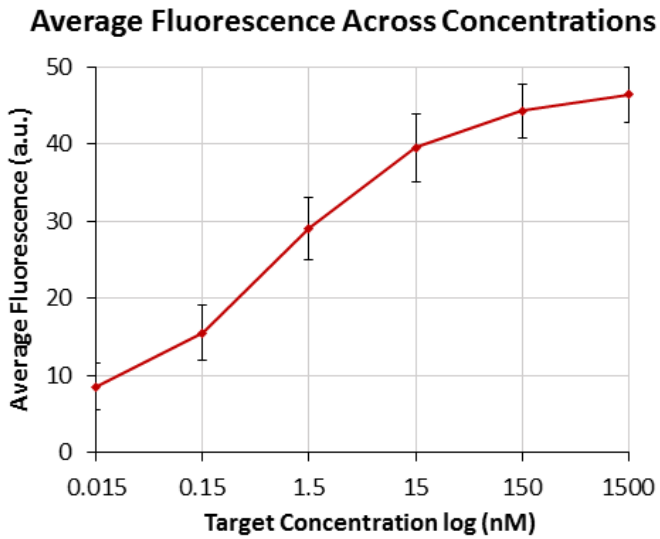
Average Fluorescence Across Concentrations
Average Fluorescence (a.u.)
50
40
30
20
10
0
0.015
0.15
1.5
15
150
1500
Target Concentration log (nM)

C.

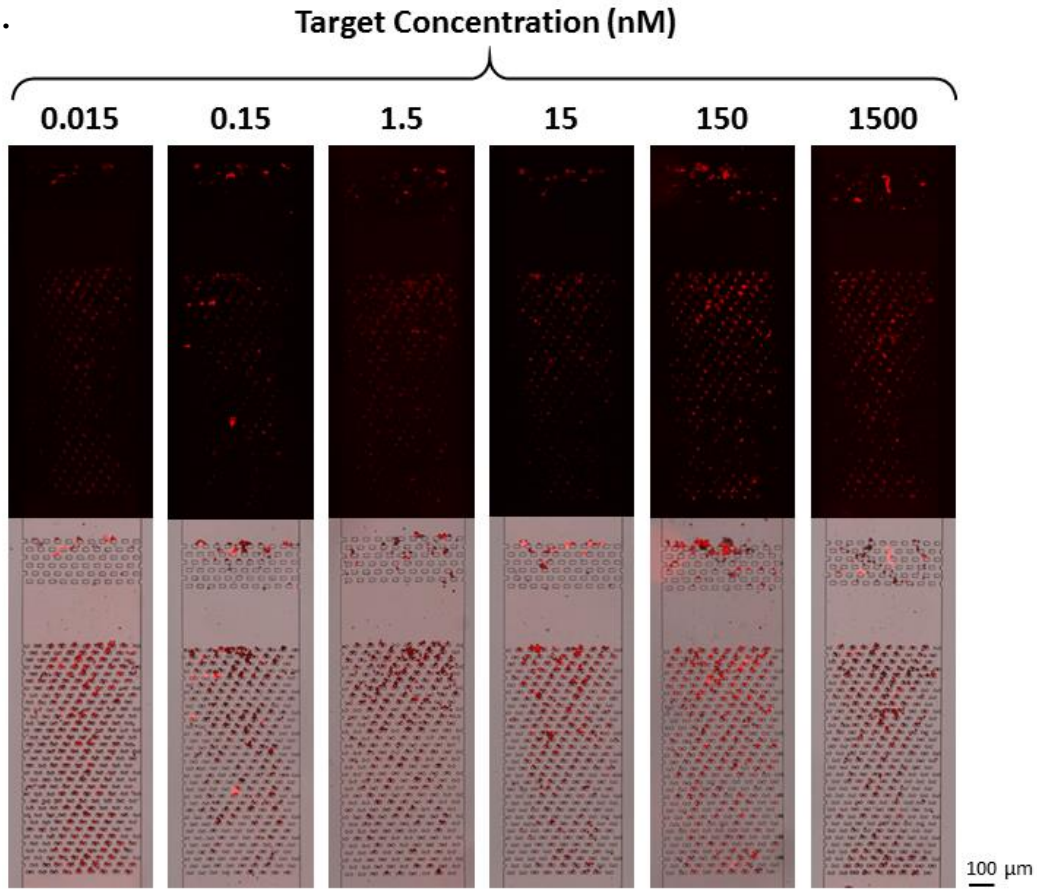
Target Concentration (nM)
0.015
0.15
1.5
15
150
1500
100 µm

D.

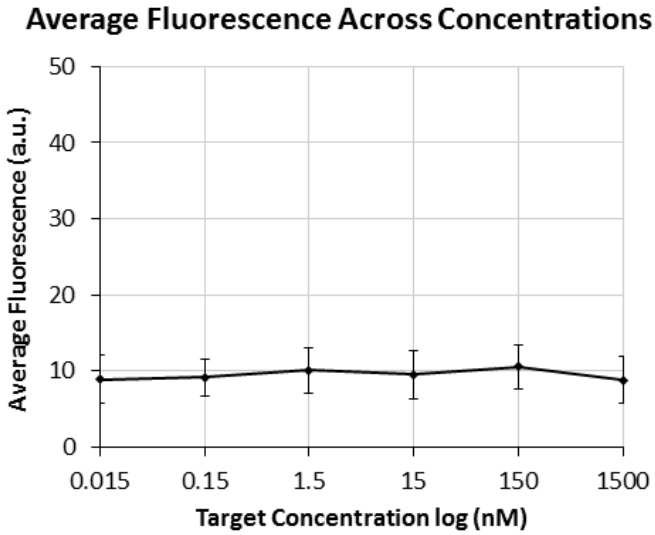
Average Fluorescence Across Concentrations
Average Fluorescence (a.u.)
50
40
30
20
10
0
0.015
0.15
1.5
15
150
1500
Target Concentration log (nM)

Figure 3.14 Titration series of RCA detection tests performed for a range of target concentrations (0.015 – 1500 nM)

Identical detection tests were performed over a range of target concentrations. **A)** Fluorescence images of the resulting DNA patterns from the series of positive detection tests. **B)** Graph mapping the average fluorescence measured over the area of the DNA pattern for each positive detection test. As expected, the fluorescence intensity increases with target concentration. **C)** Fluorescence images of the DNA patterns following completion of the negative control detection tests. **B)** Graph mapping the average fluorescence of the DNA pattern (or lack thereof) for each negative control test. As expected, the fluorescence intensity reveals a flat line of low fluorescence intensity for all the target concentrations.

A.

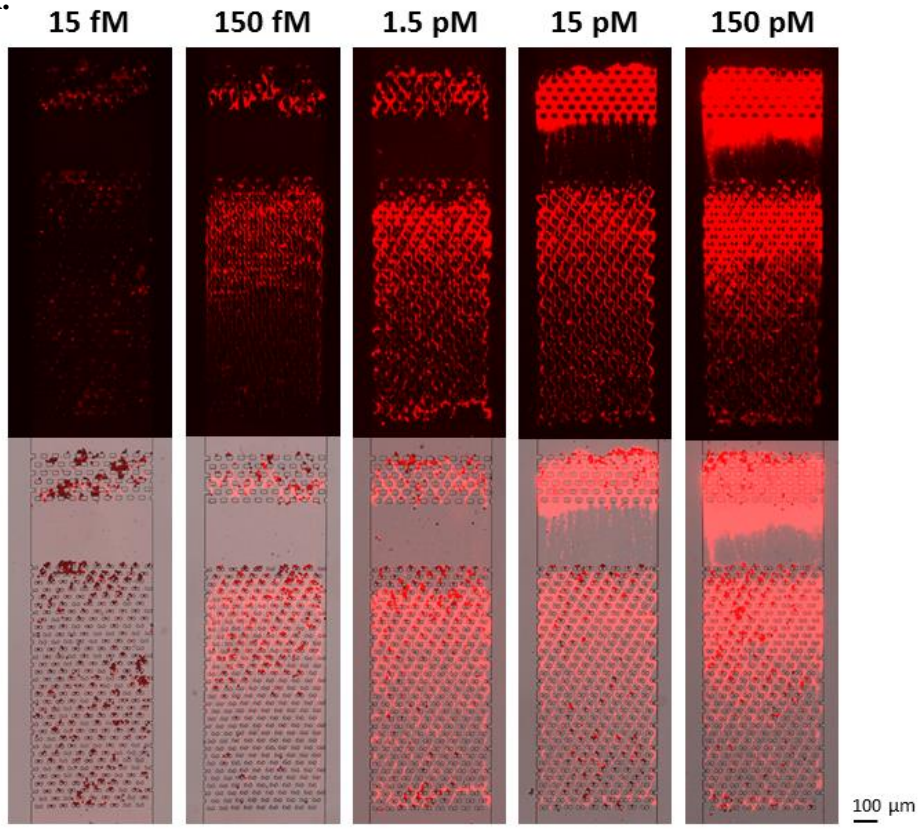

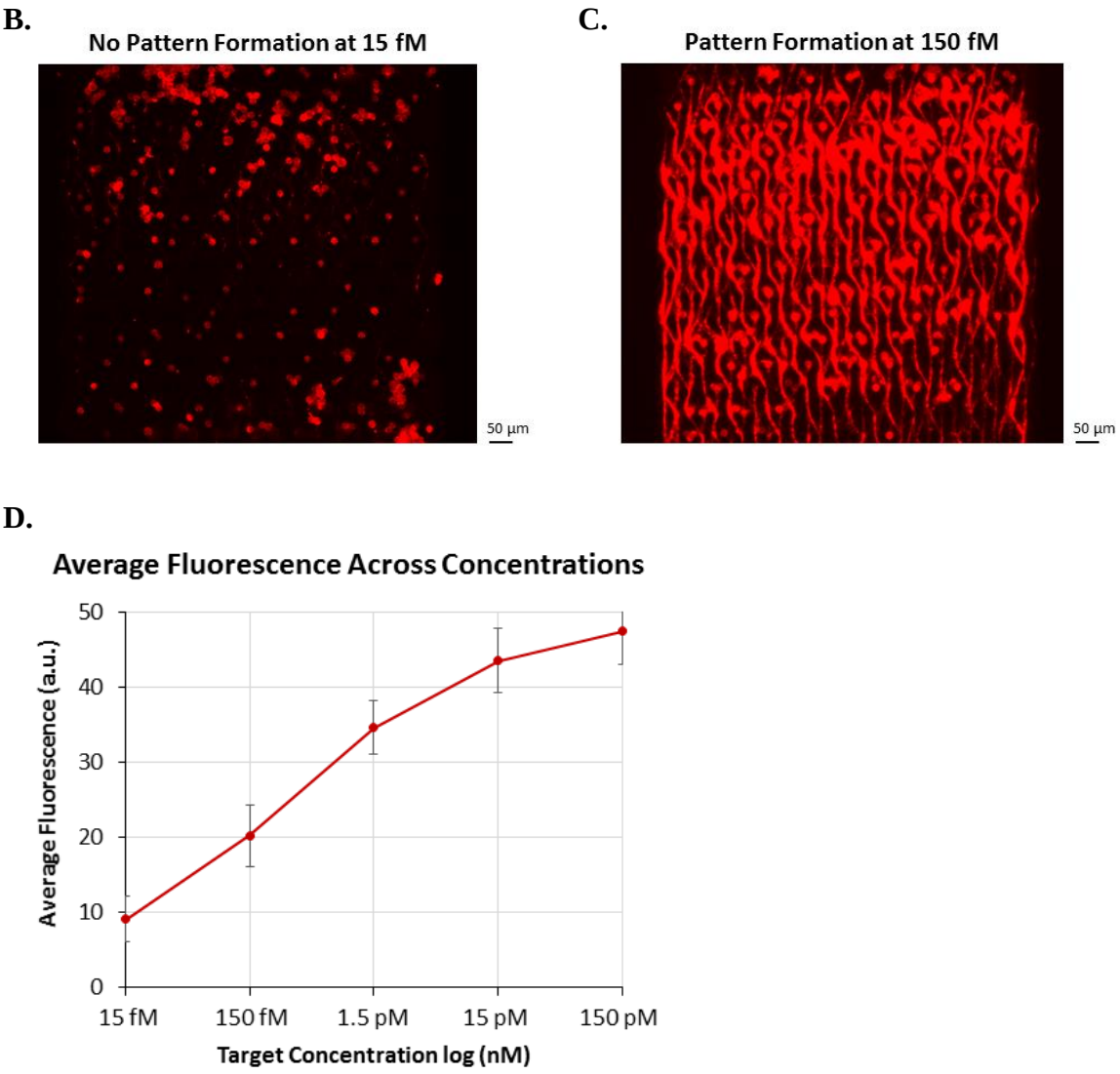

Figure 3.15 Titration series of RCA detection tests for low target concentrations (15 fM – 150 pM)

A series of RCA detection tests were performed with an extended flow period (24 hours) for improved detection sensitivity at low target sample concentrations **A)** Fluorescence and bright field images of the periodic DNA pattern formed by positive detection tests. **B-C)** Comparison of 15 and 150 fM detection results, showing the detection limit of our system is 150 fM. Only a full uniform pattern **(B)** reveals positive detection, and below the detection limit no pattern can be visualized **(C)**. **D)** Graph mapping the average fluorescence of the DNA pattern for each detection test in this series. As expected, the fluorescence intensity increases with target concentration above the detection limit.

3.3.6 *Image analysis of the DNA wave-pattern structure*

We investigated the DNA pattern structure by using ImageJ software to analyze the DNA fiber wave-form characteristics. As shown in **Figure 3.16 A**, two types of waves were observed in the DNA fiber patterns: slanted and horizontal. This is most likely because the array of microposts was designed with a distinct "tilt" angle, which leads to secondary wave form patterns in addition to the horizontal waves. Each type of DNA fiber wave pattern was evaluated as a separate data set, and for each discrete observed DNA-fiber-wave we measured key features such as wavelength, angle, and amplitude. As expected, the wavelengths, amplitudes and angles were different between the two different types of DNA fiber wave trends.

Interestingly, we discovered that the predominant wave form overall in the DNA pattern switches depending on the initial target sample concentration. In general, for thicker, high density DNA patterns (caused by higher target sample concentrations) the slanted waves dominate. In contrast, for thinner, low density DNA patterns the horizontal waves dominate. These trends are showed by the dominant wave angle histogram graphs in **Figure 3.16 B-C**. These graphs indicate that as the DNA fibers become thicker the incoming RCA DNA products favor the more dominant diagonal flow pathways as they perfuse through the micropost array. To further validate this observation, we calculated the ratio of total horizontal waves to slanted waves observed in each DNA pattern array test. **(Figure 3.16 D)** As expected, we found that the ratio decreases as the target concentration increases.

In addition to evaluating the DNA fiber patterns as waves, we examined the fluid flow mechancis within the micropost array chamber. Using 1 μm microbeads, we traced

miroparticle movement through the array using timelapse image capture and prolonged (several second) exposure times. Merging the timelapse image data set into a video file, we were able to view the continuous movement of individual particles as they flowed through the array. By drawing lines to trace the particle movement over time, we discovered that particle movement mimics the periodic, wave-like trend of the final 2D DNA patterns. These particle-trace lines are seen in **Figure 3.16 E**, and for direct comparison a high magnification fluorescence image of the DNA fibers is shown in **Figure 3.16 F**. These results support our hypothesis that the ssDNA RCA products entangle and form thick fibers along fluid streamlines and dominant flow pathways.

A.

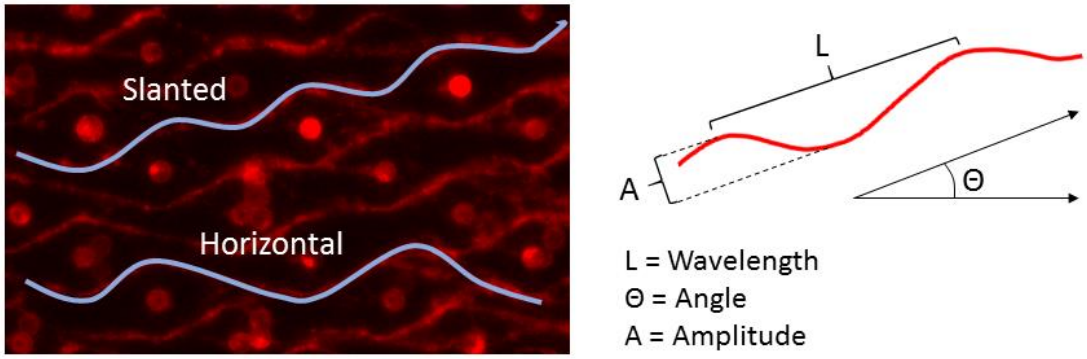
Slanted
Horizontal
L
A
Θ
L = Wavelength
Θ = Angle
A = Amplitude

B.

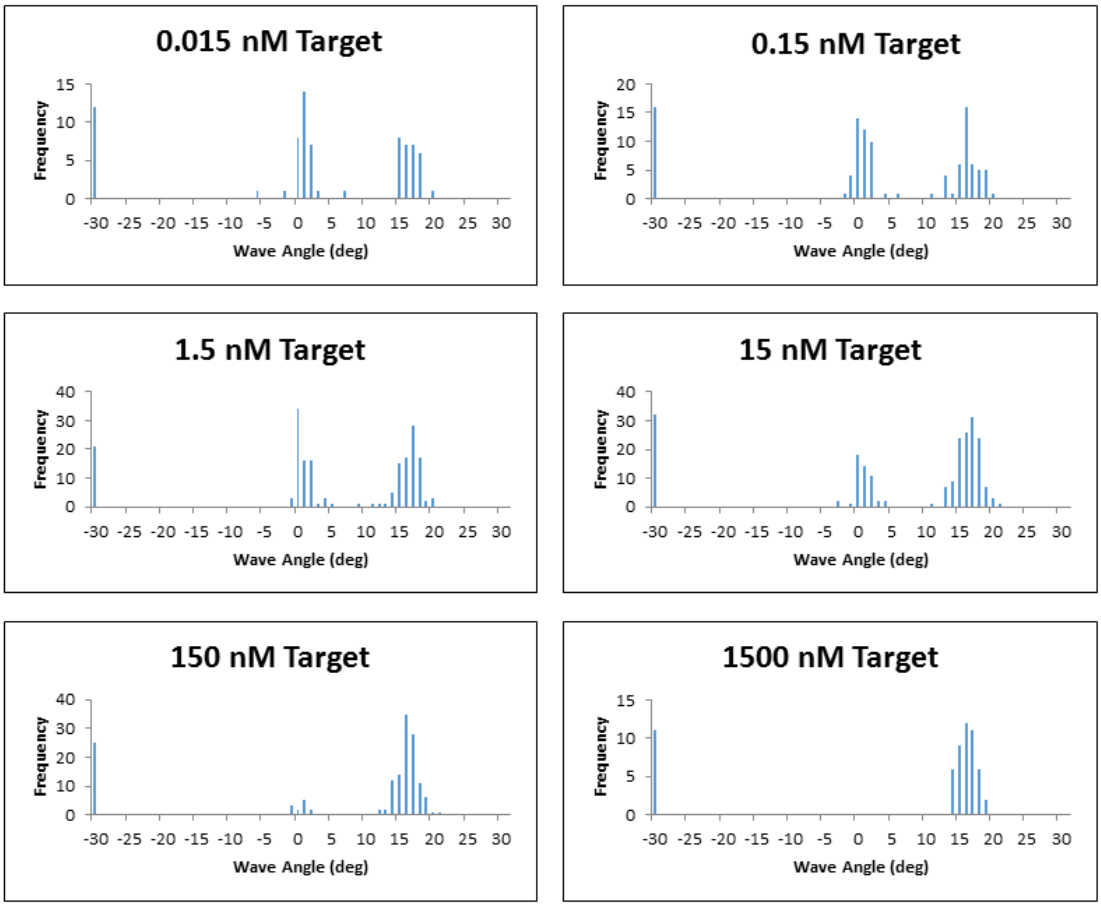
0.015 nM Target
0.15 nM Target
1.5 nM Target
15 nM Target
150 nM Target
1500 nM Target
Frequency
Wave Angle (deg)

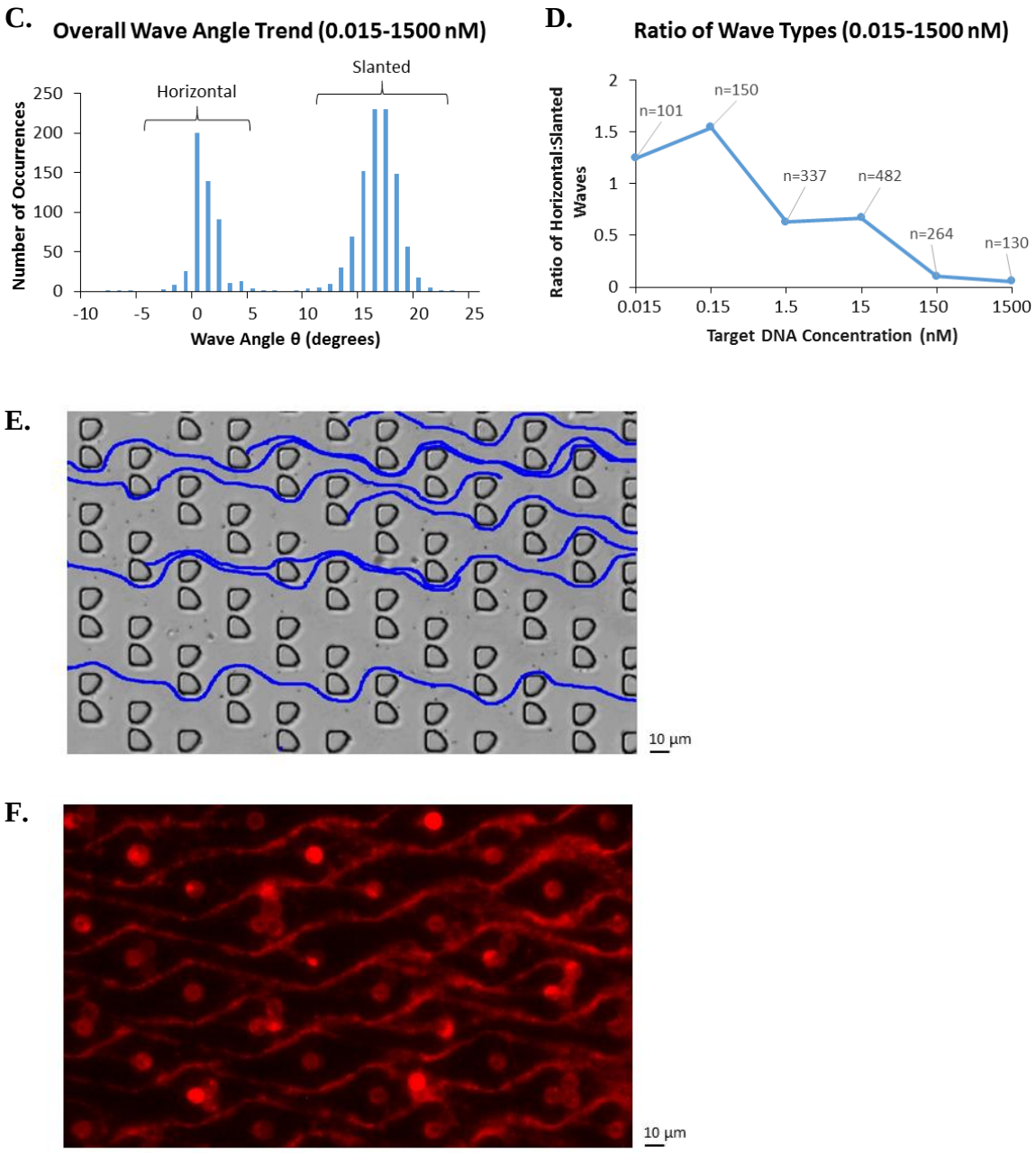

Figure 3.16 Image analysis of the DNA wave patterns and particle-flow pathways

A) Schematic illustration of the two main wave types observed in the DNA fiber patterns. **B)** Histogram data of the predominant wave type observed for different positive detection test target concentrations. As the target concentration increased, the slanted wave patterns dominated. **C)** Total wave types observed for all tests for target samples ranging from 0.015 - 1500 nM. **D)** Graph depicting the ratio of wave types (horizontal:slanted) for increasing sample concentrations. **E)** Line traces of 1 µm microbeads flowing through the microfluidic device. Flow patterns mimic fluid streamlines, and as seen in **(F)** the DNA fiber pattern also mimics the microparticle flow pathways.

3.3.7 *Fast Fourier Transform (FFT) analysis for quantitative pattern recognition*

Fourier theory states that any signal, such as a visual image, can be expressed as a sum of a series of sinusoids. To that end, the Fourier Transform has become an important image processing tool which can be used to decompose an image into its sine and cosine components. In particular, the Fourier Transform can be applied to a range of image analysis applications, including image filtering, reconstruction, and compression. In general, the output of the Fourier transformation represents the image in the Fourier or frequency domain, while the input image is the spatial domain equivalent. In the Fourier domain image, each point represents a particular frequency which can be used to describe and isolate particular features of the spatial domain image.

We have employed the Fast Fourier Transform (FFT), a discrete Fourier transform algorithm, to quantitatively verify that a periodic pattern is present in the DNA fiber read-out images. The general verification process involves using an input image, on which we perform FFT and generate a Fourier domain image. This Fourier domain image is then filtered (in our case we used a modified "star-shape" low-pass filter) and then inverse-FFT is used to reconstruct the low-pass filtered image and confirm that we isolated signals corresponding to the periodic DNA pattern. The detailed FFT analysis process that was used for our fluorescence image data is explained in **Figure 3.17.**

Overall, we aimed to demonstrate two things: 1) there are two significant angles in the FFT image, and these represent the DNA fibers' two growth directions in the wave-form pattern (which should be constant throughout all samples), and 2) we can specifically isolate and reconstruct only the DNA fiber pattern when we pick (using a low-pass filter) both angles in the FFT image and inverse-FFT them. To address these points, we designed

a star-shape low-pass filter for the FFT result, which filtered the image and focused on frequencies defining only the periodic DNA fiber patterns. As a control, we performed inverse-FFT on the excluded high-pass filter regions (the background outside of the star-shaped low-pass filter region) as well. This analysis confirmed that only the star-shaped filtered region included frequency information corresponding to the DNA fiber patterns, whereas outside the star shape there was no relevant frequency information (the inverse-FFT of the outside yielded a dark image with no pattern). All images were contrast-enhanced with identical adjustment parameters, and we used the exact same star-shape low-pass filters for all images.

Image data from both positive detection tests and negative control tests were examined with our FFT protocol. We investigated a range of tests using target concentrations from 1.5–1500 nM and the results are shown in **Figure 3.18** and **Figure 3.19**. As expected, all positive detection tests had periodic patterns which could be consistently reconstructed by inverse-FFT processing of the FFT domain image result. This consistent pattern reconstruction indicates our image processing method could repeatedly isolate the DNA pattern frequencies for verification. Using this method, we quantitatively detected the periodic DNA patterns using FFT and inverse-FFT processing down to the device detection limit of 150 fM. **Figure 3.20** shows the image analysis results from performing FFT and inverse-FFT analysis on our detection limit tests for target concentrations ranging from 15 fM – 150 pM. Using the FFT analysis steps described in **Figure 3.17**, each image was analyzed with FFT processing and inverse-FFT was used to confirm the isolated pattern frequencies. Periodic DNA patterns were accurately reconstructed with inverse-FFT for only 150 fM – 150 pM target samples. The 15 fM target

concentration falls below the system's detection limit, and thus when inverse-FFT was performed no pattern was generated from the star-shape low-pass frequency domain. This negative reconstruction image (derived from a target sample test below the detection limit) confirms that our FFT method can quantitatively distinguish DNA fiber patterns since this processing sequence correctly reproduced a negative result for a test using a target sample below the detection limit.

To conclude, we were able to differentiate positive detection tests from negative controls by using star-shaped low-pass FFT filtering with inverse-FFT reconstruction outputs. Notably, this image processing strategy exclusively reported positive results only for images drawn from positive detection tests. In contrast, negative control images that were inverse-FFT reconstructed after the FFT filtering consistently revealed dark images with no patterns. These results indicate that the low-pass filtering correctly isolated angles corresponding to the DNA fiber wave directions, and furthermore it shows that this method was accurate down to the experimentally observed detection limit of the device.

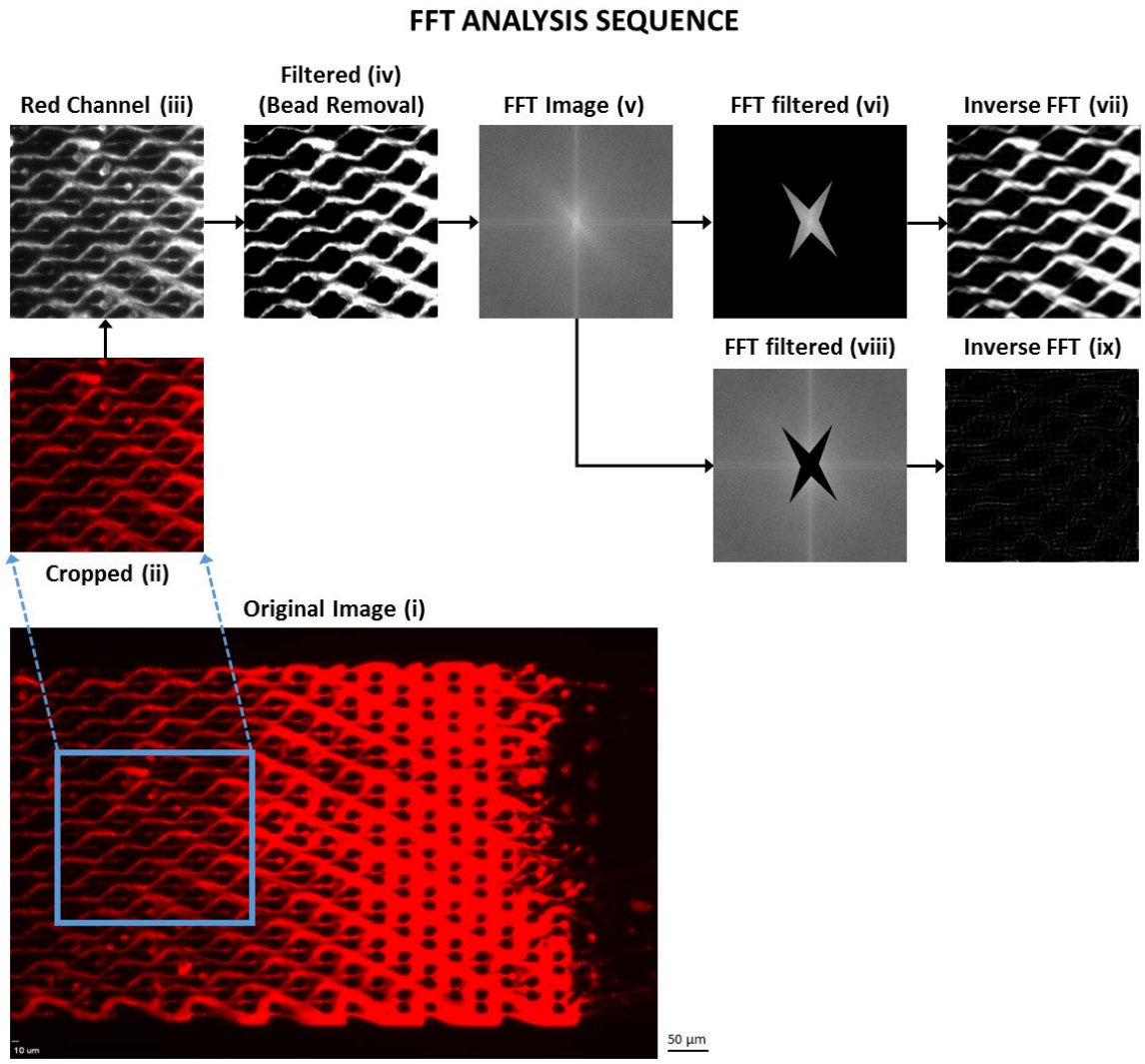

Figure 3.17 Fast Fourier Transform (FFT) analysis of DNA fiber patterns

Schematic illustration of the steps involved in FFT analysis of the DNA fiber patterns. The FFT image analysis is used to quantitatively confirm the existence of a periodic pattern read-out. Using the raw fluorescence image file of the DNA pattern read-out **(i)**, a 400 x 400 pixel sample image **(ii)** is cropped out for analysis. The red channel image is isolated **(iii)** and then filtered and contrast-enhanced to remove microbead and micropost artifacts **(iv)**. FFT is performed on the image using ImageJ software **(v)**. The relevant angles of the DNA fiber pattern are isolated from the FFT result and the background is removed **(vi)**. To check that we isolated the FFT result region representing the relevant DNA pattern frequencies, we performed inverse-FFT on the low-pass filtered FFT result **(vii)**. As a comparison, we also examined the background which was removed from the FFT result **(viii)**. The inverse-FFT of the background FFT **(ix)** shows no pattern and thus confirms that the frequencies corresponding to the periodic DNA fiber pattern were accurately isolated and reconstructed with inverse-FFT.

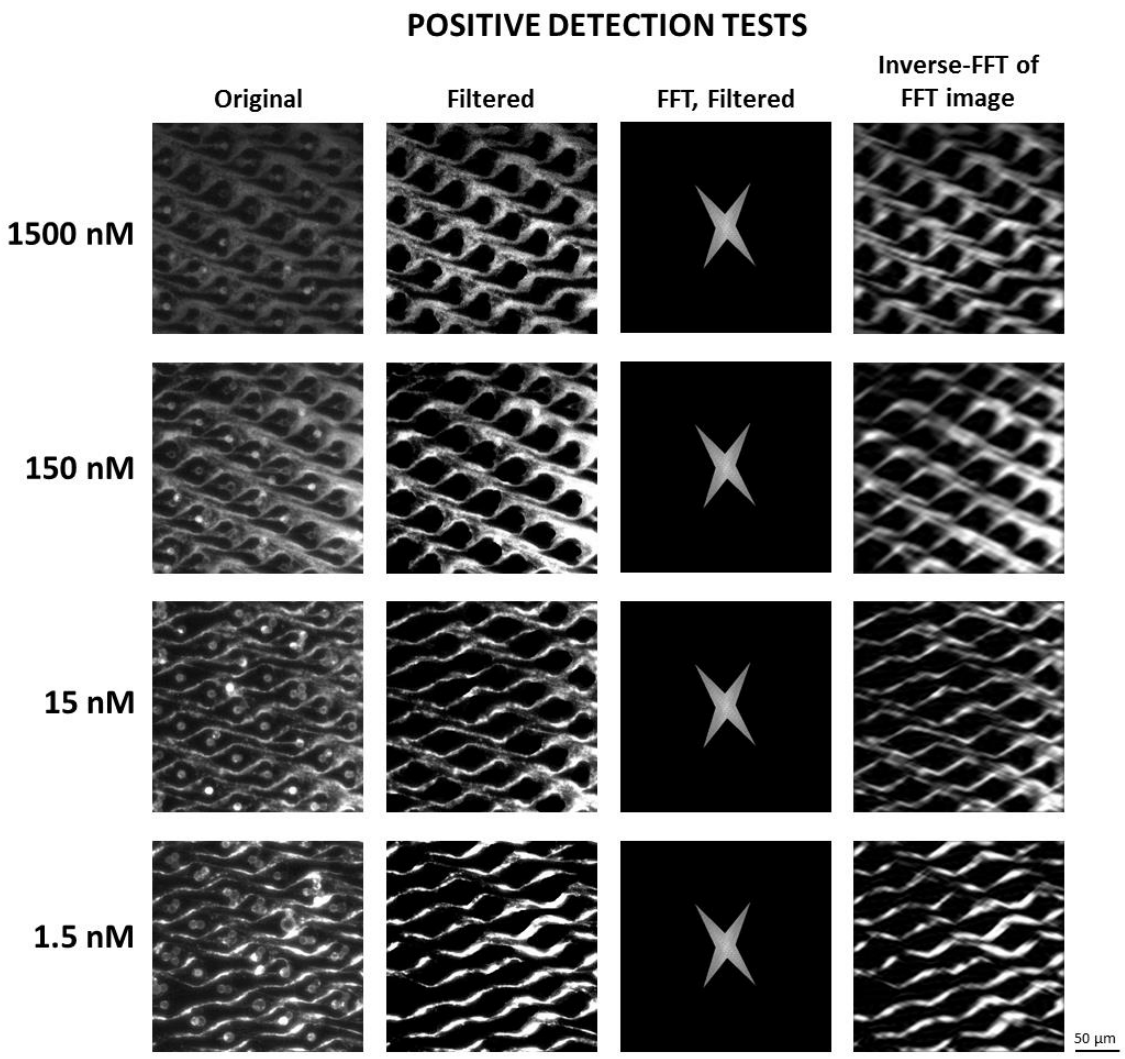

Figure 3.18 FFT analysis of positive detection tests

Image analysis results from performing FFT and inverse-FFT on positive detection tests for target amounts ranging from 1.5 – 1500 nM. Using the FFT analysis steps described in **Figure 3.17**, each sample image was filtered, contrast-enhanced, and used to generate a FFT result. The background frequencies were removed from the FFT result, and inverse-FFT was performed on the FFT result to verify that the pattern frequencies were accurately isolated. As expected, all positive detection tests had periodic patterns which could be regenerated by the inverse-FFT processing of the original FFT result.

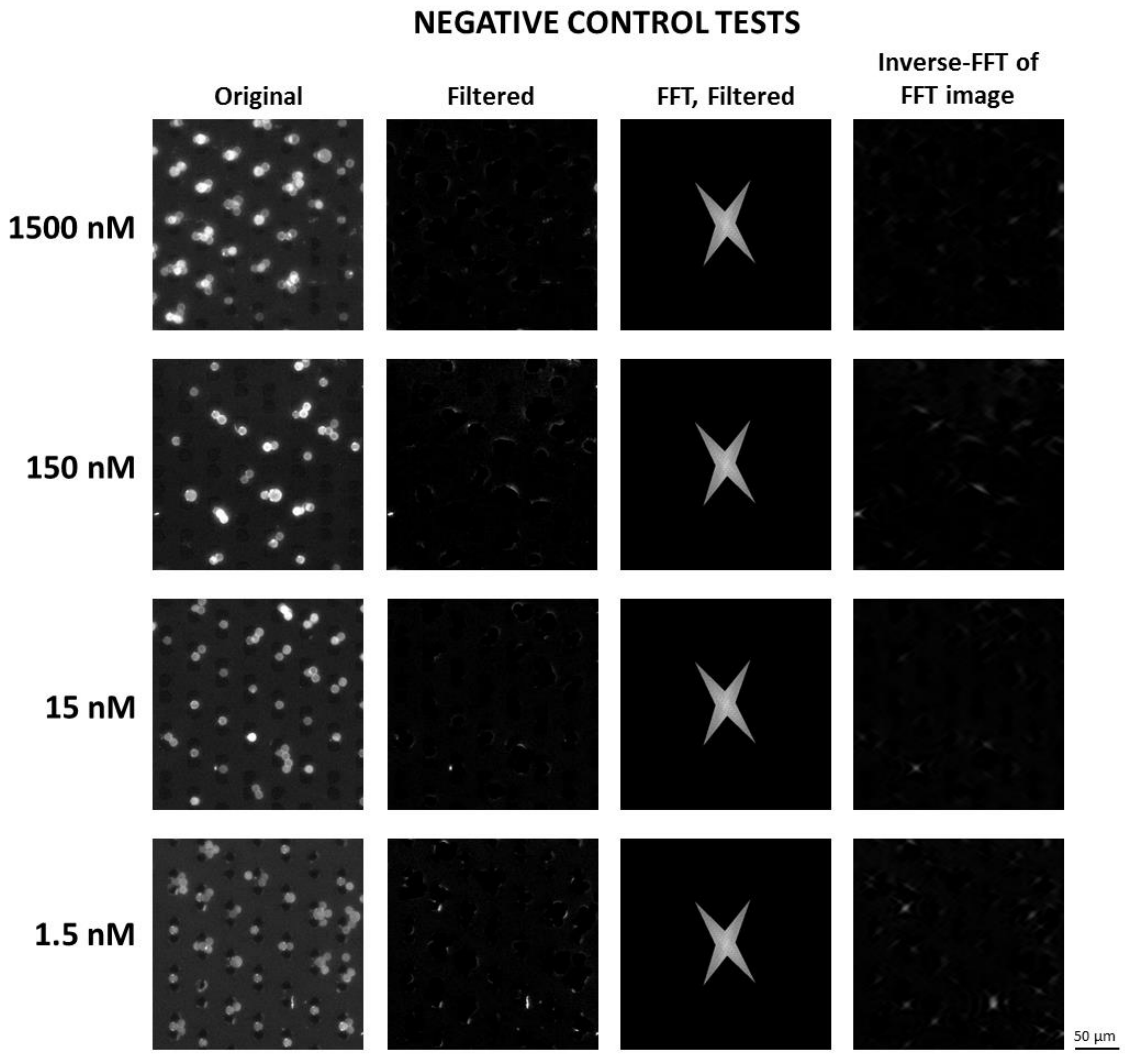

Figure 3.19 FFT analysis of negative control detection tests

Image analysis results from performing FFT and inverse-FFT on negative control detection tests for target amounts ranging from 1.5 – 1500 nM. Using the FFT analysis steps described in **Figure 3.17**, each sample image was filtered, contrast-enhanced, and used to generate a FFT result. The background frequencies were removed from the FFT result, and inverse-FFT was performed on the filtered FFT result. As expected, all negative control detection tests revealed no periodic patterns following the inverse-FFT processing step.

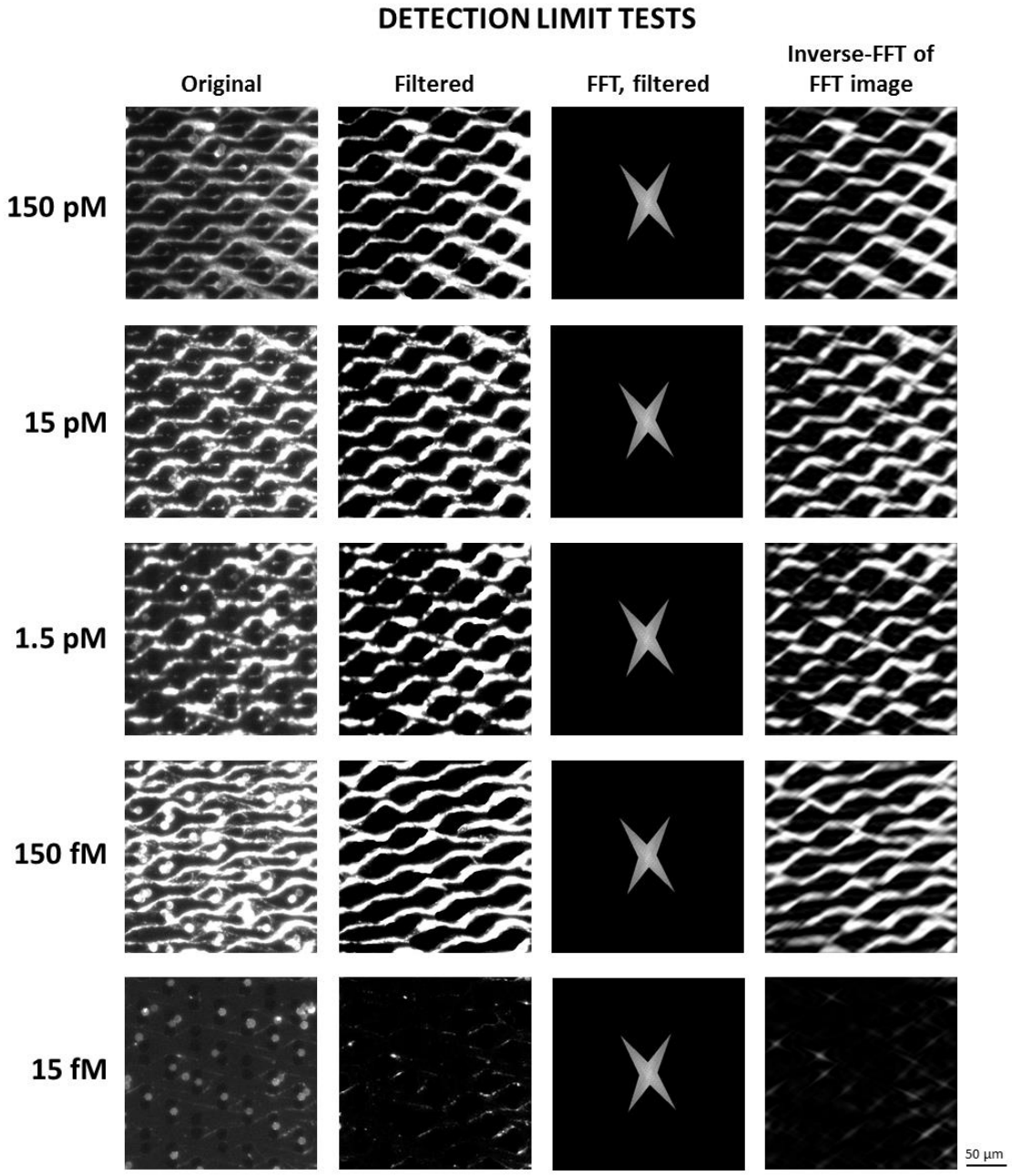

Figure 3.20 FFT analysis of detection limit tests

Image analysis results from performing FFT and inverse-FFT on detection limit tests for target concentrations ranging from 15 fM – 150 pM. Using the FFT analysis steps described in **Figure 3.17**, each sample image was analyzed with FFT processing and with inverse-FFT confirmation of the isolated pattern frequencies. Periodic DNA patterns were confirmed for only 150 fM – 150 pM target samples. The 15 fM target concentration falls below the system detection limit, and thus when inverse-FFT was performed no pattern was generated from the same frequency domain, effectively confirming our negative detection result.

3.3.8 *DNA pattern formation in rectangular post-array devices*

Although microfluidic flow is an important parameter in guiding the DNA pattern formation, the micropost array is also a key element. To evaluate the degree to which DNA patterns form in microfluidic post-arrays with varying inter-post spacing, three different microfluidic devices were designed. These three devices had rectangular post arrays with small, medium, and large inter-post spacing, in addition to different tilt-angles designed into the array. Microbeads were removed from these tests so the DNA patterns were purely formed by entanglement during fluid flow around the post array geometries. Two different sample target concentrations were used, 1.5 nM and 150 nM, and the standard 4 hour, 0.1 µl/min detection reactions were used for each type of rectangular post array device.

Overall, the results indicated that there is an upper limit to inter-post spacing, beyond which no DNA pattern forms. As seen in **Figure 3.21**, the large-spacing rectangular post array produced irregular and thin DNA fibers at the low target concentration, and in contrast, large, amorphous DNA aggregates were formed at high target concentration. Conversely, small and medium spaced arrays (which had similar dimensions to the original micropost array device) yielded uniform and periodic wave-like DNA patterns. These results also demonstrate that a variety of micropost array designs can be used to generate different 2D periodic DNA patterns. From a pure self-assembly perspective, this design versatility could be incredibly useful for 2D patterning of micro- and nano-scale objects such as proteins and nanoparticles. Furthermore, the micropost arrays could be applied to the generation of novel 2D DNA materials for sensing and biomaterial applications.

A.

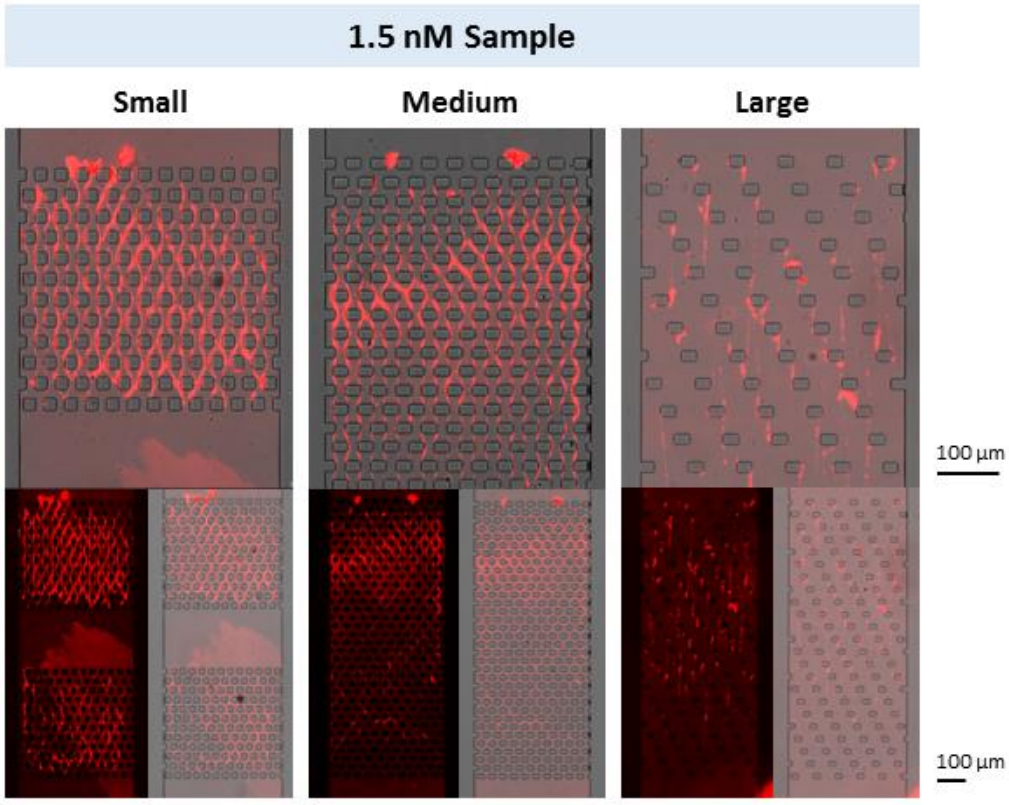
1.5 nM Sample
Small
Medium
Large
100 µm
100 µm

B.

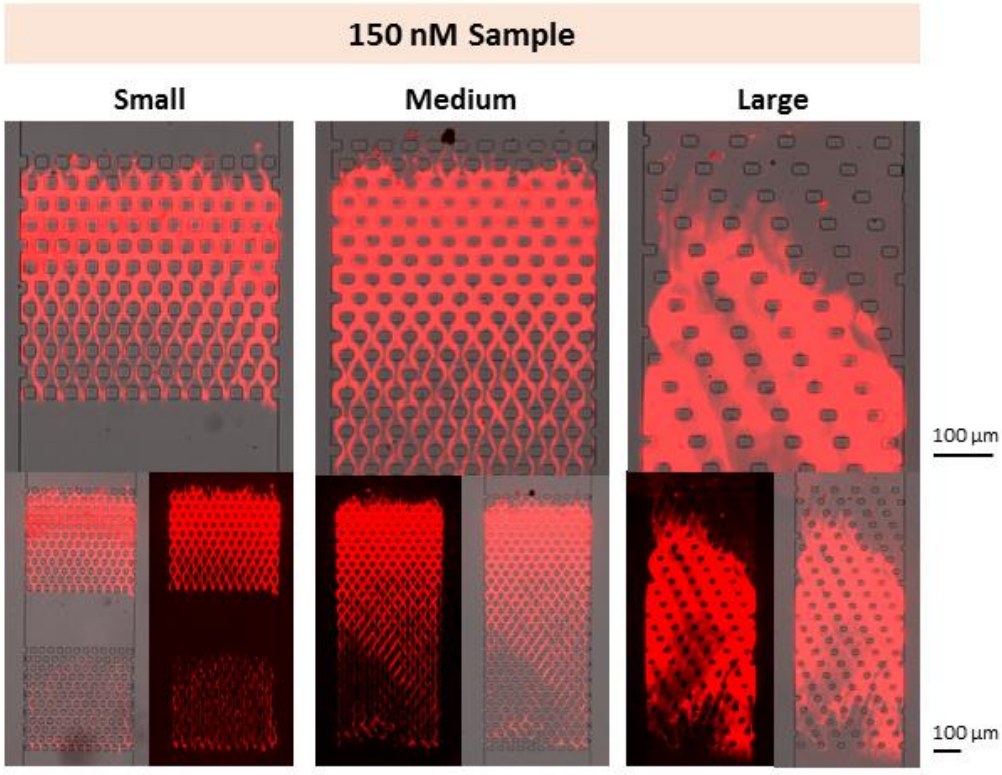
150 nM Sample
Small
Medium
Large
100 µm
100 µm

C.

Pattern	Post-Spacing (X,Y)
Small	(25 µm, 30 µm)
Medium	(50 µm, 40 µm)
Large	(75 µm, 50 µm)

Figure 3.21 DNA fiber patterns generated from rectangular post-array devices

Fluorescence images of DNA fiber patterns formed in micropost arrays with different inter-post spacing. Three device designs were tested with different distances between posts (small, medium, large) for a 1.5 nM target sample concentration **(A)** and a 150 nM target sample concentration **(B)**. Wave-like patterns were generated for only the small and medium-spaced rectangular post array designs, indicating that a balance between micropost spacing and DNA amount is needed for uniform DNA pattern formation. **C)** Chart listing the different spacing measurements for small, medium, and large rectangular post-array designs.

3.3.9 *Detection of RNA and DNA viral targets from crude leaf samples*

Many of our optimization tests were performed using transcripts amplified from isolated viral pathogens. This method allowed us to use pure samples for precise tuning and adjustment of the diagnostic system parameters. To bring our detection platform to a more real-world context, we additionally performed detection on raw crude leaf samples sourced directly from live infected plants. Using triplicate positive tests and triplicate negative controls, we demonstrated that our platform could effectively detect two different types of viral pathogens with different types of genetic material: 1) Cucumber Mosaic Virus (CMV), which has ssRNA as its genetic material, and 2) Tomato Yellow Leaf Curl Virus (TYLC), which has ssDNA as its genetic material. These findings reveal that our system is highly robust and can detect both RNA and DNA pathogens. In addition, we confirmed that our system can accurately and sensitively perform RCA-based detection from very long DNA or RNA, which often has secondary structure conformations that make it difficult for other types of detection probes to bind. The results of the triplicate tests with crude leaf samples are shown in **Figure 3.22**.

A.

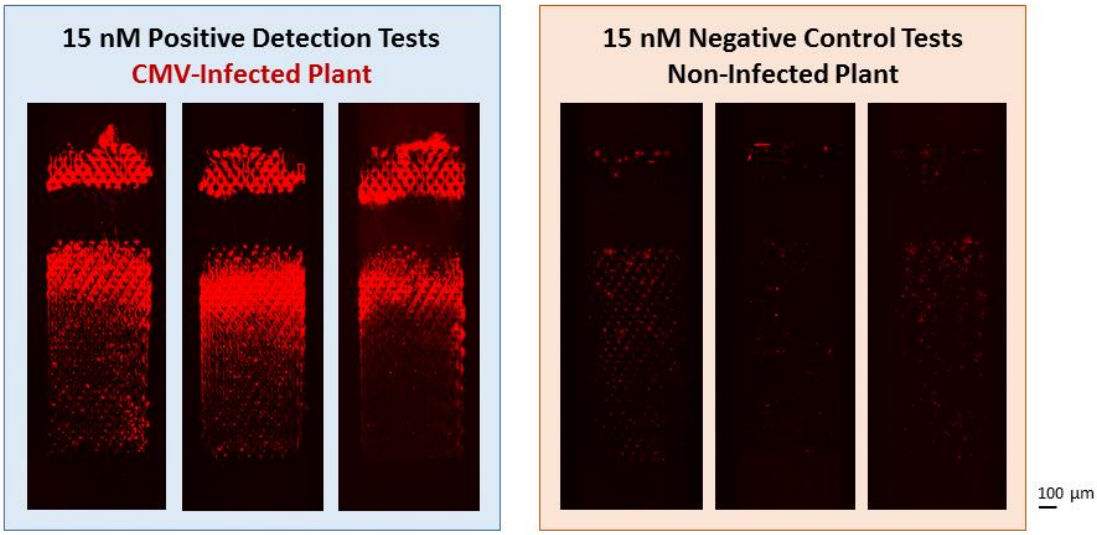

B.

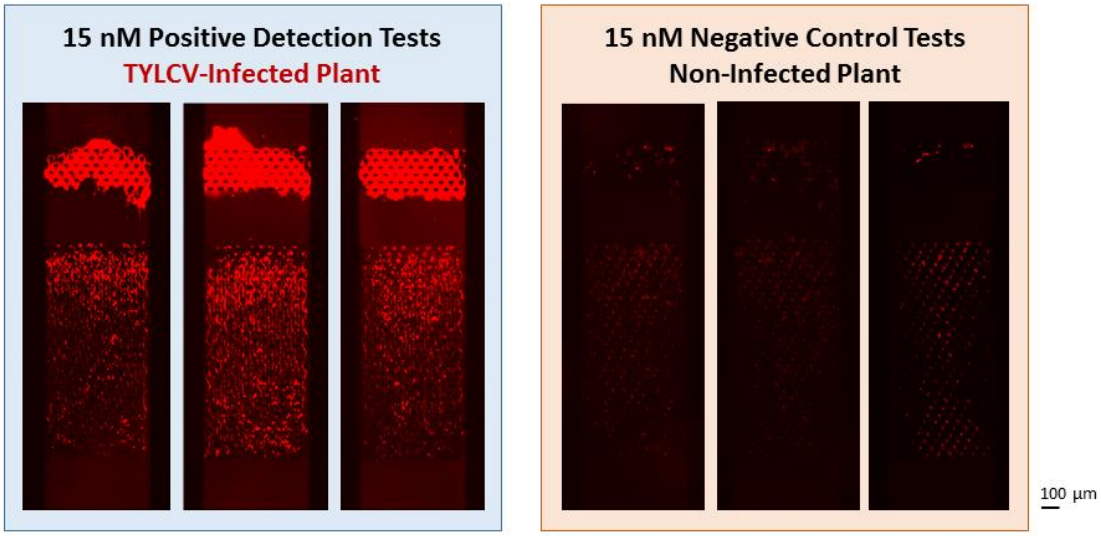

Figure 3.22 Identification of real plant viruses from crude infected leaf samples

These images show positive detection results from crude infected leaf samples. Two viruses were successfully identified, cucumber mosaic virus (CMV) which has ssRNA genetic material, and tomato yellow leaf curl virus (TYLCV), which has ssDNA genetic material. **A)** Triplicate positive test and negative control test results for CMV samples. **B)** Triplicate positive test and negative control results for TYLCV samples.

3.3.10 *Silver-staining for naked eye and smartphone POC detection*

Our ultimate vision was to achieve a POC nucleic acid detection system that is robust, simple to use, and has a consistent and sensitive read-out over a broad detection range. While DNA can be readily stained with a fluorescence dye and imaged with a fluorescence microscope, this read-out setup is technical, expensive and is difficult to use outside of a clinical environment. To overcome this challenge, we used a modified silver staining protocol to deposit silver on the DNA fiber pattern within the microfluidic device. The silver stain made the DNA fibers appear black to the naked eye. This feature enabled our device to achieve true POC detection without requiring expensive and technical microscopy or thermal cycling equipment. As seen in **Figure 3.23 A-D**, positive detection tests clearly showed a concentrated black band where the stained DNA fibers were densest. The negative controls revealed that our silver stain did not significantly stain the PDMS of the device, which is important for reducing background signal.

Incredibly, we were able to image the microfluidic RCA diagnostic device using a smartphone camera and clearly visualize the silver stained DNA fiber pattern. **Figure 3.23 E-F** are real images taken with a standard smartphone camera with no enhancements or lens attachments. This is an important step toward real-world POC detection of plant pathogens in agricultural crops, because this goal necessitates on-site field testing and highly mobile diagnostics. Moreover, we were amazed that, upon imaging the same device 4 months later with a smartphone camera, the silver stain was still clearly visible within the microfluidic device as a dark band. (**Figure 3.23 G**) We also discovered that we could zoom in on the smartphone image and still discern the periodic DNA pattern. Cropped and enlarged images of the smartphone read-out are shown in **Figure 3.23 H**.

Our RCA-based diagnostic device delivers a number of extremely valuable features: it is highly sensitive with a detection limit of 150 fM, it can be used to detect viral pathogens in raw crude samples, and the detection read-out is stable for over 4 months when stored at room temperature with no refrigeration. Not only could our diagnostic system greatly promote the health and maintenance of global agriculture, but it could also significantly advance POC detection of viral and bacterial pathogens from human samples in both clinical and non-clinical settings. Particularly for nucleic acid detection, our RCA-based diagnostic device supports important capabilities such as femtomolar detection sensitivity, crude sample processing adaptability, and environment and storage flexibility – all of which are difficult to accomplish within a single, low-cost platform.

A.

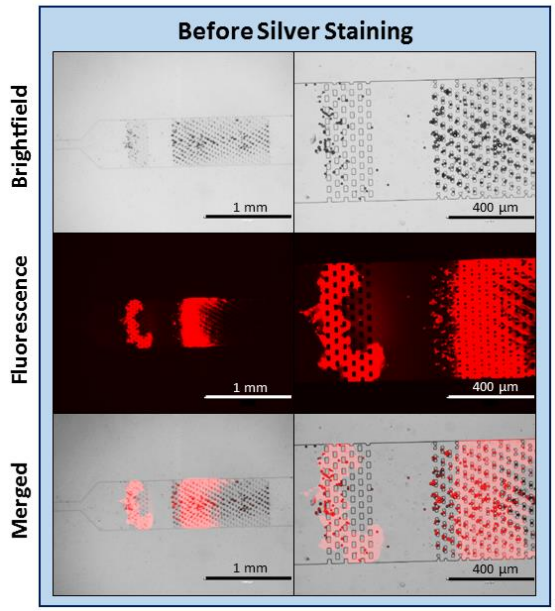
Before Silver Staining
Brightfield
Fluorescence
Merged
1 mm
400 µm

B.

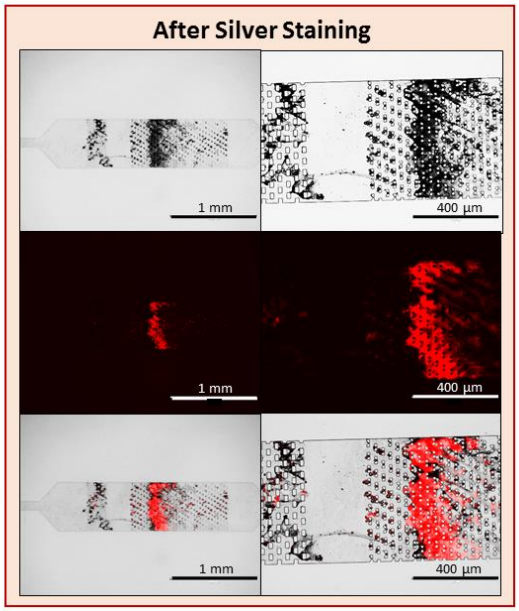
After Silver Staining
Brightfield
Fluorescence
Merged
1 mm
400 µm

C.

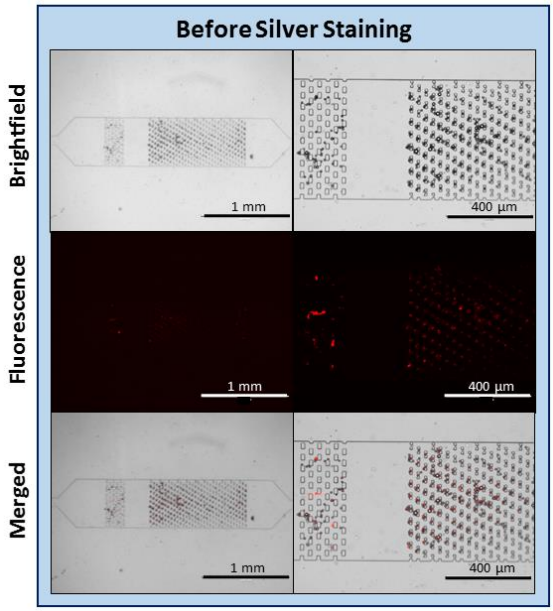
Before Silver Staining
Brightfield
Fluorescence
Merged
1 mm
400 µm

D.

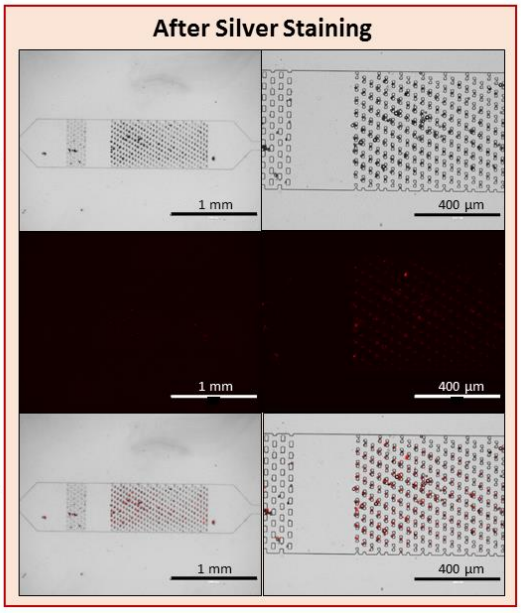
After Silver Staining
Brightfield
Fluorescence
Merged
1 mm
400 µm

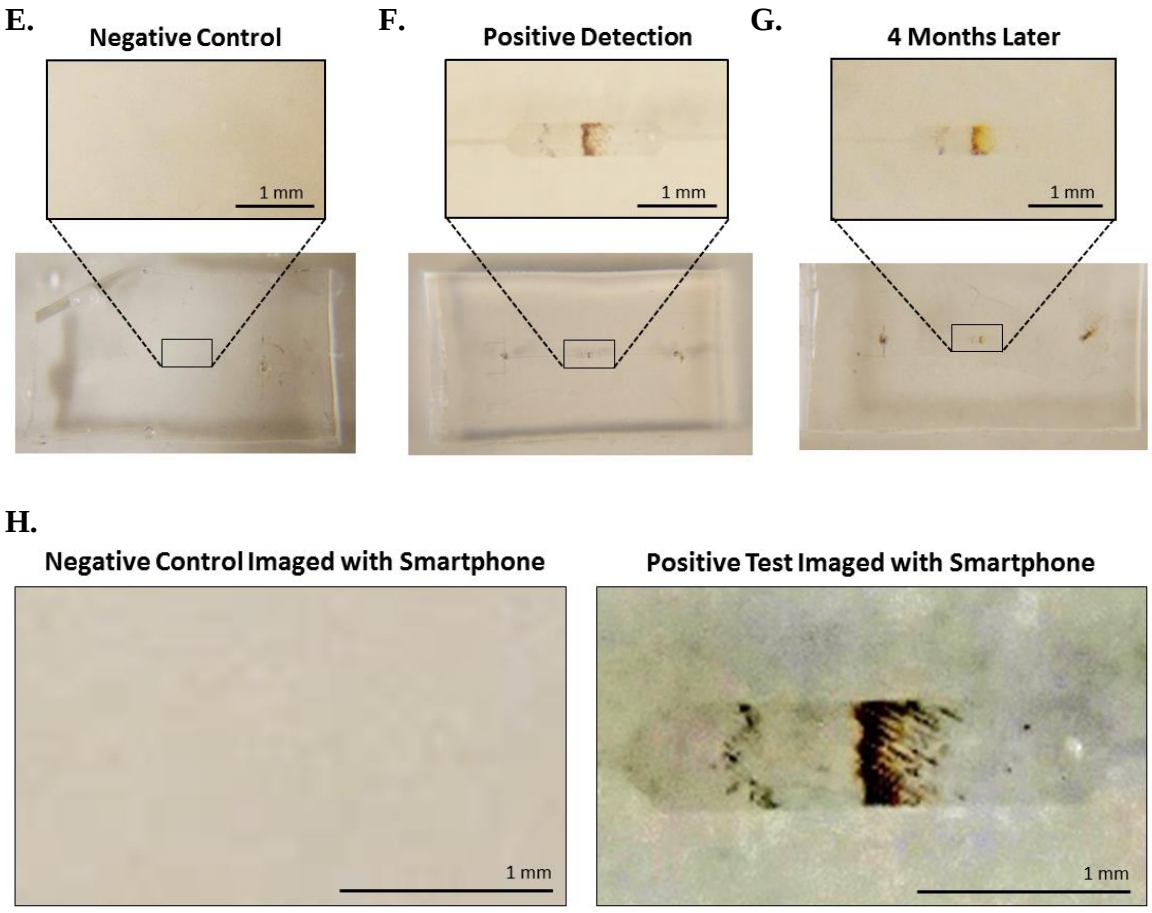

Figure 3.23 Silver staining within the microfluidic device for POC detection

A-B) Fluorescence and bright field images of the microfluidic devices after positive detection of nucleic acid targets and silver staining. Fluorescence and silver stain overlap confirm that DNA was stained accurately. **C-D)** Fluorescence and bright field images of the devices after negative control tests were performed with silver staining. Lack of silver stain confirms that the PDMS device is not stained and that there is insignificant background noise. **E-G)** Smartphone captured images of the silver stained devices. A negative control **(E),** positive detection test immediately after staining **(F),** and a positive detection test after 4 months of dry-air room temperature storage **(G)** are represented here. These results confirm that the pathogen detection can be performed without expensive equipment, and that the device results last for over 4 months without refrigeration. **H)** Enlarged and cropped images from the smartphone captured images of negative control and positive detection tests performed in our diagnostic devices.

3.5 Conclusion

We have engineered a novel diagnostic platform integrating isothermal DNA amplification, silver staining, and a portable microfluidic micropost-array device for point-of-care detection of DNA and RNA viral targets. This platform employs a new DNA hydrodynamic patterning strategy in which RCA is performed simultaneously as the entire sample mix is flowing through the system. This method generates a highly uniform 2D periodic DNA pattern which can be stained and visualized quickly by the naked eye (or a smartphone camera) without sacrificing sensitivity or accuracy. We achieved detection to as low as 150 fM of nucleic acid target, and have successfully proven accurate detection of both RNA and DNA viruses from crude infected leaf samples. These findings demonstrate that our system broadly detects multiple types of pathogens with excellent sensitivity while also avoiding the typical constraints of laboratory-based methods. Moreover, we confirmed that our system can accurately perform RCA-based detection from very long DNA or RNA genetic material, which often has secondary structure conformations that make it difficult for other types of detection probes to bind.

Interestingly, below the 150 fM detection limit no DNA fiber pattern forms. At the detection limit our platform yields a unique “yes or no” result that is entirely based on a visual pattern. The 2D DNA pattern acts as a cognitive signal which instantly provides a “yes” answer for rapid read-out of the detection result. Using a pattern as a visual cue (other than color or intensity) is a unique cognitive signal that further confirms positive target detection. When we investigated RCA detection in a static environment devoid of fluid flow the resulting DNA product did not form a uniform pattern in the microfluidic device. This finding indicated that continuous microfluidic flow is required for DNA pattern

formation. This requirement is highly unique, since DNA self-assembly both at the nano- and macro-scale typically occurs in a self-contained, static solution environment. To the best of our knowledge, our detection system is one of the first to use a DNA amplification reaction with simultaneous hydrodynamic flow as a strategy for driving self-assembly and entanglement of 2D DNA fiber patterns.

We also discovered that a variety of micropost array designs can be used for generating a broad range of periodic DNA patterns. From a self-assembly perspective, this versatility could be incredibly powerful for the specific organization and patterning of micro- and nano-scale objects such as proteins and nanoparticles. Furthermore, our system could be adapted for the assembly of free-standing 2D DNA sheets for sensing and biomaterial applications.

Our diagnostic device affords a number of highly valuable features: it is highly sensitive with a detection limit of 150 fM, it can be used to detect viral pathogens in raw crude samples, it can detect nucleic acid targets across seven orders of magnitude, and the detection read-out result is stable for over 4 months without a decrease in read-out resolution. Particularly for DNA-based detection, this is a huge leap forward since few DNA-based strategies can achieve all of these features simultaneously in a single platform. This work demonstrates successful POC diagnostics using DNA materials, which could ultimately contribute to the detection of numerous diseases in low-resource settings such as the developing world. This device could also greatly improve agricultural diagnostics, an area that has a severe lack of commercially available detection systems for on-site field testing. Finally, this work reveals that the fusion of DNA materials and microfluidics has powerful applications in not only diagnostics, but also material assembly and patterning.

CHAPTER 4

CONCLUSION AND FUTURE PERSPECTIVE

DNA enables highly programmable assembly of diverse and multifunctional materials that can interface with both inorganic (i.e. nanoparticles, quantum dots, solid substrates) and organic matter (i.e. enzymes, biomolecules, cells). DNA is unlike any other polymer because it affords several important advantages (multifunctionality, controllability, design versatility) that can be exploited and tuned for different goals. Many DNA structures have been developed, including DNA tiles, DNA origami, DNA lattice sheets, DNA coated nanoparticles, and DNA hydrogels – all of which have achieved unprecedented advancements in fields such as biology, chemistry and engineering. In addition, many unique DNA amplification reactions have been engineered for detection, drug delivery, biomaterial synthesis, and other real-world applications.

With regards to pathogen diagnostics, DNA is incredibly well-suited for performing highly controlled detection reactions with molecular-level accuracy, a capability that is extremely difficult to achieve with other materials. However, DNA-based systems can be limited in their real-world implementation because they are often high complexity, require expensive equipment, and have specific and delicate operation conditions. To overcome this challenge, I have engineered two novel diagnostic systems which incorporate DNA nanotechnology and microfluidics in portable, low cost systems that are simple to operate and capable of achieving highly accurate, sensitive, and informative detection results. The work discussed in this Dissertation provides details on

my investigation and development of these two platforms, both of which demonstrate cutting-edge strategies for translating DNA materials into real-world diagnostics.

Chapter 2 discussed our multiplexed diagnostic system, which was based on fluorescence-encoded branched DNA nanobarcode structures. We used DNA as a structural polymer to assemble novel multifunctional probes, and furthermore we utilized them within a microbead-array device for enhanced DNA detection. Our DNA nanobarcode labeling strategy (using different combinations of red and green dyes) was carefully designed and characterized, and it was also expanded by incorporating bead surface-intensity coding. We discovered a remarkable resetting capability in this DNA nanobarcode system as well. Accurate pathogen detection was repeated seven times in a single device without sacrificing detection sensitivity or accuracy, an achievement that is particularly critical in low-resource POC environments where re-usable devices with extended lifetimes could have a huge impact on public healthcare. Our device not only does this, but it also demonstrates specific detection of up to five DNA targets simultaneously, with a broad detection range of 50 pM – 1 μM. Integrating multiplexed detection with high detection sensitivity is a critical advantage, particularly for multiplexed detection of a panel of pathogens which exhibit very similar clinical symptoms in patients.

Overall, this platform used branched DNA nanostructures as molecular-recognition probes in a microfluidic microbead-array system without introducing the complexity or strict temperature and operations requirements common in standard detection methodologies such as PCR and immunoassays. Our work will significantly expand the DNA-based diagnostics repertoire, and it has powerful implications for advancing real-world clinical diagnostics. In particular, it would be extremely useful for screening difficult

to detect (and difficult to distinguish) bacterial and viral pathogens. The standard procedures in these situations can take between hours to a week, and thus quick, accurate, and highly informative (panel-based screening) diagnostics could have a huge positive impact in protecting patients from severe health complications due to misdiagnosis and delayed treatments.

Chapter 3 discussed our invention of a POC platform integrating isothermal DNA amplification, silver staining, and a micropost-array microfluidic device. Inspired by the versatility and sequence design capabilities of DNA in amplification reactions, we engineered a unique DNA system for POC detection of DNA/RNA viruses in infected agricultural plants. This platform employs a new DNA hydrodynamic patterning strategy in which DNA amplification is performed simultaneously as the reaction solution is continually flowing – this generates uniform, periodic 2D DNA patterns. These 2D patterns can be rapidly stained and visualized by the naked eye without reducing detection sensitivity or accuracy. We achieved a detection limit of 150 fM nucleic acid target using room temperature conditions, and we confirmed accurate detection of both RNA and DNA viruses from crude infected samples. These findings demonstrate that our system can broadly detect different types of viruses with high sensitivity, and furthermore they show our system can handle long DNA or RNA genetic material despite the presence of secondary architectures which typically inhibit probe detection. We also explored different micropost array designs for generating a variety of DNA patterns. In addition to generating rapid isothermal detection read-outs, this hydrodynamic DNA-patterning method could be incredibly useful in the organization and patterning of micro- and nano-scale objects such as proteins, biomolecules, and nanoparticles. Our system could be easily adapted for the

programmable assembly of free-standing 2D DNA sheets for sensing and biomaterial applications.

To the best of our knowledge, our detection system is one of the first to integrate a DNA amplification reaction with hydrodynamic flow as a means for driving self-assembly and entanglement of 2D periodic DNA fiber patterns. Our device integrates a number of highly valuable features: it is highly sensitive with a detection limit of 150 fM, it can be used to detect viral pathogens in raw crude samples, it can detect nucleic acid targets across seven orders of magnitude, and the detection result is stable for over 4 months when stored in dry, room temperature conditions. Very few DNA-based detection technologies today can achieve all of these capabilities in a single, low-cost, portable platform. We believe our platform could revolutionize agricultural diagnostics, a field that severely lacks detection systems for rapid, on-site screening of disease in agricultural crops. Furthermore, this work could dramatically improve the field of POC diagnostics, particularly for low-resource setting such as the developing world. Our diagnostic platform is also highly transferrable to other fields such as clinical, veterinary, and food-safety, thanks to the universal role of DNA as a genetic material (and detection biomarker) for many organisms.

The research investigations described in this Dissertation sought to demonstrate the feasibility and advantages of DNA materials in clinical and POC diagnostics, with the aim of highlighting the synergistic capabilities that arise from fusing DNA nanotechnology with microfluidics. Future work in this area has exciting implications, as it could lead to new, innovative platforms that overcome the main challenges of traditional diagnostic methods such as PCR, immunoassays, and cell culture. With further development, the incorporation of DNA materials into existing and new strategies for diagnostics will drive

incredible progress in global healthcare technology, help provide improved clinical outcomes, and enable more universal application of nucleic acid diagnostics.

BIBLIOGRAPHY

[1] Seeman, N.C. DNA in a material world. *Nature* **421**, 427-431 (2003).

[2] Luo, D. The road from biology to materials. *Mater Today* **6**, 38-43 (2003).

[3] Kosuri, S. & Church, G.M. Large-scale de novo DNA synthesis: technologies and applications. *Nat Methods* **11**, 499-507 (2014).

[4] Dormitzer, P.R., Suphaphiphat, P., Gibson, D.G., *et al*. Synthetic generation of influenza vaccine viruses for rapid response to pandemics. *Sci Transl Med* **5**, (2013).

[5] Roberts, R.J., Vincze, T., Posfai, J., Macelis, D. REBASE -- enzymes and genes for DNA restriction and modification. *Nucleic Acids Res* **35**, D269–D270 (2007).

[6] Cheng, W.L., Park, N.Y., Walter, M.T., Hartman, M.R. & Luo, D. Nanopatterning self-assembled nanoparticle superlattices by moulding microdroplets. *Nat Nanotechnol* **3**, 682-690 (2008).

[7] Cheng, W.L., Campolongo, M.J., Cha, J.J., *et al*. Free-standing nanoparticle superlattice sheets controlled by DNA. *Nat Mater* **8**, 519-525 (2009).

[8] Tan, S.J., Campolongo, M.J., Luo, D. & Cheng, W.L. Building plasmonic nanostructures with DNA. *Nat Nanotechnol* **6**, 268-276 (2011).

[9] Mirkin, C.A., Letsinger, R.L., Mucic, R.C. & Storhoff, J.J. A DNA-based method for rationally assembling nanoparticles into macroscopic materials. *Nature* **382**, 607-609 (1996).

[10] Alivisatos, A.P., Johnson, K.P., Peng, X.G., *et al*. Organization of 'nanocrystal molecules' using DNA. *Nature* **382**, 609-611 (1996).

[11] Park, S.Y., Lytton-Jean, A.K.R., Lee, B., Weigand, S., Schatz, G.C., & Mirkin, C.A. DNA-programmable nanoparticle crystallization. *Nature* **451**, 553-556 (2008).

[12] Elghanian, R., Storhoff, J.J., Mucic, R.C., Letsinger, R.L. & Mirkin, C.A. Selective colorimetric detection of polynucleotides based on the distance-dependent optical properties of gold nanoparticles. *Science* **277**, 1078-1081 (1997).

[13] Sano, T., Smith, C.L. & Cantor, C.R. Immuno-PCR: Very sensitive antigen detection by means of specific antibody-DNA conjugates. *Science* **258**, 120-122 (1992).

[14] Niemeyer, C.M., Wacker, R. & Adler, M. Combination of DNA-directed immobilization and immuno-PCR: Very sensitive antigen detection by means of self-assembled DNA-protein conjugates. *Nucleic Acids Research* **31**, e90 (2003).

[15] Wilner, O.I., Weizmann, Y., Gill, R., Lioubashevski, O., Freeman, R., Willner, I. Enzyme cascades activated on topologically programmed DNA scaffolds. *Nat Nanotechnol* **4**, 249-254 (2009).

[16] Bailey, R.C., Kwong, G.A., Radu, C.G., Witte, O.N. & Heath, J.R. DNA-encoded antibody libraries: A unified platform for multiplexed cell sorting and detection of genes and proteins. *J Am Chem Soc* **129**, 1959-1967 (2007).

[17] Niemeyer, C.M. The developments of semisynthetic DNA-protein conjugates. *Trends Biotechnol* **20**, 395-401 (2002).

[18] Niemeyer, C.M. Functional devices from DNA and proteins. *Nano Today* **2**, 42-52 (2007).

[19] Niemeyer, C.M. Semisynthetic DNA-protein conjugates for biosensing and nanofabrication. *Angew Chem Int Ed* **49**, 1200-1216 (2010).

[20] Alemdaroglu, F.E., Wang, J., Borsch, M., Berger, R. & Herrmann, A. Enzymatic control of the size of DNA block copolymer nanoparticles. *Angew Chem Int Ed* **47**, 974-976 (2008).

[21] Gibbs, J.M., Park, S.J., Anderson, D.R., Watson, K.J., & Mirkin, C.A. Polymer-DNA hybrids as electrochemical probes for the detection of DNA. *J Am Chem Soc* **127**, 1170-1178 (2005).

[22] Immoos, C.E., Lee, S.J. & Grinstaff, M.W. DNA-PEG-DNA triblock macromolecules for reagentless DNA detection. *J Am Chem Soc* **126**, 10814-10815 (2004).

[23] Kwak, M. & Herrmann, A. Nucleic acid/organic polymer hybrid materials: synthesis, superstructures, and applications. *Angew Chem Int Ed* **49**, 8574-8587 (2010).

[24] Safak, M., Alemdaroglu, F.E., Li, Y., Ergen, E. & Herrmann, A. Polymerase chain reaction as an efficient tool for the preparation of block copolymers. *Adv Mater* **19**, 1499-1505 (2007).

[25] Watson, K.J., Park, S.J., Im, J.H., Nguyen, S.T. & Mirkin, C.A. DNA-block copolymer conjugates. *J Am Chem Soc* **123**, 5592-5593 (2001).

[26] Mirkin, C.A., Letsinger, R.L., Mucic, R.C. & Storhoff, J.J. A DNA-based method for rationally assembling nanoparticles into macroscopic materials. *Nature* **382**, 607-609 (1996).

[27] Rosi, N.L. & Mirkin, C.A. Nanostructures in biodiagnostics. *Chem Rev* **105**, 1547-1562 (2005).

[28] Park S.Y., Lytton-Jean A.K., Lee, B., Weigand S., Schatz G.C. & Mirkin, C.A. DNA-programmable nanoparticle crystallization. *Nature* **451**, 553-556 (2008).

[29] Nykypanchuk, D., Maye, M.M., van der Lelie, D. & Gang, O. DNA-guided crystallization of colloidal nanoparticles. *Nature* **451**, 549-552 (2008).

[30] Mastroianni, A.J., Claridge S.A. & Alivisatos A.P. Pyramidal and chiral groupings of gold nanocrystals assembled using DNA scaffolds. *J Am Chem Soc* **131**, 8455-8459 (2009).

[31] Niemeyer, C.M., Sano, T., Smith, C.L. & Cantor, C.R. Oligonucleotide-directed self-assembly of proteins: semisynthetic DNA--streptavidin hybrid molecules as connectors for the generation of macroscopic arrays and the construction of supramolecular bioconjugates. *Nucleic Acids Res* **22**, 5530-5539 (1994).

[32] Niemeyer, C.M., Koehler, J. & Wuerdemann, C. DNA-directed assembly of bienzymic complexes from in vivo biotinylated NAD(P)H:FMN oxidoreductase and luciferase. *ChemBioChem* **3**, 242-245 (2002).

[33] Pathak, S., Choi, S.K., Arnheim, N. & Thompson, M.E. Hydroxylated quantum dots as luminescent probes for in situ hybridization. *J Am Chem Soc* **123**, 4103-4104 (2001).

[34] Gerion, D., Chen, F., Kannan, B., *et al.* Room-temperature single-nucleotide polymorphism and multiallele DNA detection using fluorescent nanocrystals and microarrays. *Anal Chem* **75**, 4766-4772 (2003).

[35] Han, M.Y., Gao, X., Su, J.Z. & Nie, S. Quantum-dot-tagged microbeads for multiplexed optical coding of biomolecules. *Nat Biotech* **19**, 631-635 (2001).

[36] Parak, W.J., Gerion, D., Zanchet *D, et al*. Conjugation of DNA to silanized colloidal semiconductor nanocrystalline quantum dots. *Chem Mater* **14**, 2113-2119 (2002).

[37] Mirkin, C.A., Letsinger, R.L., Mucic, R.C. & Storhoff, J.J. A DNA-based method for rationally assembling nanoparticles into macroscopic materials. *Nature* **382**, 607-609 (1996).

[38] Storhoff, J.J., Elghanian, R., Mucic, R.C., Mirkin, C.A. & Letsinger, R.L. One-pot colorimetric differentiation of polynucleotides with single base imperfections using gold nanoparticle probes. *J Am Chem Soc* **120**, 1959-1964 (1998).

[39] Soleymani, L., Fang, Z., Sargent, E.H. & Kelley, S.O. Programming nucleic acids detection sensitivity using controlled nanostructuring. *Nat Nanotechnol* **4**, 844-848 (2009).

[40] Drummond, T.G., Hill, M.G., & Barton, J.K. Electrochemical DNA sensors. *Nat Biotech* **21**, 1192-1199 (2003).

[41] Fang, Z., Soleymani, L., Pampalakis, G., *et al.* Direct profiling of cancer biomarkers in tumour tissue using a multiplexed nanostructured microelectrode integrated circuit. *ACS Nano* **3**, 3207-3213 (2009).

[42] Fan, C., Plaxco, K.W., & Heeger, A.J. Electrochemical interrogation of conformational changes as a reagentless method for the sequence-specific detection of DNA. *Proc. Natl. Acad. Sci. U.S.A.* **100**, 9134-9137 (2003).

[43] Lubin, A.A., & Plaxco, K.W. Folding-based electrochemical biosensors: the case for responsive nucleic acid architectures. *Acc Chem Res* **43**, 496-505 (2010).

[44] Park, S., Zhang, Y., Lin, S., Wang, T.-H. & Yang, S. Advances in microfluidic PCR for point-of-care infectious disease diagnostics. *Biotechnol Adv* **29**, 830-839 (2011).

[45] Zhang, C. & Xing, D. Miniaturized PCR chips for nucleic acid amplification and analysis: latest advances and future trends. *Nucleic Acids Res* **35**, 4223-4237 (2007).

[46] Kallenbach, N.R., Ma, R.I., & Seeman, N.C. An immobile nucleic acid junction constructed from oligonucleotides. *Nature* **305**, 829-831 (1983).

[47] Seeman, N.C. DNA in a material world. *Nature* **421**, 427-431 (2003).

[48] Chen J.H. & Seeman N.C. Synthesis from DNA of a molecule with the connectivity of a cube. *Nature* **350**, 631-633 (1991).

[49] Aldaye, F.A. & Sleiman. H.F. Sequential self-assembly of a DNA hexagon as a template for the organization of gold nanoparticles. *Angew Chem Int Ed* **45**, 2204-2209 (2006).

[50] Y.W. Zhang & N.C. Seeman. Construction of a DNA-truncated octahedron. *J Am Chem Soc* **116,** 1661-1669 (1994).

[51] Seeman, N.C., Chen, J., Du, S.M., *et al*. Synthetic DNA knots and catenanes. *New J Chem* **17**, 739-755 (1993).

[52] Fu, T.J. & Seeman N.C. DNA double-crossover molecules. *Biochemistry* **32**, 3211-3220 (1993).

[53] LaBean, T.H., Yan, H., Kopatsch, J. *et al*. Construction, analysis, ligation, and self-assembly of DNA triple crossover complexes. *J Am Chem Soc* **122**, 1848-1860 (2000).

[54] Shen, Z.Y., Yan, H., Wang, T., Seeman, N.C. Paranemic crossover DNA: A generalized Holliday structure with applications in nanotechnology. *J Am Chem Soc* **126**, 1666-1674 (2004),

[55] Lee, C.C., MacKay, J.A., Fréchet J.M., & Szoka, F.C. Designing dendrimers for biological applications. *Nat Biotech* **23**, 1517-1526 (2005).

[56] Li, Y, Tseng, Y.D., Kwon, S.Y *et al*. Controlled assembly of dendrimer-like DNA. *Nat Mater* **3**, 38-42 (2004).

[57] Li, Y, Tseng, Y.D., Kwon, S.Y *et al*. Controlled assembly of dendrimer-like DNA. *Nat Mater* **3**, 38-42 (2004).

[58] Nishikawa, M., Matono, M., Rattanakiat, S., Matsuoka, N. & Takakura, Y. Enhanced immunostimulatory activity of oligodeoxynucleotides by y-shape formation. *Immunology* **124**, 247-255 (2008).

[59] Rattanakiat, S., Nishikawa, M., Funabashi, H., Luo, D. & Takakura, Y. The assembly of a short linear natural cytosine-phosphate-guanine DNA into dendritic structures and its effect on immunostimulatory activity. *Biomaterials* **30**, 5701–5706 (2009).

[60] Lee, C.C., MacKay, J.A., Fréchet J.M., & Szoka, F.C. Designing dendrimers for biological applications. *Nat Biotech* **23**, 1517-1526 (2005).

[61] Lee, J.B., Roh, Y.H., Um, S.H. *et al.* Multifunctional nanoarchitectures from DNA-based ABC monomers. *Nat Nanotechnol* **4**, 430-436 (2009).

[62] Roh Y.H., Lee J.B., Kiatwuthinon P., *et al.* DNAsomes: Multifunctional DNA-based nanocarriers. *Small* **7**, 74-78 (2011).

[63] Lee, J.B., Peng, S., Yang, D., *et al*. A mechanical metamaterial made from a DNA hydrogel. *Nat Nanotechnol* **7**, 816-820 (2012).

[64] He, Y., Chen, Y., Liu, H., Ribbe, A.E. & Mao, C. *J Am Chem Soc* **127**, 12202-12203 (2005).

[65] Yan, H., Park, S.H., Finkelstein, G., Reif, J.H. & LaBean, T.H. DNA-templated self-assembly of protein arrays and highly conductive nanowires. *Science* **301**, 1882-1884, (2003).

[66] Zhang, C., Su, M., He, Y. *et al*. Conformational flexibility facilitates the self-assembly of complex DNA structures. *Proc. Natl. Acad. Sci. U.S.A.* **105**, 10665-10669 (2008).

[67] Goodman, R.P., Schaap, I.A., Tardin, C.F., *et al*. Rapid chiral assembly of rigid DNA building blocks for molecular nanofabrication. *Science* **310**, 1661-1665 (2005).

[68] Shih, W.M., Quispe, J.D., & Joyce, G.F. A 1.7-kilobase single-stranded DNA that folds into a nanoscale octahedron. *Nature* **427**, 618-621 (2004).

[69] He, Y., Ye, T., Su, M., *et al.* Hierarchical self-assembly of DNA into symmetric supramolecular polyhedral. *Nature* **452**, 198-201 (2008).

[70] Andersen E.S., Dong M., Nielsen M.M., *et al*. Self-assembly of a nanoscale DNA box with a controllable lid. *Nature* **459**, 73-76 (2009).

[71] Douglas, S.M., Dietz, H., Liedl, T., Hogberg, B., Graf, F., & Shih, W.M. Self-assembly of DNA into nanoscale three-dimensional shapes. *Nature* **459**, 414-418 (2009).

[72] Dietz, H., Douglas, S.M., & Shih, W.M. Folding DNA into twisted and curved nanoscale shapes. *Science* **325**, 725-730 (2009).

[73] Censi, R., Di Martino, P., Vermonden, T. & Hennink, W.E. Hydrogels for protein delivery in tissue engineering. *J Control Release* **161**, 680-692 (2012).

[74] Lee, S.C., Kwon, I.K. & Park, K. Hydrogels for delivery of bioactive agents: A historical perspective. *Adv Drug Deliv Rev* **65**, 17-20 (2013).

[75] Gupta, P., Vermani, K. & Garg, S. Hydrogels: From controlled release to pH-responsive drug delivery. *Drug Discov Today* **7**, 569-579 (2002).

[76] Lin, C.C. & Metters, A.T. Hydrogels in controlled release formulations: Network design and mathematical modeling. *Adv Drug Deliv Rev* **58**, 1379-1408 (2006).

[77] Peppas, N.A., Hilt, J.Z., Khademhosseini, A. & Langer, R. Hydrogels in biology and medicine: From molecular principles to bionanotechnology. *Adv Mater* **18**, 1345-1360 (2006).

[78] Hoare, T.R. & Kohane, D.S. Hydrogels in drug delivery: Progress and challenges. *Polymer* **49**, 1993-2007 (2008).

[79] Garcia, A.J. PEG-maleimide hydrogels for protein and cell delivery in regenerative medicine. *Ann Biomed Eng* **42**, 312-322 (2014).

[80] Silva, R., Fabry, B. & Boccaccini, A.R. Fibrous protein-based hydrogels for cell encapsulation. *Biomaterials* **35**, 6727-6738 (2014).

[81] Kloxin, A.M., Kloxin, C.J., Bowman, C.N. & Anseth, K.S. Mechanical properties of cellularly responsive hydrogels and their experimental determination. *Adv Mater* **22**, 3484-3494 (2010).

[82] Lutolf, M.P., Gilbert, P.M. & Blau, H.M. Designing materials to direct stem-cell fate. *Nature* **462**, 433-441 (2009).

[83] Seliktar, D. Designing cell-compatible hydrogels for biomedical applications. *Science* **336**, 1124-1128 (2012).

[84] Lutolf, M.P., Gilbert, P.M. & Blau, H.M. Designing materials to direct stem-cell fate. *Nature* **462**, 433-441 (2009).

[85] Seliktar, D. Designing cell-compatible hydrogels for biomedical applications. *Science* **336**, 1124-1128 (2012).

[86] Huh, D., Hamilton, G.A. & Ingber, D.E. From 3D cell culture to organs-on-chips. *Trends Cell Biol* **21**, 745-754 (2011).

[87] Khetan, S. & Burdick, J.A. Patterning hydrogels in three dimensions towards controlling cellular interactions. *Soft Matter* **7**, 830-838 (2011).

[88] Seliktar, D. Designing cell-compatible hydrogels for biomedical applications. *Science* **336**, 1124-1128 (2012).

[89] Huh, D., Hamilton, G.A. & Ingber, D.E. From 3D cell culture to organs-on-chips. *Trends Cell Biol* **21**, 745-754 (2011).

[90] Balakrishnan, B. & Banerjee, R. Biopolymer-based hydrogels for cartilage tissue engineering. *Chem Rev* **111**, 4453-4474 (2011).

[91] Lutolf, M.P. & Hubbell, J.A. Synthetic biomaterials as instructive extracellular microenvironments for morphogenesis in tissue engineering. *Nat Biotech* **23**, 47-55 (2005).

[92] Lee, K.Y. & Mooney, D.J. Hydrogels for tissue engineering. *Chem Rev* **101**, 1869-1879 (2001).

[93] Hoffman, A.S. Hydrogels for biomedical applications. *Adv Drug Deliv Rev* **64**, 18-23 (2012).

[94] Um, S.H., Lee, J.B., Park, N., *et al*. Enzyme-catalysed assembly of DNA hydrogel. *Nat Mater* **5**, 797-801 (2006).

[95] Cheng, E., Xing, Y., Chen, P., *et al*. A pH-triggered, fast-responding DNA hydrogel. *Angew Chem Int Ed* **48**, 7660-7663 (2009).

[96] Gehring, K., Leroy, J.L. & Gueron, M. A Tetrameric DNA structure with protonated cytosine.cytosine base pairs. *Nature* **363**, 561-565 (1993).

[97] Xing, Y.Z., Cheng, E., Yang, Y., *et al*. Self-assembled DNA hydrogels with designable thermal and enzymatic responsiveness. *Adv Mater* **23**, 1117-1121 (2011).

[98] Park, N.Y., Um, S.H., Funabashi, H., Xu, J. & Luo, D. A cell-free protein-producing gel. *Nat Mater* **8**, 432-437 (2009).

[99] Ruiz, R., Kiatwuthinon, P., Kahn, J.S., & Roh, Y.H. Cell-free protein expression from DNA-based hydrogel (p-gel) droplets for scale-up production. *Indust Biotech* **8**, 372-377 (2012).

[100] Roh, Y.H., Lee, J.B., Tan, S.J., Kim, B., Park, H. Rice, E.J. & Luo, D. Photocrosslinked DNA nanospheres for drug delivery. *Macromol Rapid Comm* **31**, 1207-1211, (2010).

[101] Lin, D.C., Yurke, B., & Langrana, N.A. Mechanical properties of a reversible, DNA-crosslinked polyacrylamide hydrogel. *J Biomech Eng* **126**, 104-110 (2004).

[102] Liedl, T., Dietz, H., Yurk, B., & Simmel, F. Controlled trapping and release of quantum dots in a DNA-switchable hydrogel. *Small* **3**, 1688-1693 (2007).

[103] Dave, N., Chan, M.Y., Huang, P.J.J., Smith, B.D., & Liu, J.W. Regenerable DNA-functionalized hydrogels for ultrasensitive, instrument-free Mercury(II) detection and removal in water. *J Am Chem Soc* **132**, 12668-12673 (2010).

[104] Lee, C.K., Shin, S.R., Lee, S.H., *et al*. DNA hydrogel fiber with self-entanglement prepared by using an ionic liquid. *Angew Chem Int Ed* **47**, 2470-2474 (2008).

[105] Lee, J.B., Peng, S., Yang, D., *et al.* A mechanical metamaterial made from a DNA hydrogel. *Nat Nanotechnol* **7**, 816-820 (2012).

[106] Dean, F.B., Nelson, J.R., Giesler, T.L. & Lasken, R.S. Rapid amplification of plasmid and phage DNA using phi29 DNA polymerase and multiply-primed rolling circle amplification. *Genome Res* **11**, 1095-1099 (2001).

[107] Qi, H., Ghodousi, M., Du, Y., Grun, C., Bae, H., Yin, P., & Khademhosseini, A. DNA-directed self-assembly of shape-controlled hydrogels. *Nat Commun* **4**, 1-10 (2013).

[108] Lee, J.B, Hong J., Bonner, D.K., Poon, Z., & Hammond, P.T. Self-assembled RNA interference microsponges for efficient siRNA delivery. *Nat Mater* **11**, 316-322 (2012).

[109] ISI Web of Science, search for a topic ‘‘microfluidic’’, www.isiknowledge.com, accessed 2015.

[110] United States Patent and Trademark office, search issued patents for ‘‘microfluidic’’ in title or abstract, http://patft.uspto.gov, accessed 2015.

[111] Shoji, S. & Esashi, M. Microflow device and systems. *J Micromech Microeng* **4**, 157-171 (1994).

[112] Laser, D.J. & Santiago, J.G. A review of micropumps. *J Micromech Microeng* **14**, R35-R64 (2004).

[113] Woias, P. Micropumps – past, progress, and future prospects. *Sens Actuators B* **105**, 28-38 (2005).

[114] Oh, K.W. & Ahn, C.H. A review of microvalves. *J Micromech Microeng* **16**, R13-R39 (2006).

[115] Nguyen, N.T. & Wu, Z.G. Micromixers – a review. *J Micromech Microeng* **15**, R1-R16 (2005).

[116] Hessel, V., Lowe, H. & Schonfeld, F. Micromixers – a review on passive and active mixing principles. *Chem Eng Sci*, **60**, 2479-2501 (2005).

[117] Kim, J., Erath, J., Rodriguez, A., & Yang, C. A high-efficiency microfluidic device for size-selective trapping and sorting. *Lab Chip* **14**, 2480-2490 (2014).

[118] Lim, L.S., Hu, M., Huang, M.C., *et al.* Microsieve lab-chip device for rapid enumeration and fluorescence in situ hybridization of circulating tumor cells. *Lab Chip* **12**, 4388-4396 (2012).

[119] World Health Organization, The World Health Report 2004, World Health Organization, Gene`ve, 2004.

[120] Batt, C.A. Food Pathogen Detection. *Science* **316**, 1579-1580 (2007).

[121] World Health Organization. *Real-time RT-PCR protocol for the detection of avian influenza A (H7N9) virus* (2013).

[122] CDC. *Diagnostics for Detecting H7N9 Using rRT-PCR* (2013).

[123] Huggett, J., Green, C. & Zumla, A. Nucleic acid detection and quantification in the developing world. *Biochem Soc Trans* **37**, 419-423 (2009).

[124] O'Connor, L. & Glynn, B. Recent advances in the development of nucleic acid diagnostics. *Expert Rev Med Devices* **7**, 529-539 (2010).

[125] Muldrew, K.L. Molecular diagnostics of infectious disease. *Curr Opin Pediatr* **21**, 102-111 (2009).

[126] Stramer, S.L., Wend, U., Candotti, D. *et al.* Nucleic acid testing to detect HBV infection in blood donors. *N Engl J Med* **364**, 236-247 (2011).

[127] Hayden, E.C. Targeted treatment tested as potential cancer cure. *Nature* **479**, 281 (2011).

[128] Sequist, L.V., Heist, R.S., Shaw, A.T. *et al.* Implementing multiplexed genotyping of non-small-cell ung cancers into routine clinical practice. *Ann Oncol* **22**, 2616-2624 (2011).

[129] Giljohann, D.A. & Mirkin, C.A. Drivers of biodiagnostic development. *Nature*, **462**, 461-464 (2009).

[130] Wang, S., Inci, F., De Libero, G., Singhal A. & Demirci, U. Point-of-care assays for tuberculosis: role of nanotechnology/microfluidics. *Biotechnol Adv* **31**, 438-449 (2013).

[131] Zhang, X., Guo, Q. & Cui, D. Recent advances in nanotechnology applied to biosensors. *Sensors* **9**, 1033-1053 (2009).

[132] Rosi, N.L. & Mirkin, C.A. Nanostructures in biodiagnostics. *Chem Rev* **105**, 1547-1562 (2005).

[133] Nam, J.M., Thaxton C.S., & Mirkin, C.A. Nanoparticle-based bio-bar codes for the ultrasensitive detection of proteins. *Science* **301**, 1884-1886 (2003).

[134] Doria, G., Conde, J., Veigas, B., *et al.* Noble metal nanoparticles for biosensing applications. *Sensors* **12**, 1657-1687 (2012).

[135] Tan, S.J., Campolongo, M.J., Luo, D. & Cheng, W. Building plasmonic nanostructures with DNA. *Nat Nanotechnol* **6**, 268-276 (2011).

[136] Lee, J., Hernandez, P., Lee, J., Govorov, A.O. & Kotov, N.A. Exciton-plasmon interactions in molecular spring assemblies of nanowires and wavelength-based protein detection. *Nat Mater*, **6**, 291-295 (2007).

[137] Zrazhevskiy, P., Sena, M. & Gao, X. Designing multifunctional quantum dots for bioimaging, detection, and drug delivery. *Chem Soc Rev*, **39**, 4326-4354 (2010).

[138] Gunasekera, U.A., Pankhurst, Q.A., & Douek, M. Imaging applications of nanotechnology in cancer. *Target Oncol* **4**, 169-181 (2009).

[139] Baker, M. Nanotechnology imaging probes: Smaller and more stable. *Nat Methods* **7**, 957-962 (2010).

[140] Saleh Ahammad, A.J., Lee, J.J. & Rahman, M.A. Electrochemical sensors based on carbon nanotubes. *Sensors* **9**, 2289-2319 (2009).

[141] Wang, J. Carbon-nanotube based electrochemical biosensors: A review. *Electroanalysis* **17**, 7-14 (2005).

[142] Lee, J.B., Campolongo, M.J., Kahn, J.S., *et al.* DNA-based nanostructures for molecular sensing. *Nanoscale*, **2**, 188-197 (2010).

[143] Lee, J.B., Roh, Y.H., Um, S.H., *et al.* Multifunctional nanoarchitectures from DNA-based ABC monomers. *Nat Nanotechnol* **4**, 430-436 (2009).

[144] Li, Y.G., Cu, Y.T.H. & D. Luo. Multiplexed detection of pathogen DNA with DNA-based fluorescence nanobarcodes. *Nat Biotechnol* **23**, 885-889 (2005).

[145] Zhang D.Y., & Seelig, G. Dynamic DNA nanotechnology using strand-displacement reactions. *Nat Chem* **3**, 103-113 (2011).

[146] Craw, P. & Balachandran, W. Isothermal nucleic acid amplification for point-of-care diagnostics: A critical review. *Lab Chip* **12**, 2469-2486 (2012).

[147] Asiello, P.J. & Baeumner, A.J. Miniaturized isothermal nucleic acid amplification, a review. *Lab Chip* **11**, 1420-1430, (2011).

[148] Park, S., Zhang, Y., Lin, S., Wang T.H. & Yang, S. Advances in microfluidic PCR for point-of-care infectious disease diagnostics. *Biotechnol Adv*, **29**, 830-839 (2011).

[149] Zhang, C. & Xing, D. Miniaturized PCR chips for nucleic acid amplification and analysis: latest advances and future trends. *Nucleic Acids Res* **35**, 4223-4237 (2007).

[150] Oblath, E.A., Henley, W.H., Alarie, J.P. & Ramsey, J.M. A microfluidic chip integrating DNA extraction and real-time PCR for detection of bacteria in saliva. *Lab Chip* **13**, 1325-1332 (2013).

[151] Jangam, S.R., Agarwal, A.K., Sur, K., & Kelso, D.M. A point-of-care PCR test for HIV-1 detection in resource-limited settings. *Biosens Bioelectron* **42**, 69-75 (2013).

[152] Maltezos, G., Johnston, M., Taganov, K., *et al.* Exploring the limits of ultrafast polymerase chain reaction using liquid for thermal heat exchange: A proof of principle. *Appl Phys Lett* **97**, 264101, (2010).

[153] Compton, J. Nucleic acid sequence-based amplification. *Nature* **350**, 91-92 (1991).

[154] Zhao, X. & Dong, T. Multifunctional sample preparation kit and on-chip quantitative nucleic acid sequence-based amplification tests for microbial detection. *Anal Chem* **84**, 8541-8548 (2012).

[155] Mader, A., Riehle, U., Brandstetter, T., Stickeler, E., & Ruehe, J. Universal nucleic acid sequence-based amplification for simultaneous amplification of messengerRNAs and microRNAs. *Anal Chim Acta* **754**, 1-7 (2012).

[156] Notomi, T., Okayama, H., Masubuchi, H., *et al.* Loop-mediated isothermal amplification of DNA. *Nucleic Acids Res* **28**, e63 (2000).

[157] Abdul-Ghani, R., Al-Mekhlafi, A.M., & Karanis, P. Loop-mediated isothermal amplification (LAMP) for malarial parasites of humans: would it come to clinical reality as a point-of-care test? *Acta Trop* **122**, 233-240 (2012).

[158] Lucchi, N.W., Demas, A., Narayanan, J. *et al.* Real-time fluorescence loop mediated isothermal amplification for the diagnosis of malaria. *PLoS One* **5**, e13733 (2010).

[159] Sun, B., Shen, F., McCalla, S. E. *et al.* Mechanistic evaluation of the pros and cons of digital RT-LAMP for HIV-1 viral load quantification on a microfluidic device and improved efficiency via a two-step digital protocol. *Anal Chem* **85**, 1540-1546 (2013).

[160] Fang, X., Liu, Y., Kong, J., & Jiang, X. Loop-mediated isothermal amplification integrated on microfluidic chips for point-of-care quantitative detection of pathogens. *Anal Chem* **82**, 3002-3006 (2010).

[161] Lalande, V., Barrault, L., Wadel, S., *et al.* Evaluation of a loop-mediated isothermal amplification assay for diagnosis of Clostridium difficile infecitons. *J Clin Microbiol* **49**, 2714-2746 (2011).

[162] McKenna, J.P., Fairley, D.J., Shields, M.D., *et al.* Development and clinical validation of a loop-mediated isothermal amplification method for the rapid detection of Neisseria meningitides. *Diagn Microbiol Infect Dis* **69**, 137-144 (2011).

[163] Neonakis, I.K., Spandidos, D.A. & Petinaki, E. Use of loop-mediated isothermal amplification of DNA for the rapid *Eur J Clin Microbiol Infect Dis* **30**, 937-942 (2011).

[164] Hanaki, K., Sekiguchi, J., Shimada, K., *et al.* Loop-mediated isothermal amplification assays for identification of antiseptic- and methicillin-resistant Staphylococcus aureus. *J Microbiol Methods* **84**, 251-254 (2010).

[165] Dinh, D.T., Thi, M., Le, Q., Vuong, C.D. & Hasebe, F. An updated loop-mediated isothermal amplification method for rapid diagnosis of H5N1 avian influena viruses. *Trop Med Health* **39**, 3-7 (2011).

[166] Parida, M., Shukla, J., Sharma, S. *et al.* Development and evaluation of reverse transcription loop-mediated isothermal amplification assay for rapid and real-time detection of the swine-origin influenza A H1N1 virus. *J Mol Diagn* **13**, 100-107 (2011).

[167] Hatano, B., Goto, M., Fukumoto, H. *et al.* Mobile and accurate detection system for infection by the 2009 pandemic influenza A (H1N1) virus with a pocket-warmer reverse-transcriptase loop-mediated isothermal amplification. *J Med Virol* **83**, 568-573 (2011).

[168] Sun, J., Najafzadeh, M.J., Vicente, V., Xi, L. & De Hoog, G.S. Rapid detection of pathogenic fungi using loop-mediated isothermal amplification, exemplified by Fonsecaea agents of chromoblastomyocosis. *J Microbiol Methods* **80**, 19-24 (2010).

[169] Niessen, L. & Vogel, R.F. Detection of Fusarium graminearum DNA using loop-mediated isothermal amplification (LAMP) assay. *Int J Food Microbiol* **140**, 183-91 (2010).

[170] Lucas, S., da Luz Martins, M., Flores, O., *et al.* Differentiation of Cryptococcus neoformans varieties and Cryptococcus gattii using CAP59-based loop-mediated isothermal DNA amplification. *Clin Microbiol Infect* **16**, 711-714 (2010).

[171] Njiru, Z.K., Mikosza, A.S., Matovu, E., *et al* African trypanosomiasis: sensitivand rapid detection of the sub-genus Trypanozoon by loop-mediated isothermal amplification (LAMP) of parasite DNA. *Int J Parasitol* **38**, 589-99 (2008).

[172] Matovu, E., Kuepfer, I., Boobo, A., Kibona, S. & Burri, C. Comparative detection of trypanosomal DNA by loop-mediated isothermal amplification and PCR from finders technology associates cards spotted with patient blood. *J Clin Microbiol* **48**, 2087-2090 (2010).

[173] Lau, Y.L., Meganathan, P., Sonaimuthu, P., *et al.* Specific, sensitive, and rapid diagnosis of active toxoplasmosis by a loop-mediated isothermal amplification method using blood samples from patients. *J Clin Microbiol* **48**, 3698-3702 (2010).

[174] Bakheit, M.A., Torra, D., Palomino, L.A., *et al.* Sensitive and specific detection of Cryptosporidium species in PCR-negative samples by loop-mediated isothermal DNA amplification and confirmation of generated LAMP products by sequencing. *Vet Parasitol* **158**, 11-22 (2008).

[175] Tomita, N, Mori, Y., Kanda, H. & Notomi, T. Loop-mediated isothermal amplification (LAMP) of gene sequences and simple visual detection of products. *Nat Protoc* **3**, 877-882 (2008).

[176] Njiru, Z.K. Loop-mediated isothermal amplification technology: towards point of care diagnostics. *PLoS Negl Trop Dis* **6**, e1572 (2012).

[177] Kimura, Y., de Hoon, M.J., Aoki, S., *et al.* Optimization of turn-back primers in isothermal amplification. *Nucleic Acids Res* 39, e59 (2011).

[178] Mori, Y. & Notomi, T. Loop-mediated isothermal amplification (LAMP): a rapid accurate, and cost-effective diagnostic method for infectious diseases. *J Infect Chemother* **15**, 62-69 (2009).

[179] Lizardi, P.M., Huang, X., Zhu, Z., *et al.* Mutation detection and single-molecule counting using isothermal rolling-circle amplification. *Nat Genet* **19**, 225-232 (1998).

[180] Liu, D., Daubendiek, S.L., Zillman, M.A., Ryan, K. & Kool, E.T. Rolling circle DNA synthesis: Small circular oligonucleotides as efficient templates for DNA polymerases. *J Am Chem Soc* **118**, 1587-1594 (1996).

[181] Zhang, D.Y., Zhang, W., Li, X. & Konomi, Y. Detection of rare DNA targets by isothermal ramification amplification. *Gene* **274**, 209-216 (2001).

[182] Zhou, Y., Huang, Q., Gao, J., Lu, J., Shen, X. & Fan, C. A dumbbell probe-mediated rolling circle amplification strategy for highly sensitive microRNA detection. *Nucleic Acids Res* **38**, e156 (2010).

[183] Bi, ., Cui, Y. & Li, L. Dumbbell probe-mediated cascade isothermal amplification: a novel strategy for label-free detection of microRNAs and its application to real sample assay. *Anal Chim Acta* **760**, 69-74 (2013).

[184] Sun, Y., Høgberg, J., Christine, T., *et al.* Pre-storage of gelified reagents in a lab-on-a-foil system for rapid nucleic acid analysis. *Lab Chip* **13**, 1509-1514 (2013).

[185] Paul, N. & Joyce, G.F. A self-replicating ligase ribozyme. *Proc Natl Acad Sci U.S.A* **99**, 12733-12740 (2002).

[186] Lam, B.J. & Joyce, G.F. Autocatalytic aptazymes enable ligand-dependent exponential amplification of RNA. *Nat Biotechnol* **27**, 288-292 (2009).

[187] Levy, M. & Ellington, A.D. Exponential growth by cross-catalytic cleavage of deoxyribozymogens. *Proc Natl Acad Sci U.S.A.* **100**, 6416-6421 (2003).

[188] Wang, F., Elbaz, J., Teller, C. & Willner, I. Amplified detection of DNA through an autocatalytic and catabolic DNAzyme-mediated process. *Angew Chem Int Ed* **50**, 295-299 (2011).

[189] Zhao, Y., Zhou, L. & Tang, Z. Cleavage-based signal amplification of RNA. *Nat Commun* **4**, 1493 (2013).

[190] Zhang, D.Y. & Seelig, G. Dynamic DNA nanotechnology using strand-displacement reactions. *Nat Chem* **3**, 103-113 (2011).

[191] Yurke, B., Turberfield, A.J., Mills, A.P., Simmel, F.C. Neumann, J.L. A DNA-fuelled molecular machine made of DNA. *Nature* **406**, 605-608 (2000).

[192] Yan, H., Zhang, X., Shen, Z. & Seeman, N. A robust DNA mechanical device controlled by hybridization topology. *Nature* **415**, 62-65 (2002).

[193] Chen, X., Briggs, N., McLain, J.R. & Ellington, A.D. Stacking nonenzymatic circuits for high signal gain. *Proc Natl Acad Sci U.S.A.* **110**, 5386-5391 (2013).

[194] Seelig, G., Yurke, B. & Winfree, E. Catalyzed relaxation of a metastable DNA fuel. *J Am Chem Soc* **128**, 12211-12220 (2006).

[195] Turberfield, A.J., Mitchell, J.C., Yurke, B., *et al.* DNA fuel for free-running nanomachines. *Phys Rev Lett* **90**, 118102 (2003).

[196] Zhang, D.Y., Turberfield, A.J., Yurke, B. & Winfree, E. Engineering entropy-driven reactions and networks catalyzed by DNA. *Science* **318**, 1121-1125 (2007).

[197] Seelig, G., Soloveichik, D., Zhang, D.Y. & Winfree, E. Enzyme-free nucleic acid logic circuits. *Science* **314**, 1585-1588 (2006).

[198] Qian, L. & Winfree, E. Scaling up digital circuit computation with DNA strand displacement cascades. *Science* **332**, 1196-1201 (2011).

[199] Zhang, D.Y., Chen, S.X. & Yin, P. Optimizing the specificity of nucleic acid hybridization. *Nat Chem* **4**, 208-214 (2012).

[200] Dirks, R.M. & Pierce, N.A. Triggered amplification by hybridization chain reaction. *Proc Natl Acad Sci U.S.A.* **101**, 15275-15278 (2004).

[201] Choi, H.M., Chang, J.Y., Trinh, L.A., *et al.* Programmable in situ amplification for multiplexed imaging of mRNA expression. *Nat Biotechnol* **28**, 1208-1212 (2010).

[202] Yin, P., Choi, H.M., Calvert, C.R. & Pierce, N.A. Programming biomolecular self-assembly pathways. *Nature* **451**, 318-322 (2008).

[203] Jiang, Y.S., Li, B., Milligan, J.N., Bhadra, S. & Ellington, A.D. Real-time detection of isothermal amplification reactions with thermostable catalytic hairpin assembly. *J Am Chem Soc* **135**, 7430-7433 (2013).

[204] Allen, P.B, Arshad, S.A., Li, B., Chen, X. & Ellington, A.D. DNA circuits as amplifiers for the detection of nucleic acids on a paperfluidic platform. *Lab Chip* **12**, 2951-2958 (2012).

[205] Li, B., Chen X. & Ellington, A.D. Adapting enzyme-free DNA circuits to the detection of loop-mediated isothermal amplification reactions. *Anal Chem* **84**, 8371-8377 (2012).

[206] Ngom, B., Guo, Y., Wang, X. & Bi, D. Development and application of lateral flow test strip technology for detection of infectious agents and chemical contaminants: a review. *Anal Bioanal Chem* **397**, 1113-1135 (2010).

[207] Posthuma-Trumpie, G.A., Korf, J. & van Amerongen, A. Lateral flow (immuno)assay: its strengths, weaknesses, opportunities, and threats. A literature survey. *Anal Bioanal Chem* **393**, 569-582 (2009).

[208] Mao, X., Ma, Y., Zhang, A., Zhang, L., Zeng, L. & Liu, G. Disposable nucleic acid biosensors based on gold nanoparticle probes and lateral flow strip. *Anal Chem* **81**, 1660-1668 (2009).

[209] Aveyard, J., Mehrabi, M., Cossins, A., Braven, H. & Wilson, R. One step visual detection of PCR products with gold nanoperticles and a nucleic acid lateral flow (NALF) device. *Chem Commun* 4251-4253 (2007).

[210] Wang, Y., Fill, C. & Nugen, S.R. Development of chemiluminescent lateral flow assay for the detection of nucleic acids. *Biosensors* **2**, 32-42 (2012).

[211] Baeumner, A.J., Pretz, J. & Fang, S. A universal nucleic acid sequence biosensor with nanomolar detection limits. *Anal Chem* **76**, 888-894 (2004).

[212] Carter, D.J. & Cary, R.B. Lateral flow microarrays: a novel platform for rapid nucleic acid detection based on miniaturized lateral flow chromatography. *Nucleic Acids Res* **35**, e74 (2007).

[213] Lie, P., Liu, J., Fang, Z., Dun, B. & Zeng, L. A lateral flow biosensor for detection of nucleic acids with high sensitivity and selectivity. *Chem Commun* **48**, 236-238 (2012).

[214] Rohrman, B.A., Leautaud, V., Molyneux, E. & Richards-Kortum, R.R. A lateral flow assay for quantitative detection of amplified HIV-1 RNA. *PLoS One* **7**, e45611 (2012).

[215] Govindarajan, A.V., Ramachandran, S., Vigil, .D., *et al.* A low cost point-of-care viscous sample preparation device for molecular diagnosis in the developing world; an example of microfluidic origami. *Lab Chip* **12**, 174-181 (2012).

[216] Yetisen, A.K., Akram, M.S. & Lowe, C.R. Paper-based microfluidic point-of-care diagnostic devices. *Lab Chip* **13**, 2210-2251 (2013).

[217] Martinez, A.W., Phillips, S.T., Whitesides, G.M. & Carrilho, E. Diagnostics for the developing world: microfluidic paper-based analytical devices. *Anal Chem* **82**, 3-10 (2010).

[218] Fu, E., Liang, T., Spicar-Mihalic, P., *et al.* Two-dimensional paper network format that enables simple multistep assays for use in low-resource settings in the context of malaria antigen detection. *Anal Chem* **84**, 4574-4579 (2012).

[219] Mirkin, C.A., Letsinger, R.L., Mucic, R.C. & Storhoff, J.J. A DNA-based method for rationally assembling nanoparticles into macroscopic materials. *Nature* **382**, 607-609 (1996).

[220] Mollasalehi, H. & Yazdanparast, R. Non-crosslinking gold nanoprobes for detection of nucleic acid sequence-based amplification products. *Anal Biochem* **425**, 91-95 (2012).

[221] Shen, W., Deng, H. & Gao, Z. Gold nanoparticle-enabled real-time ligation chain reaction for ultrasensitive detection of DNA. *J Am Chem Soc* **134**, 14678-14681 (2012).

[222] Xu, W., Xue, X., Li, T., Zeng, H. & Liu, X. Ultrasensitive and selective colorimetric DNA detection by nicking endonuclease assisted nanoparticle amplification. *Angew Chem Int Ed Engl* **48**, 6849-6852 (2009).

[223] Conde, J., de la Fuente, J.M. & Baptista, P.V. RNA quantification using gold nanoprobes – application to cancer diagnostics. *J Nanobiotechnol* **8**, 5 (2010).

[224] Loweth, C.J., Caldwell, W.B., Peng, X., Alivisatos, A.P. & Schultz, P.G. DNA-based assembly of gold nanocrystals. *Angew Chem Int Ed* **38**, 1808-1812 (1999).

[225] Alivisatos, A.P., Johnsson, K.P., Peng, X., Wilson, T.E., Loweth, C.J., Bruchez, M.P. Jr. & Schultz, P.G. Organization of 'nanocrystal molecules' using DNA. *Nature* **382**, 609-611 (1996).

[226] Zhu, H., Isikman, S.O., Mudanyali, O., Greenbaum, A. & Ozcan, A. Optical imaging techniques for point-of-care diagnostics. *Lab Chip* **13**, 51-67 (2013).

[227] Myers, F.B. & Lee, L.P. Innovations in optical microfluidic technologies for point-of-care diagnostics. *Lab Chip* **8**, 2015-2031 (2008).

[228] Sin, M.L., Gao, J., Liao, J.C. & Wong, P.K. System integration – A major step toward lab on a chip. *J Biol Eng* **5**, 6 (2011).

[229] Sidorova, J.M., Li, N., Schwartz, D.C., Folch, A. & Monnat, R.J. Jr. Microfluidic-assisted analysis of replicating DNA molecules. *Nat Protoc* **4**, 849-861 (2009).

[230] Zhu, H., Isikman, S.O., Mudanyali, O., Greenbaum, A. & Ozcan, A. Optical imaging techniques for point-of-care diagnostics. *Lab Chip* **13**, 51-67 (2013).

[231] Miller, A.R., Davis, G.L., Oden, Z.M., *et al.* Portable, battery-operated, low-cost, bright field and fluorescence microscope. *PLoS One* **5**, e11890 (2010).

[232] Ghosh, K.K., Burns, L.D., Cocker, E.D., *et al.* Miniaturized integration of a fluorescence microscope. *Nat Methods* **8**, 871-878 (2011).

[233] McCall, B., Pierce, M., Graviss, E.A., Richards-Kortum, R. & Tkaczyk, T. Toward a low-cost compact array microscopy platform for detection of tuberculosis. *Tuberculosis* **91** (suppl. 1), S54–S60 (2011).

[234] Greenbaum, A., Luo, W., Su, T.W., *et al.* Imaging without lenses: achievements and remaining challenges of wide-field on-chip microscopy. *Nat Methods* **9**, 889-895 (2012).

[235] Lee, S.A., Leitao, R., Zheng, G., Yang, S., Rodriguez, A. & Yang, C. Color capable sub-pixel resolving optofluidic microscope and its application to blood cell imaging for malaria diagnosis. *PLoS One* **6**, e26127 (2011).

[236] Balsam, J., Ossandon, M., Kostov, Y., Bruck, H.A. & Rasooly, A. Lensless CCD-based fluorometer using a micromachined optical Söller collimator. *Lab Chip* **11**, 941-949 (2011).

[237] Zhu, H., Yaglidere, O., Su, T.W., Tseng, D. & Ozcan, A. Cost-effective and compact wide-field fluorescent imaging on a cell-phone. *Lab Chip* **11**, 315-322 (2011).

[238] Breslauer, D.N., Maamari, R.N., Switz, N.A., Lam, W.A. & Fletcher, D.A. Mobile phone based clinical microscopy for global health applications. *PLoS One* **4**, e6320 (2009).

[239] Smith, Z.J., Chu, K., Espenson, A. R., *et al*. Cell-phone-based platform for biomedical device development and education applications. *PLoS One* **6**, e17150 (2011).

[240] Oncescu, V., O'Dell, D. & Erickson, D. Smartphone based health accessory for colorimetric detection of biomarkers in sweat and saliva. *Lab Chip* **13**, 3232-3238 (2013).

[241] Martinez, A.W., Phillips, S.T., Carrilho, E., *et al.* Simple telemedicine for developing regions: camera phones and paper-based microfluidic devices for real-time, off-site diagnosis. *Anal Chem* **80**, 3699-3707 (2008).

[242] Mudanyali, O., Dimitrov, S., Sikora, U. *et al*. Integrated rapid-diagnostic-test reader platform on a cellphone. *Lab Chip* **12**, 2678-2686 (2012).

[243] Mancuso, M. & Erickson, D. CLEO: 2013, OSA, Washington, D.C., 2013, p. AM3M.2.

[244] Li, Y., Cu, Y.T. & Luo, D. Multiplexed detection of pathogen DNA with DNA-based fluorescence nanobarcodes. *Nat Biotechnol* **23**, 885-889 (2005).

[245] Um, S.H., Lee, J.B., Kwon, S.Y., Li, Y. & Luo, D. Dendrimer-like DNA-based fluorescence nanobarcodes. *Nat Protoc* **1**, 995-1000 (2006).

[246] Lee, J.B., Roh, Y.H., Um, S.H., *et al.* Multifunctional nanoarchitectures from DNA-based ABC monomers. *Nat Nanotechnol* **4**, 430-436 (2009).

[247] Hartman, M.R., Yang, D., Tran, T.N., *et al*. Thermostable branched DNA nanostructures as modular primers for polymerase chain reaction. *Angew Chem Int Ed Engl* **52**, 8699-8702 (2013).

[248] Feng, X., Duan, X., Liu, L. *et al*. Fluorescence logic-signal-based multiplex detection of nucleases with the assembly of a cationic conjugated polymer and branched DNA. *Angew Chem Int Ed Engl* **48**, 5316-5321 (2009).

[249] Lin, C., Jungmann, R., Leifer, A.M., *et al*. Submicrometre geometrically encoded fluorescent barcodes self-assembled from DNA. *Nat. Chem* **4**, 832-839 (2012).

[250] Seeman, N.C. DNA in a material world. *Nature* **421**, 427-431 (2003).

[251] Feldkamp & Niemeyer, C.M. Rational design of DNA nanoarchitectures. *Angew Chem Int Ed Engl* **45**, **12**, 1856-76 (2006).

[252] Bath, J. & Turberfield, A.J. DNA nanomachines. *Nat Nanotechnol* **2**, 275-284, (2007).

[253] Pinheiro, A.V., Han, D., Shih, W.M., & Yan, H. Challenges and opportunities for structural DNA nanotechnology. *Nat Nanotechnol* **6**, 763-772, (2011).

[254] Rothemund, P.W. Folding DNA to create nanoscale shapes and patterns. *Nature* **440**, 297-302 (2006).

[255] Wei, B. Dai, M., & Yin, P. Complex shapes self-assembled from single-stranded DNA tiles. *Nature* **485**, 623-626, (2012).

[256] Zhang, C., Tian, C., Guo, F., *et al.* DNA-directed three-dimensional protein organization. *Angew Chem Int Ed* **51**, 3382-3385, (2012).

[257] Fu, Y., Zen, D., Chao, J., *et al.* Single-step rapid assembly of DNA origami nanostructures for addressable nanoscale bioreactors. *J Am Chem Soc* **135**, 696-702 (2013).

[258] Lin, C., Jungmann, R., Leifer, A.M., *et al.* Submicrometre geometrically encoded fluorescent barcodes self-assembled from DNA. *Nat Chem* **4**, 832-389 (2012).

[259] Niemeyer, C.M., Adler, M., & Wacker R. Detecting antigens by quantitative immuno-PCR. *Nat Prot* **2**, 1918-1930 (2007).

[260] Li, L.L., Wu, P., Hwang, K., & Lu, Y. An exceptionally simple strategy for DNA-functionalized up-conversion nanoparticles as biocompatible agents for nanoassembly, DNA delivery, and imaging. *J Am Chem Soc* **135**, 2411-2414 (2013).

[261] McLaughlin, C.K., Hamblin, G.D., Hänni, K.D., *et al.* Three-dimensional organization of block copolymers on 'DNA-minimal' scaffolds. *J Am Chem Soc* **134**, 4280-4286 (2012).

[262] Xing, Y., Cheng, E., Yang, Y., *et al.* Self-assembled DNA hydrogels with designable thermal and enzymatic responsiveness. *Adv Mater* **23**, 1117-1121 (2011).

[263] Um, S.H., Lee, J.B., Park, N., Kwon, S.Y., Umbach, C.C. & Luo, D. Enzyme-catalysed assembly of DNA hydrogel. *Nat Mater* **5**, 797-801 (2006).

[264] Lee, J.B. Peng, S. Yang, D., *et al.* A mechanical metamaterial made from a DNA hydrogel. *Nat Nanotechnol* **7**, 816-820 (2012).

[265] Li, Y., Tseng, Y.D., Kwon, S.Y., *et al.* Controlled assembly of dendrimer-like DNA. *Nat Mater* **3**, 38-42 (2004).

[266] Lee, J.B., Roh, Y.H., Um, S.H., *et al.* Multifunctional nanoarchitectures from DNA-based ABC monomers. *Nat Nanotechnol* **4**, 430-436 (2009).

[267] Luo, D. The road from biology to materials. *Mater Today* **6**, 38-43 (2003).

[268] Roh, Y.H., Ruiz, R.C.H., Peng, S.M., Lee, J.B. & Luo, D. Engineering DNA-based functional materials. *Chem Soc Rev* **40**, 5730-5744 (2011).

[269] Li, Y., Tseng, Y.D., Kwon, S.Y., *et al.* Controlled assembly of dendrimer-like DNA. *Nat Mater* **3**, 38-42 (2004).

[270] Han, M., Gao, X., Su, J.Z. & Nie, S. Quantum-dot-tagged microbeads for multiplexed optical coding of biomolecules. *Nat Biotechnol* **19**, 631-635 (2001).

[271] Fulton, R.J., McDade, R.L., Smith, P.L., Kienker, L.J. & Kettman, J.R. Jr.. Advanced multiplexed analysis with the FlowMetrix system. *Clin Chem* **43**, 1749-1756 (1997).

[272] Steemers, F.J., Ferguson, J.A. & Walt, D.R. Screening unlabeled DNA targets with randomly ordered fiber-optic gene arrays. *Nat Biotechnol* **18**, 91-94 (2000).

[273] Braeckmans, K., De Smedt, S.C., Leblans, M., Pauwels, R. & Demeester, J. Encoding microcarriers: Present and future technologies. *Nat Rev Drug Discov* **1**, 447-456 (2002).

[274] Duggan, D.J., Bittner, M., Chen, Y., Meltzer, P. & Trent, J.M. Expression profiling using cDNA microarrays. *Nat Genet* **21**, 10-14 (1999).

[275] Cheung, V.G., Morley, M., Aguilar, F. *et al*. Making and reading microarrays. *Nat Genet* **21**, 15-19 (1999).

[276] Schena, M., Shalon, D., Davis, R.W. & Brown, P.O. Quantitative monitoring of gene expression patterns with a complementary-DNA microarray. *Science* **270**, 467-470 (1995).

[277] Braeckmans, K., De Smedt, S.C., Leblans, M., Pauwels, R. & Demeester, J. Encoding microcarriers: Present and future technologies. *Nat Rev Drug Discov* **1**, 447-456 (2002).

[278] Cunin, F., Schmedake, T.A., Link, J.R., *et al.* Biomolecular screening with encoded porous-silicon photonic crystals. *Nat Mater* **1**, 39-41 (2002).

[279] Wang, J., Liu, G. & Rivas, G. Encoded beads for electrochemical identification. *Anal Chem* **75**, 4667-4671 (2003).

[280] Nam, J.M., Thaxton, C.S. & Mirkin, C.A. Nanoparticle-based bio-bar codes for the ultrasensitive detection of proteins. *Science* **301**, 1884-1886 (2003).

[281] Han, M., Gao, X., Su, J.Z. & Nie, S. Quantum-dot-tagged microbeads for multiplexed optical coding of biomolecules. *Nat Biotechnol* **19**, 631-635 (2001).

[282] Braeckmans, K., De Smedt, S.C., Leblans, M., Pauwels, R. & Demeester, J. Encoding microcarriers: Present and future technologies. *Nat Rev Drug Discov* **1**, 447-456 (2002).

[283] Nicewarner-Pena, S.R., Freeman, R.G., Reiss, B.D., *et al.* Submicrometer metallic barcodes. *Science* **294**, 137-141 (2001).

[284] Li, Y., Cu, Y.T., & Luo, D. Multiplexed detection of pathogen DNA with DNA-based fluorescence nanobarcodes. *Nat Biotechnol* **23**, 885-889 (2005).

[285] Di Carlo, D., Wu, L.Y. & Lee, L.P. Dynamic single cell culture array. *Lab Chip* **6**, 1445-1449 (2006).

[286] Skelley, A.M., Kirak, O., Suh, H., Jaenisch, R., & Voldman, J. Microfluidic control of cell pairing and fusion. *Nat Meth* **6**, 147-152 (2009).

[287] Wu, L.Y., Di Carlo, D. & Lee, L.P. Microfluidic self-assembly of tumor spheroids for anticancer drug discovery. *Biomed Microdevices* **10**, 197-202 (2008).

[288] Wlodkowic, D., Faley, S., Zagnoni, M., Wikswo, J.P. & Cooper, J.M. Microfluidic single-cell array cytometry for the analysis of tumor apoptosis. *Anal Chem* **81**, 5517-5523 (2009).

[289] Chung, K., Kim, Y., Kanodia, J.S., Gong, E., Shvartsman, S.Y. & Lu, H. A microfluidic array for large-scale ordering and orientation of embryos. *Nat Methods* **8**, 171-177 (2011).

[290] Levario, T.J., Zhan, M., Lim, B., Shvartsman, S.Y. & Lu, H. Microfluidic trap array for massively parallel imaging of Drosophila embryos. *Nat Protoc* **8**, 721-736 (2013).

[291] Shi, W., Qin, J., Ye, N. & Lin, B. Droplet-based microfluidic system for individual Caenorhabditis elegans assay. *Lab Chip* **8**, 1432-1435 (2008).

[292] Sochol, R.D., Li, S., Lee, L.P. & Lin, L. Continuous flow multi-stage microfluidic reactors via hydrodynamic microparticle railing. *Lab Chip* **12**, 4168-4177 (2012).

[293] Sochol, R.D., Casavant, B.P., Dueck, M.E., & Lee, L.P. A dynamic bead-based microarray for parallel DNA detection. *J Micromech Microeng* **21**, 054019 (2011).

[294] Lilliehorn, T., Nilsson, M., Simu, U., *et al.* Dynamic arraying of microbeads for bioassays in microfluidic channels. *Sensors and Actuators B* **106**, 851-858 (2005).

[295] Burger, R., Reith, P., Kijanka, G., *et al.* Array-based capture, distribution, counting and multiplexed assaying of beads on a centrifugal microfluidic platform. *Lab Chip* **12**, 1289-1295 (2012).

[296] Dubus, S., Gravel, J.F., Le Drogoff, B., *et al.* PCR-free DNA detection using a magnetic bead-supported polymeric transducer and microelectromagnetic traps. *Anal Chem* **78**, 4457-4464 (2006).

[297] Um, S.H., Lee, J.B., Kwon, S.Y., Li, Y. & Luo, D. Dendrimer-like DNA-based fluorescence nanobarcodes. *Nat Protoc* **1**, 995-1000 (2006).

[298] Blake, R.D. & Delcourt, S.G. Thermodynamic effects of formamide on DNA stability. *Nucleic Acids Res* **24**, 2095-2103 (1996).

[299] Blake, R.D. & Delcourt, S.G. Thermodynamic effects of formamide on DNA stability. *Nucleic Acids Res* **24**, 2095-2103 (1996).

[300] McConaughy, B.L., Laird, C.D. & McCarthy, B.J. Nucleic acid reassociation in formamide. *Biochemistry* **8**, 3289-3295 (1969).

[301] Sadhu, C., Dutta, S. & Gopinathan, K.P. Influence of formamide on the thermal stability of DNA. *J Biosci* **6**, 817-821 (1984).

[302] Yufeng, L., Hayes, D.N., Nobel, A. & Marron, J.S. Statistical significance of clustering for high-dimension, low-sample size data. *J Am Stat Assoc* **103**, 12811293 (2008).

[303] Rothemund, P.W. Folding DNA to create nanoscale shapes and patterns. *Nature* **440**, 297-302 (2006).

[304] Yin, P., Hariadi, R.F., Sahu, S., *et al.* Programming DNA tube circumferences. *Science* **321**, 824-826 (2008).

[305] Lee, J.B., Peng, S., Yang, D. *et al.* A mechanical metamaterial made from a DNA hydrogel. *Nat Nanotechnol* **7**, 816-820 (2012).

[306] Lee, J.B., Peng, S., Yang, D. *et al.* A mechanical metamaterial made from a DNA hydrogel. *Nat Nanotechnol* **7**, 816-820 (2012).

[307] Lin, C., Xie, M., Chen, J.J., Liu, Y. & Yan, H. Rolling-circle amplification of a DNA nanojunction. *Angew Chem Int Ed* **45**, 7537-7539 (2006).

[308] Lin, C. Wang, X., Liu, Y., Seeman, N.C. & Yan, H. Rolling circle enzymatic replication of a complex multi-crossover DNA nanostructure. *J Am Chem Soc* **129**, 14475-14481 (2007).

[309] Dean, F.B., Nelson, J.R., Giesler, T.L. & Lasken, R.S. Rapid amplification of plasmid and phage DNA using Phi 29 DNA polymerase and multiply-primed rolling circle amplification. *Genome Res* **11**, 1095-1099 (2001).

[310] Blanco, L., Bernad, A., Lazaro, J.M. *et al.* Highly efficient DNA synthesis by the phage phi 29 DNA polymerase. Symmetrical mode of DNA replication. *J Biol Chem* **264**, 8935-8940 (1989).

[311] Larsson, C., Koch, J., Nygren, A., *et al.* In situ genotyping individual DNA molecules by target-primed rolling-circle amplification of padlock probes. *Nat Methods* **1**, 227-232 (2004).

[312] Nilsson, M. Lock and roll: single-molecule genotyping in situ using padlock probes and rolling-circle amplification. *Histochem Cell Biol* **126**, 159-164 (2006).

[313] Li, N., Li, J. & Zhong, W. CE combined with rolling circle amplification for sensitive DNA detection. *Electrophoresis* **29**, 424-432 (2008).

[314] Wang, B., Potter, S.J., Lin, Y., *et al.* Rapid and sensitive detection of severe acute respiratory syndrome coronavirus by rolling circle amplification. *J Clin Microbiol* **43**, 2339-2344 (2005).

[315] Pickering, J., Bamford, A., Godbole, V., *et al.* Integration of DNA ligation and rolling circle amplification for the homogeneous, end-point detection of single nucleotide polymorphisms. *Nucleic Acids Res* **30**, 60e (2002).

[316] Zhang, S., Wu, Z., Shen, G. & Yu, R. A label-free strategy for SNP detection with high fidelity and sensitivity based on ligation-rolling circle amplification and intercalating of methylene blue. *Biosens. Bioelectron* **24**, 3201-3207 (2009).

[317] Cheng, Y., Li, Z., Zhang, X., Du, B. & Fan, Y. Homogeneous and label-free fluorescence detection of single-nucleotide polymorphism using target-primed branched rolling circle amplification. *Anal. Biochem* **378**, 123-126 (2008).

[318] Zhou, H., Bouwman, K., Schotanus, M. *et al.* Two-color, rolling-circle amplification on antibody microarrays for sensitive, multiplexed serum-protein measurements. *Genome Biology* **5**, R28 (2004).

[319] Konry, T., Smolina, I., Yarmush, J.M., *et al.* Ultrasensitive detection of low-abundance surface-marker protein using isothermal rolling circle amplification in a microfluidic nanoliter platform. *Small* **7**, 395-400 (2011).

[320] Zhao, W., Cui, C.H., Bose, S., *et al.* Bioinspired multivalent DNA network for capture and release of cells. *Proc Natl Acad Sci U.S.A.* **109**, 19626-19631 (2012).

[321] Zhang, Z., Ali, M.M., Eckert, *et al.* A polyvalent aptamer system for targeted drug delivery. *Biomaterials* **34**, 9728-9735 (2013).

[322] Ali, M.M. & Li, Y. Colorimetric sensing by using allosteric-DNAzyme-coupled rolling circle amplification and a peptide nucleic acid-organic dye probe. *Angew Chem Int Ed* **48**, 3512-3515 (2009).

[323] Tang, L., Liu, Y., Ali, M.M., Kang, D.K., Zhao, W. & Li, J. Colorimetric and ultrasensitive bioassay based on a dual-amplification system using aptamer and DNAzyme. *Anal Chem* **84**, 4711-4717 (2012).

[324] Zhao, W., Gao, Y., Kandadai, S.A., Brook, M.A. & Li, Y. DNA polymerization on gold nanoparticles through rolling circle amplification: towards novel scaffolds for three-dimensional periodic nanoassemblies. *Angew Chem Int Ed* **45**, 2409-2413 (2006).

[325] Ali, M.M, Su, S., Filipe, C.D., Pelton, R. & Li, Y. Enzymatic manipulations of DNA oligonucleotides on microgel: towards development of DNA-microgel bioassays. *Chem Commun* 4459-4461 (2007).

[326] Linck, L., Reiss, E., Bier, F. & Resch-Genger, U. Direct labeling rolling circle amplification as a straightforward signal amplification technique for biodetection formats. *Anal Methods* **4**, 1215-1220 (2012).

[327] Berr, A. & Schubert, I. Direct labelling of BAC-DNA by rolling-circle amplification. *Plant J* **45**, 857-862 (2006).

[328] Su, H., Yuan, R., Chai, Y. Mao, L. & Zhuo, Y. Ferrocenemonocarboxylic–HRP@Pt nanoparticles labeled RCA for multiple amplification of electro-immunosensing. *Biosens Bioelectron* **26**, 4601-4604 (2011).

[329] Beyer, S., Nickels, P. & Simmel, F.C. Periodic DNA nanotemplates synthesozed by rolling circle amplification. *Nano Lett* **5**, 719-722 (2005).

[330] Faruqi, A.F., Hosono, S., Driscoll, M.D., *et al.* High-throughput genotyping of single nucleotide polymorphisms with rolling circle amplification. *BMC Genomics* **2**, 4.

[331] Christian, A.T., Pattee, M.S., Attix, C.M., *et al.* Detection of DNA point mutations and mRNA expression levels by rolling circle amplification in individual cells. *Proc Natl Acad Sci U.S.A* **98**, 14238-14243 (2001).

[332] Jonstrup, S.P., Koch, J. & Kjems, J. A microRNA detection system based on padlock probes and rolling circle amplification. *RNA* **12**, 1747-1752 (2006).

[333] Cheng, Y., Zhang, X., Li, Z., *et al.* Highly sensitive determination of microRNA using target-primed and branched rolling-circle amplification. *Angew Chem Int Ed* **48**, 3268-3272 (2009).

[334] Wen, Y., Xu, Y., Mao, X., *et al.* DNAzyme-based rolling-circle amplification DNA machine for ultrasensitive analysis of microRNA in Drosophila larva. *Anal Chem* **84**, 7664-7669 (2012).

[335] Cao, A. & Zhang, C.Y. Sensitive and label-free DNA methylation detection by ligation-mediated hyperbranched rolling circle amplification. *Anal Chem* **84**, 6199-6205 (2012).

[336] Paprotka, T., Deuschle, K., Metzler, V. & Jeske, H. Conformation-selective methylation of geminivirus DNA. *J Virol* **85**, 12001-12012 (2011).

[337] Larsson, C., Koch, J., Nygren, A., *et al.* In situ genotyping individual DNA molecules by target-primed rolling-circle amplification of padlock probes. *Nat Methods* **1**, 227-232 (2004).

[338] Larsson, C., Grundberg, I. Soderberg, O. & Nilsson, M. In situ detection and genotyping of individual mRNA molecules. *Nat Methods* **7**, 395-397 (2010).

[339] Yaroslavsky, A.I. & Smolina, I.V. Fluorescence imaging of single-copy DNA sequences within the human genome using PNA-directed padlock probe assembly. *Chem Biol* **20**, 445-453 (2013).

[340] Smolina, I., Miller, N.S. & Frank-Kamenetskii, M.S. PNA-based microbial pathogen identification and resistance marker detection: An accurate, isothermal rapid assay based on genome-specific features. *Artif DNA PNA XNA* **1**, 76-82 (2010).

[341] Ou, L.J., Liu, S.J., Chu, X., Shen, G.L. & Yu, R.Q. DNA encapsulating liposome based rolling circle amplification immunoassay as a versatile platform for ultrasensitive detection of protein. *Anal Chem* **81**, 9664-9673 (2009).

[342] Yan, J., Song, S., Li, B., *et al.* An on-nanoparticle rolling-circle amplification platform for ultrasensitive protein detection in biological fluids. *Small* **6**, 2520-2525 (2010).

[343] Xue, Q., Wang, Z., Wang, L. & Jiang, W. Sensitive detection of proteins using assembled cascade fluorescent DNA nanotags based on rolling circle amplification. *Bioconjug Chem* **23**, 734-739 (2012).

[344] Yang, L., Fung, C.W., Cho, E.J. & Ellington, A.D. Real-time rolling circle amplification for protein detection. *Anal Chem* **79**, 3320-3329 (2007).

[345] Ma, C., Wang, W., Yang, Q., Shi, C. & Cao, L. Cocaine detection via rolling circle amplification of short DNA strand separated by magnetic beads. *Biosens Bioelectron* **26**, 3309-3312 (2011).

[346] Söderberg, O., Gullberg, M., Jarvius, M., *et al.* Direct observation of individual endogenous protein complexes in situ by proximity ligation. *Nat Methods* **3**, 995-1000 (2006).

[347] Jung, J., Lifland, A.W., Zurla, C., Alonas, E.J. & Santangelo, P.J. Quantifying RNA-protein interactions in situ using modified-MTRIPs and proximity ligation. *Nucleic Acids Res* **41**, e12 (2012).

[348] Gu, G.J., Friedman, M., Jost, C., *et al.* Protein tag-mediated conjugation of oligonucleotides to recombinant affinity binders for proximity ligation. *N Biotechnol* **30**, 144-152 (2013).

[349] Ali, M.M., Aguirre, S.D., Xu, Y., Filipe, C.D., Pelton, R. & Li, Y. Detection of DNA using bioactive paper strips. *Chem Commun* 6640-6642 (2009).

[350] Su, Q., Xing, D. & Zhou, X. Magnetic beads based rolling circle amplification-electrochemiluminescence assay for highly sensitive detection of point mutation. *Biosens Bioelectron* **25**, 1615-1621 (2010).

[351] Konry, T., Hayman, R.B. & Walt, D.R. Microsphere-based rolling circle amplification microarray for the detection of DNA and proteins in a single assay. *Anal Chem* **81**, 5777-5782 (2009).

[352] Chapin, C.C. & Doyle, P.S. Ultrasensitive multiplexed microRNA quantification on encoded gel microparticles using rolling circle amplification. *Anal Chem* **83**, 7179-7185 (2011).

[353] Wang, H., Ach, R.A. & Curry, B. Direct and sensitive miRNA profiling from low-input total RNA. *RNA* **13**, 151-159 (2007).

[354] Shingara, J., Keiger, K., Shelton, J., *et al.* An optimized isolation and labeling platform for accurate microRNA expression profiling. *RNA* **11**, 1461-1470 (2005).

[355] Lee, J., Icoz, K., Roberts, A., *et al.* Diffractometric detection of proteins using microbead-based rolling circle amplification. *Anal Chem* **82**, 197-202 (2010).

[356] Lee, J.B., Peng, S., Yang, D., *et al.* A mechanical metamaterial made from a DNA hydrogel. *Nat Nanotechnol* **7**, 816-820 (2010).

[357] Um, S.H., Lee, J.B., Park, N., Kwon, S.Y., Umbach, C.C. & Luo, D. Enzyme-catalysed assembly of DNA hydrogel. *Nat Mater* **5**, 797-801 (2006).

[358] Park, N., Um, S.H., Funabashi, H., Xu, J. & Luo, D. A cell-free protein-producing gel. *Nat Mater* **8**, 432-437 (2009).

[359] Roh, Y.H., Lee, J.B., Tan, S.J., *et al.* Photocrosslinked DNA nanospheres for drug delivery. *Macromol Rapid Commun* **31**, 1207-1211 (2010).

[360] Lee, J.B., Hong, J., Bonner, D.K., Poon, Z. & Hammond, P.T. Self-assembled RNA interference microsponges for efficient siRNA delivery. *Nat Mater* **11**, 316-322 (2012).

[361] Beyer, S., Nickels, P. & Simmel, F.C. Periodic DNA nanotemplates synthesized by rolling circle amplification. *Nano Lett* **5**, 719-722 (2005).

[362] Deng, Z., Tian, Y., Lee, S.H., Ribbe, A.E. & Mao, C. DNA-encoded self-assembly of gold nanoparticles into one-dimensional arrays. *Angew Chem Int Ed* **44**, 3582-3585 (2005).

[363] Zhao, W., Gao, Y., Kandadai, S.A., Brook, M.A. & Li, Y. DNA polymerization on gold nanoparticles through rolling circle amplification: towards novel scaffolds for three-dimensional periodic nanoassemblies. *Angew Chem Int Ed* **45**, 2409-2413 (2006).

[364] Wilner, O.I., Shimron, S., Weizmann, Y., Wang, Z.G. & Willner, I. Self-assembly of enzymes on DNA scaffolds: en route to biocatalytic cascades and the synthesis of metallic nanowires. *Nano Lett* **9**, 2040-2043 (2009).

[365] Cheglakov, Z., Weizmann, Y., Braunschweig, A.B., *et al.* Increasing the complexity of periodic protein nanostructures by the rolling-circle-amplified synthesis of aptamers. *Angew Chem Int Ed* **47**, 126-130 (2008).

[366] Hamblin, G.D., Carneiro, K.M., Fakhoury, J.F., Bujold, K.E. & Sleiman, H.F. Rolling circle amplification-templated DNA nanotubes show increased stability and cell penetration ability. *J Am Chem Soc* **134**, 2888-2891 (2012).

[367] Carneiro, K.M.M., Hamblin, G.D., Hanni, K.D., *et al.* Stimuli-responsive organization of block copolymers on DNA nanotubes. *Chem Sci* **3**, 1980-1986 (2012).

[368] Ma, Y., Zheng, H., Wang, C. *et al.* RCA strands as scaffolds to create nanoscale shapes by a few staple strands. *J Am Chem Soc* **135**, 2959-2962 (2013).

[369] Ouyang, X., Li, J., Liu, H.*et al*. Rolling Circle Amplification-Based DNA Origami Nanostructrures for Intracellular Delivery of Immunostimulatory Drugs. *Small* **9**, 3082-3087 (2013).

[370] Zhao, W., Cui, C.H., Bose, S., *et al.* Bioinspired multivalent DNA network for capture and release of cells. *Proc Natl Acad Sci U.S.A.* **109**, 19626-19631 (2012).